DOCTOR OF PHILOSOPHY

Mathematical Modelling of Cancer Growth and Spread
The Role of Matrix Metalloproteinases

Deakin, Niall Ewan

Award date:
2015

Mathematical Modelling of Cancer Growth and Spread: The Role of Matrix Metalloproteinases

By

Niall Ewan Deakin

A Thesis submitted for the degree

of Doctor of Philosophy

University of Dundee

December 2015

Contents

Acknowledgements

I am most grateful to my PhD supervisor Mark Chaplain for his Olympian patience and understanding. Without him you would not be subjected to my thoughts.

I have been privileged to undertake my doctoral work in a department willing to provide unending support and friendship. To properly thank each individual who has supported me professionally or personally would easily double the length of this thesis. Despite this, I will attempt to highlight the individuals I am most grateful for having met over my time with the department. It is in these friendships gained that I am most proud.

Mark, in whom I remain thankful.

Gibin for his perspectives on life.

Zhenlin for his brotherhood.

Elaine for her honest opinions.

Daniella for her academic insight.

Mariya for her inspiring work ethic.

Simon for his happiness.

Niall for spelling his name properly.

Botong for her distant friendship.

Marc for driving me to improve.

A doctorate is not only the result of academic input and so I would like to express my thanks to all members of my family and friends who have encouraged and cajoled me through my studies.

My sister-in-law, Caroline, for becoming a doctor first.

My mother, Myra, for empathy.

My father, Rob, for laughter.

My brother, Mark, for inspiring.

My nephew, James, for joy.

My dog, Vreckan, for spirit.

My closest friend, Max, for prove reeding and ade.

My person-I-know, Carrie, for teaching me cryptic crosswords.

All others unmentioned for being too many to list.

In the depths of my thesis writing I found comfort and perspective from the night sky. Therefore, in closing, I would like to thank my lucky stars, the easily located Orion constellation.

Declaration

I declare that the following thesis is my own composition and that it has not been submitted before in application for a higher degree.

Niall Ewan Deakin

Certification

This is to certify that Niall Ewan Deakin has complied with all the requirements for the submission of this Doctor of Philosophy thesis to the University of Dundee.

Prof. Mark A. J. Chaplain

Abstract

A mass of cells that grow without normal bounds is termed a benign tumour if it does not invade locally into the tissue and malignant when it invades into its surrounding tissue. Benign tumours are often harmless unless the pressure they exhibit onto the tissue surrounding it causes trouble to the functioning of the human body as is often the case in brain tumours (gliomas) or other vital organs of the body. It is malignant tumours that are deemed to be made up of cancer cells and it is this process of invasion that defines them and will be studied in this thesis.

We do this by considering two scales of interest in cancer cell invasion. In Chapters 4 and 5, we focus on tissue scale dynamics of a cancerous mass and the processes by which the cancerous mass is able to invade the surrounding tissue. Correspondingly, we focus on a continuum, deterministic approach to protease-dependent invasion where matrix degrading enzymes cleave collagen fibrils and other ECM components. Specifically, in Chapter 4 we formulate a PDE model of cancer cell invasion primarily through haptotaxis as the result of degradation of tissue from the proteolytic activity of the membrane bound MT1-MMP protein and the soluble MMP-2 protein in addition to the complexes formed, and consequences thereof, from interactions they have with one another and their endogenous inhibitor TIMP-2. In Chapter 5 we develop the PDE model of cancer

cell invasion to incorporate additional dynamics of the tissue and how these may hamper cancer cell invasion and tissue degradation. Further, we investigate how the tissue may be reconditioned by MT1-MMP proteins to allow for additional cancer cell movement and tissue degradation.In Chapter 6, we consider how small protrusions from the cell termed *invadopodia* can affect the production of MMP-2 proteins and the focussing of ECM degradation, which has the consequence of allowing cancer cells to overcome barriers in the extracellular matrix.

Chapter 1

Introduction

Cancer cell invasion is of particular significance when considering the development of the disease as it is intrinsically linked with metastasis, which is responsible for approximately 90% of cancer deaths. Matrix degrading proteins are of critical importance when it comes to the degradation of healthy tissue that allows for the growth and spread of cancer cells and these proteins and their inhibitors can have non-linear dynamics (cf. the activation system for matrix metalloproteinase 2; MMP-2). This motivates the use of mathematical models to fully understand the complex process of invasion.

In Chapter 2, we outline some of the biological dynamics that are important in cancer cell invasion in order to provide evidence for the incorporation of these biological motivations in the proposed mathematical models. In Chapter 3, we provide a summary of the historical and current mathematical models of cancer invasion which form the foundations on which the current work stands.

We have developed a continuum (PDE) model of cancer cell invasion incorporating the activation system for matrix metalloproteinase 2 in Chapter 4 and

provided details on how it is formulated and parameterised. We explore the significance of the level of tissue inhibitor of metalloproteinases 2 (TIMP2) on cancer cell invasion and identify the individual roles that MMP-2 and the membrane bound-1 matrix metalloproteinases (MT1-MMP) play.

The surrounding environment of the cancer cells plays a significant role in cancer cell invasion and so while we have considered a relatively simple formulation of the environment in Chapter 4, in Chapter 5 we proceed to expand upon the proposed model with the incorporation of additional roles of the environment, including pore size, etc., on cancer cell invasion. Additionally we explore how the significance of MT1-MMP changes when the additional dynamics that are solely the domain of MT1-MMP are considered.

In Chapter 6, we investigate how small protrusions of a single cell (invadopodia) into the surrounding tissue may cause additional and significant changes as to how cancer cell invasion proceeds. The inclusion of shuttling of MT1-MMP to invadopodia is investigated with relation to the activations system of MMP-2 as well as how this may affect the lifespan of invadopodia. This is modelled through a stochastic approach where only a small spatial scale, and therefore small number of proteins are considered.

A discussion of the proposed works focusing on results obtained from the modelling efforts is included in Chapter 7 before a discussion of the proposed works including both their usefulness as prognostic tools and the exploration of as-of-yet not fully defined biological systems The presented work is then brought to an end with the offering of potential avenues of continued research.

Chapter 2

The Biology of Cancer Invasion

Cancer is a classification of over 200 diseases which all arise progressively from an alteration in a single cell's genetic structure. A cancer cell is defined as one which proliferates beyond the bounds a normal cell experiences and one which invades and replaces cells of neighbouring areas. Alberts et al. (2008) describes the body as a *"society or ecosystem where dynamics such as self-preservation are put below that of self-sacrifice"*, a statement which we will support by describing the functions of healthy cells, before continuing on to show how cancerous cells demonstrate behaviour that violates this description.

Cancers gain their classification from either the location from which they arise (brain cancer, breast cancer, cervical cancer, etc.) or from their tissue type (blastomas-embryonic tissues, carcinomas-epithelial tissue, leukemias-blood production site, lymphomas-lymphatic tissue, myeloma-bone marrow, sarcomas-connective tissue etc.). Carcinomas are the most common classification accounting for approximately 90% of all cancers.

Cancer grading measures the abnormality of the cancer cells from biopsies and

generally follows the three grades (some cancers and countries have varying grading systems) of: (i) the cancer cells appear normal (differentiated) and grow slowly, (ii) the cancer cells are abnormal (poorly differentiated) and grow quickly and (iii) the cancer cells are very abnormal (undifferentiated) and grow very quickly.

Cancer staging measures the extent of the disease's spread. There are a number of systems to measure this. However we present only one numerical system here: stage 0 (cancer limited to surface cells), stage 1 (cancer exhibiting growth but remains at original site), stage 2 (local invasion of cancer cells), stage 3 (further reaching invasion of cancer cells) and stage 4 (metastasis).

2.1 Biology of Healthy Cells and Tissue

In order to understand the processes that cancerous cells perform, a basic understanding of the processes a healthy cell may undergo is required. This also applies when we look at how a mass of cancer cells interact with their surrounding healthy stroma and so here we provide a minimal overview of both.

A cell (discovered by Hooke in 1665 (Hooke, 1665)) is the biological entity which all living organisms are made up of, whether single cell organisms or multicellular (humans contain approximately 3.72×10^{13} cells (Bianconi et al., 2013)). A cell is the fundamental building block of life as nothing smaller than it can perform all of the following: contain hereditary data (DNA), obtain resources/nutrients from its environment, convert these resources/nutrients to energy, use this energy to multiply by creating a duplicate of itself.

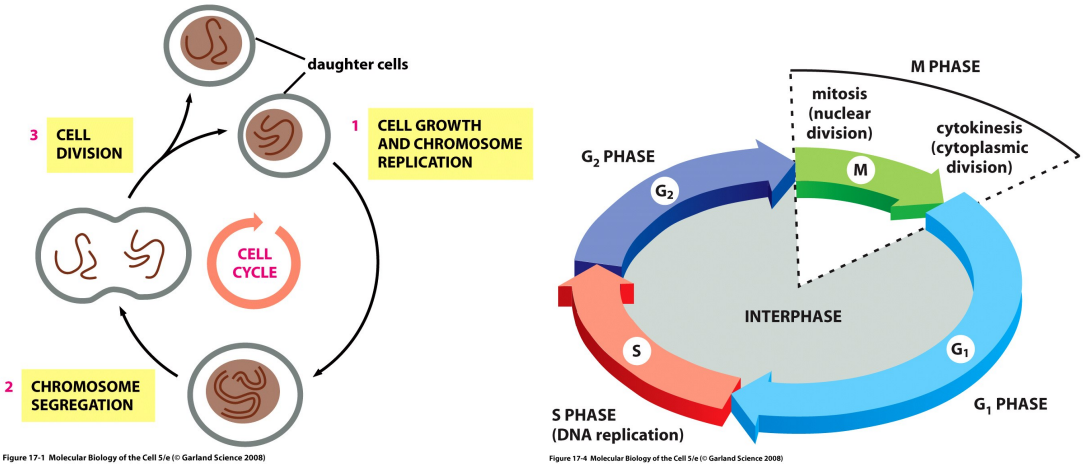

Figure 2.1: *The four stages of G1, S, G2 and M that a cell cycles through are illustrated where G0 represents a removal, however temporary, from this cycle. ©Alberts et al. (2008), reproduced by permission of Garland Science/Taylor & Francis LLC.*

The communication between cells is extensive and is done by a myriad of extracellular signals. A cell needs to receive multiple signals in order to survive. Depriving a cell of one or more of these signals can initiate cell death. If a cell receives the required signals to survive, it can then either divide or differentiate if appropriate additional signals are received. Despite receiving the same signals, different cells may react in different ways to the same signals depending on their ability to interpret these signals through receptor proteins.

The cell-cycle, as outlined in Figure 2.1, describes the functional stages a cell goes through in order to continually divide and is defined by four stages. The interphase is the period that contains the first three of these stages: G1 phase (cell grows), S phase (DNA synthesis resulting in a doubling of each chromosome), G2 phase (the cell continues to grow). The interphase is followed by the M phase (mitosis-nuclear division and cytokinesis-cell division). G0 phase is the state a cell goes into when it is no longer taking part in this cell-cycle where the cell is considered to be resting.

Healthy tissue constructs made up of the extracellular matrix (ECM) are rigid structures of cellular components that are constantly undergoing remodelling. The rate at which this remodelling takes place is boosted during development and wound repair. What determines the remodelling of ECM can be one of the following factors: cell-surface receptors, matrix degrading proteins and stress/tension. Comprehensive overviews for the structure of the ECM are provided in Vakonakis and Campbell (2007), Daley et al. (2008) and Hynes (2009).

In order for cellular structures to be formed, there must a way of linking cells together. This is done either directly with cell-cell bonds of either homophilic or heterophilic type, or by the use of a medium such as the rigid ECM structure, which multiple cells can connect to. Integrins are transmembrane/cell-surface receptors that allow for cell-cell or cell-ECM bonds to form. This gives rise to the two forms of animal tissue. Epithelial tissues are formed of closely packed epithelial cells while connective tissues, which the ECM is, has a much sparser distribution of cells. Epithelial cells are themselves architectures of cells that form sheets that line cavities and structures throughout the body. Typically, a layer of epithelial cells will create the surface of a structure encasing the basement membrane, beyond which lies the connective tissue made up of collagen and a variety of other ECM material. This is outlined in the diagrams of Figure 2.2.

Collagens are a family of triple helical proteins that are responsible for tissue assembly and maintenance. This definition leaves some blurring in the distinction between collagens and collagen-like proteins (Kadler et al., 2007). Of the collagens, collagen type-I is the most abundant and can be found in connective tissue throughout the body. The three chains that form the collagen protein are α chains while the majority of collagen proteins are homotrimers. Collagen type-I in its standard form is heterotrimeric and consists of two identical $\alpha - 1$ chains while the third is an $\alpha - 2$ chain.

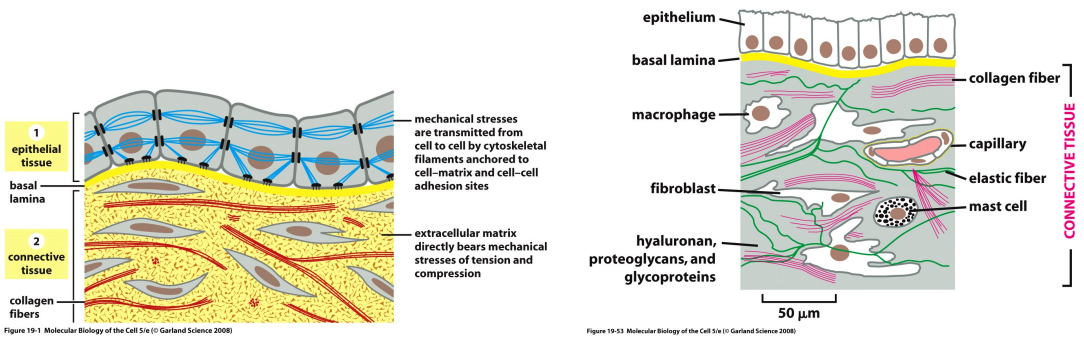

Figure 2.2: *Schematic of epithelium leading into connective tissue. ©Alberts et al. (2008), reproduced with permission from Garland Science/Taylor & Francis LLC.*

The family of collagens in the ECM are triple-helical proteins (cf. Figure 2.3) proteins that are extremely strong and flexible and provide the ECM with its tensile strength. The triple helix form of collagen is resistant to many forms of degradation. The end segments of collagen fibres are not in the triple-helical form and feature N- and C-termini. The crosslinking of collagen fibres to form fibrils occurs at these termini where the C-terminus of one collagen molecule is linked to the N-terminus of another collagen molecule. A collection of three stranded collagen type-I molecules can form collagen fibrils of diameter 50-200nm which have the structure outlined in Figure 2.3. Collagen fibrils are then organised into fibrous structures by fibroblasts (Ehrlich and Krummel, 1996; Alberts, Johnson, Lewis, Raff, Roberts and Walter, 2008).

The three-dimensional aspect of the ECM plays a pivotal role in regulating cellular adhesion, migration, morphogenesis, growth and apoptosis (see Klein et al., 2003, and references therein) by affecting cells at the level of signal transduction (Daley et al., 2008).

Matrix Turnover, or matrix degradation, occurs in normal tissue and is in fact an essential process in healthy tissue. There are biological processes in a healthy

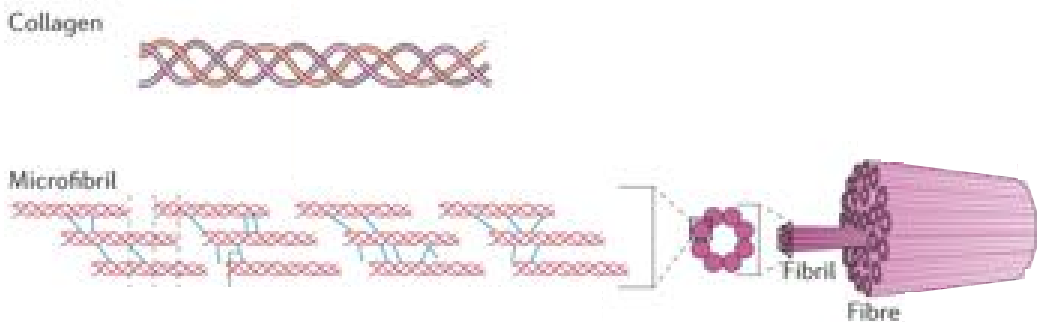

Figure 2.3: *The triple-helical nature of the rope-like collagen strands and their formation within the larger constructs of fibrils and fibres. ©Nature Publishing Group, reproduced with permission from Mouw et al. (2014).*

body that require the degradation of extracellular matrix to either provide the space required by a cell to replicate or to allow the cell to travel through the matrix. These processes occur in bones adapting to stresses (Chiquet et al., 1996), the branching growth of mammary glands during embryonic development (Vu and Werb, 2000) and other epithelial structures and in immune response where white blood cells migrate across the basal lamina of blood vessels. An essential part of investigating ECM turnover, whether in a positive case such as wound healing or a negative case such as cancer, is the the consideration of MMPs and TIMPs (Kerrigan et al., 2000).

As natural turnover of ECM is required within a healthy body, MT1-MMP and MMP-2 are produced at certain times outside of cancer invasion. MT1-MMPs can be seen as a method for fibroblast (these lay down the foundation of the ECM) invasion of tissue (happens on a single based scale that causes only small degradation of tissue far below what we would see in cancer) to allow the fibroblasts to reach areas of tissue that have been damaged and need to be repaired. This process involves MT1-MMP (and therefore MMP-2) being expressed continuously until the wound has been healed. When we consider this process in the

context of cancer invasion we can see that this feedback loop (technical details involve collagen activating ERK which upregulates MT1-MMP which causes a feedback loop by encouraging the ERK again) causes the wholesale destruction of tissue (Lu et al., 2011).

2.2 Biology of Cancerous Cells and Their Environment

The most common form of cancer is the grouping of solid carcinoma accounting for $\sim 80 - 90\%$ of all cancers. Carcinomas are formed from epithelial cells.

If we recall the body as a *"society of cells"* then it is clear that cancer cells subvert this society towards their own ends.

Meyskens et al. (1984) estimated the number of cells per cancerous cell mass (from order $10^0 - 10^2$ number of cancer cells of cell diameter $12.0 - 44.5\mu$m in oblate spheroid masses of diameter up to 150μm in a semisolid medium) as $2.40 \times \frac{(\text{diameter of mass of cells})^{2.378}}{(\text{diameter of cell})^{2.804}}$.

Here, we will use the framework provided by Hanahan and Weinberg (2000) in Figure 2.4 where they characterise cancer as having 6 "hallmarks", with an additional 3 hallmarks proposed in their follow-up paper (Hanahan and Weinberg, 2011): enabling replicative immortality, inducing angiogenesis, resisting cell death, sustaining proliferative signalling, evading growth suppressors, activating invasion and metastasis, deregulating cellular energetics. These are the basic characteristics that they believe have emerged that can define most, if not all, human cancers. We note that there exists some criticism in the literature of these "hallmarks", for example, in the paper of Sonnenschein and Soto (2013) where

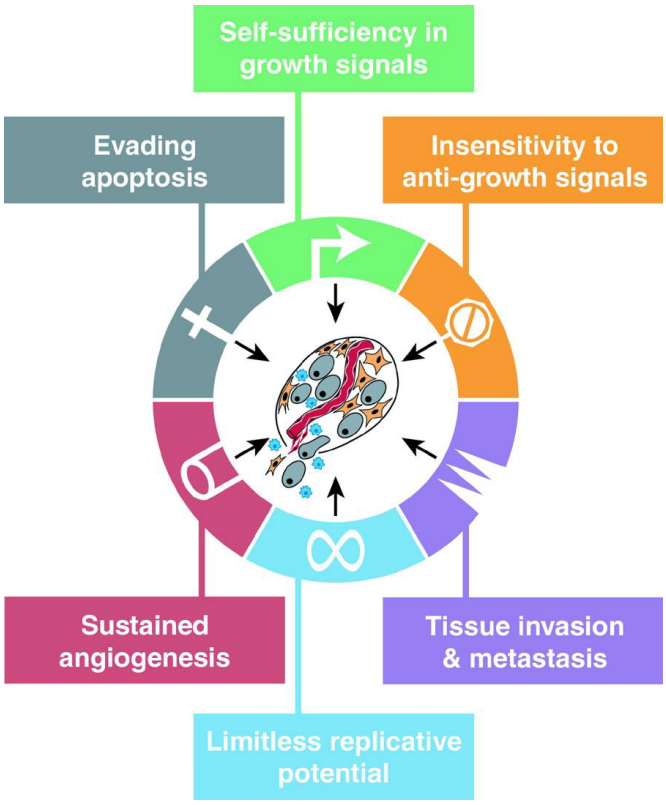

Figure 2.4: *The six originally identified "hallmarks of cancer". ©Elsevier, reproduced with permission from Hanahan and Weinberg (2000).*

they instead extol the tissue organisation field theory where cancer is viewed as a tissue-based disease.

Replicative immortality of cancer cells allows them to be able to undergo mitosis limitlessly. This is in contrast with normal healthy cells which can only do so a limited number of times. Human cells can perform mitosis approximately 40-60 times under the Hayflick limit (Hayflick and Moorhead, 1961).

Resisting cell death permits the growth rate of a mass of cancer cells, defined by the balance between the production and death rates of the cell, to increase beyond levels that would be considered normal in healthy tissues. Apoptosis (cell-death) can be triggered by environmental stimuli and was proposed by Kerr et al. (1972).

Inducing angiogenesis provides cancer cells with the required nutrients necessary for them to grow. This can be supplied in the form of oxygen diffusing from blood vessels. As such, it is profitable for masses of cancer cells to stimulate the growth of blood vessels in the same vicinity as the cancer cells and is indeed a requirement for solid tumours to grow past $\sim$2-3mm in diameter. This is done by the release of tumour angiogenic factors (TAF) that provide signals to the blood vessels to grow toward the cancerous mass.

Sustaining proliferative signalling of cancer cells, where these cells gain the capability of continued generation of their own growth signals through oncogenes (characterised as growth factors, growth factor receptors, signal transduction proteins, nuclear regulatory proteins and cell cycle regulators), independent of the surrounding tissue, allowing for the overcoming of homeostasis.

Evading growth suppressors that would promote homeostasis. Homeostasis occurs where there is a balance of both promoting growth and suppressing growth,

where appropriate. Malignant tumours are clear violators of homeostasis and as such it is not surprising that they feature both sustained growth, as discussed in the previous sub-topic, as well as insensitivity to anti-growth signals. The part of homeostasis that is violated in this context is the ability of signals to force cells into the quiescient state (G_0 of the cell cycle) or postmitotic state. These antigrowth signals are picked up by integrins on the cell-surface, which in turn internalise the signal. As such, one manner of cancerous cells evading these growth signals in the manipulation of the expression of cell surface receptors away from those that pick up antigrowth signals.

Tissue invasion and metastasis where tissue invasion depends on cell motility through neighbouring regions of healthy tissue. This may be achieved by either enzyme dependent means through the degradation of the surrounding extracellular matrix or enzyme independent means through collective cell migration (Khalil and Friedl, 2010; Vargas and Zaman, 2011; Schlüter, 2013). Metastasis is the seeding of new environs, which occurs when certain barriers within the body are overcome, such as allowing cancer cells to enter into the blood vessels or lymph system, allowing for the creation of secondary tumours to form.

Deregulating cellular energetics causes glycolysis to be upregulated, resulting in additional cellular respiration.

Tumour-promoting inflammation occurs where the co-opting of the immune system causes it to promote cancer cell invasion.

Genome instability and mutation, where most types of cancer cells have chromosomes that deviate form the norm (aneuploidy state instead of euploid karyotypic state) to the extent that they may have an extra copy of chromosome(s), missing chromosome(s) or the fusion of two or more chromosomes.

2.3 Cancer Cell Invasion

Different types of collagen act as a physical barrier to cancer cell invasion or as a surface to move along depending on the structure. For invasion and metastasis to occur, cancer cells are required to overcome several collagen-endowed tissue barriers. One such obstacle is the basement membrane that lines vascular endothelial cells and is made up of largely collagen type IV. Another obstacle is the structural ECM in the tissue (stroma), which can be largely made up of collagen type I. The ECM is a fairly rigid and stable structure which has displayed decades long half-life in vivo. Protease-dependent invasion (as opposed to force based models of movement along fibres) rely on enzymes (such as MMPs) to cleave the collagen fibrils that would otherwise impede movement through the region.

One form of cancers, gliomas (brain cancers), can have an identifiable tumour centre, boundary and invasive region ahead of the boundary with MT1-MMP being overexpressed in cells at the border of the tumour and in invasive cells ahead of the tumour (Guo et al., 2005). Guo et al. (2005) perform a statistical analysis of their results and find that for all grades of tumour (I-IV), there exists a significant association between the upregulation of MT1-MMP and MMP-2 with the invasiveness of the glioma. However, glioblastomas, the most highly malignant of gliomas, are characterised by rapid invasion into the surrounding parenchyma and blur tumour margins with single cell invasion occurring at the invasive front and the formation of small colonies of cancer cells in advance of the tumour. This renders the potentially curative treatments of surgery, immunotherapy, radiotherapy and chemotherapy to be palliative care only (Nakada et al., 2007).

Metastates (secondary tumours/cancers) account for more than 90% of cancer deaths (Steeg, 2006). For metastasis to occur, cancer cells must exhibit invasion

through a variety of structured media such as the highly dense collagen constitution of some peritumoral stroma (Hanahan and Weinberg, 2000, 2011). This can occur by the secretion of enzymes that are capable of degrading components of the ECM or by the adoption of an amoeboid phenotype that allows cancer cells to travel through the medium in a protease-independent manner (Friedl and Wolf, 2003*a*; Sahai, 2005). Cancer cells from a primary tumour break away from the central mass and are disseminated throughout the body where they regrow to form secondary tumours. The main steps of metastasis are intravasation, survival/travelling of the blood stream, extravasation. A tumour may release millions of cells in a day to only have a few survive these final two processes.

2.3.1 Matrix Degrading Enzymes

Matrix degradation is accomplished by proteins such as the urokinase plasminogen activator (uPA) and the family of matrix metalloproteinases (MMPs). There are 24 MMPs in humans (named MMP-,1-3,7-17,19-21,23A,23B,24-28, Quesada et al., 2009), 18 of which are freely-diffusive with the remaining 6 being bound to the membrane of the cell. Collectively they can degrade all components of healthy tissue (Kleiner and Stetler-Stevenson, 1999; Egeblad and Werb, 2002). This in turn facilitates cancer growth and spread by virtue of the available space left in the absence of the degraded ECM as well as by VGEF proteins that are released by the degraded tissue encouraging the cancer growth (López-Otín and Overall, 2002), (Werb, 1997). MMPs are zinc-dependent endopeptidases whose main function is the homeostatic regulation of the ECM, that is to say the regular turnover of the ECM (Nagase and Woessner, 1999). This process is exploited in cancer growth and invasion where various MMPs are over expressed. The expression of MMPs faces control at the level of transcription but can also face

inhibition when moving from the proMMP precursor state to an active MMP as well as inhibition when it exists in its active state (Overall and López-Otín, 2002; Clark et al., 2008).

The first member of the matrix metalloproteinase family discovered was MMP-1 (originally named tadpole interstitial collagenase) from evidence of collagenolytic activity in tadpole tail metamorphosis (Gross and Lapiere, 1962). While MMPs have gone through several name changes, the generally accepted naming convention for them is now MMPs. Even once we have settled upon the notation of MMP, we still find that numerous expansions of this abbreviation exist: namely, metalloendopeptidase, metallopeptidase, metalloproteinase, or metalloprotease.

MMPs feature a lack of upregulation by gene amplification/activation in cancer cells but instead transcriptional changes result in the over-expression of MMPs in cancer invasion Shapiro and Senior (1999). This distinguishes them from typical oncogenes. It is important to note that MMPs play a part in many diseases as well as in healthy tissue, for example, cancer, arthritis, skeletal development and growth plate disorders, heart disease, central nervous system (CNS), meningitis, multiplesclerosis, Alzheimers disease, inflammatory myopathies (Malemud, 2005).

The family of MMPs can exhibit both pro- and anti-invasive characteristics (Nöel et al., 2012) but in this work we focus on the pro-invasive MMPs of MMP-2 and MT1-MMP. MMP-2 is secreted in the inactive zymogen form of proMMP-2 whereas the fully active MT1-MMP is expressed on the cell surface after being activated internally. This interplay between the enzymes is emphasised by the coexpression of proMMP-2, MT1-MMP, MMP-2 and TIMP2 in a variety of tissues (Kinoh et al., 1996). While MT1-MMP was initially thought to have activity limited to activating MMP-2, it has since been found to also have a direct role in tissue degradation (d'Ortho et al., 1997).

MMPs that play a crucial role in cancer invasion are MMP-2, MMP-9 and the various MT-MMPs (mainly MT1-MMP). Some MMPs even have the opposite effect with MMP-8 in particular exhibiting anti-invasive properties. Even amongst the pro-cancer MMPs there seems to be some location specific properties with MMP-2 and-9 being more important in liver cancer with a minimal (at best) role of MT1-MMP whereas other locations (breast in particular) has a high dependence on the specific properties offered by the MT1-MMPs due to the make-up of the 3D collagen type-I structure.

MMP-2 was one of the earliest discovered MMPs, it has known many names: matrix metallopeptidase 2, gelatinase A, 72kDa gelatinase, 72kDa type IV collagenase, $M_r 72,000$ MMP.

ECM substrates of MMP-2 are: elastin, fibronectin, various collagens, laminin, aggrecon, vitronectin. MMP-2 has a non-ECM substrate of TGF-beta (consequence uncertain but it is a growth factor), IGFBP3 (causes increased cell proliferation and survival) and CCL7 (a chemokine that allows the transformation of a chemotactic agonist into a chemotactic antagonist).

MMP-2 and MMP-9 are seen to strongly correlate with glioma progression and malignancy. MMP-2 and MT1-MMP are overexpressed in invading cells of gliomas in humans (Guo et al., 2005).

Integrin $\alpha_v\beta_3$ is found to be implicated in the activation process of MMP-2 by MT1-MMP and TIMP2 in glioma cells (Deryugina et al., 2001). However Sakai et al. (2011) confirm the findings of Gilles et al. (1997) and Nguyen et al. (2000) that the MMP-2 activation from 3D collagen induced MT1-MMP is independent of integrins and matrix stiffness.

MT1-MMP is activated from proMT1-MMP by furin-like proprotein convertases

into active MT1-MMP (a process that can be inhibited by the convertase inhibitors of α 1-PDX and HIV aspartyl protease inhibitor). This means that by the time it reaches the surface of the cell, it is in its active form.

MT1-MMP localises to the front of migrating cells. This allows degradation of ECM components that are in front of the invading cancer cells that would otherwise be a physical barrier to invasion. ECM substrates of MT1-MMP are: fibronectin, vitronectin, laminin-1,-5, fibrin, collagen type I, II, III, gelatin, casein and elastin. MT1-MMP has a non-ECM substrate of pro-α_v integrin (offers an increase motility). As well as degrading and remodelling components of the ECM, MT1-MMP can cause the detachment of cell-cell and cell-substrate adhesion links by cleaving cell adhesion molecules such as CD44 and integrin α_v chain.

MT1-MMP confers cancer cells with the ability to proteolytically degrade the basement membrane scaffolding, initiate invasive pseudopodia (where a single cell changes its geometry to reach out in a specific direction) and facilitate transmigration through the endothelial monolayer and the basement membrane ($\sim$100 nm thick and consisting of largely collagen type-IV).

MT1-MMPs are responsible for the invasive potential of fibroblasts and other single cell invasion capabilities. Hotary et al. (2000) find that MT1-MMP invasion is independent of the activation of MMP-2. While MT1-MMP is essential for cancer cell invasion in 3D (Sabeh, Shimizu-Hirota and Weiss, 2009; Li et al., 2008), Lund et al. (2014) find that it is not sufficient in itself for invasion of 3D collagen by human muscle satellite cells.

Of MMP-mutant gene knockout mice, only the mmp14 gene-knockout is lethal in mice. They are born without abnormalities but develop these and die aged 3-12 weeks (Holmbeck et al., 1999; Zhou et al., 2000). Key findings of their work includes that MT1-MMP and MMP-2 knock-out mice die fastest followed by

MT1-MMP knockout mice followed by MMP-2 knockout mice (who may not even die from the internal failures that they suffer). MT1-MMP deficient mice produce only a faint level of MMP-2. Angiogenesis and tumour growth are severely limited in MMP-2-null and MT1-MMP-null mice.

TIMP2 is one of four members of the gene family of "tissue inhibitor of metalloproteinases" consisting of: TIMP1, 2, 3, 4. These genes encode the proteins that act as protease inhibitors and can collectively inhibit all members of the MMP family. proMMP-2 and proMMP-9 (the latent forms of MMP-2 and MMP-9) are the only pro-enzymes of the MMP family that are capable of forming complexes with TIMPs. proMMP-2 can bind to TIMP2 and this complex plays a role in its activation mediated by MT1-MMP to MMP-2. TIMP2 has an N-terminal domain and a C-terminal domain. When TIMP2 inhibits MT1-MMP, the N-terminal domain of the TIMP2 binds to the catalytic domain of the MT1-MMP. When TIMP2 is involved in the activation of MMP-2, the proMMP-2 uses its hemopexin-like domain to bind to the remaining free C-terminal domain. As TIMP2 has a multifaceted function, any potential inhibitor that selectively targets only MT1-MMP has been described as the "*Holy Grail in MMP inhibitor drug development*" (Zucker and Cao, 2009).

2.3.2 The Extracellular Matrix in Relation to Matrix Metalloproteinases

The microenvironment of the tumour plays a significant role in cancer progression (Hu and Polyak, 2008; Bissell et al., 2002) with matrix metalloproteinases, among other matrix degrading enzymes, acting as regulators, allowing obstacles to be overcome (Rowe and Weiss, 2009; Kessenbrock et al., 2010).

While collagen type-I will normally exist as a heterotrimer, it can also exist in a homotrimeric form in the cases of fetal tissues, fibrosis and human cancers (see Chang et al., 2012, and references therein). This difference in possible structure may play a significant but not yet fully understood role in cancer invasion. McBride et al. (1997) propose that the structure formed by collagen type-I is proposed to be due to the $\alpha - 2$ chain and Kuznetsova et al. (2003) find that homotrimeric collagen denaturates 100 times slower than heterotrimeric collagen when performed at the same temperature. Denatured collagen is gelatin, a substrate of MMP-2.

The main constituent of the stroma (dense connective tissue) is the insoluble, structural, cross-linked type I collagen. MT1-MMP exhibits strong type I collagenolytic capabilities and weak gelatinolytic capabilities. Conversely, MMP-2 exhibits weak type I collagenolytic capabilities and strong gelatinolytic capabilities (Tam et al., 2004) where it is unable to degrade cross-linked collagen type I and type IV but is able to degrade the uncross-linked variants (Zhang et al., 2013). MMP-2 can, however, critically degrade type IV collagen, the main component of the basement membrane and an extracellular barrier. As MT1-MMP is bound to cancer cells, its region of proteolytic activity is more restricted than that of the freely-diffusive proteolytic enzyme MMP-2.

While MT1-MMP activity is restricted in range, it has an advantage in its capability of overcoming environments of higher collagen density such as exists in some peritumoral stroma. Sabeh, Shimizu-Hirota and Weiss (2009) have shown that when cancer cells are faced with structural barriers created in reconstituted gels by covalently cross-linked fibrils of type I collagen, or that exist in the stromal environment of the mammary gland, invasion is dependent on MT1-MMP-mediated proteolysis.

2.3.3 Invadopodia

Cells move across a substrate by forming protrusions which attach to the ECM before retracting, dragging the cell along. While all the protrusions are capable of forming adhesion sites with the ECM and receiving signals, only podosomes and invadopodia are capable of non-negligible ECM degradation when compared to the scale of cellular invasion. These membrane protrusions are dependent on intracellular actin structures and are classified as: filopodia, lamellopodia, invadopodia, podosomes.

While there are many shared roles between these cell protrusions, we highlight the main form and function of each protrusion:

Lamellipodia: sheet-like, 10–15 μm wide but only 0.1–0.3μm thick. Lifespan: minutes. The broadest structure on the cell membrane.

Filopodia: finger-like, Lifespan: minutes. sensors that are responsible for exploration of the cell surroundings and provide feedback to the cell. Located near lamellipodia and probe the region ahead of lamellipodia. More significant in 3D than 2D substrates. - Three-dimensional reconstruction and motion analysis of living, crawling cells.

Podosomes: conical, Lifespan: minutes. Responsible for cellular motility through both the degradation of matrix and the formation of adhesion sites.

Invadopodia: conical, Lifespan: hours. The overcoming of cellular barriers for cancer cells by the degradation of ECM as well as an increased cancer cell motility.

Focal adhesions: 2–6μm. Lifespan: hours. A bridge between the cell and ECM through which signals are received.

Localisation of proteins to cellular protrusions has a large impact on the function of the protrusion. One example is proMMP-2 and MT1-MMP localising at invadopodia while proMMP-2, MT1-MMP and TIMP2 localise at lamellipodia. This higher level of TIMP2 at lamellipodia in comparison to invadopodia leads to invadopodia being more responsible for cellular invasion and locomotion instead of lamellipodia in cancer (Chen and Wand, 1999).

The maturation of invadopodia formation can be divided into distinct stages as outlined in the work of Artym et al. (2006). These are: (i) aggregation of cortactin, which is responsible for the shape of the actin cytoskeleton, (ii) shuttling of MT1-MMP to invadopodia, (iii) matrix degradation and (iv) MT1-MMP mediated dissociation of cortactin.

Chapter 3

Mathematical Modelling of Cancer Cell Invasion

3.1 Continuum Modelling

Mathematical modelling of cancer growth and invasion has expanded from the seminal, though not necessarily the first, work of Greenspan (1976) as it has attempted to fill the ever-expanding areas that cancer biology research has examined/unearthed/discovered. The burgeoning levels of mathematical models in the field owes, in part, its existence to the surge in computational power that has facilitated ever-complex numerical simulations that could not have been undertaken in decades past. However, simulations of any organ in full is still not possible despite the particular advances towards such models of the liver (Holzhütter et al., 2012; Drasdo et al., 2014).

While we highlight the most relevant of mathematical works on cancer cell invasion, for a more expansive overview of the following topics, we refer the reader

to the review papers and the references therein: Araujo and McElwain (2004), Roose et al. (2007), Quaranta et al. (2008) Bellomo et al. (2008), Bellomo and Delitala (2008), Tracqui (2009), Preziosi and Tosin (2009), Lowengrub et al. (2010), Byrne (2010), Rejniak and McCawley (2010), Deisboeck et al. (2011), Rejniak and Anderson (2011) and Scianna and Preziosi (2012).

The general mathematical form for how a species (variable c) moves in response to a gradient in either its own concentration/density or that of another species is modelled by the equation:

$$\frac{\partial c}{\partial t} + \nabla \cdot \underline{J} = \sum_{i=1}^{m} f_i, \tag{3.1}$$

where J is the sum of the flux terms and m is the number of source terms, f_i.

One such movement that can be modelled by this type of formulation is that of chemotaxis where chemotaxis describes the process by which an object, e.g. a cell, moves in response to a chemical concentration gradient. For example, *Escherichia coli* moves in response to gradients in its nutrient's concentration (Adler, 1973) as can be mathematically modelled in continuum form by the Patlak-Keller-Segel (P-K-S) equations (Patlak, 1953; Keller and Segel, 1970, 1971*a*,*b*).

The P-K-S equations were introduced to study the movement of the diffusible *Escherichia coli* (variable c) in response to gradients in a diffusible nutrient (variable v) that the *Escherichia coli*, themselves, produce. They considered this to take place in a multi-dimensional space with zero-flux boundary conditions. Therefore $c \equiv c(\underline{x}, t) = c(x, y, z, t)$, $v \equiv v(x, y, z, t)$ and $\underline{n} \cdot \nabla c = \underline{n} \cdot \nabla v = 0$ on the boundary $\partial\Omega$, where $\underline{n}$ is the outward unit normal. The P-K-S equations can therefore be of the form:

$$\frac{\partial c}{\partial t} = \nabla \cdot (D_c \nabla c - \chi c \nabla v), \tag{3.2}$$

$$\frac{\partial v}{\partial t} = D_v \Delta v - \beta_v v + \mu_v c, \tag{3.3}$$

where D_c is the diffusion rate of the *Escherichia coli*, χ is the chemotaxis sensitivity function (in this case a parameter), D_v is the diffusion rate of the nutrient, β_v is the death rate of the nutrient and μ_v is the production rate of the nutrient.

The generalised form of considering the chemotactic flux is:

$$J = \chi(\cdot)\nabla v, \tag{3.4}$$

where various functional forms of chemotactic sensitivity function, $\chi(\cdot)$, are presented in Hillen and Painter (2001), Painter and Hillen (2002) and Hillen and Painter (2009) where they discuss appropriate forms to avoid overcrowding (finite time blow-up solutions).

From the initial mathematical models of chemotaxis (Keller and Segel, 1971*a*,*b*), there has developed a wide variety of problems that can be modelled by variations on these equations as seen in the reference paper of Horstmann (2003), as well as the expansive work of Hillen and Painter (2009) and the references therein. While chemotaxictic flux is defined as being in response to a chemical gradient, haptotactic flux is defined as being in response to a density gradient. In the presented work, we will consider cancer cells to react haptoactically towards density gradients in the non-diffusible tissue.

This movement in response to gradients may not only act as an attractant for a species but instead as a chemo-repellent (Adler and Tso, 1974; Tso and Adler, 1974) as is the case in the work of Perumpanani et al. (1998), where they consider degradation of tissue to release solubilised fibronectin that then impedes invasion by acting as a chemo-attractant in the opposite direction of overall travel.

Invasion mediated by oxygen distribution where cancer cells use oxygen as a nutrient has been one of the first methods of studying cancer growth mathematically. We present a brief journey through the developments to mathematical models of

cancer growth over a twenty year period from Thomlinson and Gray (1955) to Deakin (1975) before considering the works of Orme and Chaplain (1996) and referring the reader to the review works of Araujo and McElwain (2004) and Roose et al. (2007). We note that the mathematical models of cancer invasion considering oxygen distribution after this period tend to consider cancer cells as discrete entities, e.g., Powathil et al. (2012) and so will be considered in more depth later in this chapter.

Thomlinson and Gray (1955) and Burton (1966) established mathematical models where oxygen was modelled as a nutrient diffusing from the outer edge (boundary) of a tumour inwards to investigate its role in necrosis. Burton (1966) obtained approximations for how wide this viable ring of cancer cells was in relation to the entirety of the tumour. These works were expanded in Greenspan (1972) and Greenspan (1974) where the addition of surface tension resulted in the removal of cells due to necrosis in the centre of the tumour being countered by the surface tensions of the tumour causing a compact tumour to form. Deakin (1975) used a varying consumption rate of oxygen by cells to expand these works to include the result of the viable rim reducing in size slowly in response to necrosis at the centre of the tumour.

More recent works that have continued this work on multicellular spheroids and avascular tumour development with a necrotic core include the works of Byrne and Chaplain (1995), Byrne and Chaplain (1996), Orme and Chaplain (1996). For mathematical models of tumour-induced angiogenesis, we refer the reader to the review papers of Mantzaris et al. (2004), Chaplain et al. (2006) as well as Scianna et al. (2013) and the references therein.

Invasion mediated by the acidity of the environment was championed by Gatenby

and Gawlinski (1996) where they formulated a system of partial differential equations (P.D.Es) to model cancer cell (variable c) invasion of the extracellular matrix (ECM) where the ECM (v) is degraded by H^+ ions (Λ). They consider cancer cells to experience flux in the form of non-linear diffusion, modelled by $J = D_c(1-v)\nabla c$, which has a maximum diffusive rate at $v = 0$, which decreases for increasing density of v where there is no diffusion for $v = 1$. The non-linear diffusion term models the limiting/prevention of cancer cells diffusing into a region of highly dense ECM where diffusion at a higher rate occurs once the ECM has begun to be degraded by H^+ ions.

Their model can be presented in the form:

$$\frac{\partial c}{\partial t} = \nabla \cdot (D_c(1-v)\nabla c) + \mu_c c(1-c), \tag{3.5}$$

$$\frac{\partial v}{\partial t} = -\delta_v \Lambda v + \mu_v v(1-v), \tag{3.6}$$

$$\frac{\partial \Lambda}{\partial t} = \nabla \cdot (D_\Lambda \nabla \Lambda) + \mu_\Lambda (c - \Lambda), \tag{3.7}$$

where cancer cells self reproduce at a rate of μ_c, limited by the amount of cancer cells already at that location. The ECM is degraded at rate δ_v by the amount of H^+ ions and self reproduces in a manner that is limited by the amount of ECM at that location. The H^+ ions can diffuse at rate D_Λ and are produced by the cancer cells until a value defined by the amount of H^+ ions.

We present the two key results of their model where, firstly, they identify an interstitial gap as a result of a pH gradient extending into the ECM surrounding the cancer cells (caused by the diffusion of excess H^+ ions produced by the cancer cells) where there is a region between the cancer cells and ECM where neither are present. This is backed up by in vitro experiments and clinical observations. Secondly, they identify the value of the degradation rate of ECM by excess H^+

ions ($\delta_v = 1$) at which there is a transformation of the cancer cells from non-invasive tumours ($\delta_v < 1$) into invasive tumours ($\delta_v > 1$).

We make the observation that in the case where an interstitial gap is found to exist, haptotaxis cannot, by definition, be a force that causes cancer cells to migrate.

Gatenby and Gawlinski (2003) and Gatenby et al. (2006) then further developed the above model in three ways. First, they changed the volume filling terms of $(1-v)$ and $(1-c)$ to $(1-c-v)$ in the diffusion of cancer cells, production of cancer cells and productions of ECM to incorporate competition for space between the two populations. Secondly, they modified the H^+ ion concentration removal by considering it to be proportional to the difference between H^+ ion concentration in the considered domain and that in serum. Finally, they changed the way in which the excess H^+ ions degrade the ECM to be the function:

$$\delta_v(1 - exp(-(\frac{H - H_v^{\text{opt}}}{2H_v^{\text{width}}})^2)), \tag{3.8}$$

and introduced a term to model the death of cancer cells from acidity of:

$$\delta_c(1 - exp(-(\frac{H - H_c^{opt}}{2H_c^{width}})^2)), \tag{3.9}$$

where δ_c, δ_v are the death and degradation rates, $H_c^{\text{opt}}, H_v^{\text{opt}}$ are defined to be the H^+ concentration at an optimal level of pH and $H_c^{\text{width}}, H_v^{\text{width}}$ represent the half-widths of the inverted Gaussian functions (the distance from the centre of the distribution to the inflection point).

Further mathematical models of acid-mediated invasion have been investigated by Webb et al. (1999) and Smallbone et al. (2005).

Invasion mediated by matrix degrading proteins whereby the matrix degrading proteins degrade the ECM resulting in cancer cells moving in response to the

resultant ECM gradients has given rise to many mathematical works, with the framework for these models initially laid out in Perumpanani et al. (1996). Haptotaxis is the process by which a cell moves as a result of a physical gradient through adhesion. It was stated in the form that is considered today by Carter (1967) who found that cellulose acetate did not offer adhesion sites for cells to adhere to and as such cells would not move across the surface unless the cellulose acetate was first coated with a layer of the adhesion site-offering palladium upon which cells would move in response to the gradient of the palladium.

Hilltopping is another form of haptotaxis and is the act of the male of a species locating to the highest area while demonstrating territorial behaviour to attract a mate which results in there being a high proportion of males at the hill top. This behaviour is common in low density species of insects and lepidoptera (Scott, 1968). Individual cancerous cells migrate along stromal collagen fibres (Wang et al., 2002) which when examined at the tissue scale would show cancer cells moving from regions of lower collagen fibre density to that of higher collagen density.

Haptotaxis of cancer cells in response to ECM gradients during cancer invasion was first modelled mathematically by Perumpanani et al. (1996) and can be seen to compare with the P-K-S equations outlined above. Their model considered...

and can be presented in the following form:

$$\begin{aligned}
\frac{\partial c(\mathbf{X},t)}{\partial t} &= \nabla \cdot (\theta(v)(\Gamma_c(c,n_1,n_2)\nabla c - c\chi(v)\nabla v - c\Psi(s)\nabla s)) \\
&\quad + c f_2(c,n_1,n_2), && (3.10)\\
\frac{\partial v(\mathbf{X},t)}{\partial t} &= \nabla \cdot K(v\theta(v)(\Gamma_{n_1}(\nabla c + \nabla n_2) + \Gamma_c \nabla c - c\chi(v)\nabla v - c\Psi(s)\nabla s)) \\
&\quad - \delta(v,m), && (3.11)\\
\frac{\partial n_1(\mathbf{X},t)}{\partial t} &= \nabla \cdot (\theta(v)(\Gamma_{n_1}(c,n_1,n_2)\nabla c)) + n_1 f_1(c,n_1,n_2), && (3.12)\\
\frac{\partial n_2(\mathbf{X},t)}{\partial t} &= \nabla \cdot (\theta(v)(\Gamma_{n_1}(c,n_1,n_2)\nabla n_2)) + n_2 f_2(c,n_1,n_2), && (3.13)\\
\frac{\partial m(\mathbf{X},t)}{\partial t} &= \nabla \cdot (D_m \nabla m) + \alpha_m(c,v) - \beta_m c, v, m, && (3.14)\\
\frac{\partial s(\mathbf{X},t)}{\partial t} &= \nabla \cdot (D_s \nabla s) + \alpha_s(v,m), && (3.15)
\end{aligned}$$

where, to consider the effects of the ECM density either blocking or retarding cellular motion,

$$\theta(v) = \begin{cases} k_{26}, & \text{if } 0 < v < k_{27}, \\ \dfrac{k_{28} - v}{k_{28} - k_{27}}, & \text{if } k_{27} < v < k_{28}, \\ 0, & \text{if } k_{28} < v. \end{cases} \qquad (3.16)$$

Cells exhibit logistic growth, i.e.,

$$f_1 = k_1(k_2 - n_1 - n_2 - c), \qquad (3.17)$$

$$f_2 = k_4(k_5 - n_1 - n_2 - c). \qquad (3.18)$$

To represent adhesion in the cellular diffusion terms,

$$\Gamma_n = k_3 \frac{k_{18}}{k_{19} + k_{25}(k_{25}n_1 + k_{25}n_2 + k_{20}c)}, \qquad (3.19)$$

$$\Gamma_c = k_6 \frac{k_{18}}{k_{19} + k_{20}(k_{25}n_1 + k_{25}n_2 + k_{20}c)}. \qquad (3.20)$$

While the haptotaxis and chemotaxis terms were considered to be constants of

$\chi(v) = k_{17}$ and $\psi(s) = k_{16}$ and the forced movement of ECM components is considered proportional to the flux of the cellular motions.

The production of proteolysed ECM is considered as proportional to the degradation of ECM, $\alpha_s(v, m) \propto \delta(v, m)$. Matrix degrading proteins are considered to only be produced at the cancer-ECM interface with the function $\alpha_m(c, v) = k_1 cv$ while the inhibition and natural decay of these proteins is represented by the function $\beta_m(c, v, m) = -k_{12}m - k_{13}mc - k_{14}mv$.

The number of mathematical models that have similar frameworks to Perumpanani et al. (1996), where the underlying solutions can have travelling wave or travelling wave-like solutions, is expansive where a partial listing of these models includes the study of vasculature-mediated taxis movement of cancer cells in Orme and Chaplain (1996), cancer cell flux as a form of taxis towards degraded ECM components, which opposes cancer cell invasion in Perumpanani et al. (1998), cancer cell flux as taxis up an ECM gradient supporting cancer cell invasion in Perumpanani et al. (1999) and Anderson et al. (2000), where the latter is additionally discretised to form a discrete model of cancer cell invasion, the investigation of travelling waves of shock-like appearance in a model with minimal cellular diffusion and dominated by haptotaxis in Marchant et al. (2001), the introduction of the uPa system with tactic-driven instabilities giving rise to highly dynamic, spatially heterogeneous solutions in Chaplain and Lolas (2005) and Chaplain and Lolas (2006), non-local adhesion in the haptotactic flux of cancer cells used to represent cell-cell and cell-ECM adhesion in Gerisch and Chaplain (2008) and Painter et al. (2010), further expansion of the uPA system in Andasari et al. (2011), the role of MT1-MMP and its impact on MMP-2 activation and both restructuring and degradation of the ECM in Deakin and Chaplain (2013), the coupling of MMP reactions at the invasive front with tissue-scale dynamics of cancer cell and ECM densities in a multi-scale, moving boundary model in Trucu

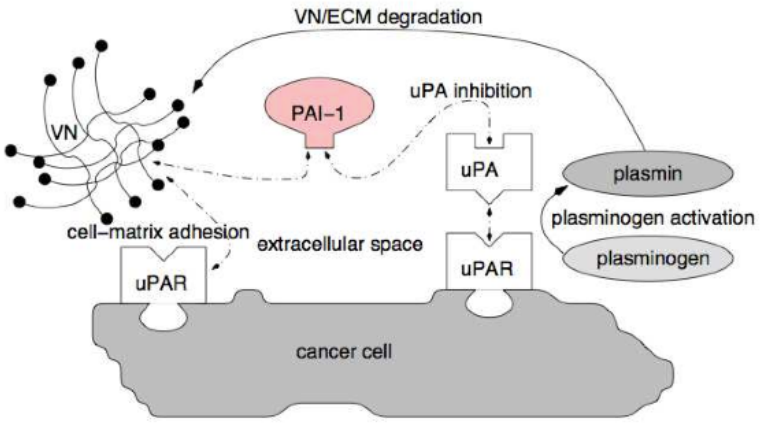

Figure 3.1: *The urokinase plasminogen activation system. ©Springer, reproduced with permission from Andasari et al. (2011).*

et al. (2013).

While the presented form of taxis is frequently used to model cancer cell invasion, Mallet and Pettet (2006) examine an integrin-mediated haptotaxis where they consider the matrix-mediated haptotaxis to be a subset of their model. Additionally, non-local models of cellular adhesion exist and use a system of integro-PDE equations, as will be discussed later.

Invasion mediated by the uPA system can be considered as one possible subset of the above model where the matrix degrading protein is plasmin and its associated activation system, which is presented in Figure 3.1. Chaplain and Lolas (2005) pioneered the following mathematical model of cancer cell invasion when mediated by the urokinase plasminogen activator system by explicitly modelling the proteins uPA (variable u), PAI-1 (T) and plasmin (m), which can be written in the following form:

$$\frac{\partial c}{\partial t} = \nabla \cdot (D_c \nabla c - \xi c \nabla u - \zeta c \nabla T - \chi c \nabla v) + \mu_c c(1-c) + \phi_{13} cu, \quad (3.21)$$

$$\frac{\partial v}{\partial t} = -\delta v m + \mu_v (1-v) + \phi_{21} uT - \phi_{22} Tv, \quad (3.22)$$

$$\frac{\partial u}{\partial t} = \nabla \cdot (D_u \nabla u) - \phi_{31} uT - \phi_{33} cu + \alpha_u c, \quad (3.23)$$

$$\frac{\partial T}{\partial t} = \nabla \cdot (D_T \nabla T) + \alpha_T m - \phi_{41} uT - \phi_{42} Tv, \quad (3.24)$$

$$\frac{\partial m}{\partial t} = \nabla \cdot (D_m \nabla m) - \phi_{51} uT + \phi_{52} Tv + \phi_{53} cu, \quad (3.25)$$

The proposed model was then modified by the inclusion of $\phi_{14} Tv - \omega_1 m$ in the cancer cell source terms to consider an indirect proliferation of cancer cells in response to an eventual activation of cancer cell-bound uPA by ECM-bound PAI-1 as well as apoptosis in response to the overproduction of plasmin.

Models where chemotaxis influences the invasive profile of cancer by destabilising the steady state solution are presented in Chaplain and Lolas (2005), Chaplain and Lolas (2006) and Andasari et al. (2011), where cancer cells produce uPA and can be bound to these molecules and causes a taxis-driven instability while the haptotaxis reacting towards ECM gradients as a pro-invasive factor and it is the balance of pro- and anti- invasive haptotaxis and chemotaxis that causes the distinctive dynamics in these works of highly heterogeneous spatial-temporal dynamics as evidenced by the dispersion relation plots presented therein.

Invasion mediated by non-local effects is studied in multiple models that result from the novel method developed in Armstrong et al. (2006) where cellular adhesion is considered in a continuum model of two interacting populations in 2 spatial dimensions where the adhesion is considered to be non-local.

$$\frac{\partial c}{\partial t} = \nabla \cdot (D_c \nabla c - cK_c(c,v)), \tag{3.26}$$

$$\frac{\partial v}{\partial t} = \nabla \cdot (D_v \nabla c - vK_v(c,v)), \tag{3.27}$$

where the non-local advection terms, K_c, K_v, named adhesion velocity, are (in 2D space):

$$\begin{aligned} K_c(c,v) = & \int_0^1 \int_0^{2\pi} r\eta[S_c g_{cc}(c(\underline{x}+r\underline{\eta}), v(\underline{x}))\Omega_{cc}(r) \\ & + C g_{cv}(c(\underline{x}+r\underline{\eta}), v(\underline{x}+r\underline{\eta}))\Omega_{cv}(r)]d\theta dr, \end{aligned} \tag{3.28}$$

$$\begin{aligned} K_c(c,v) = & \int_0^1 \int_0^{2\pi} r\eta[S_v g_{vv}(c(\underline{x}+r\underline{\eta}), v(\underline{x}))\Omega_{vv}(r) \\ & + C g_{cv}(c(\underline{x}+r\underline{\eta}), v(\underline{x}+r\underline{\eta}))\Omega_{cv}(r)]d\theta dr, \end{aligned} \tag{3.29}$$

which allows for the consideration of the dependence on the strength of the adhesive binding, Ω, with consideration to the radial distance (sensing radius), S, of both self adhesion and cross species adhesion. η represents the unit outer normal, which depends on the angle θ, where $\eta(\theta) = (cos\theta, sin\theta)^T$ while g represents the adhesive strength functions, outlined as follows:

$$g_{cc}(c,v) = g_{cv}(c,v) = \begin{cases} c(1-c-v), & \text{if } c+v<1, \\ 0, & \text{otherwise.} \end{cases} \tag{3.30}$$

Armstrong et al. (2006) consider $\Omega_{cc} = \Omega_{cv} = \Omega_{vv} = 1$ for simplicity, whereas Gerisch and Chaplain (2008) develop upon this formulation when considering different formulations for this strength of the adhesive binding in a continuum based cancer cell invasion of form similar to Anderson et al. (2000). Additionally, they modify the adhesive velocity equation so that the integration is to R instead of 1 with the result being divided by R, i.e., previously, Armstrong et al. (2006)

had $K_c(c,v) = \int_0^1 f(c,v)\mathrm{d}r$ whereas Gerisch and Chaplain (2008) have $K_c(c,v) = \frac{1}{R}\int_0^R f(c,v)\mathrm{d}r$.

$$\frac{\partial c}{\partial t} = \nabla \cdot (D_c \nabla c - cK_c) + \mu_c c(1-c-v), \tag{3.31}$$

$$\frac{\partial v}{\partial t} = \delta v m + \mu_v (1-c-v), \tag{3.32}$$

$$\frac{\partial m}{\partial t} = \nabla \cdot (D_m \nabla m) + \alpha c - \beta m, \tag{3.33}$$

where the function f in the non-local adhesion term K_c remains as defined above. Gerisch and Chaplain (2008) note that the integral over the sensing radius should have a value of 1 in order to not alter the magnitude of the velocity due to adhesion. They propose two forms of the radial dependency function in 2D:

$$\Omega_1(r) = \frac{1}{\pi R^2}, \tag{3.34}$$

$$\Omega_2(r) = \frac{3}{\pi R^2}(1 - \frac{r}{R}), \tag{3.35}$$

where the first proposed form results in an integrand independent of r while the second form results in linear decay to the point R where $\Omega_2(R) = 0$. By incorporating a linear decay into the strength of adhesive binding, it allows for the consideration of adhesion sites further away from the initial location to have less of an effect than adhesion sites closer to the initial location. Armstrong et al. (2006) show that for $R = 0$ there remains the possibility of finite time blow-up solutions whereas for small R, $R > 0$, there is an avoidance of finite time blow-up solutions while there is still the allowance of aggregation dynamics.

Further results of biological interest are obtained in Gerisch and Chaplain (2008) where they find that local overcrowding ($c + v \geq 1$) is permitted in cases where the total amount of c and v within a region of radius R from the location X is bound such that $\int_{X-R}^{X+R} c + v \leq R$. They identify the value of cell-cell adhesion of $S_{cc} = 0.5$ when considered with their parameter set blocks all cancer cell invasion

to the point of creating a spatially heterogeneous steady state solution as the cells are bound strongly together in a small region near the origin. However, when they increase the cell-ECM adhesion, S_{cv}, they find that invasion is permissible and that more cancer cells break off from the original mass of cells with increasing cell-ECM adhesion. Andasari (2011) incorporates the non-local advection terms presented in Gerisch and Chaplain (2008) into the model developed in Chaplain and Lolas (2005).

Mathematical models of MMP-2 activation exist in the literature where we here remind the reader that we will develop upon these directly in the presented work within the context of cancer cell invasion. Karagiannis and Popel (2004) were the first to propose a mathematical model of the activation system of MMP-2 in a model of collagen type-I degradation with a system of ODEs to represent bulk collagenolysis in a well-mixed state. We note that while they provide a "sample equation" in the supplementary material of their work, they do not provide the equations for all proteins or protein complexes. However, the ODEs can be reconstructed from the reactions listed where we present these in Figure 3.2.

Their model combines the ectodomain shedding of MT1-MMP, collagen degradation by both MMP-2 and MT1-MMP, MMP-2 inhibition by TIMP2 as well as the activation of MMP-2. Here, we present a reconstruction of the equations likely underpinning their results, broken down into the different processes of ectodomain shedding, degradation of collagen, MMP-2 inhibition by TIMP2 and the activation of MMP-2.

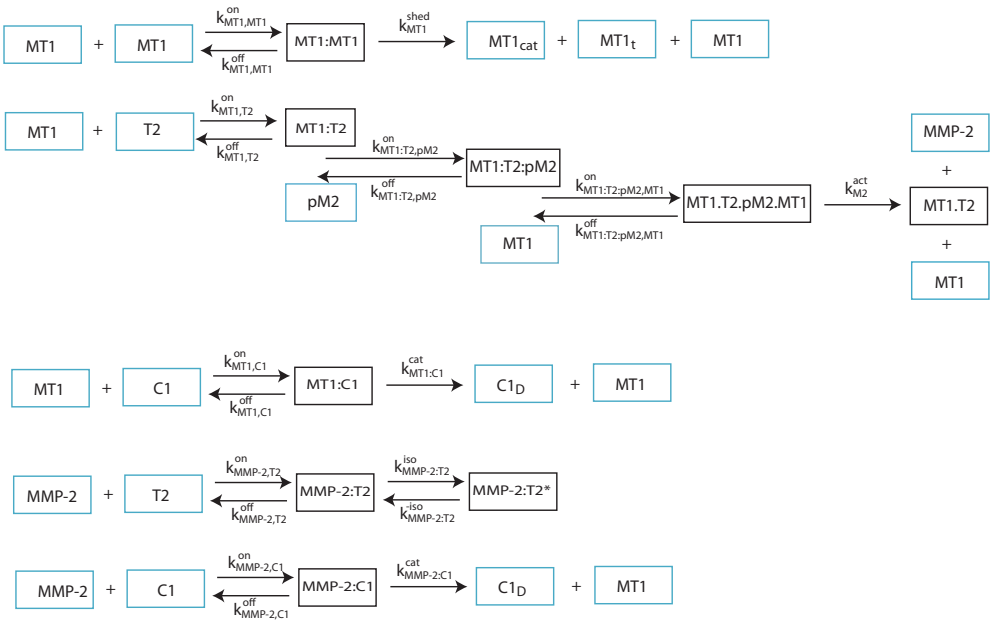

Figure 3.2: *The MMP-2 activation system in combination with collagen type-I degradation and ectodomain shedding of MT1-MMP (Karagiannis and Popel, 2004). MT1 represents MT1-MMP, $MT1_{cat}$ represents the catalytic domain of MT1-MMP when it has been isolated from the rest of the molecule, $MT!_t$ represents the truncated part of the MT1-MMP that is left when the catalytic domain has been severed from the molecule, T2 represents TIMP2, pM2 represents proMMP-2, C1 represents collagen type-I and $C1_D$ represents denatured collagen type-I.*

Ectodomain shedding is modelled by:

$$\begin{aligned}
\frac{d[MT1]}{dt} = \quad & 2k^{off}_{MT1,MT1}[MT1 \cdot MT1] - 2k^{on}_{MT1,MT1}[MT1]^2 \\
& + k^{shed}_{MT1}[MT1 \cdot MT1] = ES_{MT1}, && (3.36)\\
\frac{d[MT1 \cdot MT1]}{dt} = \quad & -k^{off}_{MT1,MT1}[MT1 \cdot MT1] + k^{on}_{MT1,MT1}[MT1]^2 \\
& - k^{shed}_{MT1}[MT1 \cdot MT1] = ES_{MT1 \cdot MT1}, && (3.37)\\
\frac{d[MT1_{cat}]}{dt} = \quad & + k^{shed}_{MT1}[MT1 \cdot MT1] = ES_{MT1_{cat}}, && (3.38)\\
\frac{d[MT1_t]}{dt} = \quad & + k^{shed}_{MT1}[MT1 \cdot MT1] = ES_{MT1_t}. && (3.39)
\end{aligned}$$

Degradation of collagen type-I by both MMP-2 and MT1-MMP is modelled by:

$$\begin{aligned}
\frac{d[MT1]}{dt} = \quad & k^{off}_{MT1,CI}[MT1 \cdot CI] - k^{on}_{MT1,CI}[MT1][CI] \\
& + k^{cat}_{MT1,CI}[MT1 \cdot CI] = DC_{MT1}, && (3.40)\\
\frac{d[CI]}{dt} = \quad & k^{off}_{MT1,CI}[MT1 \cdot CI] - k^{on}_{MT1,CI}[MT1][CI] = DC_{CI}, && (3.41)\\
\frac{d[MT1 \cdot CI]}{dt} = \quad & -k^{off}_{MT1,CI}[MT1 \cdot CI] + k^{on}_{MT1,CI}[MT1][CI] \\
& - k^{cat}_{MT1,CI}[MT1 \cdot CI] = DC_{MT1 \cdot CI}, && (3.42)\\
\frac{d[CI_D]}{dt} = \quad & + k^{cat}_{MT1,CI}[MT1 \cdot CI] + k^{cat}_{M2,CI}[M2 \cdot CI] = DC_{CI_D}, && (3.43)\\
\frac{d[M2]}{dt} = \quad & k^{off}_{M2,CI}[M2 \cdot CI] - k^{on}_{M2,CI}[M2][CI] + k^{cat}_{M2,CI}[M2 \cdot CI] \\
& = DC_{M2}, && (3.44)\\
\frac{d[M2 \cdot CI]}{dt} = \quad & -k^{off}_{M2,CI}[M2 \cdot CI] + k^{on}_{M2,CI}[M2][CI] - k^{cat}_{M2,CI}[M2 \cdot CI] \\
& = DC_{M2 \cdot CI}. && (3.45)
\end{aligned}$$

MMP-2 inhibition by TIMP2 is modelled by:

$$\frac{d[M2]}{dt} = +k^{off}_{M2,T2}[M2\cdot T2] - k^{on}_{M2,T2}[M2\cdot T2] = MI_{M2} \tag{3.46}$$

$$\frac{d[T2]}{dt} = +k^{off}_{M2,T2}[M2\cdot T2] - k^{on}_{M2,T2}[M2\cdot T2] = MI_{T2} \tag{3.47}$$

$$\begin{aligned}\frac{d[M2\cdot T2]}{dt} = {} & k^{on}_{M2,T2}[M2\cdot T2] - k^{off}_{M2,T2}[M2\cdot T2] + k^{-inh}_{M2,T2}[M2\cdot T2^*] \\ & -k^{inh}_{M2,T2}[M2\cdot T2^*] = MI_{M2\cdot T2}\end{aligned} \tag{3.48}$$

$$\frac{d[M2\cdot T2^*]}{\partial t} = +k^{inh}_{M2,T2}[M2\cdot T2^*] - k^{-inh}_{M2,T2}[M2\cdot T2^*] = MI_{M2\cdot T2^*} \tag{3.49}$$

Activation of MMP-2 is modelled by:

$$\begin{aligned}\frac{d[MT1]}{dt} = {} & k^{off}_{MT1,T2}[MT1\cdot T2] - k^{on}_{MT1,T2}[MT1][T2] \\ & -k^{on}_{MT1,T2,M2p,MT1}[MT1\cdot T2\cdot M2p][MT1] \\ & k^{act}_{M2}[MT1\cdot T2\cdot M2p\cdot MT1] = AM_{MT1},\end{aligned} \tag{3.50}$$

$$\frac{d[T2]}{dt} = k^{off}_{MT1,T2}[MT1\cdot T2] - k^{on}_{MT1,T2}[MT1][T2] = AM_{T2}, \tag{3.51}$$

$$\begin{aligned}\frac{d[MT1\cdot T2]}{dt} = {} & k^{on}_{MT1,T2}[MT1][T2] - k^{off}_{MT1,T2}[MT1\cdot T2] \\ & +k^{off}_{MT1,T2,M2p}[MT1\cdot T2\cdot M2p] \\ & -k^{on}_{MT1,T2,M2p}[MT1\cdot T2][M2p]AM_{MT1\cdot T2},\end{aligned} \tag{3.52}$$

$$\begin{aligned}\frac{d[M2p]}{dt} = {} & k^{off}_{MT1,T2,M2p}[MT1\cdot T2\cdot M2p] \\ & -k^{on}_{MT1,T2,M2p}[MT1\cdot T2][M2p]AM_{M2p},\end{aligned} \tag{3.53}$$

$$\begin{aligned}\frac{d[MT1\cdot T2\cdot M2p]}{dt} = {} & k^{on}_{MT1,T2,M2p}[MT1\cdot T2][M2p] - k^{off}_{MT1,T2,M2p}[MT1\cdot T2\cdot M2p] \\ & +k^{off}_{MT1,T2,M2p,MT1}[MT1\cdot T2\cdot M2p\cdot MT1] \\ & -k^{on}_{MT1,T2,M2p,MT1}[MT1\cdot T2\cdot M2p][MT1] \\ & = AM_{MT1\cdot T2\cdot M2p},\end{aligned} \tag{3.54}$$

$$\begin{aligned}\frac{d[MT1\cdot T2\cdot M2p\cdot MT1]}{dt} = {} & k^{on}_{MT1,T2,M2p,MT1}[MT1\cdot T2\cdot M2p][MT1] \\ & -k^{off}_{MT1,T2,M2p,MT1}[MT1\cdot T2\cdot M2p\cdot MT1] \\ & -k^{act}_{M2}[MT1\cdot T2\cdot M2p\cdot MT1] = AM_{MT1\cdot T2\cdot M2p\cdot MT1},\end{aligned} \tag{3.55}$$

$$\frac{d[MT1\cdot T2^*]}{dt} = k^{act}_{M2}[MT1\cdot T2\cdot M2p\cdot MT1] = AM_{MT1\cdot T2^*}, \tag{3.56}$$

$$\frac{d[M2]}{dt} = k^{act}_{M2}[MT1\cdot T2\cdot M2p\cdot MT1] = AM_{M2}. \tag{3.57}$$

Which, when combined into one system of ODEs can be written as:

$$\frac{dY_i}{dt} = ES_{Y_i} + DC_{Y_i} + MI_{Y_i} + AM_{Y_i} \tag{3.58}$$

for i =1 to 17 with $\mathbf{Y} = (MT1, MT1 \cdot MT1, MT1_{cat}, MT1_t, CI, MT1 \cdot CI, CI_D, M2, M2 \cdot CI, T2, M2 \cdot T2, M2 \cdot T2^*, MT1 \cdot T2, M2p, MT1 \cdot T2 \cdot M2p, MT1 \cdot T2 \cdot M2p \cdot MT1, MT1 \cdot T2^*)^T$, where undefined values of ES_j, DC_j, MI_j and AM_j are set to be equal to zero for j=1 to 17.

Key results of the model are providing characterisation of the MMP-2 activation system while finding that TIMP2 levels which are either too high or too low inhibit the activation process. By studying the ectodomain shedding of MT1-MMP in conjunction with the activation process of MMP-2, they determine that the more MT1-MMP molecules that have undergone ectodomain shedding, the fewer free MT1-MMP molecules that are available to take part in the activation of MMP-2. Additionally, they found that the level of TIMP2 modified the amount of ectodomain shedding where the complex of TIMP2·MT1-MMP was protected from the shedding process. As they are the first to mathematically model this system, with the addition of collagen degradation by both MT1-MMP and MMP-2, they provide a base for future development on quantitative approaches in identifying the ranges at which collagen is degraded most extensively by the combination of activated MMP-2 and MT1-MMP.

They later expanded upon the outlook of their ODE formulation of the processes outlined above to consider the impacts on angiogenisis in Karagiannis and Popel (2006) by examining collagen degradation at the tip endothelial cell of a sprouting vessel. Specifically, they considered cell migration to be a function of proteolysis in the vicinity of the cell and included production of MT1-MMP, proMMP-2 and TIMP2 by the tip cell of the sprouting vessel and changed the system of ODEs into one of PDEs where MMP-2, TIMP2·MMP-2 and proMMP-2 are all freely

diffusible. By doing so they found estimates for cell velocities through a variety of collagen compositions. Additionally, they found that at higher levels of collagen density, proteolysis was largely performed by MT1-MMP and limited to the invading edge of the cell whereas at lower collagen densities there was a concurrent degradation of collagen by MT1-MMP and MMP-2 and this degradation was less localised. Donzé et al. (2011) performed global robustness and sensitivity of the model and explored the possibility of oscillatory dynamics in the system.

A second notable attempt to characterise the activation of MMP-2 along with secondary issues is presented in Hoshino et al. (2012) where they considered an extensive set of potential complexes that may eventually lead to forms that are relevant to the activation of MMP-2 from proMMP-2 by the process involving TIMP2 and MT1-MMP, outlined in Figure 3.3. They consider two "pools" to represent two regions that consider differing internalisation processes for MT1-MMP of pool X and Y where internalisation is dependent on bafilomycin concentration and surface density, respectively. A-Cell (Ichikawa, 2001) is then used to generate the equations which form the basis of their model, which are provided in the supporting information of their paper, and consists of 39 ODEs. Experimental validation alongside their computational model is used to investigate the significance of turnover of MT1-MMP for proteolysis at an invadopodium.

They find that the rapid turnover of MT1-MMP is responsible for the increased degradation of ECM at invadopodia and found that the blocking of vesicle transport in their model, and in their experiment, blocked ECM degradation.

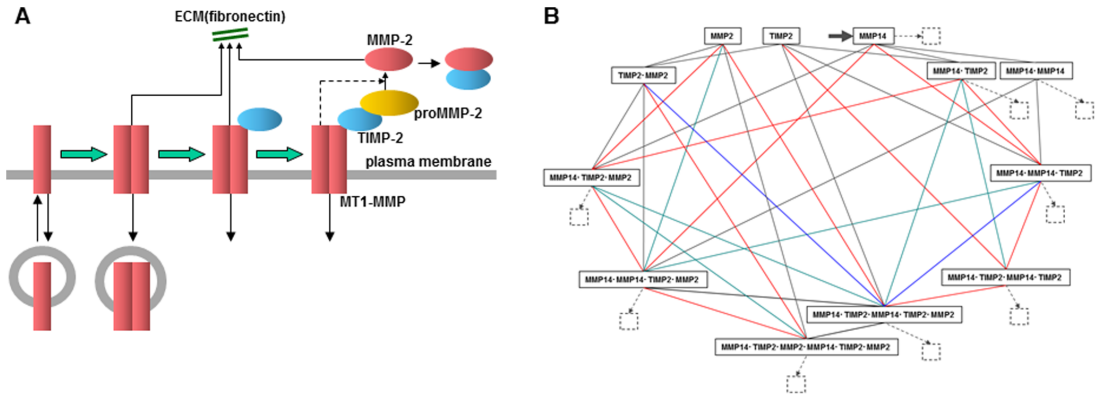

Figure 3.3: *The MMP-2 activation system and related complex formation. The bold arrow indicates insertion of MT1-MMP while the dotted arrow indicates internalisation of MT1-MMP. Reproduced from Hoshino et al. (2012).*

3.2 Discrete Modelling

Discrete models of individual cancer cell invasion focus on the individual cancer cells through the lattice-based cellular automata (CA) models (extensions include the cellular Potts models (CPMs) and lattice-gas cellular automata (LGCA) models) or through lattice-free, force-based models.

In the context of cancer cell invasion, CAMs are discrete lattices in 2 or 3 spatial dimensions where each lattice point can be considered to be in two states ("on" or "off") to represent there either being a subcellular element of a cancer cell/an entire cancer cell in that location or an absence of cancer in that location. A 2D spatial lattice where each point represents an area where an individual cancer cell can exist allows for cancer cells to move with either 4 or 8 degrees of freedom. The initial state of the model evolves trough predefined rules where each lattice point considers several factors (the neighbouring lattice points on/off status, local oxygen distribution, intracellular signalling, etc.) to determine if the cancer cell at that location will move to a neighbouring lattice point, remain unchanged

or die. By the inclusion of intracellular processes and/or the impact of oxygen concentration, determined from a PDE covering the entire lattice, these models are frequently multiscale in nature.

Examples of models where each grid point describes an individual cancer cell can be found in the works of Anderson and collaborators (Anderson et al., 2000; Anderson, 2005; Anderson et al., 2006) where they discretise a PDE governing cancer cells to determine the rules that govern the movement, proliferation and apoptosis of cancer cells in invasion. The individual cancer cells respond to a system of PDEs governing the density of the extracellular matrix and some matrix degrading proteins. Their framework is capable of considering cancer cells having different phenotypes where each lattice point was considered to have more data than the "on" and "off" states of a typical CAM. As such, it has been expanded to look at evolutionary dynamics of the cancer cells and how the microenvironment affects the evolutionary process in the works of Anderson and Gerlee (Gerlee and Anderson, 2007, 2008, 2009*a*,*b*, 2010).

A CA model with a hexagonal lattice was proposed in Aubert et al. (2006) to study the migration of glioma cells where the cells were defined to have an attraction to each other that preferentially biases movement.

In order to maintain the distinctness of each cancer cell, an approach is to use a Potts model where each cell is assigned a unique index, Q, termed the *spin number*. Potts models have cancer cell populations evolving in ways that minimise the effective energy. Cells move by an iterative process of the movement of the boundary elements of the cell. Models that consider a large amount of cancer cells are termed large-Q Potts models. The Potts model considers a single surface energy across multiple cells whereas an extended large-Q Potts model, known as a cellular Potts model (CPM), considers each cell to have an individual

surface energy that allows for the growth and shrinking of cells in response to its neighbouring cells and lattice points. This also allows for the consideration of each cell going through different physical sizes and can be used to prescribe maximum and minimum cell sizes. This allows for more complex morphologies of the cancer cells to be considered along with their respective adhesion properties and other cell-cell dynamics.

Models that focus specifically on cancer cell growth and invasion using a CPM include the works of Stott et al. (1999); Turner and Sherratt (2002); Jiang et al. (2005); Rubenstein and Kaufman (2008); Andasari et al. (2012). We refer the reader to the review papers of Moreira and Deutsch (2002); Hatzikirou et al. (2008); Szabó and Merks (2013) for a review of CPM in cancer cell growth, invasion and evolution.

CPMs have seen a number of developments in the last decade (see the recent review paper of Scianna and Preziosi, 2012), one of which is the introduction of a lattice-gas cellular automaton (LGCA) model. How a LGCA model varies from a CAM/CPM is through the inclusion of cellular velocity where cells are also capable of colliding with one another. Of the LGCA models, Wurzel et al. (2005) consider apoptosis, proliferation and movement of cancer cells in gliomas while Hatzikirou and Deutsch (2008) model the effect of a more general hetereogeneous ECM layout on cancer cell movement in the absence of apoptosis and proliferation. Further LGCA models of cancer invasion include the works of Hatzikirou et al. (2010); Tektonidis et al. (2011); Böttger et al. (2012). Additionally, a hybrid LGCA-CPM has been proposed in Ghaemi and Shahrokhi (2006) to model avascular cancer growth. Another notable modified CPM is that proposed in Li and Lowengrub (2014) where they no longer consider cell size to depend on cell velocity.

Not all individual models of cancer cell invasion consider cancer cells to be fixed to lattice points. These models are termed *off-lattice* and can be force-based, such as cell-centred models (Drasdo and Höhme, 2003; Drasdo and Hoehme, 2005), in which there is a proliferating rim and cancer cells either move there centre point or reorientate to minimise the energies resulting from adhesion to local neighbouring cells and the pressure caused by the mitosis of neighbouring cells. They used their model to investigate the transition of exponential growth of cancer cells in a multicellular spheroid to a sub-exponential growth as the result of the depletion of a nutrient. Ramis-Conde et al. (2008) developed a lattice-free model of discrete cancer cells to study cellular adhesion through the interaction of the intracellular proteins of E-cadherin and β-catenin. It is the distance between the centre of each cell that determines the size of the contact area between two cells. This work was then developed in Ramis-Conde et al. (2009) to study the role of these proteins in the intravasation of cancer cells in one of the few mathematical works focussing on metastasis. Further, Kim et al. (2007) developed a hybrid model of a tumour spheroid where the core of necrotic cells and quiescent cells are governed by PDE dynamics whereas the rim of the tumour is modelled discretely to allow for cellular adhesion to be incorporated at the cellular level.

An alternative approach to modelling off-lattice dynamics is to use the immersed boundary method. Here, the ECM is considered as a viscous incompressible fluid in which cancer cells are immersed, has been implemented by Rejniak, Dillon and coauthors to study tumour growth and invasion (Rejniak, 2005, 2007; Rejniak and Dillon, 2007; Dillon et al., 2008). Cancer cells are considered to be viscous fluids with elastic links on the cell membrane. Fluid can be gained by the cell, initiating cell growth, which causes the shape of the cell to change. The process of the splitting of the cell into two daughter cells is determined by elastic forces where each cell is defined as having elastic links, termed the *contractile force link*, linking

each point of the cell membrane with a corresponding point on the opposite side of the cell. The cell cycle is modelled independently in each cell. Cells are therefore capable of having individually defined sizes as well as the biomechanical properties relating to cell growth, division, senescence, adhesion and the receiving of signals from the ECM. The ECM is modelled by the inclusion of elastic links between cells, which model cellular adhesion. Further, Rejniak et al. (2010); Rejniak (2012) have used the same technique to study the development of preinvasive, intraductal tumours and their development into invasive tumours.

The level-set method has been used to incorporate complex morphologies in moving boundary models of cancer cell invasion (Macklin and Lowengrub, 2006, 2008). These nonlinear works can be coupled with angiogenesis (Zheng et al., 2005), including the blood flow in these networks (Macklin et al., 2009) and emphasise the significance of the heterogeneity of the tissue in tumour morphologies (Macklin and Lowengrub, 2007).

3.3 Multiphase Modelling

Multiphase models attempt to deal with the mechanical forces and stresses that tissues and cancer cells are exposed to through the use of the theory of mixtures. It is in invoking the theory of mixtures that these models differ most significantly from the previous methods of modelling cancer cell growth and invasion as where previously, a spatial domain is said to be made up of only one element, the theory of mixtures defines each location to be made up of fractions of the considered components. Multiphase models of cancer invasion therefore consider tumours to be made up of a multiphase mixture of cancer cells, ECM and extracellular fluid. Tumours are defined to be moving within a porous domain made up of the ECM,

which is wetted by extracellular fluid. For a greater understanding of multiphase models, see Preziosi and Tosin (2009) and the references therein.

3.4 Modelling Techniques of the Presented Work

Having acknowledged that there are a large number of papers of varying approaches/types on the topic of cancer invasion, we will present 3 research chapters in this thesis where the first two will feature P.D.E. models that have been formulated and analysed as far as possible (linear stability analysis Keener and Sneyd, 1998; Murray, 2002; Britton, 2012) with appropriate computational simulations. The third of the research chapters will focus on a non-spatial, stochastic approach to modelling MMP-2 activation mediated by MT1-MMP and TIMP2 at invadopodia.

Chapter 4

A PDE Model of Cancer Invasion Focussing on the Role of MMPs

4.1 Introduction

One of the hallmarks of cancer growth and metastatic spread is the process of local invasion of the surrounding tissue. Cancer cells achieve protease-dependent invasion by the secretion of enzymes involved in proteolysis. These overly-expressed proteolytic enzymes then proceed to degrade the host tissue allowing the cancer cells to disseminate throughout the microenvironment by active migration and interaction with components of the extracellular matrix (ECM) such as collagen.

In this chapter we develop a mathematical model of cancer invasion using a system of partial differential equations to consider the role matrix metalloproteinases (MMPs) play in local invasion as the result of an existing, minimally invasive tumour. Specifically our model will focus on two distinct types of MMP i.e.

soluble, diffusible MMPs (e.g. MMP-2) and membrane-bound MMPs (e.g. MT1-MMP), and the roles each of these has when the cancer cells move into areas of differing extracellular environments.

Mathematical modelling has been used to investigate a number of topics in cancer progression and invasion, including models taking into account: oxygen/nutrient driven dynamics, the immune response, the acidity of the environment, force-based pressure, the microenvironment in general and protease-dependent invasion. These effects can be modelled using a variety of techniques, including partial differential equations for densities of cells, individual-based models including cellular automaton models and multi-scale models as outlined in the review papers of Araujo and McElwain (2004), Rejniak and McCawley (2010) and Lowengrub et al. (2010) and the references therein. Alternatively, the variables involved in these modelling works can be modelled through the theory of mixtures, as done in the multiphase works outlined in the review paper of (Preziosi and Tosin, 2009) and the references therein.

4.2 Model Development

MMPs fall into two broad categories: soluble and bound. Soluble MMPs, such as, MMP-2, MMP-9, etc. have some comparable dynamics to the generic secretory matrix degrading enzymes investigated in previous mathematical models (Perumpanani et al., 1996; Anderson et al., 2000; Anderson, 2005; Gerisch and Chaplain, 2008) such as the ability to freely diffuse and degrade the ECM it comes in contact with. As such, these previous models may be suitable for the consideration of these MMPs. We note, however, that there are both additional processes in the activation of these enzymes that are critical to invasion that have

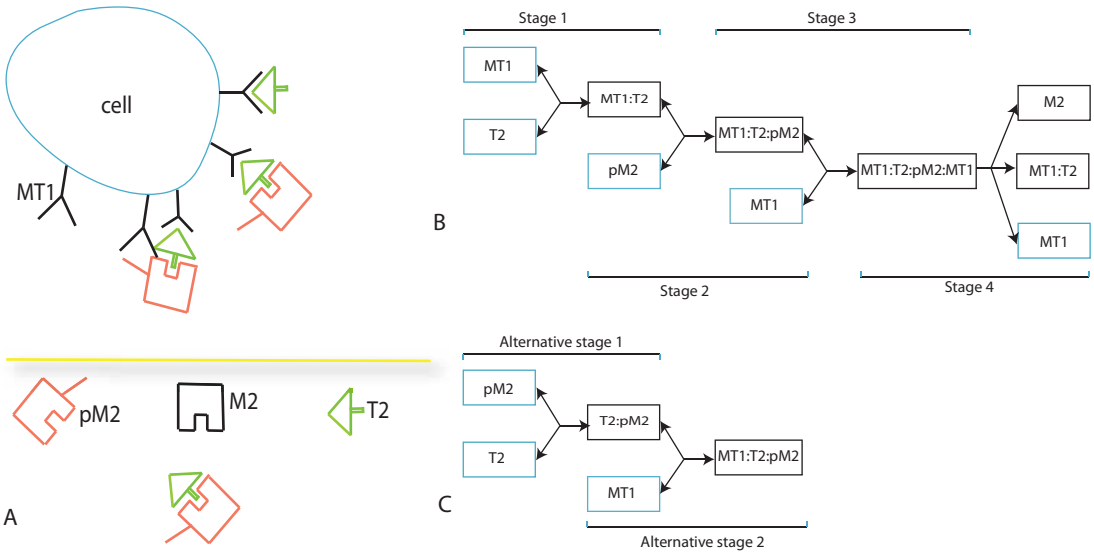

Figure 4.1: *The full schematic diagram of MMP-2 activation. Plot A indicates whether a protein or complex is bound to the membrane of the cell or capable freely diffusing throughout the domain. Plot B illustrates the first pathway by which proMMP-2 can become activated while plot C illustrates the alternative route by which proMMP-2 can become activated. In all plots, 'MT1' represents MT1-MMP, 'T2' represents TIMP2, pM2 represents proMMP-2 and M2 represents MMP-2, while in plots B and C, a protein/complex is in a blue box if it is directly produced by a cancer cell and black if it is formed from later reactions.*

not been considered, along with the exemption of membrane-bound MMPs, and thus there is still much to be investigated. In this chapter, we develop this style of modelling with partial differential equations when considering how such a model will be formulated for the soluble MMP, MMP-2, the membrane-bound MMP, MT1-MMP, and the activation process of MMP-2 that requires MT1-MMP, as outlined in Figure 4.1.

In our model we denote by $c(\mathbf{x}, t)$ the cancer cell density, $v(\mathbf{x}, t)$ the ECM density, $m_s(\mathbf{x}, t)$ the MMP-2 concentration and by $m_t(\mathbf{x}, t)$ the MT1-MMP concentration. In addition, we let $T(\mathbf{x}, t)$ denote the TIMP2 concentration, $f(\mathbf{x}, t)$ the

concentration of the complex of MT1-MMP:TIMP2 (with an assumed proMMP-2 attached). As we simulate our model in 2 spatial dimensions, we define a vector $\mathbf{u}$ such that:

$$\mathbf{u} \equiv (c(x,y,t), v(x,y,t), m_s(x,y,t), m_t(x,y,t), T(x,y,t), f(x,y,t))^T. \tag{4.1}$$

We develop our model according to the conservation of mass equations, i.e.:

$$\frac{\partial \mathbf{u}}{\partial t} + \nabla \cdot \mathbf{J} = \mathbf{H}, \tag{4.2}$$

with flux and source terms as modelled by $\mathbf{J} = (J_1, ..., J_6)^T$ and $\mathbf{H} = (H_1, ..., H_6)^T$, respectively.

Cancer cell density, c:

The cancer cell density flux, J_1, considers the movement of cancer cells according to cellular diffusion, modelled by $D_c \nabla c$, for some constant D_c, in addition to a haptotactic flux of $c\chi(c,v)\nabla v$, for some haptoptactic sensitivity function $\chi(c,v)$.

The cancer cell density source, H_1, is formed from the production of cancer cells in accordance to the availability of *"free space"* as determined by the densities of the cancer cells and ECM, represented by $F(c,v)$.

As the cancer cells and ECM are in a form of *"competition for space"*, we consider their growth functions, as well as the haptotactic sensitivity function, to be linked. Therefore, we will define the ECM reaction equations before providing the precise forms of the growth functions $F(c,v)$, for the production of cancer cells and $G(c,v)$, for the production of components of the ECM as well as the haptotactic sensitivity function $\chi(c,v)$.

$$\frac{\partial c}{\partial t} = \nabla \cdot (D_c \nabla c - c\chi(c,v)\nabla v) + F(c,v). \tag{4.3}$$

ECM density, v:

The ECM flux, J_2 is zero as the ECM is considered to be normally static in healthy tissues over the scale of cellular invasion where a healthy tissue will have a half-life of decades.

The ECM source, H_2, incorporates matrix degradation (proteolysis) by either MMP-2, m_s, or MT1-MMP, m_t. This results in a loss of ECM density, as modelled by $-\delta_{ms} m_s v$ and $-\delta_{mt} m_t v$, respectively. Further, the ECM is remodelled according to the available space, as determined by the densities of the cancer cell population and the ECM. We identify this remodelling rate as the function G. We can define a constant δ such that $\delta\delta_1 = \delta_{ms}$ and $\delta\delta_2 = \delta_{mt}$, for some constants δ_1 and δ_2.

$$\frac{\partial v}{\partial t} = -\delta v(\delta_1 m_s + \delta_2 m_t) + G(c, v). \tag{4.4}$$

An overview of the forms that the growth functions for cancer cell and ECM densities have taken in the modelling literature is presented in Table 4.1. To justify our choice of functions F and G, we provide a summary of the biological means by which cancer cells and ECM components are produced. A more expansive description of these processes can be found in the biological review presented in Chapter 2 of this work. In essence, cancer cells produce copies of themselves through mitosis and therefore must have zero production rate where $c = 0$ whereas ECM components are produced by fibroblasts and are therefore capable of having a non-zero production rate where $v = 0$.

We incorporate these dynamics into a coupled volume filling, or "competition for space", approach, where we define constants Z, k, l to represent the maximum amount, Z, of k cancer cells and l ECM constituent parts that are able to either fill a region of space or be supported by the region. Further, we note that as we

F(c,v)	**G(c,v)**	**Source**
0	0	Anderson et al. (2000), Anderson (2005).
$-c$	0	Sherratt (1993).
$fc(Z-kc)$	0	Painter et al. (2010), Marchant et al. (2001), Perumpanani et al. (1999).
$Lc(Z-kc)$	0	where L represents the intracellular acidity, Webb et al. (1999).
$c(Z-kc)$	$v(Z-lv)$	Gatenby and Gawlinski (1996), Chaplain and Lolas (2005), Andasari et al. (2011).
$c(Z-kc-lv)$	$v(Z-kc-lv)$	Chaplain and Lolas (2006), Gatenby et al. (2006).
$c(Z-kc-lv)$	$(Z-kc-lv)$	Gerisch and Chaplain (2008), Andasari et al. (2011), Deakin and Chaplain (2013).

Table 4.1: *Existing forms of the functions representing cancer cell growth, $F(c,v)$, and ECM remodelling, $G(c,v)$, are presented in a dimensionalised form where Z represents the maximum amount of either k cancer cells or l ECM components, along with their respective sources.*

consider the proteins and protein complexes to take up a negligible amount of space, the populations of these do not influence the volume filling between the cancer cell and ECM densities. We are therefore able to identify $(Z - kc - lv)$ as an appropriate multiplier to represent such a competition for space with forms of the functions $F(c, v)$ and $G(c, v)$ of:

$$\begin{aligned} F &= \mu_c c(Z - kc - lv), \\ G &= \mu_v(Z - kc - lv), \end{aligned}$$

for some constants μ_c and μ_v. Central in the use of volume filling terms is that there is reduced production as the free space is filled by cancer cells and ECM constituent parts to the point where there is no production where there is no free space. Further, the volume filling terms can act as a correcting term when there is a location with more cancer cells and/or ECM constituent parts than are able to be stably supported.

As such, we can consider there to be volume filling criteria of:

$$\begin{aligned} kc + lv < Z, &\quad \text{for production,} \\ kc + lv = Z, &\quad \text{for stasis,} \\ kc + lv > Z, &\quad \text{for death/degradation,} \end{aligned}$$

with the strict conditions for production or stasis to exist of:

$$\begin{aligned} kc >= 0, \\ lv >= 0, \\ kc <= Z, \\ lv <= Z. \end{aligned}$$

We note that by the definition of the volume filling maximum, a small breach of the maximum amount of cancer cells and/or ECM constituent parts that are at

a spatial location is still biologically relevant as the volume filling terms will act to correct the over subscription of that spatial location beyond that which can be supported. What is at odds with a biological interpretation of the model is when such a correction is outstripped by further cancer cells or ECM constituent parts being moved or produced at the spatial region, as is the case in finite-time blow up solutions where an infinite number of cells would be said to exist within a defined spatial region. Such finite-time blow up solutions can be avoided by considering the above approach to volume filling in the haptotactic sensitivity function, $\chi(c, v)$ (Stevens and Othmer, 1997; Painter and Hillen, 2002; Hillen and Painter, 2009). As such, we choose a haptotactic sensitivity function of $\chi(c, v) = v(Z - kc - lv)$. As the haptotactic flux happens at a rate of $c\chi(c, v)\nabla v$, there is no haptotaxis possible when either there are no cancer cells to move ($c = 0$), no ECM constructs for cancer cells to move through ($v = 0$) or no free space for cancer cells to move into ($Z = kc + lv$).

As the volume filling terms in the production of cancer cells, ECM constituent parts and cancer cell haptotaxis can be trivially seen to not cause an increase in the populations above the critical values of kc=Z, lv=Z, kc+lv=Z in isolation, we consider the cases of production or stasis to be normal, whereas the case of death/degradation as a result of volume filling terms to be abnormal. Once we have established the full model, an examination of what may cause such a breach of the critical values along with the implications on the model will be discussed.

The remaining equations of the model describe the interplay between MMPs in cancer invasion, specifically MT1-MMP activation of MMP-2, the balance between TIMP2 inhibition of both MT1-MMP and MMP-2, and the dual role of TIMP2 as inhibitor of active MMP-2 and being necessary for the activation process of MMP-2. The full process of MMP-2 activation is shown in Figure 4.1. The proteins in a blue box are produced directly by a cancer cell while those in the

black box are only formed through later interactions. Whether a species/complex is free to move, without considering lateral diffusion on a cell and the relative movement of a cell, is also indicated. Proteins of proMMP-2 have their "pro" domain cleaved to form fully active MMP-2 through a process involving both MT1-MMP and (paradoxically) TIMP2. This process is accomplished through two methods, which while differing in their first two stages, share the same third and fourth stage.

For the first method, the first two stages involve the binding of a protein of TIMP2 to the catalytic domain of an MT1-MMP protein. This inhibits the MT1-MMP protein from degrading the surrounding ECM but leaves it otherwise intact on the cell surface. A proMMP-2 protein then binds to this complex to form the trimer MT1-MMP:TIMP2:proMMP-2. Alternatively, the first two stages of the second method features a proMMP-2 protein binding to a TIMP2 protein, a reaction that does not necessarily happen near the membrane of a cancer cell. This complex then binds to a MT1-MMP protein on the surface of the cell to form the trimer MT1-MMP:TIMP2:proMMP2.

The remaining two stages, which are shared between the two methods of MMP-2 activation, are the binding of a free MT1-MMP to this trimer and then the cleavage of the pro domain of the proMMP-2, which results in a complex of MT1-MMP:TIMP2, MT1-MMP and a fully active MMP-2 protein.

As we feel that these dynamics can be sufficiently captured by only two stages, we simplify the full schematic of reactions into the two stages, as laid out in Figure 4.2. This involves making the assumption that every protein of TIMP2 has an attached proMMP-2 protein, reducing stage 1 and stage 2 of Figure 4.1 into one stage. Further, as the dissociation rate of the complex MT1-MMP:TIMP2:proMMP-2:MT1-MMP is much smaller than the rate of the pro domain of the proMMP-2

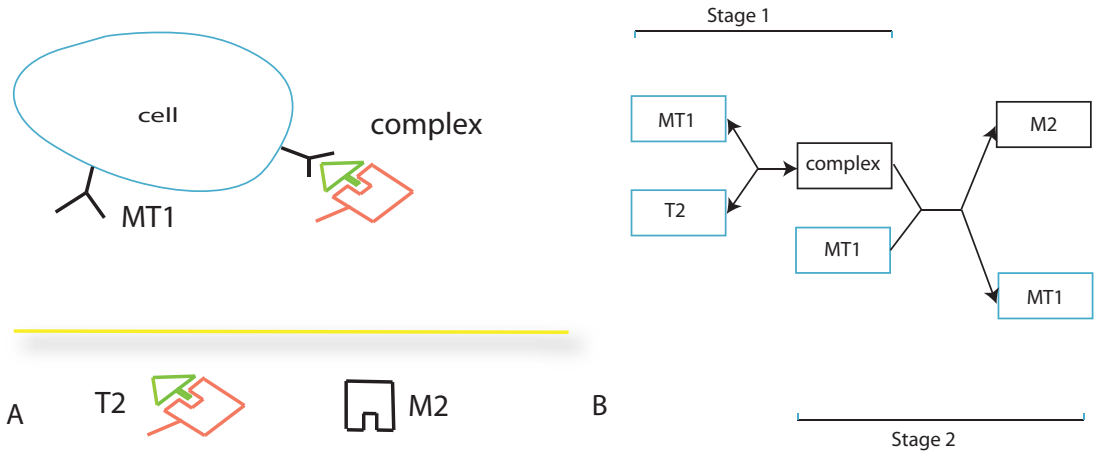

Figure 4.2: *Simplified schematic diagram of MMP-2 activation which will be implemented in the PDE model presented herein. 'MT1' represents MT1-MMP, 'T2' represents a TIMP2 molecule with an assumed proMMP-2 molecule attached, 'complex' represents the intermediate complex f defined as the complex of MT1-MMP, TIMP2 and proMMP-2 and 'M2' represents MMP-2.*

being shed, we assume that these processes can be adequately condensed into one stage, reduced from stage 3 and stage 4 of Figure 4.1.

The use of the reduced schematic for MMP-2 activation outline in Figure 4.2 therefore relies on three conditions: (i) there is a sufficiently high concentration of proMMP-2 (ii) the majority of proMMP-2 proteins in the body are already bound to a protein of TIMP2 (Eroschenko and Di Fiore, 2013) and (iii) unbound proMMP-2 proteins can quickly bind to any free TIMP2 protein (reaction rate of $3.26 \times 10^4 M^{-1}s^{-1}$ Olson et al., 1997).

MMP-2 concentration, m_s:

The MMP-2 flux, J_3, is determined from MMP-2 being a freely diffusible protein and so we model the flux as $D_{ms}\nabla m_s$, for some constant D_{ms}.

The MMP-2 source, H_3, has several components where MMP-2 is inhibited by

TIMP2 at a rate of ϕ_{31}, produced from the cleavage of complex f by a free MT1-MMP at a rate of ϕ_{32} and has a natural decay rate of β_{ms}.

$$\frac{\partial m_s}{\partial t} = \nabla \cdot (D_{ms} \nabla m_s) - \phi_{31} T m_s + \phi_{32} m_t f - \beta_{ms} m_s. \tag{4.5}$$

MT1-MMP concentration, m_t:

The MT1-MMP flux, J_4, is determined by the movement of cancer cells as MT1-MMP proteins are tethered to the membrane of cancer cells. While MT1-MMP proteins can diffuse along the surface of the cell and internalise before appearing on the membrane of the cell at a different location, we consider these processes to be unimportant in regards to the overall movement of MT1-MMP in cancer cell invasion. Movement of cancer cells will directly result in the movement of the all tethered proteins and complexes and so the flux of the MT1-MMP proteins is in proportion with both amount of MT1-MMP proteins and the flux of the cancer cells, J_1, i.e. $\nabla \cdot J_4 = \gamma m_t \nabla \cdot J_1$.

As this is a non standard method for obtaining the flux of a variable, we provide further description in order to justify our choice. If we consider the cancer cell density equation, c, as the sum of discrete cancer cells within a unit region, i.e. $c = \sum_{1}^{p} 1$. Further, we can group these individual cancer cells into subpopulations delineated by the amount of MT1-MMP proteins attached to the individual cells, i.e. $c = \sum_{i=1}^{q} \alpha_i$, where $alpha_i$ is the total amount of cancer cells with i MT1-MMP proteins attached.

We note that as the amount of free MT1-MMP proteins on any individual cancer cell can be changed through the reaction terms of m_t, the individual cancer cells can freely move from one defined subpopulation of cancer cells to another.

The movement of α_i cancer cell will therefore result in the movement of $\alpha_i i$ proteins of MT1-MMP in the same direction.

As the total flux of cancer cells is expressed as $\nabla \cdot J_1$, which can also be written as $\nabla \gamma J_\gamma = \gamma \nabla \cdot J_\gamma$, the flux term for the MT1-MMP proteins is $\gamma m_t \nabla \cdot J_\gamma$.

The MT1-MMP source, H_4, is found from the following reactions. MT1-MMP proteins are inhibited reversibly by TIMP2 at a rate of ϕ_{41} with a dissociation rate of ϕ_{42}. MT1-MMP proteins are produced by the cancer cells at a rate of $\alpha_{mt} Z$. Additionally, we include collagen-induced expression (Haas et al., 1998; Zigrino et al., 2001; Guo et al., 2005) in our model at a rate of $\alpha_{mt} n$. This may take into account observations showing that collagen-dense mouse mammary tissues result in cancer cells with a more invasive phenotype (Provenzano et al., 2008). Auto-degradation of MT1-MMP on the cancer cell surface means that there is never too much MT1-MMP on the surface at one time. The MT1-MMP is internalised (inside the cell) and is recycled before being put back on the cell surface. This is how the lifespan of active MT1-MMP is increased. We incorporate this by having a natural decay term of $\beta_{m_t} m_t$.

$$\begin{aligned} \frac{\partial m_t}{\partial t} &= \gamma m_t \nabla \cdot (D_c \nabla c - \chi c v (Z - kc - lv) \nabla v) \\ &\quad - \phi_{41} T m_t + \phi_{42} f - \beta_{m_t} m_t + \alpha_{mt} c (Z + nv). \end{aligned} \tag{4.6}$$

TIMP2, T:

The flux of TIMP2, J_5, is determined from TIMP2 proteins being freely diffusible and so we model this flux as $D_T \nabla T$, for some constant D_T.

The source of TIMP2, H_5, models the characteristics of TIMP2 proteins binding to the catalytic domains of MMP-2 and MT1-MMP proteins at rates ϕ_{51} and ϕ_{52}, respectively. While the binding of TIMP2 to MMP-2 is considered to be irreversible, we consider the dissociation of the complex MT1-MMP:TIMP2 to occur at the rate ϕ_{53}. In addition, we consider TIMP2 proteins to be produced

at a rate of α_T by cancer cells.

$$\frac{\partial T}{\partial t} = \nabla \cdot (D_T \nabla T) - \phi_{51} T m_s - \phi_{52} T m_t + \phi_{53} f + \alpha_T c. \tag{4.7}$$

The intermediate complex, f:

The flux of the intermediate complex of MT1-MMP:TIMP2:proMMP2, J_6, is determined in a similar way to that of free MT1-MMP as they are both tethered to cells' membranes. As such, we have $\nabla \cdot J_6 = \gamma f \nabla \cdot J_1$.

The source of the intermediate complex, H_6 is determined from the reversible binding of a TIMP2 protein to an MT1-MMP protein at a formation rate of ϕ_{61} and a dissociation rate of ϕ_{63}. The cleavage of the prodomain of a proMMP-2 protein by a free MT1-MMP protein, that is illustrated in stage 4 of Figure 4.2, occurs at a rate of ϕ_{62}. We note that auto-degradation of MT1-MMP on the cancer cell surface is blocked when a MT1-MMP protein is bound to TIMP2 and so it plays no role in the intermediate complex source term.

$$\begin{aligned} \frac{\partial f}{\partial t} &= \gamma f \nabla \cdot (D_c \nabla c - \chi c v (Z - kc - lv) \nabla v) \\ &\quad + \phi_{61} T m_t - \phi_{62} f m_t - \phi_{63} f. \end{aligned} \tag{4.8}$$

The system of equations are closed by applying zero-flux boundary conditions of:

$$J_i \cdot \mathbf{n} = 0,$$

for $i = 1, ..., 6$ at all spatial locations on the boundary where $\mathbf{n}$ is the outward unit normal.

Non-dimensionalisation of equations (4.3)–(4.8) is achieved by using the reference variables $\tau = 10^4$s and $L = 0.1$cm where numerical simulations will be run over a non-dimensionalised spatial domain of length 0-4 (0-4mm) and non-dimensionalised temporal range of either 0-40 (0-4.6 days) or 0-100 (0-11.5 days).

This provides sufficient space and time allowances for the consideration of local cancer invasion. As we have developed a model in a field that has a rich history of PDE models (Anderson et al., 2000; Gerisch and Chaplain, 2008; Andasari et al., 2011) we follow these models by obtaining the non-dimensionalisation reference parameters of c_0 and v_0 by the same method, namely, $c_0 = 6.7 \times 10^7$cells cm^{-3} and $v_0 = 10^{-1}nM$ (Terranova et al., 1985).

While the exact enzyme concentration ranges in ECM can be difficult to obtain, we take the reference enzyme concentration to be 1nM with concentrations throughout the considered timeframe to be within the range 0-25nM. This is broadly in line with experimental data for concentrations obtained from serum although precisely how the concentrations in serum relate to the concentrations in ECM is not known. Tutton et al. (2003) find pre-operative MMP-2 levels in plasma of colorectal cancer patients of 568.9ng/ml = 7.89nM, Song et al. (2012) find preoperative serum levels of MMP-2 in breast cancer of ∼200ng/ml = 2.81nM, Gohji et al. (1998) find serum levels of MMP-2 in men with prostrate cancer of mean values 570.6ng/ml = 7.91nM to 723.0ng/ml = 10.03nM when using the Japanese system of T1-T4 for clinical stage. MT1-MMP concentrations of 0.38nM were found in Baker et al. (1994), 3 ng/mL = 0.04nM in Petrella and Brinckerhoff (2006) and TIMP2 concentrations of 2-9.19nM were found in Baker et al. (1994) while Butler et al. (1998) and English et al. (2001) performed *in vitro* experiments with enzyme concentrations of order $10^1 - 10^2$nM.

We non-dimensionalise by using the substitutions of $c = \hat{c}c_0$, $v = \hat{v}v_0$, $m_s = \hat{m}_s m_{s_0}$, $m_t = \hat{m}_t m_{t_0}$, $T = \hat{T}T_0$, $f = \hat{f}f_0$ and $t = \hat{t}\tau$ and by setting the parameters:

$$\hat{D}_c = \frac{D_c\tau}{L^2}, \qquad \hat{\chi} = \frac{\chi {v_0}^2 \tau Z}{L^2}, \qquad \hat{\mu_c} = \mu_c \tau Z, \qquad \frac{kc_0}{Z} = 1,$$
$$\frac{lv_0}{Z} = 1, \qquad \hat{\delta_1} = \delta\delta_1\tau m_{s_0}, \qquad \hat{\delta_2} = \frac{\delta_2 m_{t_0}}{\delta_1 m_{s_0}}, \qquad \hat{\mu_v} = \frac{Z\mu_v\tau}{v_0},$$
$$\hat{D_{m_s}} = \frac{D_{m_s}\tau}{L^2}, \qquad \hat{\phi_{31}} = \phi_{31}T_0\tau, \qquad \hat{\beta_{m_s}} = \beta_{m_s}\tau, \qquad \gamma = \frac{1}{c_0},$$
$$\hat{\phi_{41}} = \phi_{41}T_0\tau, \qquad \hat{\phi_{42}} = \frac{\phi_{42}f_0\tau}{m_{t_0}}, \qquad \hat{\beta_{m_t}} = \beta_{m_t}\tau, \qquad \hat{\alpha_{m_t}} = \frac{\alpha_{m_t}c_0\tau Z}{m_{t_0}},$$
$$\frac{nv_0}{Z} = 1, \qquad \hat{\phi_{61}} = \frac{\phi_{61}T_0 m_{t_0}\tau}{f_0}, \quad \hat{\phi_{62}} = \phi_{62}m_{t_0}\tau \qquad \hat{\phi_{63}} = \phi_{63}\tau.$$

Upon dropping the hats for notational simplicity, we obtain the non-dimensionalised system of equations of:

$$\frac{\partial c}{\partial t} = \nabla\cdot(D_c\nabla c - \chi cv(1-c-v)\nabla v) + \mu_c c(1-c-v), \tag{4.9}$$
$$\frac{\partial v}{\partial t} = -\delta_1 v(m_s + \delta_2 m_t) + \mu_v(1-c-v), \tag{4.10}$$
$$\frac{\partial m_s}{\partial t} = \nabla\cdot(D_{m_s}\nabla m_s) - \phi_{31}Tm_s + \phi_{32}m_t f - \beta_{m_s}m_s, \tag{4.11}$$
$$\frac{\partial m_t}{\partial t} = m_t\nabla\cdot(D_c\nabla c - \chi cv(1-c-v)\nabla v)$$
$$-\phi_{41}Tm_t + \phi_{42}f - \beta_{m_t}m_t + \alpha_{m_t}c(1+v), \tag{4.12}$$
$$\frac{\partial T}{\partial t} = \nabla\cdot(D_T\nabla T) - \phi_{51}Tm_s - \phi_{52}Tm_t + \phi_{53}f + \alpha_T c, \tag{4.13}$$
$$\frac{\partial f}{\partial t} = f\nabla\cdot(D_c\nabla c - \chi cv(1-c-v)\nabla v)$$
$$+\phi_{61}Tm_t - \phi_{62}fm_t - \phi_{63}f, \tag{4.14}$$

where we present both the dimensionalised and dimensionless parameters in Table 4.4.

In order to close the system, we perform computational simulations with zero-flux boundary conditions to equations (4.9), (4.11)–(4.14). The initial conditions imposed depend on the precise invasion scenario we are considering. In our the first set of simulation results (Invasion Scenario 0A, cf. Figures 4.8–4.10) we have a cluster of cancer cells in the centre of a homogeneous ECM with a minimal removed section in which the cancer cells exist with a small amount of activated enzymes already released i.e. $c(0) = e^{(\frac{-(x^2+y^2)}{0.02})}$, $v(0) = 1 - c(0)$, $m_s(0) = m_t(0) =$

$T(0) = f(0) = 5c(0)$.

4.2.1 Parameter Estimation

Parameters are largely obtained from either the biological literature or comparable mathematical models and are presented here and in Table 4.4. As we will have to perform some further simulations to obtain the parameters used in the reduced schematic of Figure 4.2 that is used in the cancer invasion model, we will also present how the parameters used in these further simulations represented by equations (4.15)–(4.21) and equations (4.22)–(4.25) are obtained.

As previously discussed, there are a large number of PDE models in this field and while we require new sources for parameters relating to the MMPs, we do not need to begin *de novo* for the remaining parameters. These can be obtained from the comparable models of Anderson et al. (2000), Anderson (2005), Chaplain and Lolas (2006), Gerisch and Chaplain (2008), Andasari et al. (2011) and the references therein. As such, we follow these models to obtain estimates for the parameters of $D_c, \chi, \mu_c, \mu_v, \delta_1, \delta_2$

Anderson et al. (2000) use the experimental data of Bray (1992) to find a range of cancer cell diffusion of $10^{-10} - 10^{-9} cm^2 s^{-1}$ and so we choose to use the dimensionalised parameter of $D_c = 3.5 \times 10^{-10} cm^2 s^{-1}$. A haptotaxis rate of cancer cells towards ECM gradients of $2.6 \times 10^{-6} cm^2 s^{-1} nM^{-1}$ is assumed in Anderson et al. (2000) and many of the models following on from their work while we note that movement along collagen is found to be slower than movement along fibronectin (Wojciak-Stothard et al., 1997) and as such we use the value of $\chi = 5 \times 10^{-7} cm^2 s^{-1} M^{-1}$. Chaplain and Lolas (2006) provide extensive biological references for the parameter defining cell division of $0.02h^{-1} - 0.72h^{-1}$ and as such we

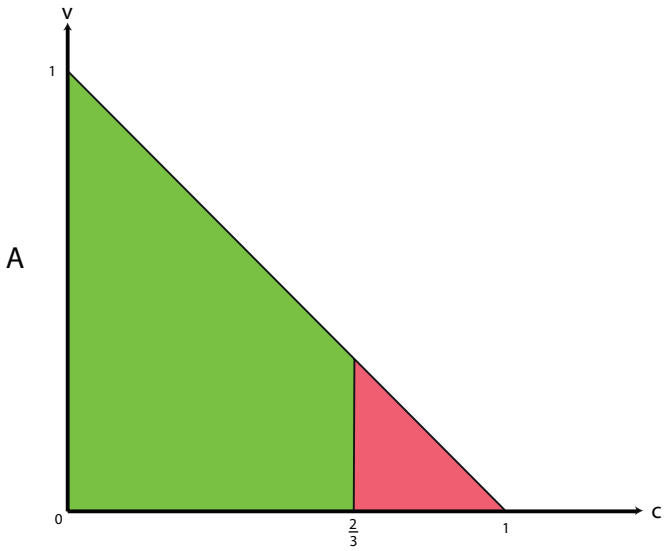

Figure 4.3: *A comparison of the functions determining the production of the cancer and ECM densities in order to determine which is larger for a range of cancer and ECM densities. The functions of* $0.3c(1-c-v)$ *and* $0.2(1-c-v)$ *are compared for the full range of values of* $0 \leq c \leq 1$ *and* $0 \leq v \leq 1$*. When the first function is larger, we indicate this with the colour red and when the second function is larger, we indicate this with the colour green. The two functions are equal to one another along the white line.*

choose a dimensionalised parameter value of $\mu_c = 0.108h^{-1}$. Gerisch and Chaplain (2008) use a value of ECM remodelling to be $3.6 \times 10^{-3}h^{-3}nM^{-1}$ while we choose an ECM remodelling term of double that where $\mu_v = 7.2 \times 10^{-3}h^{-3}nM^{-1}$. We have chosen a value for μ_c and μ_v in accordance with Figure 4.3 which identifies which is greater between $\mu_c c(1-c-v)$ and $\mu_v(1-c-v)$ when $\mu_c = 0.3$ and $\mu_v = 0.2$. This shows which is reaching closer to the fully filled stage, however it does not necessarily show which is producing cells more quickly.

As the rates taken for the degradation of ECM constituents vary with regard to acidity, temperature and the exact make-up of the constituent parts, we choose to consider matrix degradation by MMP-2 and MT1-MMP to be equal ($\delta_2 = 1$), however this would not be true for each of the constituent parts of the ECM at all acidity levels. What we are measuring is not then the exact amount of ECM degraded but instead the amount of potential tissue that may be degraded. For exact measurement of ECM degradation to be accurately predicted by our model, precise imaging of both the position and identification of the constituents would need to be analysed along with a consideration of the acidity of the environment. By varying the parameters δ_1, and δ_2, it would be possible to gain an overview of how the overall proportion of degradation performed by either MMP aids cancer cell invasion. This is not necessary in the current work and would provide most benefit when a patient specific assessment is carried out.

Collier et al. (2011) find the diffusion of MMP-2 on collagen type-1 to be $1.29 \times 10^8 cm^2 s^{-1}$ and we consider the diffusion of proMMP-2, TIMP2 to be of the same order. Therefore we have $D_{m_s} = D_{pm_s} = D_T = 1.29 \times 10^8 cm^2 s^{-1}$.

The parameters $\beta_{m_s}, \beta_{m_t}, \alpha_{m_t}$ and α_T were chosen so that the concentrations of active MT1-MMP and MMP-2 are in the range 0-25nM for the entire domain and 0-10nM for the cancer-ECM interface. As the values of serum level of free

MMP-2 and TIMP2 do not correlate with tumour staging Kolomecki et al. (2001); Oberg et al. (1999) as well as the MMP-2/TIMP2 complex (Oberg et al., 1999) and as we have previously discussed that serum levels of MMP-2 have been seen in the range 2.81-10.03nM, we consider this to be an appropriate range for our continuum based mathematical model.

However some parameters cannot be obtained from the literature directly (ϕ_{32}, ϕ_{62}) as we are using the reduced schematic of Figure 4.2, thus here we show how they are estimated.

We consider a model (submodel A) of the full MMP-2 activation system represented in Figure 4.1 to take place in the spatial domain represented in Figure 4.4 to estimate the rate at which MT1-MMP binds to TIMP2 which has an attached proMMP-2. We then compare this rate to a model (submodel B) of the simplified representation of the MMP-2 activation system represented in Figure 4.2 that is consider in the full model of equations (4.9)–(4.14). We note that for both submodels that as the diffusive enzymes have such a high diffusion rate, there is little difference between that of the spatial and ordinary differential equation model despite having interactions that can only happen near the cell boundary.

Toth et al. (2000) find the binding rate of MT1-MMP to TIMP2 to be $2.74 \times 10^6 M^{-1}s^{-1}$ as well as the dissociation of this complex of $2 \times 10^{-4}s^{-1}$. Therefore we have the non-dimensionalised parameters of $a_1 = b_1 = 2.74 \times 10^{-3}$ and $a_2 = b_2 = 2 \times 10^{-4}$ with $\phi_{41} = \phi_{52} = \phi_{61} = 27.4$ with $\phi_{51} = \phi_{63} = 2$.

Olson et al. (1997) find the binding rate of the complex of MT1-MMP and TIMP2 to that of proMMP-2 to be $1.4 \times 10^5 M^{-1}s^{-1}$ as well as the dissociation of this three enzyme complex of $4.7 \times 10^{-3}s^{-1}$. Therefore we have $a_3 = 1.4 \times 10^{-4}$ with $a_4 = 4.7 \times 10^{-3}s^{-1}$.

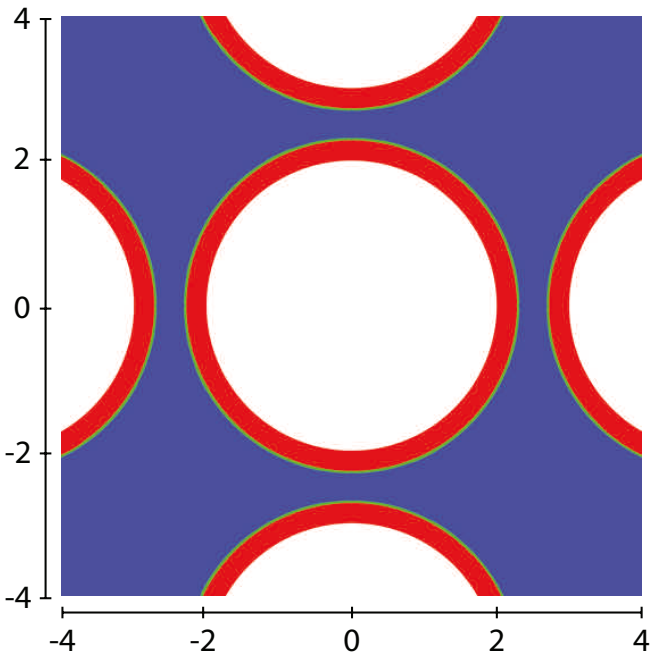

Figure 4.4: *The domain and boundary conditions used in submodel A and B. The domain is square and contains an entire cancer cell in addition to parts of four cells. The cancer cells are of equal shape with a diameter of 40 μm. The red region is the area that membrane-bound interactions can take place and the blue region is where the freely-diffusive enzymes can move into. The boundary between the white and red region is considered to be zero-flux and the boundary between red region and blue region, presented in green, has conservation of flux across it.*

SubModel A:

We formulate submodel A, where all parameters have estimates or estimated ranges in the literature, with the sole purpose of simulating a specific circumstance to provide a resultant profile of MMP-2 that submodel B can be compared with. This allows for the estimation of the unknown parameter of b_3 in submodel B, which is equivalent to $\phi_{32} = \phi_{62}$ in the proposed model of cancer invasion of equations (4.9)–(4.14).

We use the non-dimensionalisation parameters of $\tau = 1s, L = 0.001$cm and a reference enzyme concentration of 1nM to determine the following non-dimensionalised system of equations where we have chosen $\alpha_{pM2} = \alpha_{MT1} = \alpha_{T2} = 0$ to close the system to be able to compare the results obtained from the schematic used in this submodel and the later submodel B.

$$\frac{\partial[pM2]}{\partial t} = \nabla \cdot (D_{pM2}\nabla[pM2]) + \alpha_{pM2} - a_3[MT1:T2][pM2] + a_4[MT1:T2:pM2] \quad (4.15)$$

$$\frac{\partial[M2]}{\partial t} = \nabla \cdot (D_{M2}\nabla[M2]) + a_7[MT1:T2:pM2:MT1] \quad (4.16)$$

$$\frac{\partial[MT1]}{\partial t} = +\alpha_{MT1} + a_2[MT1:T2] - a_1[MT1][T2] - a_5[MT1:T2:pM2][MT1] + a_6[MT1:T2:pM2:MT1] + a_7[MT1:T2:pM2:MT1] \quad (4.17)$$

$$\frac{\partial[T2]}{\partial t} = \nabla \cdot (D_{T2}\nabla[T2]) + \alpha_{T2} + a_2[MT1:T2] - a_1[MT1][T2] \quad (4.18)$$

$$\frac{\partial[MT1:T2]}{\partial t} = +a_4[MT1:T2:pM2] - a_3[MT1:T2][pM2] + a_7[MT1:T2:pM2:MT1] + a_1[MT1][T2] - a_2[MT1:T2] \quad (4.19)$$

$$\frac{\partial[MT1:T2:pM2]}{\partial t} = a_3[MT1:T2][pM2] - a_4[MT1:T2:pM2] - a_5[MT1:T2:pM2][MT1] + a_6[MT1:T2:pM2:MT1] \quad (4.20)$$

$$\frac{\partial[MT1:T2:pM2:MT1]}{\partial t} = a_5[MT1:T2:pM2][MT1] - a_6[MT1:T2:pM2:MT1] - a_7[MT1:T2:pM2:MT1] \quad (4.21)$$

We use initial conditions in the region near the cell of proMMP-2=100nM, MT1-MMP=200nM and TIMP2=160nM with Figure 4.5 showing the subdomain integration of concentration levels for chosen species changing over the combined region.

The one parameter which we have chosen to estimate is the rate at which free

	Dimensionless value	**Original value**	**Source**
D_{pM2}	1.29×10^2	$1.29 \times 10^8\ cm^2 s^{-1}$	Collier et al. (2011)
D_{M2}	1.29×10^2	$1.29 \times 10^8\ cm^2 s^{-1}$	Collier et al. (2011)
D_{T2}	1.29×10^2	$1.29 \times 10^8\ cm^2 s^{-1}$	Collier et al. (2011)
a_1	2.74×10^{-3}	$2.74 \times 10^6\ M^{-1} s^{-1}$	Toth et al. (2000)
a_2	2×10^{-4}	$2 \times 10^{-4}\ s^{-1}$	Toth et al. (2000)
a_3	1.4×10^{-4}	$1.4 \times 10^5\ M^{-1} s^{-1}$	Olson et al. (1997)
a_4	4.7×10^{-3}	$4.7 \times 10^{-3}\ s^{-1}$	Olson et al. (1997)
a_5	4.3×10^{-5}	$4.3 \times 10^4\ M^{-1} s^{-1}$	estimated
a_6	9×10^{-7}	$9 \times 10^{-7}\ s^{-1}$	Karagiannis and Popel (2004)
a_7	2×10^{-2}	$2 \times 10^{-2}\ s^{-1}$	Karagiannis and Popel (2004)
α_{pM2}	0		
α_{MT1}	0		
α_{T2}	0		

Table 4.2: *Parameter set A as used in submodel A, relating to the full activation system of MMP-2 at the cellular scale.*

MT1-MMP proteins bind to the complex of MT1-MMP:TIMP2:proMMP-2, parameter a_5. The reason for doing so is that the literature offers a wide range of values for this rate. The mathematical model of Karagiannis and Popel (2004) estimates the value to be $3 \times 10^3 M^{-1} s^{-1}$ through comparisons with the biological data of English et al. (2001). Indeed, when we use the biological data of English et al. (2001) and Butler et al. (1998) (as shown in the later stochastic model introduced in Chapter 6, Figure 6.5), we find a comparable value of $3 \times 10^3 M^{-1} s^{-1}$. However, the mathematical work of Hoshino et al. (2012), where they have also performed original biological experiments, estimate the parameter to be a much larger value of $2 \times 10^6 M^{-1} s^{-1}$.

This discrepancy in parameter value estimates may in part be explained where experiments performed in Butler et al. (1998) and English et al. (2001) used the severed catalytic region of MT1-MMP proteins and performed experiments in a well-mixed bulk. This may result in a parameter estimate that is smaller than the case *in vivo*. We have chosen to estimate the parameter a_5 as a value between these estimates and as such have used $a_5 = 4.3 \times 10^4 M^{-1} s^{-1}$ for all computational simulations of our presented model.

SubModel B:

We formulate submodel B using known parameters in conjunction with one unknown parameter, b_3. In comparing the results with that obtained from submodel A, we are able to obtain an estimate for the unknown parameter b_3, which can then be used in the proposed model of cancer invasion of equations (4.9)–(4.14) where b_3 is equivalent to $\phi_{32} = \phi_{62}$.

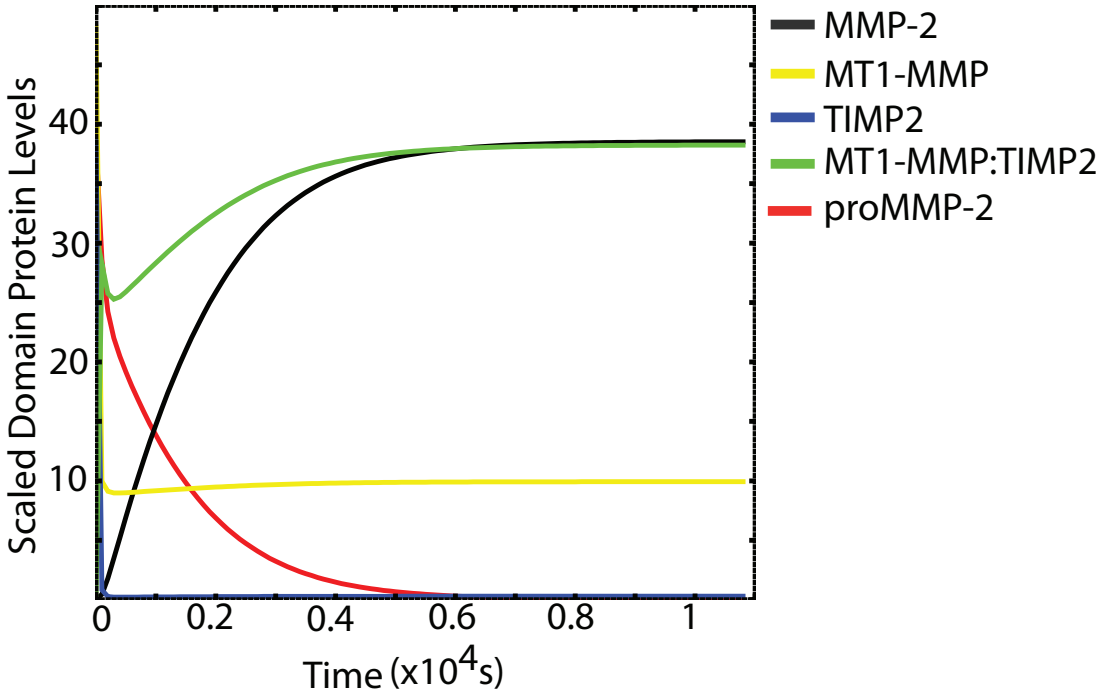

Figure 4.5: *Submodel A. Total protein levels as determined by domain integrations of the variables of the models are presented where MMP-2 is black, MT1-MMP is yellow, TIMP2 is blue, proMMP-2 is red and the complex of MT1-MMP:TIMP2:MT1-MMP:proMMP-2 is shown in green.*

Parameter	Dimensionless value	Original value	Source
D_{pM2}	1.29×10^2	$1.29 \times 10^8\ cm^2 s^{-1}$	Collier et al. (2011)
D_{M2}	1.29×10^2	$1.29 \times 10^8\ cm^2 s^{-1}$	Collier et al. (2011)
b_1	2.74×10^{-3}	$2.74 \times 10^6\ M^{-1} s^{-1}$	Toth et al. (2000)
b_2	2×10^{-4}	$2 \times 10^{-4}\ s^{-1}$	Toth et al. (2000)
b_3	1.95×10^{-5}	$1.95 \times 10^4\ M^{-1} s^{-1}$	fitted
α_{MT1}	0		
α_{T2}	0		

Table 4.3: *Parameter set B as used in submodel B relating to the reduced activation system of MMP-2 at the cellular scale.*

$$\frac{\partial [MT1]}{\partial t} = +\alpha_{MT1} + b_2[f] - b_1[MT1][T2] \tag{4.22}$$

$$\frac{\partial [T2]}{\partial t} = \nabla \cdot (D_{T2} \nabla [T2]) + \alpha_{T2} + b_2[f] - b_1[MT1][T2] \tag{4.23}$$

$$\frac{\partial [f]}{\partial t} = +b_1[MT1][T2] - b_2[f] - b_3[f][MT1] \tag{4.24}$$

$$\frac{\partial [M2]}{\partial t} = \nabla \cdot (D_{M2} \nabla [M2]) + b_3[f][MT1] \tag{4.25}$$

We use initial conditions in the region near the cell of MT1-MMP=200nM and TIMP2=160nM with Figure 4.6 showing the subdomain integration of concentration levels for chosen species changing over the combined region. Comparisons of Figure 4.5 with Figure 4.6 yield the non-dimensionalised $b_3 = 1.95 \times 10^{-5}$.

Steady states of the underlying, spatially homogeneous system of equations (4.26)–(4.32) are obtained by solving simultaneous equations in Maple 13$^{\mathrm{TM}}$, using the baseline parameters found in Table 4.4.

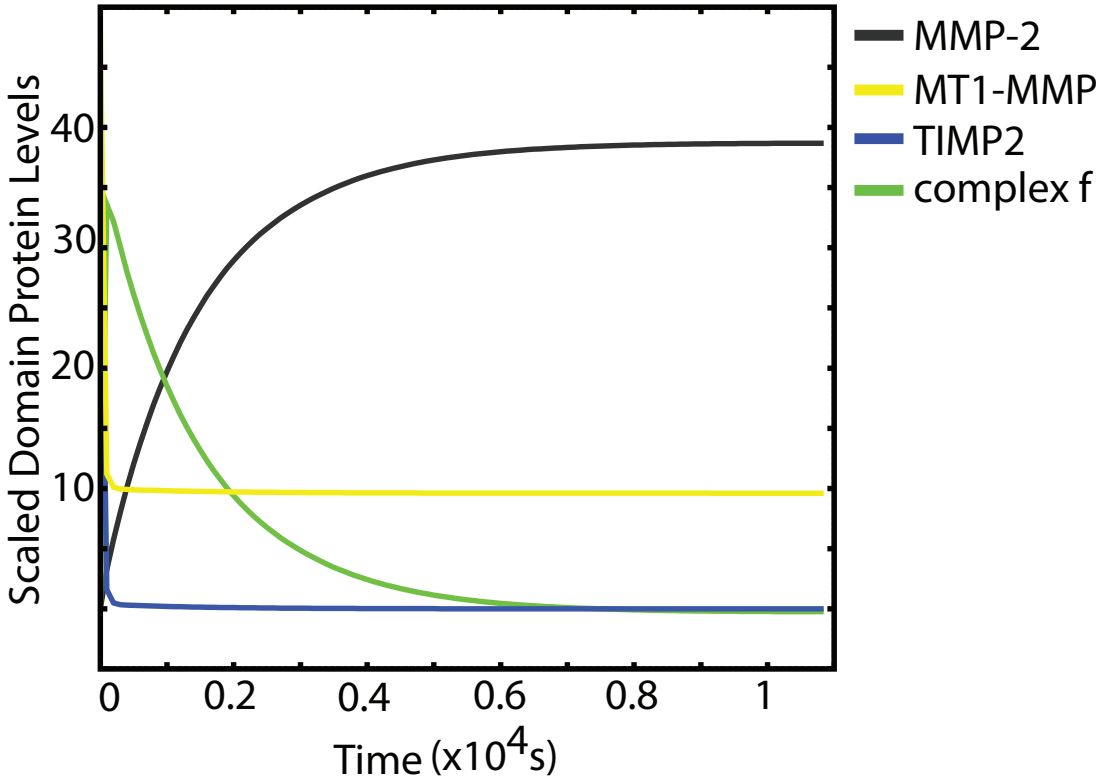

Figure 4.6: *Submodel B. Total protein levels as determined by domain integrations of the variables of the models are presented where MMP-2 is black, MT1-MMP is yellow, TIMP2 is blue, the intermediate complex, f, is shown in green.*

	Dimensionless value	**Original value**	**Source**
D_c	3.5×10^{-4}	$3.5 \times 10^{-10} cm^2 s^{-1}$	Anderson et al. (2000)
χ	5×10^{-3}	$5 \times 10^{-7} cm^2 s^{-1} M^{-1}$	Anderson et al. (2000)
μ_c	0.3	$0.108 h^{-1}$	Chaplain and Lolas (2006)
δ_1	1	$1 \times 10^{-4} n M^{-1} s^{-1}$	Anderson et al. (2000)
δ_2	1	scaling factor	estimated
μ_v	0.2	$7.2 \times 10^{-3} h^{-1} n M^{-1}$	Gerisch and Chaplain (2008)
D_{m_s}	1.29×10^{-2}	$1.29 \times 10^{8}\ cm^2 s^{-1}$	Collier et al. (2011)
ϕ_{31}	5	$5 \times 10^{5}\ M^{-1} s^{-1}$	estimated
ϕ_{32}	0.195	$1.95 \times 10^{4}\ M^{-1} s^{-1}$	estimated
β_{m_s}	0.1	$1 \times 10^{-5}\ s^{-1}$	estimated
α_{m_t}	5	$5 \times 10^{-4}\ s^{-1}$	estimated
ϕ_{41}	27.4	$2.74 \times 10^{6}\ M^{-1} s^{-1}$	Toth et al. (2000)
ϕ_{42}	2	$2 \times 10^{-4}\ s^{-1}$	Toth et al. (2000)
β_{m_t}	0.1	$1 \times 10^{-5}\ s^{-1}$	estimated
D_T	1.29×10^{-2}	$1.29 \times 10^{8}\ cm^2 s^{-1}$	Collier et al. (2011)
α_T	4	$4 \times 10^{-4}\ s^{-1}$	estimated
ϕ_{51}	5	$5 \times 10^{5}\ M^{-1} s^{-1}$	estimated
ϕ_{52}	27.4	$2.74 \times 10^{6}\ M^{-1} s^{-1}$	Toth et al. (2000)
ϕ_{53}	2	$2 \times 10^{-4}\ s^{-1}$	Toth et al. (2000)
ϕ_{61}	27.4	$2.74 \times 10^{6}\ M^{-1} s^{-1}$	Toth et al. (2000)
ϕ_{62}	0.195	$1.95 \times 10^{4}\ M^{-1} s^{-1}$	estimated
ϕ_{63}	2	$2 \times 10^{-4}\ s^{-1}$	Toth et al. (2000)

Table 4.4: *Baseline parameter set for the model*

$$
\begin{aligned}
0 &= \mu_c c(1-c-v), && (4.26)\\
0 &= -\delta(s-1+v)(m_s+m_t)+\mu_v(1-c-v), && (4.27)\\
0 &= -\phi_{31}Tm_s+\phi_{32}m_t f-\beta_{m_s}m_s, && (4.28)\\
0 &= -\phi_{41}Tm_t+\phi_{42}f-\beta_{m_t}m_t+\alpha_{m_t}c(1+v), && (4.29)\\
0 &= -\phi_{51}Tm_s-\phi_{52}Tm_t+\phi_{53}f+\alpha_T c, && (4.30)\\
0 &= \phi_{61}Tm_t-\phi_{62}fm_t-\phi_{63}f, && (4.31)\\
0 &= \delta_s m_t(1-s). && (4.32)
\end{aligned}
$$

The seven mathematical solutions of this system are:

$$
\begin{pmatrix} c^* \\ v^* \\ m_s^* \\ m_t^* \\ T^* \\ f^* \end{pmatrix} = \begin{pmatrix} 1 \\ 0 \\ 21.25 \\ 19.37 \\ 0.01 \\ 0.81 \end{pmatrix}, \begin{pmatrix} 0 \\ 1 \\ 0 \\ 0 \\ T^* \\ 0 \end{pmatrix}, \begin{pmatrix} 0 \\ -0.04 \\ -11.79 \\ 5.89 \\ -0.01 \\ -0.51 \end{pmatrix}, \begin{pmatrix} 2 \\ -1 \\ -80 \\ 0 \\ -0.02 \\ 0 \end{pmatrix}, \begin{pmatrix} 1 \\ 0 \\ 94.48 \\ -17.24 \\ -0.01 \\ -2 \end{pmatrix},
$$

$$
\begin{pmatrix} 1 \\ 0 \\ 112.94 \\ -26.47 \\ -0.01 \\ -1.48 \end{pmatrix}, \begin{pmatrix} 0.01 \\ 0.99 \\ -1.26 \\ 1.26 \\ -0.01 \\ -0.19 \end{pmatrix}, \begin{pmatrix} 1.61 \\ -0.61 \\ 1.65 \\ -1.65 \\ 0.38 \\ -10.25 \end{pmatrix}, \begin{pmatrix} 2.16 \\ -1.16 \\ 121.07 \\ -121.07 \\ 0.00 \\ -0.44 \end{pmatrix},
$$

where only the first two solutions satisfy the non-negative requirement for being biologically relevant. As such, further examination of only these first two solutions is presented.

Before finding the stability of these steady states, we note that the first steady state represents a region where cancer has fully invaded the tissue and the ECM is completely degraded while the second steady state represents the case where all cancer cells have died out and only healthy tissue makes up the entirety of the domain but doesn't put any conditions on the values that T can take.

For the steady state of $(c^*, v^*, m_s^*, m_t^*, T^*, f^*)^T = (1, 0, 21.25, 19.37, 0.01, 0.81)^T$, the associated eigenvalues are: $\lambda_1 = -0.10, \quad \lambda_2 = -0.22, \quad \lambda_3 = -0.30, \quad \lambda_4 = -0.48, \quad \lambda_5 = -4.06, \quad \lambda_6 = -40.83, \quad \lambda_7 = -639.10$. As all the eigenvalues λ_i for $i = 1, ..., 7$ are negative, we have that the steady state is stable.

For the steady state of $(c^*, v^*, m_s^*, m_t^*, T^*, f^*)^T = (0, 1, 0, 0, T^*, 0)^T$, the associated eigenvalues are: $\lambda_1 = -0.2, \quad \lambda_2 = -0.1 - 5T^*, \quad \lambda_3 = -13.7T^* - 1.05 + 0.05(75076T^{*2} + 11508T^* + 361)^{0.5}, \quad \lambda_4 = -13.7T^* - 1.05 - 0.05(75076T^{*2} + 11508T^* + 361)^{0.5}, \quad \lambda_5 = 0, \quad \lambda_6 = 0, \quad \lambda_7 = 0.$

In order to determine the stability of the steady state associated with λ_3, we plot (not shown) $13.7T^* - 1.05$ and $0.05(75076T^{*2} + 11508T^* + 361)^{0.5}$. From this, we determine that $\text{Re}(0.05(75076T^{*2} + 11508T^* + 361)^{0.5}) > \text{Re}(13.7T^* - 1.05)$ for all $T \in \mathbb{R}(0, \infty)$, therefore $\text{Re}(\lambda_3) > 0$ and this steady state is unstable.

As discussed previously, using volume filling terms can result in "normal" or "abnormal" states of the production functions for cancer cell density and ECM density where normal conditions are defined as those allowing for growth or stasis from the production function while abnormal conditions are defined as those resulting in a loss. As these functions are primarily intended to provide growth or stasis to the ECM and cancer cell densities, we term the switch in states to be a "breach" in the volume filling function.

We note that while the conditions of $c \geq 0$ and $v \geq 0$ are inviolable in a biological

understanding of the model. The remaining three conditions required for stasis or production of $c \leq 1$, $v \leq 1$, $c + v \leq 1$ can be violated to cause a breach resulting in a switch in role of the production terms to that of encouraging loss in the cancer cell and ECM densities. Biologically, this means that while we cannot have a negative amount of either cancer cells or ECM components, only a certain amount of cancer cells or ECM components can be supported. As such, a minimal or temporary breach can be considered to be biologically relevant. However, an unchecked breach can result in finite-time blow up solutions, which is at odds with a biological interpretation of the model.

We separate the proposed model into two systems of equations considering either only the reaction terms in equations (4.33)–(4.38) or only the flux of cancer cells, ECM components and associated proteins in equations (4.39)–(4.44). This is done to provide a clear indication of the role of each term in causing or recovering from a breach.

$$\frac{\partial c}{\partial t} = \mu_c c v(1 - c - v), \tag{4.33}$$

$$\frac{\partial v}{\partial t} = -\delta v(m_s + m_t) + \mu_v(1 - c - v), \tag{4.34}$$

$$\frac{\partial m_s}{\partial t} = -\phi_{31} T m_s + \phi_{32} m_t f - \beta_{m_s} m_s, \tag{4.35}$$

$$\frac{\partial m_t}{\partial t} = -\phi_{41} T m_t + \phi_{42} f - \beta_{m_t} m_t + \alpha_{m_t} c(1 + v), \tag{4.36}$$

$$\frac{\partial T}{\partial t} = -\phi_{51} T m_s - \phi_{52} T m_t + \phi_{53} f + \alpha_T c, \tag{4.37}$$

$$\frac{\partial f}{\partial t} = \phi_{61} T m_t - \phi_{62} f m_t - \phi_{63} f, \tag{4.38}$$

$$\frac{\partial c}{\partial t} = \nabla \cdot (D_c \nabla c - \chi c v(1-c-v)\nabla v), \tag{4.39}$$

$$\frac{\partial v}{\partial t} = 0 \tag{4.40}$$

$$\frac{\partial m_s}{\partial t} = \nabla \cdot (D_{m_s} \nabla m_s) \tag{4.41}$$

$$\frac{\partial m_t}{\partial t} = m_t \nabla \cdot (D_c \nabla c - \chi c(1-c-v)\nabla v) \tag{4.42}$$

$$\frac{\partial T}{\partial t} = \nabla \cdot (D_T \nabla T) \tag{4.43}$$

$$\frac{\partial f}{\partial t} = f \nabla \cdot (D_c \nabla c - \chi c(1-c-v)\nabla v) \tag{4.44}$$

It can trivially be seen that the reaction terms found in equations (4.33) and (4.34), satisfy the three criteria for production or stasis for all t, provided it is true for $t = 0$. As there are no flux terms for the ECM, v, we can declare that $v \leq 1 \forall t$ where $v(t=0) \leq 1$ and $c, v(t=0) \geq 0$ thus any breach must be the result of the flux terms of the cancer cell density found in equation (4.39).

When we examine the spatial terms in isolation from the kinetics, equations (4.39)–(4.44), it becomes clear that there exists two ways in which the volume filling criterion of $1 - c - v \geq 0$ can be breached. This can be caused by either the diffusion or the haptotaxis term. We illustrate three cases where this breach can either occur due to diffusion only in the plots of Figure 4.7 A&B, either haptotaxis or diffusion in the plots of Figure 4.7 C&D or by haptotaxis only in the plots of Figure 4.7 E&F. We will then proceed to consider the consequences of this breached criterion, including any affect on the remaining volume filling criteria. In all three cases outlined by Figure 4.7, we define the ECM, v to be green and the cancer cells, c to be red and we consider only the two spatial locations of X and Y at the two times of t_i and $t_i + \epsilon$ where we define ϵ to be a sufficiently small value. We do not specify the proportion of ECM to cancer and represent this graphically with the break conditions on the density axes.

In all cases, we have conservation of mass for both the cancer cell population and the ECM density such that $c(X,t_i) + c(Y,t_i) = c(X,t_i+\epsilon) + c(Y,t_i+\epsilon)$ and $v(X,t_i) + v(Y,t_i) = v(X,t_i+\epsilon) + v(Y,t_i+\epsilon)$. Furthermore, as there is no flux terms for the ECM components, we have that $v(X,t_i) = v(X,t_i+\epsilon)$ and $v(Y,t_i) = v(Y,t_i+\epsilon)$. We remark that diffusion of cancer cells causes movement from regions of higher c to regions of lower c and that haptotaxis of cancer cells causes movement from regions of lower v to regions of higher v at a rate that is limited by the haptotactic sensitivity function, which in our model is $\chi v(1-c-v)$.

To construct the scenario outlined in the plots of Figure 4.7 A&B ,where it is possible for diffusion but not haptotaxis to violate this criteria, we consider $c(X,t_1) > c(Y,t_1)$, $c(X,t_1) + v(X,t_1) = 1$, $v(X,t_1) < v(Y,t_1)$ and $c(Y,t_1) + v(Y,t_1) = 1-\delta$, where $0 \leq \delta << 1$. We now consider how such a setup would be modified by the flux terms. We would have diffusion from locations X to Y by $t = t_1 + \epsilon$ which for some sufficiently small δ would cause an increase in cancer cells at location Y such that $c(Y,t_1+\epsilon)+v(Y,t_1+\epsilon) > 1$. This violates the volume filling criterion of $1 - c + v \geq 0$. Haptotaxis would move cells from location X to Y as $v(X,t_1) < v(Y,t_1)$, however no haptotaxis can take place as the volume filling term in the haptotactic sensitivity function is zero when $1 - c - v = 0$ as is is the case at location X at $t = t_1$.

We now discuss the third scenario outlined in Figure 4.7 E&F where it is possible for haptotaxis but not diffusion to violate the volume filling criteria before returning to the second scenario. We construct this scenario by considering $c(X,t_3) = c(Y,t_3)$, $c(X,t_3) + v(X,t_3) = 1-\gamma$, $c(Y,t_3) + v(Y,t_3) = 1-\delta$ and $v(X,t_3) < v(Y,t_3)$ where $0 < \gamma < 1$ and $0 \leq \delta << 1$. As we move from t_3 to $t_3 + \epsilon$ for some sufficiently small ϵ, we note that no diffusion can take place as $c(X,t_3) = c(Y,t_3)$ and that haptotaxis would move cancer cells from location X to Y as $v(X,t_3) < v(Y,t_3)$. Unlike the first case, we do not have

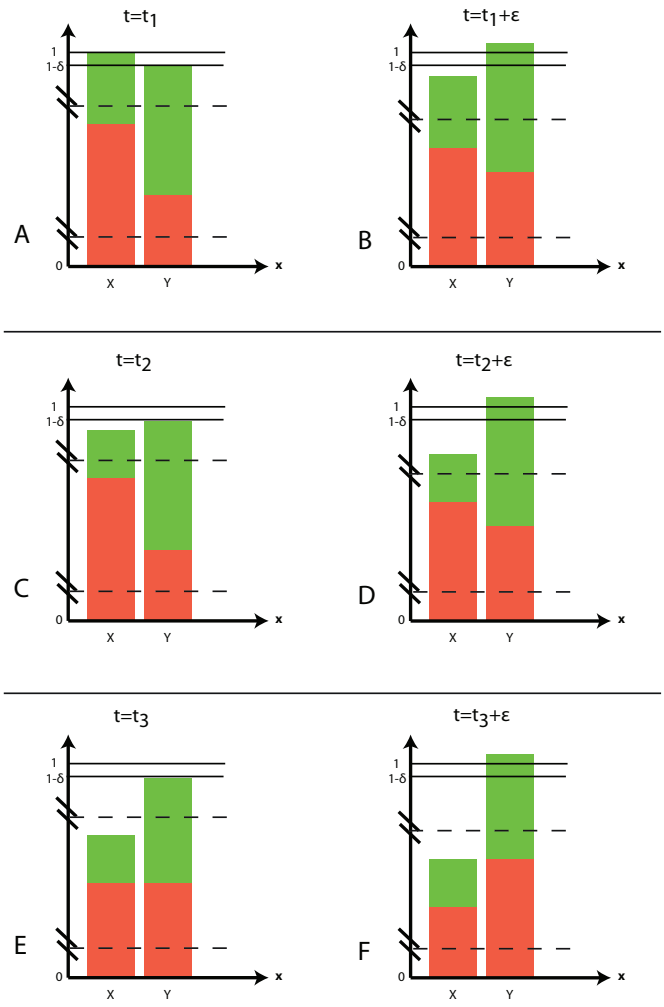

Figure 4.7: *We illustrate three scenarios where the flux terms can cause a breach of the volume filling criterion of* $1-c-v \geq 0$. *Plots A and B illustrates the case where this breach is caused by diffusion. Plots C and D illustrate the case where either diffusion or haptotaxis can cause the breach and the plots of E and F illustrate the case where the breach can be caused by haptotaxis but not diffusion. We represent the ECM by green and the cancer cells by red and consider two spatial locations of* X *and* Y *at two time points of* t_i *and* $t_i + \epsilon$ *for* $i = 1, 2, 3$.

$1 - c(X, t_1) - v(X, t_1) = 0$ and so the haptotactic event can take place. Provided that δ is sufficiently small and γ sufficiently large, we will have a breach of the volume filling criterion of $1 - c - v \geq 0$ as $c(Y, t_3 + \epsilon) + v(Y, t_3 + \epsilon) > 1$.

If we construct the second scenario as outline in Figure 4.7 C&D in the same way as the third scenario with the exception of $c(X, t_2) > c(Y, t_2)$, it is now trivial to show a breach of the volume filling criterion by either the diffusion or haptotaxis as $c(Y, t_2 + \epsilon) + v(Y, t_2 + \epsilon) > 1$ provided δ is sufficiently small and γ sufficiently large.

As we have found that the two conditions required for production or stasis of $c + v \leq 1$ and $c \leq 1$ can be violated, we must consider the consequences of such a breach. We do this by by considering both the effects on the flux terms and the reaction terms. For the flux term of equation (4.39), we note that the diffusion term is unaffected by any such breach and will continue to act in the same manner, however the haptotaxis term will change sign resulting becoming what is known as a chemorepellent in chemotaxis models, and as such we coin it to be haptorepellent. This change causes cancer cells to instead move away from regions of higher v towards regions of lower v.

We now consider what effect the breaking of the volume filling criterion of $1 - c - v \geq 0$ has on the reaction terms (the examining of the after effects of this change is the equivalent to examining the effect of having an initial condition for the spatially homogeneous equations of (4.33)–(4.38) that doesn't satisfy the condition of $1 - c - v \geq 0$) but still satisfies $0 \leq v \leq 1$ (i.e. $0 < c$). As such we consider the reactions that will affect location Y at $t = t_i + \epsilon$ where $c(Y, t_i + \epsilon) + v(Y, t_i + \epsilon) > 1$.

From equations (4.33) and (4.34), we have that

$$\begin{aligned}
\frac{\partial c(Y,t_i+\epsilon)}{\partial t} &= \mu_c c(Y,t_i+\epsilon)(1-c(Y,t_i+\epsilon)-v(Y,t_i+\epsilon)) < 0, \quad (4.45)\\
\frac{\partial v(Y,t_i+\epsilon)}{\partial t} &= -\delta v(m_s(Y,t_i+\epsilon)+m_t(Y,t_i+\epsilon))\\
&\quad +\mu_v(1-c(Y,t_i+\epsilon)-v(Y,t_i+\epsilon)) < 0, \quad (4.46)
\end{aligned}$$

which can be interpreted as there being a decrease in c and v at this location as a direct consequence of the breach in the volume filling criterion of $1-c-v \geq 0$. This cycle would remain active until $1-c-v \geq 0$. We have therefore shown that neither the reaction or flux terms can cause an increase in v above the value of 1 despite the increase in c such that $c+v>1$ caused by the flux terms.

Provided there were no further increase from location X to Y from the flux terms, we have shown that there will be a decrease in c at location Y from the haptotaxis term acting as a haptorepellent and a decrease in both c and v from the reaction terms. We have however, shown that a further increase in c at location Y is possible from both the haptotaxis term and the diffusion. As such, it is possible that a breach in the volume filling criterion of $1-c-v \geq 0$ will not immediately fix itself.

As for the other criterion of volume filling, namely $c \geq 0$ and $v \geq 0$, we note that these are inviolable in a biological sense as it is impossible for negative amount of cancer cells or ECM components to be present at any location. We note that neither the diffusion or haptotaxis terms can possibly cause a decrease to either c or v when either are at zero and so have only the reaction terms to consider. The reaction terms can trivially be shown to not decrease c or v past zero when we have $1-c-v \geq 0$.

We therefore consider the cases where $1-c-v<0$ as caused by either haptotaxis or diffusion and the effect this has on the reaction terms. In order for the violation

to be the result of haptotaxis, we must have $v(Y, t_i + \epsilon) > \gamma$ for some small γ where the haptotactic sensitivity function produces a displacement proportional to $v(c - c^2 - cv)$ and so is unlikely to provide a movement greater than γ for reasonable choices of χ. In order for the violation to be the result of diffusion, we have that $0 \leq c \leq 1$ with $1 - c - v < 0$ therefore $v > \gamma$. As $1 - c - v \geq 0$ when $v = 0$, we have that there will no longer be a decrease in c and v as a result of a breach in the volume filling. We have therefore shown that the remaining volume filling criteria of $c \geq 0$ and $v \geq 0$ are satisfied for all t.

We then have that finite time blow-up solutions are only avoided provided that haptorepellence, degradation of ECM, production of cancer cells and remodelling of ECM are able to move cancer cells away from location Y at a rate quicker than any additional cancer cells that are moved to location Y from the reaction-boosted flux terms. We remark that finite time blow-up solutions do not appear for all ranges of parameter values considered for this model and that any results breaking the volume filling criterion of $1 - c - v \geq 0$ appear to be quickly righted. In addition, we note that the choice of volume filling in the chemotaxis sensitivity function, cancer cell production and ECM remodelling all decrease the likelihood of finite time blow-up solutions. Finally, we remark that as there appears to only be a minor violation of $1 - c - v \geq 0$, we can consider this to still make biological sense as the definition for maximum amount of cancer cells at one location may be slightly increased at times when there are additional pressures abusing the plasticity of the cell.

4.3 Results

We will present two invasion scenarios in this chapter: Invasion Scenario 0A and 0B. The former represents the growth and spread of cancer cells from an initial central mass as may be representative of an *in vivo* evolution of a cancerous mass while the latter represents cancer cell invasion from an initial strip along the LHS of the domain as may be more representative of a style of *in vitro* experiments.

Here we present numerical simulations of the proposed model represented by equations (4.9)–(4.14) under zero flux boundary conditions prescribed by the homogenous Neumann boundary conditions in two spatial dimensions, although we note that as the initial conditions and results are radially symmetric in Invasion Scenario 0A and the multiplicity of results and the initial conditions along the y-axis of Invasion Scenario 0B that interpretation of results obtained under a one dimensional spatial region would be as full and as valid as those obtained from the presented model.

In some of the plots of the figures presented in this chapter we have added an overlay of the contour of $c = 0.01$ in either white or black where we have defined this to be the extent of cancer invasion. This is done to add clarity when interpreting the data represented in the plots and is stated in the caption of each plot where relevant.

In addition to the model variables of c, v, m_s, m_t, T and f, we employ two "dummy variables" of Δv_{m_s}, where $\dfrac{\partial \Delta v m_s}{\partial t} = \delta_1 v m_s$, and $\Delta v m_t$, where $\dfrac{\partial \Delta v_{m_t}}{\partial t} = \delta_1 \delta_2 v m_t$, to record how much ECM has been degraded by either MMP-2 or MT1-MMP at each point within the considered domain. We will also present functions of these variables where it is beneficial to the interpretation of the results, namely, $\varnothing = 1 - c - v$ to represent the unfilled space left by the cancer cells and ECM

components and $\Delta v_{total} = \Delta vm_s + \Delta vm_t$ to represent the total degradation as caused by both MMP-2 and MT1-MMP. We note that for $0 < \varnothing \leq 1$ we have some empty space where $\varnothing = 1$ means there are no cancer cells or ECM components present, $\varnothing = 0$ no empty space and $\varnothing < 0$ we have an overcrowding problem. For Δv_{total} we note that there would be a initial value of zero at all coordinates and there would be an upper bound of 1 in the case where there is no ECM remodelling ($\mu_v = 0$) but as we have presented a model with ECM remodelling ($\mu_v > 0$), we have no upper bound on this function.

We begin with the following remarks that all results obtained from the model defined by the equations (4.9)–(4.14) will have: (i) the spatially homogeneous condition of $1 - c - v \geq 0$, (ii) the solutions are tending to the only stable spatially homogeneous steady state of $(1, 0, 21.25, 19.37, 0.01, 0.81)^T$ when using the parameters found in Table 4.4 and that this is most clear in the plots of Figure 4.13 E&H, Figure 4.14 B&E and Figure 4.15 C&F, (iii) $\varnothing > 0$ for all cases where ECM is degraded beyond the cancer cell invasion boundary.

If we assume at some time $t = \check{t}_1$ there is an area of cancer cells of "P" and want to compare this area to that found at a later time of $t = \check{t}_2$ where there has been an increase in depth of invasion by "r" in a square domain of length "d", we find this difference in areas to be $\pi r^2 - P$ for Invasion Scenario 0A and $dr - P$ for Invasion Scenario 0B. In other words, we have a quadratic increase of region where there exists at least some cancer cells in Invasion Scenario 0A compared to the linear increase in Invasion Scenario 0B when we increase the invasion depth of the cancer cell boundary into the ECM.

Invasion Scenario 0A is the first Invasion Scenario that we consider, where a cancer mass in the centre of a domain invades outwards in a radial fashion with the

initial conditions representing the initial cancer mass distributed in a Gaussian distribution of $e^{-((x^2+y^2)/0.02)}$ (Figure 4.8, plot A) in the centre of a square region of tissue that satisfies the initial condition $v(t=0) = 1 - c(t=0)$ (Figure 4.8, plot D). This cancer mass is determined to have an initial concentration of the enzymes and enzyme complexes of the same distribution of the cancer cell mass but with the increased magnitude of $5 \times c(t=0)$ and is therefore implicitly shown as a scaled-by-5 version of Figure 4.8, plot A. We use the baseline parameters of Table 4.4 to solve over a 2D spatial square domain of length 0.4cm and time range 0-4.6 days with results plotted at 0, 2.3 and 4.6 days ($t = 0, 20, 40$).

As can be seen from the plots in Figure 4.8 A–C, we observe a radially symmetric growth of the cancer cell mass with an equivalent reduced state of ECM shown in the plots of Figure 4.8 D-F and the degraded ECM of Figure 4.8 G&H. We note that the spatially homogeneous, stable steady state calculated above of $(c^*, v^*, m_s^*, m_t^*, T^*, f^*)^T = (1, 0, 21.25, 19.37, 0.01, 0.81)^T$ is beginning to emerge in the centre of the region where $c(\mathbf{x} = (0,0)) = 1, v(\mathbf{x} = (0,0)) = 0$.

If we consider the region where $c \geq 0.01$ and $v \geq 0.01$ as the cancer-ECM interface and provide approximations for the concentrations of MMP-2 (1-4nM) and MT1-MMP (0.1-5nM) within this region, then we can provide further approximations for these concentrations to the spatially homogeneous steady state and compare favourably with biological data found in for MMP concentration in serum for various forms of cancer, as previously outlined, of MMP-2 = 2.81-10.03nM and MT1-MMP= 0.04-0.38nM.

From the plots of Figure 4.8 G&H we see the location and amount of ECM that has been degraded in total. We note that this goes above the non-dimensionalised value of 1 which was defined to be the maximum amount of ECM in any location. The degradation of an amount above the value of 1 is due to the remodelling term

in the ECM equation ($\mu_v(1-c-v)$) creating new macromolecules of ECM when there is sufficient space for fibroblasts to do so. In the centre of the domain, where there is considered to be an initial mass of cancer cells reaching the maximum density ($c(\mathbf{x}=(0,0),t=0)=1$) and a complete lack of ECM components ($v(\mathbf{x}=(0,0),t=0)=0$, there is a lack of ECM degradation throughout the considered timeframe. This fulfils the volume filling criterion at that location for the remodelling term and so no ECM macromolecules are produced throughout the considered timeframe and therefore no ECM is degraded at this location. Finally, we observe that there has been degradation of the ECM beyond the cancer cell invasion boundary.

We can see an increase in the distribution of enzymes to a more radially expansive region as motivated by the spread of the cancer cells as well as an increase in maximum concentration towards the stable, spatially homogeneous steady state for m_s and m_t and a decrease in maximum concentration towards the stable, spatially homogeneous steady state for T and f as seen in the distributions shown in the plots of Figure 4.9 at $t=20$ and Figure 4.10 at $t=40$.

When we examine the variables m_s and m_t in particular we see the increase in region and magnitude from 5×Figure 4.8 A to Figure 4.9 A&B to Figure 4.10 A&B but to focus on the characteristics of the MMPs at the interface between the cancer cells and the ECM, we look at the plots of Figure 4.9 D&E and Figure 4.10 D&E. The plots of specific MMP-2 concentration ranges of $0.25 \leq m_s \leq 1$ (red region) and $m_s > 1$ (blue region) in Figure 4.9 D and Figure 4.10 D demonstrate that MMP-2 is free to diffuse beyond what is defined to be the boundary of the cancer cell mass to the point where almost all of the red region at $t=20$ is outside the cancer cell invasion boundary while at $t=40$ all of the red region and a minimal amount of the blue region is outside the cancer cell invasion boundary. This is in stark contrast to the MT1-MMP profile shown in Figure4.9 E and

Figure 4.10 E (where we define $0.25 \leq m_t \leq 1$ to be the red region and $m_t > 1$ to be the blue region) where neither the red nor the blue regions have been able to move past the boundary of the cancer cells as the only movement that MT1-MMP proteins can make is while attached to a cancer cell. This shows that all degradation of the ECM ($\delta v(m_s + m_t)$) beyond the cancer cell boundary must be due to MMP-2 rather than MT1-MMP while the increased concentration of MT1-MMP over MMP-2 in the region closest to the centre of the cancer mass (defined as the region where $m_t > m_s$). We also note that the distance between the red and blue regions is increased for MMP-2 from that of MT1-MMP.

We examine the variables of T and f and find that there is not an increase in the magnitude of the variables as they tend towards the stable, spatially homogeneous steady state values of 0.01 and 0.81 respectively however we do see the region in which they exist expanding due to the spread of c (cf. Figure 4.9 C&F and Figure 4.10 C&F). We note that there is a similarity between their relation and the relation between m_s and m_t where T is freely diffusible and can therefore travel beyond the extent of the cancer cell invasive boundary while f is limited in movement to the transport by cancer cells. We consider that there is such low concentration of T to mean that any free TIMP2 that is produced or released from a complex is quickly bound to either free MT1-MMP or MMP-2. We note that there is an increase in both the T and f variable at the leading edge of the cancer cell invasion.

Expanding on the observations made from the plots of Figure 4.8 G&H, in Figure 4.11 we have that ECM degradation beyond the cancer invasive front is the sole domain of the freely diffusible MMP-2, m_s while the degradation of ECM components within this cancer invasion front is shared by both the MMPs. The precise amount of ECM that has been degraded by each MMP is elucidated in the plot of Figure 4.12 B.

In the final figure presented for this Invasion Scenario, Figure 4.12, we compare the subdomain integrations of the variables and functions of $v, c, \varnothing, \Delta v_{total}, \Delta v_{m_s}$ and Δv_{m_t} to examine the contributions of the variables to the dynamics of the model across the considered timeframe of $t = 0 - 40$, corresponding to a 4.6 days consideration. We note that the non-dimensionalisation where we defined the maximum amount cancer cells or ECM components to exist as being equal to 1 has the consequence of the maximum of the total amount of cancer cells or ECM components (subdomain integration of c and v) over a square domain of length 4 to be 16. This does not, however, provide a maximum value for the summation of the total ECM degraded as the ECM is continually remodelled (density increased) where there is the space for it to do so, i.e., where $\varnothing > 0$.

In the plot of Figure 4.12 A, we focus on the summation of total density of the ECM, cancer cells and the free space, $\varnothing$, that is left for either of these to be produced or be moved into. We note that there appears to be a near linear growth in free space, $\varnothing$, over the considered timeframe while the total ECM density is reduced quadratically and the total amount of cancer cells increases quadratically. We observe that while the total of cancer cells is strictly increasing, after some small initial time it is always below the total free space. This means that for this Invasion Scenario 0A we have an ECM that is reduced to a level more than twice than would be needed to simply provide space for the cancer cells to be produced/move into for the entirety of the considered timeframe (after some small time has elapsed). In fact, for this specific scenario we have that the ECM is reduced to a level over three times the required amount for the entirety of the considered timeframe, again after some small elapsed time.

In the plot of Figure 4.12 B, it is abundantly clear that the bulk of degradation of the ECM over the considered timeframe is due to the soluble MMP-2 where degradation by either of the MMPs increases quadratically. This is due to the

t	c	v	$\varnothing$	m_s	m_t	T	f	Δv_{total}	Δv_{m_s}	Δv_{m_t}
0	0.06	15.94	0	0.31	0.31	0.31	0.31	0	0	0
20	0.57	13.14	2.29	5.29	6.02	0.04	1.19	7.29	6.21	1.08
40	2.01	9.11	4.88	24.75	25.69	0.07	3.14	25.72	23.04	2.68

Table 4.5: *Invasion Scenario 0A. Table showing the subdomain integration at* $t = 0, 20$ *and* $t = 40$ *(corresponding to 0 days, ∼2.3 days and ∼4.6 days) of the model variables in addition to the inclusion of how much degradation has occurred due to each and both of the MMPs considered.*

ability of MMP-2 to diffuse beyond the cancer cell boundary into regions where there is a higher amount of intact ECM components.

Data which is not be immediately clear from the figures in this subsection of Section 4.3 is shown in Table 4.6 where $\varnothing$ represents the empty space of $1-c-v$ and $\Delta v_{total}, \Delta v_{ms}$ and Δv_{mt} represent the amounts of of ECM degraded in total, by MMP-2 and by MT1-MMP, respectively. Additional interpretation of the data presented in this table is offered up in Section 5.3.

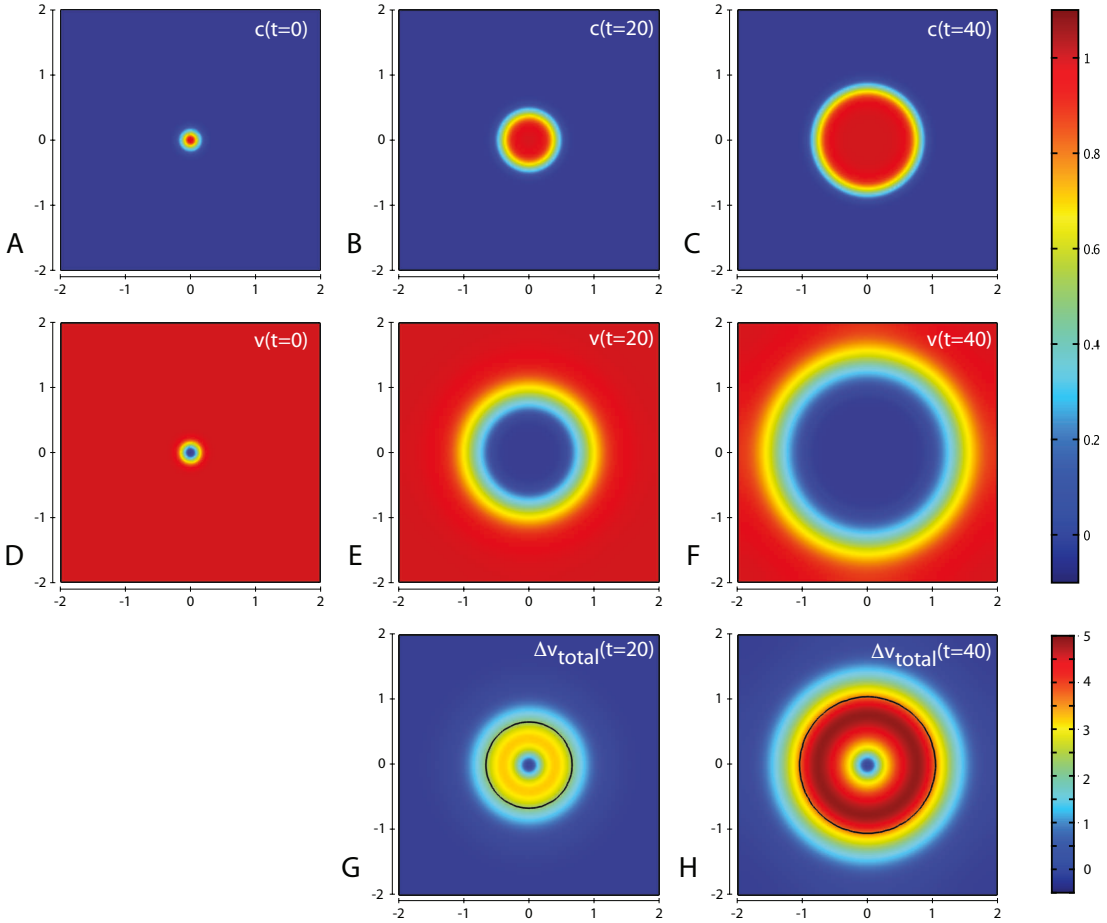

Figure 4.8: *Invasion Scenario 0A. Plots A-C show the time evolution of the cancer cell densities from* $t = 0$ *through* $t = 20$ *(corresponding to ∼2.3 days) to* $t = 40$ *(corresponding to ∼4.6 days) with plots D-F showing the corresponding ECM densities and plots G&H showing how much ECM has been degraded across the domain where the black contour line shows the cancer cell density at level 0.01, chosen to represent the maximum extent of invasion. Simulations are performed using the baseline parameter set of Table 4.4.*

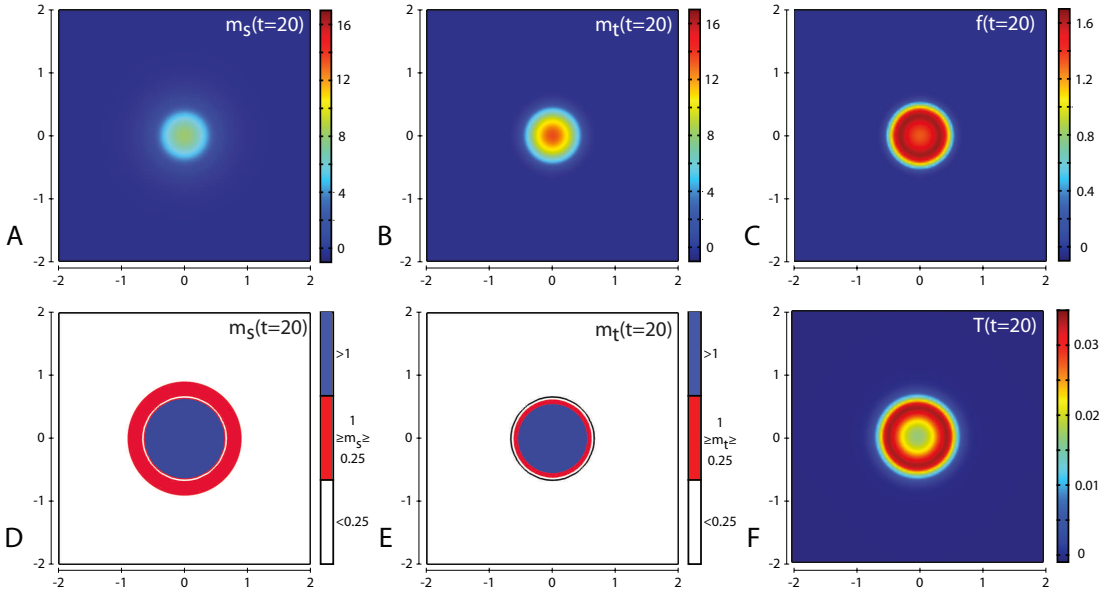

Figure 4.9: *Invasion Scenario 0A. The concentrations of MMP-2, MT1-MMP, the intermediary complex f and TIMP2 at $t = 20$ (corresponding to ∼2.3 days) are shown in plots A,B,C and F respectively. Plots D&E show the MMP-2 and MT1-MMP concentrations again at $t = 20$ but with appropriate thresholds to indicate the enzyme distributions near the invasive front of the cancer cell invasion. The white contour line in plot D and black contour line in Plot E show the cancer cell density at level 0.01 chosen to represent the maximum extent of invasion. Simulations are performed using the baseline parameter set of Table 4.4.*

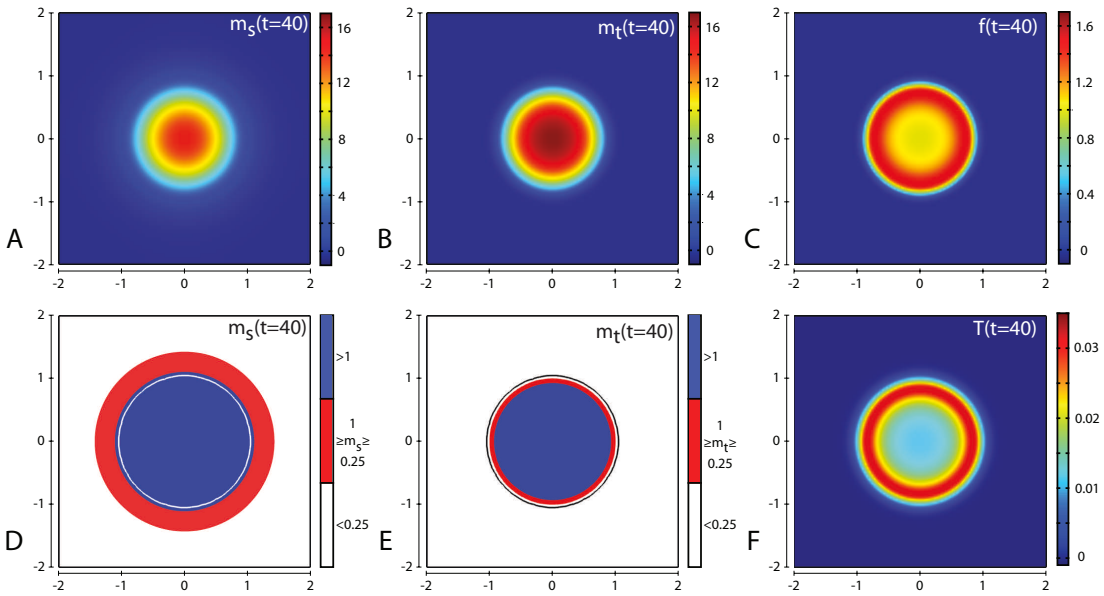

Figure 4.10: *Invasion Scenario 0A. The concentrations of MMP-2, MT1-MMP, the intermediary complex f and TIMP2 at $t = 40$ (corresponding to ∼4.6 days) are shown in Plots A,B,C and F respectively. Plots D&E show the MMP-2 and MT1-MMP concentrations again at $t = 40$ but with appropriate thresholds to indicate the enzyme distributions near the invasive front of the cancer cell invasion. The white contour line in plot D and black contour line in plot E show the cancer cell density at level 0.01 chosen to represent the maximum extent of invasion. Simulations are performed using the baseline parameter set of Table 4.4.*

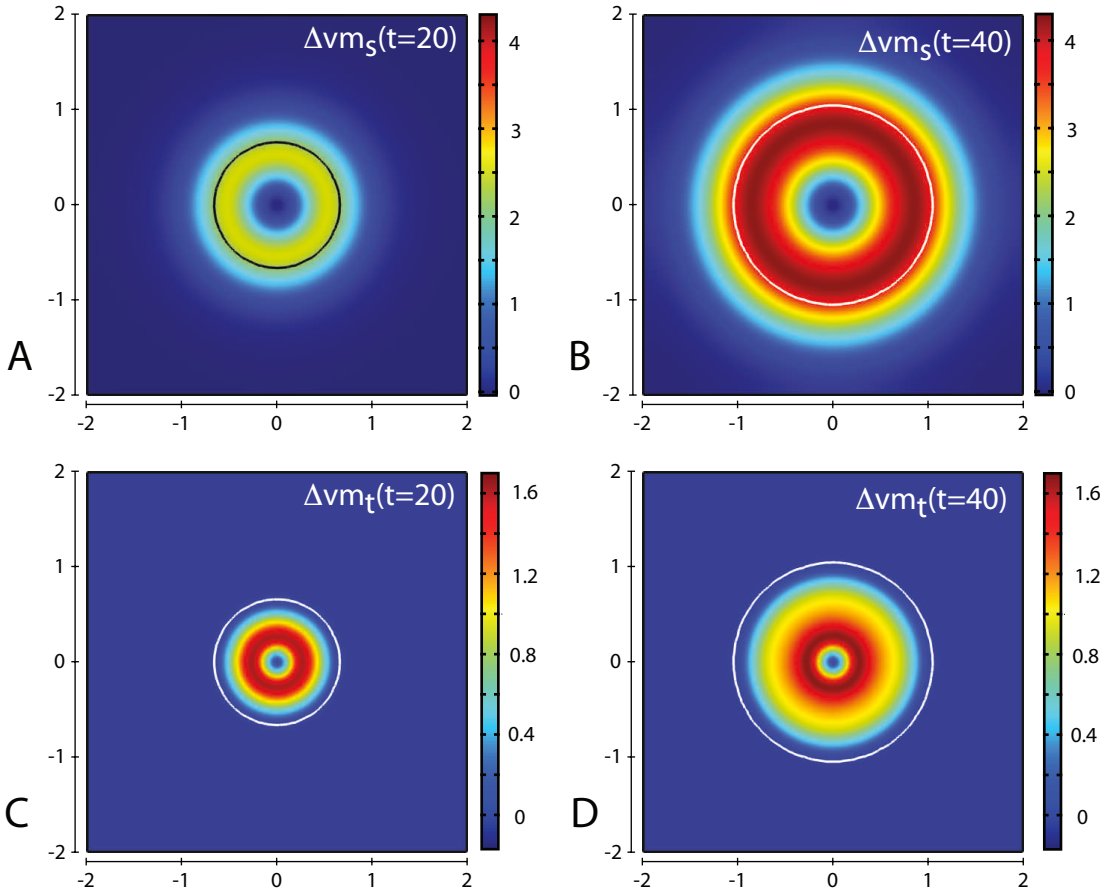

Figure 4.11: *Invasion Scenario 0A. Plots A & B show the profiles of the density of ECM degraded solely by m_s, while plots C & D show the profiles of the density of ECM degraded solely by m_t at $t = 20$ and 40 (corresponding to ∼2.3 and 4.6 days, respectively). The white contour line in plots B-D and black contour line in plot A shows the cancer cell density at level 0.01 chosen to represent the maximum extent of invasion. Simulations are performed using the baseline parameter set of Table4.4.*

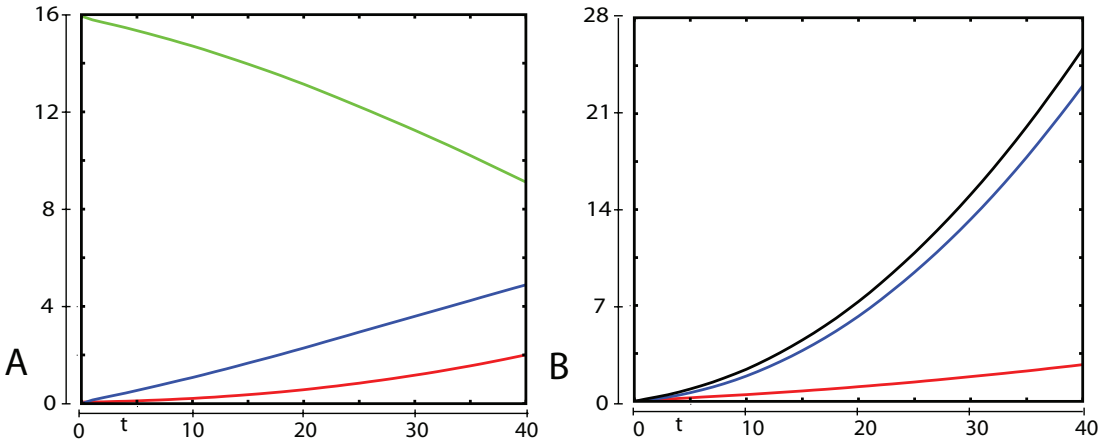

Figure 4.12: *Invasion Scenario 0A. Plot A shows the subdomain integration of the density of ECM (green), cancer (red) and empty space (blue) over the full time range considered (t=0-40). Plot B shows the subdomain integration of the amount of ECM degraded in total (black), solely by m_s (blue) and solely by m_t (red). Simulations are performed using the baseline parameter set of Table4.4.*

Invasion Scenario 0B is the second Invasion Scenario that we consider, where a set of initial conditions to create a situation where the cancer cell mass forms a strip along the LHS of the domain and invades an ECM construct defined initially as $v(t=0) = 1 - c(t=0)$ from left to right as is illustrated in the plots of Figure 4.13 A&B. While in the previous Invasion Scenario we considered the enzymes to have an initial condition of a scaled $5\times$ the distribution of c, in this scenario we consider the enzyme concentrations to be of the same magnitude as the initial cancer cell distribution, i.e. $m_s(t=0) = m_t(t=0) = f(t=0) = T(t=0) = c(t=0)$. We solve the system of equations over a 2D spatial square domain of length 0.4cm and time range 0-11.5 days and plot the data at 0, 1.15, 5.75 and 11.5 days ($t = 0, 10, 50, 100$). We use the same baseline parameter set as in the previous Invasion Scenario of Table 4.4 and as such we have the same stable, spatially homogeneous steady state that the solutions tend to over time of $(c^*, v^*, m_s^*, m_t^*, T^*, f^*)^T = (1, 0, 21.25, 19.37, 0.01, 0.81)^T$, however this dynamic

is much clearer here as can be seen by the plots of Figures 4.13 E&H, 4.14 C&F and 4.15 C&F.

As can be seen from the plots in Figure 4.13 A,C-E, we observe an invasion through the domain from left to right where unlike the previous scenario, we have linear rather than quadratic growth of the cancer invasion boundary with corresponding ECM density profiles shown in the plots of Figure 4.13 F–H. The plot of Figure 4.17 A offers further clarification where it can be seen that after $\sim t = 40$ there appears to be a linear increase in cancer cell density of approx. 1 per $12.5t$ matched by an equal decrease in total ECM component density.

To focus on the characteristics of the MMPs at the interface between the cancer cells and the ECM, as well as at other locations, we examine Figure 4.14 for the time evolution of these enzymes and Figure 4.16 for the amount of ECM that each MMP is able to degrade. The plots of specific MMP-2 concentration ranges of $0.25 \leq m_s \leq 1$ (red region) and $m_s > 1$ (blue region) in Figure 4.14 C demonstrates the ability of MMP-2 to freely diffuse beyond what is defined to be the boundary of the cancer cell mass to the point where it can become the sole cause of ECM degradation (cf. Figure 4.16) while the limits of MT1-MMP being present only on the cancer cells surface limits its range to the cancer invasion boundary Figure 4.15 F and impacts upon its influence on ECM degradation (cf. plots of Figure 4.16 D–F).

If we consider the region between c=0.01 and v=0.01 as the cancer-ECM interface and provide approximations for the concentrations of MMP-2 (1-5.5nM) and MT1-MMP (0.1-5nM) within this region, then we can provide further approximations for these concentrations to the spatially homogeneous steady state and can compare favourably with biological data found in various forms of cancer (outlined previously on Page 60) of MMP-2 = 2.81-10.03nM and MT1-MMP=

0.04-0.38nM. We can see an increase in the growth and spread of enzymes to more of the domain as motivated by the spread of the cancer cells and the diffusion of m_s with the stable, spatially homogeneous steady state solutions for m_s and m_t of 21.25 and 19.37 respectively in Figure 4.14 C&F.

We examine the variables of T and f in Figure 4.15 can see that the intermediate complex, f, while beginning near its own stable, spatially homogeneous steady state of 0.81, increases to a value of almost double that in the plot of Figure 4.15 A while experiencing a steep descent to 0nM beyond the cancer cell boundary. There is a rapid drop in concentration of TIMP2 from the initial condition where there was a maximum value of 1 by time $t = 10$ towards the stable, spatially homogeneous steady state, however it is free to diffuse beyond the cancer cell boundary. We consider that there is such low concentration of T to mean that any free TIMP2 that is produced or released from a complex is quickly bound to either free MT1-MMP or MMP-2. We note that there is an increase in both the concentrations of TIMP2 and the intermediate complex, f at the leading edge of the cancer cell invasion while the concentrations of these variables have reached their steady state values for a large region of the established cancer mass.

In Figure 4.16 we note that at the furthest LHS of the domain ($\mathbf{x} = (-2, y)$), where there is considered to be an initial mass of cancer cells reaching the maximum density ($c = 1$) and a complete lack of ECM components ($v = 0$), there is a lack of ECM degradation throughout the considered timeframe (Figure 4.16 A–F) as a result of the volume filling component of the "growth" term of the ECM forbidding the production of ECM components and therefore their degradation. Secondly, we have that ECM degradation beyond the cancer invasive front is the sole domain of the freely soluble MMPs, m_s while the degradation of ECM components within this cancer invasion front is shared by both the soluble and bound MMPs.

Third and finally, in Figure 4.17, we compare the subdomain integrations of the variables and functions of $v, c, \varnothing, \Delta v_{total}, \Delta v_{m_s}$ and Δv_{m_t} to examine the contributions of the variables to the dynamics of the model across the considered timeframe of $t = 0 - 100$, corresponding to a 11.5 days consideration. We note that the non-dimensionalisation where we defined the maximum amount cancer cells or ECM components to exist as being equal to 1 has the consequence of the maximum of the total amount of cancer cells or ECM components (subdomain integration of c and v) over a square domain of length 4 to be 16. This doesn't, however, provide a maximum for the summation of the total ECM degraded as the ECM is continually remodelled (density increased) where $\varnothing > 0$.

In the plot of Figure 4.17 A, we focus on the summation of total density of the ECM, cancer cells and the free space, $\varnothing$, that is left for either of these to be produced/moved into. We note that the free space, $\varnothing$ appears to reach a steady state of 3.7 after $t = 40$ although this would not be able to continue indefinitely due to boundary effects. It is at the point where the free space reaches that the total amount of cancer cells reaches a linear increase of approx. 1 per $12.5t$ matched by an equal decrease in total ECM component density.

In the plot of Figure 4.17 B, it is abundantly clear that the bulk of degradation of the ECM over the considered timeframe is due to the soluble MMP-2 where degradation by either of the MMPs increases quadratically. This is due to the ability of MMP-2 to diffuse beyond the cancer cell boundary into regions where there is a higher amount of intact ECM components.

Data which is not be immediately clear from the figures in this subsection of Section 4.3 is shown in Table 4.6 where $\varnothing$ represents the empty space of $1 - c - v$ and $\Delta v_{total}, \Delta v_{ms}$ and Δv_{mt} represent the amounts of of ECM degraded in total, by MMP-2 and by MT1-MMP, respectively.

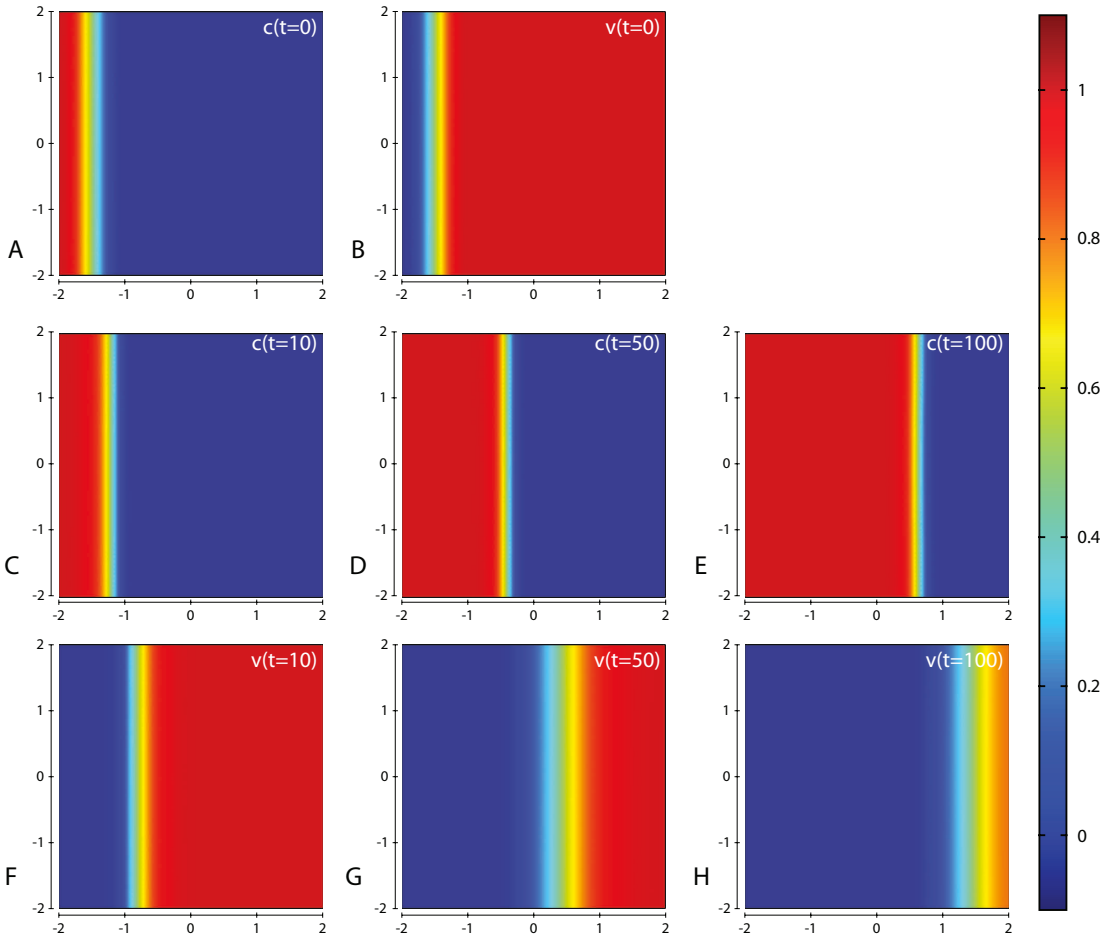

Figure 4.13: *Invasion Scenario 0B. Plots A & B show the profiles of the initial conditions for the cancer cell density and ECM density. Plots C-E show the time evolution of the profile of cancer cell density at* $t = 10, 50$ *and* 100 *(corresponding to* $\sim$*1.15, 5.75 and 11.5 days, respectively). Plots F-H show the profiles of the ECM density at* $t = 10, 50$ *and* 100*. Simulations are performed using the baseline parameter set of Table4.4.*

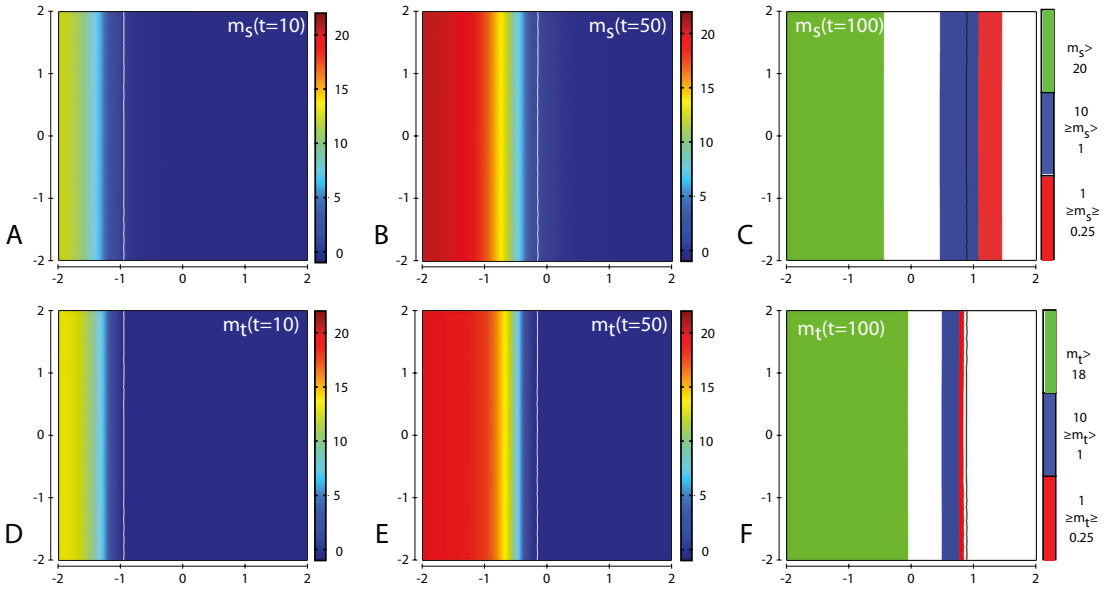

Figure 4.14: *Invasion Scenario 0B. Plots A-C show the profiles of MMP-2 concentration, while plots D-F show the profiles of MT1-MMP concentration at* $t = 10, 50$ *and* 100 *(corresponding to* $\sim$*1.15, 5.75 and 11.5 days, respectively). The white contour line in plots A, B, D & E and the black contour line in plots C & F shows the cancer cell density at level 0.01 chosen to represent the maximum extent of invasion. Simulations are performed using the baseline parameter set of Table4.4.*

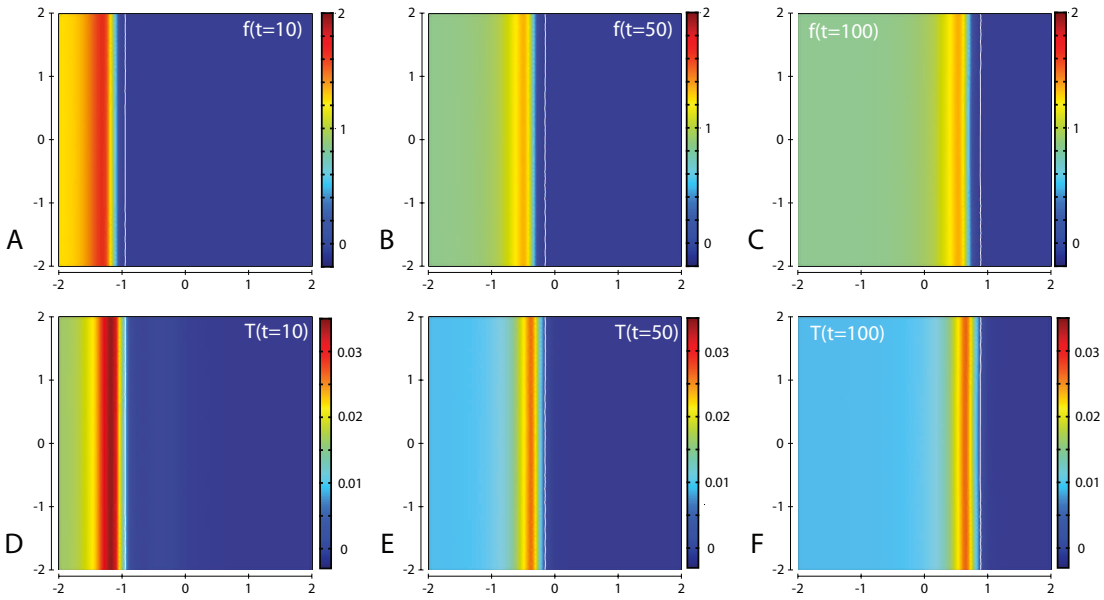

Figure 4.15: *Invasion Scenario 0B. Plots A-C show the profiles of the complex function f (where f is MT1-MMP:TIMP2:proMMP-2) concentration, while plots D-F show the profiles of TIMP2 concentration at $t = 10, 50$ and 100 (corresponding to $\sim$1.15, 5.75 and 11.5 days, respectively). The white contour line in plots A-F shows the cancer cell density at level 0.01 chosen to represent the maximum extent of invasion. Simulations are performed using the baseline parameter set of Table4.4.*

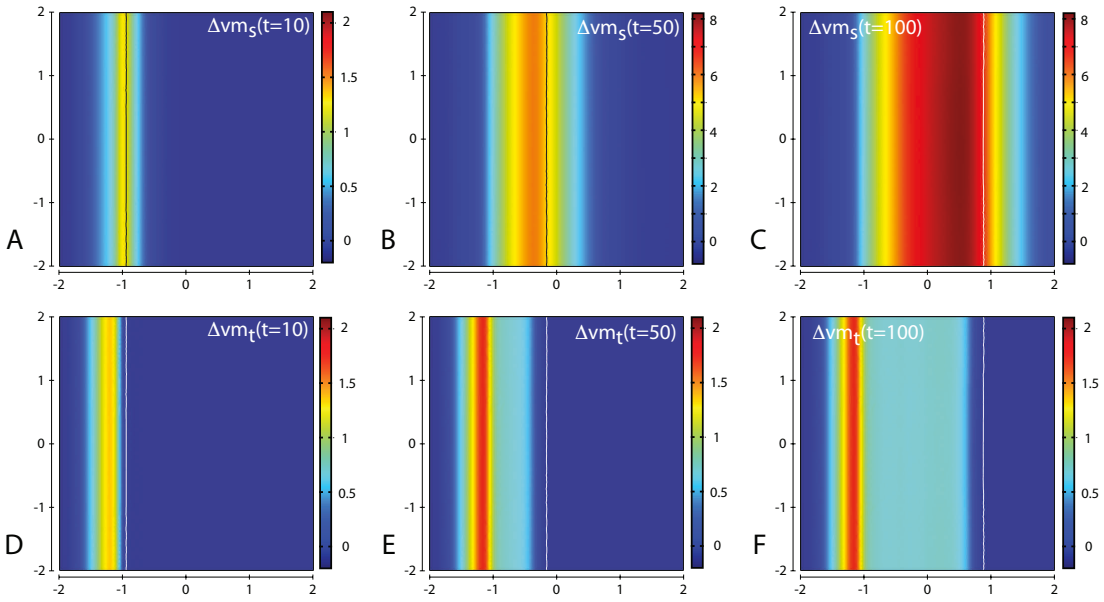

Figure 4.16: *Invasion Scenario 0B. Plots A-C show the profiles of the density of ECM degraded solely by m_s, while plots D-F show the profiles of the density of ECM degraded solely by m_t at $t = 10, 50$ and 100 (corresponding to ∼1.15, 5.75 and 11.5 days, respectively). The white contour line in plots C-F and black contour line in plots A &B shows the cancer cell density at level 0.01 chosen to represent the maximum extent of invasion. Simulations are performed using the baseline parameter set of Table4.4.*

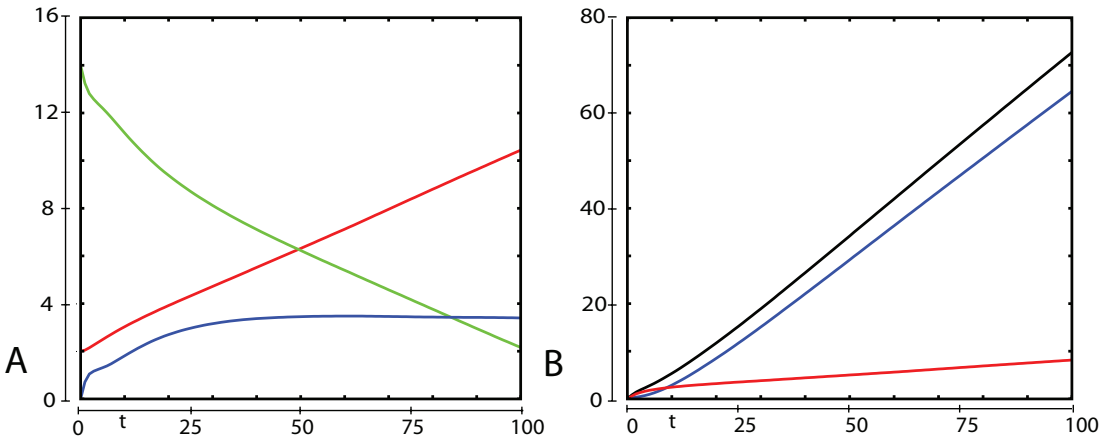

Figure 4.17: *Invasion Scenario 0B. Plot A shows the subdomain integration of the density of ECM (green), cancer (red) and empty space (blue) over the full time range considered (t=0-100). Plot B shows the subdomain integration of the amount of ECM degraded in total (black), solely by m_s (blue) and solely by m_t (red). Simulations are performed using the baseline parameter set of Table4.4.*

t	c	v	$\varnothing$	m_s	m_t	T	f	Δv_{total}	Δv_{m_s}	Δv_{m_t}
0	2.00	14.00	0	2.00	2.00	2.00	2.00	0	0	0
10	3.03	11.16	1.81	31.55	34.79	0.10	4.96	5.36	2.89	2.47
50	6.32	6.23	3.45	113.82	107.82	0.09	6.38	34.20	29.18	5.02
100	10.44	2.16	3.4	201.07	187.57	0.13	9.75	72.73	64.56	8.17

Table 4.6: *Invasion Scenario 0B. Table showing the subdomain integration at $t = 0, 10, 50$ and 100 (corresponding to 0 days, ∼1.15 days, ∼5.75 days and ∼11.5 days) of the model variables in addition to the inclusion of how much degradation has occurred due to each and both of the MMPs considered.*

4.3.1 Parameter Sensitivity

In order to determine the sensitivity of the result dependent on the individual parameters of the model, we perform additional simulations almost identical to Invasion Scenario 0A where the only change is a single parameter by an increase of 50%. We record the value of the subdomain integral of c ($\int c \, \mathrm{d}\mathbf{x}$) at $t = 25$ and present this data in Figure 4.18 where we consider how much each parameter change has affected the result of $\int c \, \mathrm{d}\mathbf{x}$ as a proportion of the maximum change achieved by a single parameter change (ϕ_{53} has an 83% decrease in $\int c \, \mathrm{d}\mathbf{x}$ at $t = 25$).

By showing the sensitivity to each parameter we have performed a partial mathematical parameter sensitivity of the total amount of c at $t = 25$ to an increase of 50% to the parameters of the model but to consider biological concerns where we consider the sensitivity of the model to the sources of the parameters, we have to consider the cases where we not only have caused a 50% increase to the individual parameters but also to certain groupings of parameters. We define the specified groupings of parameters to be where parameters are linked by either having the same source or where one is defined in terms of the other. Included at the bottom right of Figure 4.18 are the 5 cases where we have considered changes to multiple, grouped parameters at once. Namely, $\phi_{31}\&\phi_{51}$, $\phi_{32}\&\phi_{62}$, $\phi_{41}\&\phi_{52}\&\phi_{61}$, $\phi_{42}\&\phi_{53}\&\phi_{63}$ and δ_1 (where $\delta_1\delta_2$ unchanged). By performing this additional sensitivity analysis we have found that while there was a large decrease in the total amount of cancer cells at $t = 25$ by the parameters of ϕ_{41} and ϕ_{53}, when the coupled sets of biological parameters of $\phi_{41}, \phi_{52}, \phi_{61}$ and $\phi_{42}, \phi_{53}, \phi_{63}$ are each increased by 50%, there is in fact an increase in total amount of cancer cells at $t = 25$.

The parameters that have the biggest affect on an increase in the overall number

of cancer cells when they are increased by 50% are μ_c and D_c. While the cancer cell production rate is unsurprisingly the parameter with the largest effect, we note that the increase in diffusion rate of cancer cells having a larger effect than the increase in haptotaxis is likely due to the volume filling that exists for the haptotaxis but not diffusion of cancer cells where the diffusion allow cancer cells to travel through regions where $1 - c - v = \epsilon$ for some $0 \leq \epsilon << 1$ which would act as a barrier or significant reduction factor to the haptotaxis mediated displacement of cancer cells.

We note that an increase in δ_1 where $\delta_1\delta_2$ is unchanged causes a higher increase in total cancer cells than an increase in δ_2. This is unsurprising as MMP-2 is found to be responsible for the bulk of collagenolysis when compared with MT1-MMP.

We therefore identify the parameters of μ_v and α_T as being the most relevant parameters that cause an decrease in the total amount of cancer cells at $t = 25$ when they are increased by 50%. While these parameters for ECM remodelling and TIMP2 production would reasonably be expected to fulfil this described role, we note that the parameter α_T actually has a much more complicated relationship with the progression of cancer. We expand on this by showing the effect of changing α_T in Figures 4.19 and 4.20 on the steady state values of m_s, m_t, f and T by representing the percentage change from the values obtained when $\alpha_T = 4$, the rate of TIMP2 production found in Table 4.4. As we note that the amount of free TIMP2 plays a significant role in determining whether there is MMP-2 activated and in how much free MT1-MMP or MMP-2 are able to degrade the ECM.

Figure 4.19 shows that for too small or too high a value of α_T, there is a decrease in the total amount of active MMP-2 and that the total amount of active MT1-MMP is strictly decreasing for an increasing TIMP2 production. This is line

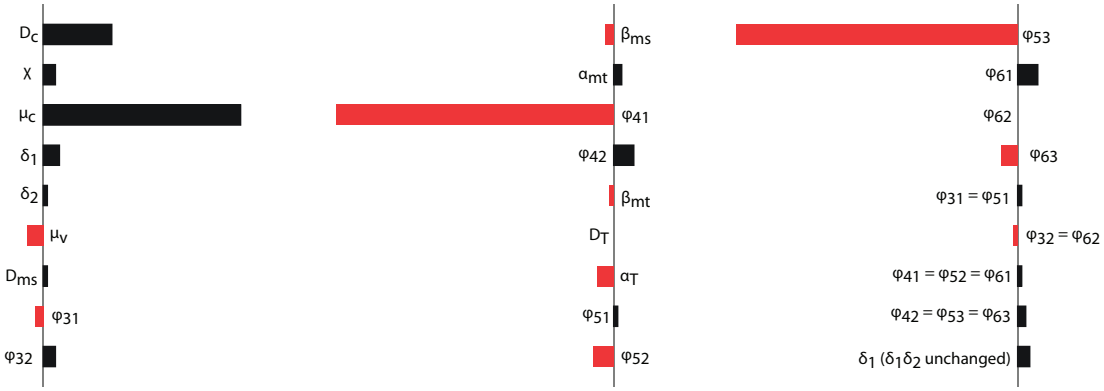

Figure 4.18: *We show how much of a change there is in* $\int c\,\mathrm{d}\mathbf{x}$ *at* $t = 25$ *when each individual parameter listed in Table4.4 is increased by 50%. The black bars indicate the amount of increase while the red bars indicate the amount of decrease. We scale each result by the maximum decrease of 83% that was achieved by* ϕ_{53}

with the numerical study of the activation system of MMP-2 by Karagiannis and Popel (2004) where they find the same relation when considering a system of ODEs that lack production of enzymes but have that there is a value for the initial concentration of TIMP2 that provides a maximum rate of MMP-2 activation from proMMP-2 and which a lower or higher concentration of TIMP2 reduces this rate.

4.4 Discussion

In this chapter we established a PDE model for cancer invasion of tissue, focussing on the roles of the soluble MMP, MMP-2 and the bound MMP, MT1-MMP. We also considered their interactions with one another where MT1-MMP plays a role in the activation of MMP-2 from its proenzyme state. This advanced upon previous mathematical models of cancer cell invasion that used either generic matrix degrading enzymes and could be considered to be parallel to works that focus on the uPA system in cancer cell invasion. The presented work also furthers mathematical modelling of MMP-2 activation that has thus far tended to focus

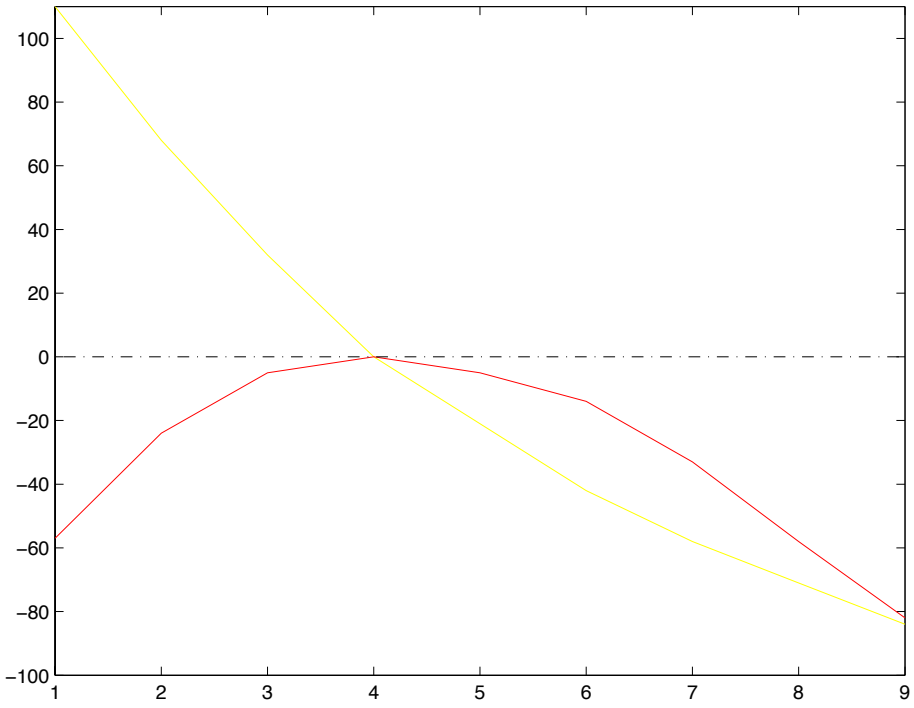

Figure 4.19: *The percentage increase or decrease in the steady state values of the variables m_s and m_t from the steady state values obtained from Table 4.4 when the parameter α_T is increased or decreased by a unit amount from the initial value of $\alpha_T = 4$ to a minimum of 1 and maximum of 9. We represent the change in active MMP-2 by the red line and the change in active MT1-MMP by the yellow line.*

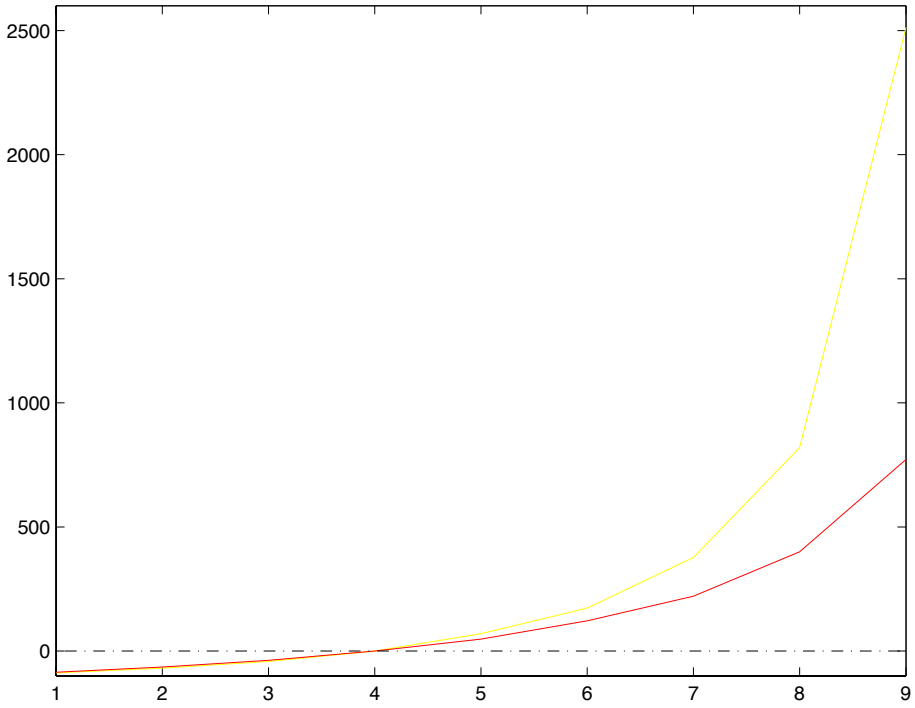

Figure 4.20: *The percentage increase or decrease in the steady state values of the variables T and f from the steady state values obtained from Table 4.4 when the parameter α_T is increased or decreased by a unit amount from the initial value of $\alpha_T = 4$ to a minimum of 1 and maximum of 9. We represent the change in the intermediate function f by the red line and the change in TIMP2 by the yellow line.*

upon ODE models. The potential of the presented model to consider rich ECM environments is examined in the following chapter.

We determined the appropriate forms of functions as defined by the background biology that would cause an increase to the cancer cell and ECM component populations while showing functions that previously pubished models have chosen to use. This incorporated the key biological rules of mitosis in cancer cells and the remodelling of ECM by fibroblasts not being reliant on the presence of ECM while also incorporating the competition for space in these inter- and intra- cancer cells and ECM reactions. The paradigms of a volume filling model of two variables were established to be $1 - c - v \geq 0, c \geq 0$ and $v \geq 0$.

To formulate our model, we first had to establish which dynamics of the MMP-2 activation system would be incorporated into our model and settled on a reduced version of the system as outlined in Figure 4.2. We then presented the model in dimensionalised and non-dimensionalised forms before determining the best parameters for the model from either previous mathematical models or the biological literature. Where parameters were not directly obtainable, we presented two smaller mathematical models of the MMP-2 activation system to determine appropriate estimations of the parameters.

A steady state analysis was performed to find that there exists one stable, spatially homogeneous steady state that the solution of the model will tend to as $t \to \infty$. This solution represented the case where cancer has fully invaded the domain and no ECM was present. With the baseline parameter set of Table 4.4, values for the steady state approximation of the concentration of MMP-2 was found to be 21.25nM and for MT1-MMP this was found to be 19.37nM. The concentrations of TIMP2 and the intermediate complex of TIMP2:MT1-MMP were

noticeably lower at 0.01nM and 0.81nM, respectively. This lower value is determined to be due to the relation of the production of TIMP2 and the unbinding of TIMP2 from the interim complex being outstripped by the binding of TIMP2 to MT1-MMP and MMP-2.

We noted that the variables were able to breach the volume filling criterion of $1 - c - v \geq 0$ and found that this could be the result of either of the flux terms of diffusion or haptotaxis and found that such a breach did not facilitate the breaking of the remaining volume filling criteria of $c \geq 0$ and $v \geq 0$. We found that the inclusion of volume filling in the terms representing haptotaxis, cancer cell production and ECM remodelling decreased the likelihood of finite time blow-up solutions occurring. In the event that finite time blow-up solutions are found for parameter values not yet examined or for small modifications to the model, we note that the inclusion of a non-local volume filling in the haptotaxis term would allow for a sensing radius and would would limit the breach of the volume filling criterion of $1 - c - v \geq 0$ to that from diffusion. It can be trivially shown that a breach due to diffusion would not break the remaining volume filling criteria of $c \geq 0$ and $v \geq 0$ as diffusion cannot increase c above the value of 1 and so the production term for the cancer cells and the remodelling term for the ECM will both cause a decrease when $1 - c - v \leq 0$ however they will allow v to approach but not pass zero. As such, the consideration of integro-PDE models in the future (as considered in Gerisch and Chaplain (2008), Andasari et al. (2011), Domschke et al. (2014) and others) may be of use.

We considered two scenarios of initial conditions to examine cancer growth and spread of Invasion Scenario 0A and 0B which were shown to have quadratic and linear growth, respectively. In Invasion Scenario 0A, we considered a central mass of cancer cells invading radially outwards as may be seen in some *in vivo* experiments or cases where a cancerous mass is surrounded by ECM and detailed

the variables through a progression of time in Figures 4.8–4.12 and Table 4.5. For Invasion Scenario 0B, we considered a second set of initial conditions to create a situation similar to what may appear in some *in vitro* experiments where the cancer cell mass forms a strip along the LHS of the domain and invades an ECM construct from left to right as seen in Figures 4.13–4.17 and Table 4.6.

We find that MMP-2 and TIMP2 are able to diffuse past the boundary of the cancer cell mass in contrast to the intermediate complex f and MT1-MMP, and that the MMP-2 profile has a less steep front than that of MT1-MMP. As such, all matrix degradation in advance of the cancer invasion boundary is the sole domain of MMP-2 while the degradation of ECM components within this cancer invasion front is shared by both MMP-2 and MT1-MMP. In addition, the majority of bulk ECM degradation was due to MMP-2 over the considered timeframe where the role of MT1-MMP mediated degradation was diminished in comparison to that of MMP-2 over time (cf. Figure 4.12 and Figure 4.17). This relationship between MMP-2 and MT1-MMP when it comes to bulk degradation supports the paradigm proposed by Sabeh, Li, Saunders, Rowe and Weiss (2009) of secreted MMPs being functionally limited to bulk collagenolytic processes whereas MT1-MMP is capable of acting in a focussed manner that supports subsequent collagenolysis and therefore invasion.

Where we considered the cancer-ECM interface to be defined as the region between c=0.01 and v=0.01, we were able to provide approximations for the concentrations of MMP-2 (0A: 1-4nM, 0B:1-5.5nM) and MT1-MMP (0A&OB: 0.1-5nM) within this region, then we can provide further approximations for these concentrations to the spatially homogeneous steady state and can compare favourably with biological data found in serum from various forms of cancer of MMP-2 = 2.81nM, 7.89nM, 7.91-10.03nM and MT1-MMP= 0.04nM, 0.38nM.

Near the leading front of the cell invasion boundary (though not directly upon the boundary) there is an increase in both the concentrations of the intermediate complex f and TIMP2 from the concentration where the cancer population has stabilised at the maximum non-dimensionalised value of 1. This increase in the intermediate complex, f, was shown to not be due to the initial condition being higher than this increased amount where in Invasion Scenario 0B f began near its steady state and reached a maximum of almost twice this value.

A parameter sensitivity analysis finds that an increase in D_c has a larger impact upon invasion than χ where we assume this to be due to the volume filling term in the haptotactic sensitivity function limiting the movement of cancer cells in the cancer-ECM interface. Additionally, we find that there is a value for α_T at which the steady state value of MMP-2 is at a maximum where either an increase or decrease to this value reduces the value of MMP-2.

Chapter 5

The Restructuring of ECM by MT1-MMP in a PDE Model of Cancer Invasion

5.1 Introduction

In the previous chapter, MT1-MMP was seen to be important in the early stages of invasion where it outperformed MMP-2 in ECM degradation. However its primary significance appeared to be due to its activation of MMP-2 which was then able to diffuse into and degrade the bulk of the ECM (cf. Figure 4.12 A and Figure 4.17). Although this corresponds to some of the known properties of MT1-MMP proteins in cancer cell invasion (Sato et al., 1994), it lacks insight into other roles of MT1-MMP which have been found to be of particular significance in cancer invasion. For example, Hotary et al. (2003) consider MT1-MMP to be a growth factor for cancer cells in a 3D ECM made up of collagen type-I, both *in vivo* and *in vitro* due to its effect of enabling cancer cells to modify their

shape. In this chapter we will examine MT1-MMP in its role of modifying the local environment of cancer cells in ways that MMP-2 cannot. This will be done through the inclusion of the effect the ECM architecture may have when applied to a model of cancer invasion developed in the previous chapter. Elements of the ECM architecture to be investigated include the pore size of the matrix and the crosslinking of collagen fibres. We note that in some highly dense collagen structures such as breast tissue, the cancer cells are unable to physically fit through a porous region. In this chapter we consider some cases where cancer cells are reliant upon their attached MT1-MMP proteins to either forge a path or modify the cell shape so that it can pass through an otherwise impassable ECM region allowing degradation by either MT1-MMP or MMP-2 to take place and permitting movement of cancer cells otherwise impossible.

The ECM will therefore need to be examined in greater detail than has been done so far in the presented work where the architecture of the ECM plays a pivotal role in cancer cell invasion (Kumar and Weaver, 2009; Friedl and Wolf, 2008; Lu et al., 2012). Type I collagen fibres are non-branching, fibrous proteins that resist tensile stresses and are the most common fibres found in the connective tissue of almost all organs, as well as tendons, ligaments, fasciae, fibrocartilage and bone (Eroschenko and Di Fiore, 2013). MMP-2 can degrade type-I collagen in bulk, albeit at a rate 8 times slower than MT1-MMP. However Sabeh, Shimizu-Hirota and Weiss (2009); Li et al. (2008) investigated embedding multicellular spheroids of HT-1080 fibrosarcoma cells within gels of cross-linked native type I collagen and found that MT1-MMP silencing blocks virtually all collagenolytic and invasive activity. As such, Sabeh, Li, Saunders, Rowe and Weiss (2009) proposed the paradigm that secreted MMPs are responsible for, but ultimately limited to, bulk collagenolytic processes whereas MT1-MMP can cause focalised degradation of ECM through which cancerous cells can then move and further

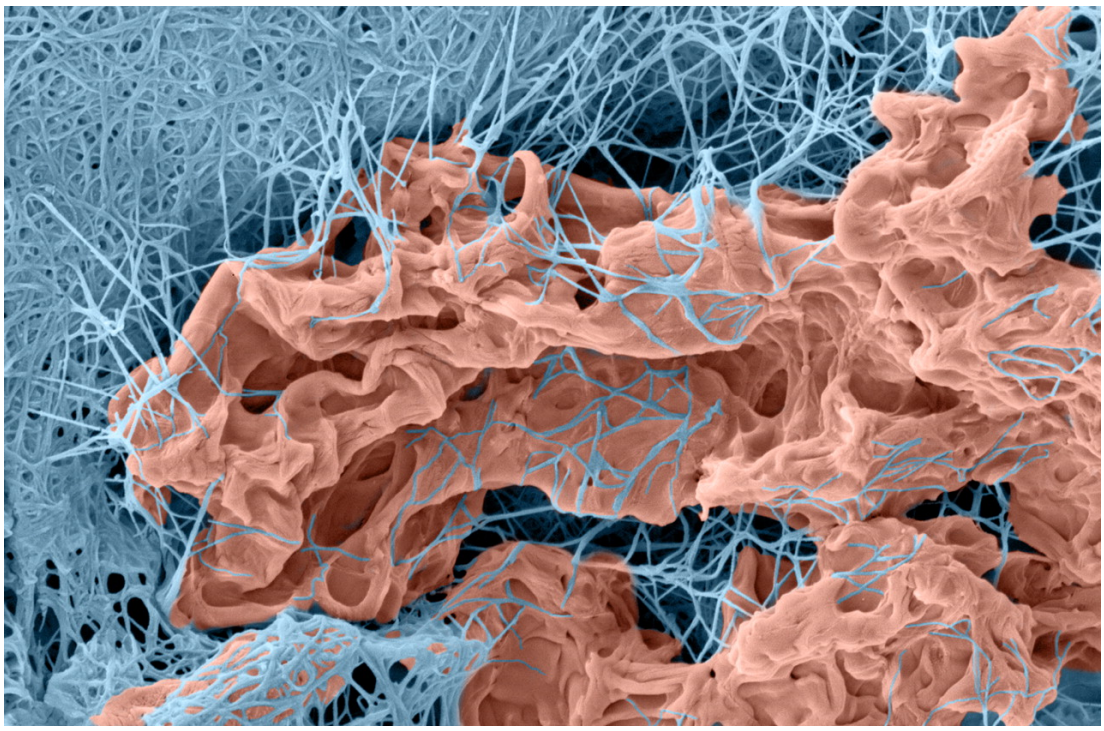

Figure 5.1: *Invasion of cancer cells through a 3 dimensional,* in vivo *generated network of collagen type-I. Reproduced from Sabeh, Shimizu-Hirota and Weiss (2009) under a Creative Commons license.*

degradation by other MMPs can take place. Connective tissue is mainly formed of collagen type-I whereas the stability of the basement membrane is determined primarily by collagen type IV (Kühn, 1995).

While MMPs can collectively degrade virtually all components of the ECM (Kleiner and Stetler-Stevenson, 1999), when considering an environment of mainly type I collagen, we must consider the substrates of MMP-2 and MT1-MMP, since MMP-2 may not be able to degrade fully-formed collagen *in vivo*. Further, 3-D collagen-induced surface localization of MT1-MMP leads to MMP-2 activation (Sakai et al., 2011). There is also uncertainty over the ability of MMP-2 proteins to degrade collagen type-IV in vivo (Barrett et al., 2012). Zhang et al. (2013) suggest that MMP-2 is unable to degrade cross-linked forms of collagen type -I

and -IV.

As more expansively discussed in Chapter 2 of the presented work, collagen fibres are cross-linked collagen molecules, where collagen molecules are formed from three strands of collagen proteins. In the case of type I collagen, the three proteins involved are of two types termed α-1 type I collagen and α-2 type I collagen. The standard construction of type I collagen is formed from two α-1 type I collagens and a single α-2 type I collagen, although some variants are formed of three identical proteins of α-1 type I collagen (Chang et al., 2012). Gioia et al. (2007) show (*in vivo*) that MT1-MMP proteins and MMP-2 proteins have functionally different ways of degrading type I collagen where the ectodomain of MT1-MMP can bind to either α-1 or α-2 followed by their degradation whereas MMP-2 binds preferentially to the α-1 chain from which it degrades the α-2 chain. However, 3D *in vivo* models of collagen type-I have found MT1-MMP proteins and not MMP-2 proteins modulating cancer cell invasion (Hotary et al., 2000; Sabeh, Shimizu-Hirota and Weiss, 2009).

Monaco et al. (2006) found that the rate that MMP-2 proteins degrade type IV collagen to be $1.2 \times 10^4 M^{-1}s^{-1}$ at 42 and $5 \times 10^3 M^{-1}s^{-1}$ at 37, while Inada et al. (2004) found that at 25, MMP-2 degradation of collagen type I is virtually non-existent. Thus it may be that the partial unwinding of type IV collagen that happens at increased temperatures (Dölz et al., 1988) is what deforms the cross-linked collagen fibrils into a form that MMP-2 can degrade. Further, Kuznetsova et al. (2003) find *in vitro* that homotrimeric type I collagen denaturates 100 times slower than heterotrimeric collagen when experiments are performed at the same temperature.

We operate under the assumption that *in vitro* models of MMP-2 degrading collagen either make use of uncross-linked variants of collagen that do not resemble

the makeup of collagen *in vivo*, have MT1-MMP causing partial unwinding of the collagen before degradation or are performed at temperatures such that the collagen has become at least partially unwound. As such, we consider the ECM to be, at times, "protected" from degradation by MMP-2 until remodelled into an appropriate form by MT1-MMP.

5.1.1 Suitability Modifier: The Means by which Biological Traits of the ECM are Modelled

In our model we denote by $s(\mathbf{x}, t)$ the *suitability modifier* as introduced in Deakin and Chaplain (2013). The suitability modifier acts as an environmental factor by reducing the proportion of a cell population that can physically move through the matrix by attempting to take into account the pore size of the collagen substrate along with reducing the amount of matrix that is considered available to be degraded.

The two main motivations we consider as means by which the suitability of the ECM can be changed is:

- regions of smaller pore size can be traversed by cancer cell that have had their shape adapted; a process that can be achieved by MT1-MMP proteins (Hotary et al., 2003).
- degradation of cross-linked type I collagen fibrils by MMP-2 proteins may only be possible once partial degradation by MT1-MMP has occurred.

While we acknowledge that there are other ways of modelling the effects that have been used to illustrate why the suitability modifier may be used (e.g. multiple ECM populations), we believe that the consideration of the suitability of the

matrix may allow for quantifiable comparisons of tissues that will allow for simpler models and faster computational results. Further, we find that this method offers a simplified means of considering any combination of these effects, as well as further effects that may be as of yet uncharacterised, while using the same model. The combination of these effects would require extensive quantifying of tissues before allowing for an individual analysis of imaging as input for a patient-specific approach that is as of yet undeveloped. This would include properties such as the effects of differing pore sizes on promotion or retardation of cancer cell movement, specifically in bulk. Once imaging data has been obtained and quantified into a form compatible with the suitability modifier for $s(t = 0)$, a quicker calculation of many complicating factors is possible than a more expansive model of split ECM variables for each component with a more complex initial ECM distribution with unique properties.

While MMP-2 may not be able to degrade type I collagen in vitro, it is able to degrade gelatin *in vitro* and unwound collagen *in vivo* and we know that MT1-MMP can degrade collagen into gelatin *in vivo*, can degrade gelatin in vitro and can cause the partial unwinding of collagen in vitro. We therefore have a justification for a suitability matrix that is remodelled by MT1-MMP into a neural state.

What we do not have is a perfect biologically representative treatment of the various interactions of ECM constituent parts and the cancer cells, since they are grouped together into a single term (suitability modifier). However we note that we do have a simplified presentation of many features that can now be implicitly incorporated into the model without adding significant complication to the model equations and therefore computational cost.

5.2 A PDE Model of Cancer Invasion Including Further Biological Effects of the ECM

We define a matrix environment with a neutral/no affect on cancer cell invasion to have a suitability modifier value of 1. This represents a case where the results of the model are identical to the reduced model where no consideration is placed on the suitability of the environment, as presented in Chapter 4. A matrix environment containing difficult regions of ECM for cancer cells to invade will be represented by a suitability modifier with a value $0 \leq s < 1$, with values towards zero describing an environment that is more difficult for cancer cells to navigate through the tissue, as well as a reduction in the amount of ECM that is available to be degraded. A suitability modifier greater than 1 may be considered where the environment is structured to encourage cell migration such as is the case in a "follow the leader"/"Indian chain" dynamic (Schlüter, 2013; Friedl and Wolf, 2003*b*), although this is not investigated in the present work.

We note that two spatial locations with the same value of ECM density, v, will not necessarily present the same dynamics depending on the value of the suitability modifier at these locations. In addition, an interpretation of the suitability modifier can be made as follows: a value of $s = \frac{1}{4}$ may represent a region that contains a tissue where (i) $\frac{3}{4}$ of the constituent parts of the ECM are cross-linked collagen, (ii) $\frac{3}{4}$ of the considered ECM has a pore size below a threshold α that blocks invasion, (iii) more than $\frac{3}{4}$ of the considered ECM has a pore size in the range $\alpha - \beta$ that slows invasion or (iv) some combination of the factors presented in (i)-(iii) that has the equivalent effect.

We present a modified PDE model of cancer invasion in equations (5.1)-(5.7) where we have indicated through the functions $g_i(s, v)$ reactions that we feel

further investigation into the effects of the ECM should be considered. We ensure that there are appropriate functions of $g_i(s, v)$ where the model presented in Chapter 4 can be recovered.

We highlight a minor difference in the way that the terms of ECM degradation are presented where in the previous chapter, we considered there to be a degradation rate of both MMP-2 and MT1-MMP which then experiences some scaling factor of δ_2 for the total degradative capability of MT1-MMP. This does not allow for an examination of cases where MMP-2 is unable to degrade our chosen ECM structures and so we modify the ECM degradation term of Chapter 4, from $-\delta_1 v(m_s + \delta_2 m_t)$ to $-(\delta_1 g_2(s, v)m_s + \delta_2 g_3(s, v)m_t)$ where the parameter choices for $\delta_1 = 1$ and $\delta_2 = 1$ in Table 4.4 are left unchanged and we note that the forms of ECM degradation in both chapters are equivalent for this parameter choice.

The full non-dimensionalised model is therefore:

$$\begin{aligned}
\frac{\partial c}{\partial t} &= \nabla \cdot (D_c \nabla c - \chi c g_1(s, v)(1 - c - v)\nabla v) + \mu_c c(1 - c - v), && (5.1)\\
\frac{\partial v}{\partial t} &= -(\delta_1 g_2(s, v)m_s + \delta_2 g_3(s, v)m_t) + \mu_v(1 - c - v), && (5.2)\\
\frac{\partial m_s}{\partial t} &= \nabla \cdot (D_{m_s} \nabla m_s) - \phi_{31} T m_s + \phi_{32} m_t f - \beta_{m_s} m_s, && (5.3)\\
\frac{\partial m_t}{\partial t} &= m_t \nabla \cdot (D_c \nabla c - \chi c g_1(s, v)(1 - c - v)\nabla v) \\
&\quad -\phi_{41} T m_t + \phi_{42} f - \beta_{m_t} m_t + \alpha_{m_t} c(1 + v), && (5.4)\\
\frac{\partial T}{\partial t} &= \nabla \cdot (D_T \nabla T) - \phi_{51} T m_s - \phi_{52} T m_t + \phi_{53} f + \alpha_T c, && (5.5)\\
\frac{\partial f}{\partial t} &= f \nabla \cdot (D_c \nabla c - \chi c g_1(s, v)(1 - c - v)\nabla v) \\
&\quad +\phi_{61} T m_t - \phi_{62} f m_t - \phi_{63} f, && (5.6)\\
\frac{\partial s}{\partial t} &= \delta_s m_t (1 - s). && (5.7)
\end{aligned}$$

We apply zero-flux boundary conditions to close the system. The initial conditions imposed depend on the precise invasion scenario we are considering. In first

three Invasion Scenarios (1A, 1B, 2) we have a cluster of cancer cells in the centre of a homogeneous density ECM and suitability defined in the appropriate section with a small amount of activated enzymes already released. The second grouping of three Invasion Scenarios will be similar to the first three with the exception of the layout where we consider a mass of cancer cells moving from left to right.

We simulate the model in 2 spatial dimensions and use the baseline parameters outlined in Table 4.4, unless otherwise specified, along with the introduction of δ_s which will have its value specified on a case by case basis. The key concepts of the "suitability modifier" are dependent upon 3 dimensional effects such as the pore sizes of the cross-linked collagen constituent of the ECM, which are then represented by a numerical value that is applied as a modifier to interactions involving the ECM. This means that the ECM density does not explicitly consider these issues and, crucially, two ECM densities of value 0.5 will not necessarily facilitate invasion in the same way if the corresponding "suitability matrix" values are different at the two locations.

In Chapter 4, we considered the density of the ECM components to be the sole factor of importance of the ECM when it came to the ability of MMPs to degrade ECM components and cancer cells to move. As such, when the choice of $g_1(s, v) = g_2(s, v) = g_3(s, v) = v$ is made, the model presented in Chapter 4 is recovered. In this chapter, we now consider other characteristics of the ECM that may impact on cancer cell growth and invasion before proposing alternative forms for the functions $g_1(s, v), g_2(s, v), g_3(s, v)$.

Identifying appropriate functions (g_i) by which the suitability modifier may be modelled is done by first recognising that the choice of $g_1(s, v) = g_2(s, v) = g_3(s, v) = v$ recovers the model presented in Chapter 4. This, however, completely ignores the introduction of the suitability modifier but as we hope to extend the

previous model, we impose the condition that where the suitability modifier is neutral, i.e. $s = 1$, the previous model of equations (4.9)-(4.14) is recovered, $g_1(1, v) = g_2(1, v) = g_3(1, v) = v$. For example:

- $s = 1$ provides a neutral environment when $g_1(1, v) = g_2(1, v) = g_3(1, v) = v$.
- $0 \leq s < 1$ provides an environment that is less effective than the neutral case.
- $s > 1$ provides an environment that actively facilitates invasion.
- if $s_1 < s_2$ then s_2 is an environment that offers increased invasive potential.

There are many possible forms for the functions $g_1(s, v), g_2(s, v), g_3(s, v)$ that may be appropriate. Some such forms are as follows: $v, sv, s^n{-}1{+}v, (s{-}1)^n{+}v, \dfrac{s^n + a}{a + 1}$. In Figure 5.3 we plot the suitability modifier against the ECM density for the examples where $n = 1$ and $a = 1$ of $v, sv, s - 1 + v, \dfrac{s + 1}{2}v$.

In Figure 5.3 A we have a case where the suitability modifier plays no role and there is a linear increase in v. In plot B we have very small output from the function unless $v + s \geq 1$. In plot C we find have to incorporate the condition of $v{+}s \geq 1$ and so the function is not valid where this condition is not met. We have contours of constant values along the line $v = s$. In plot D we have a stretched version of plot B where we note that plot B would be the result of $\dfrac{s^n + a}{a + 1}$ where $a = 0$ and plot D is the case where $a = 1$. Notably from this representation of $g_j(s, v)$ we have that when $s = 1$, we have a v that varies between $\frac{1}{2}$ and 1. In all four plots we have that v increases linearly from 0 to 1 when $s = 1$.

The precise form of $g_1(1, v), g_2(1, v), g_3(1, v)$ that we choose to use for the remainder of this chapter is $g_1(s, v) = g_2(s, v) = g_3(s, v) = -(1 - s - v)$. This is an

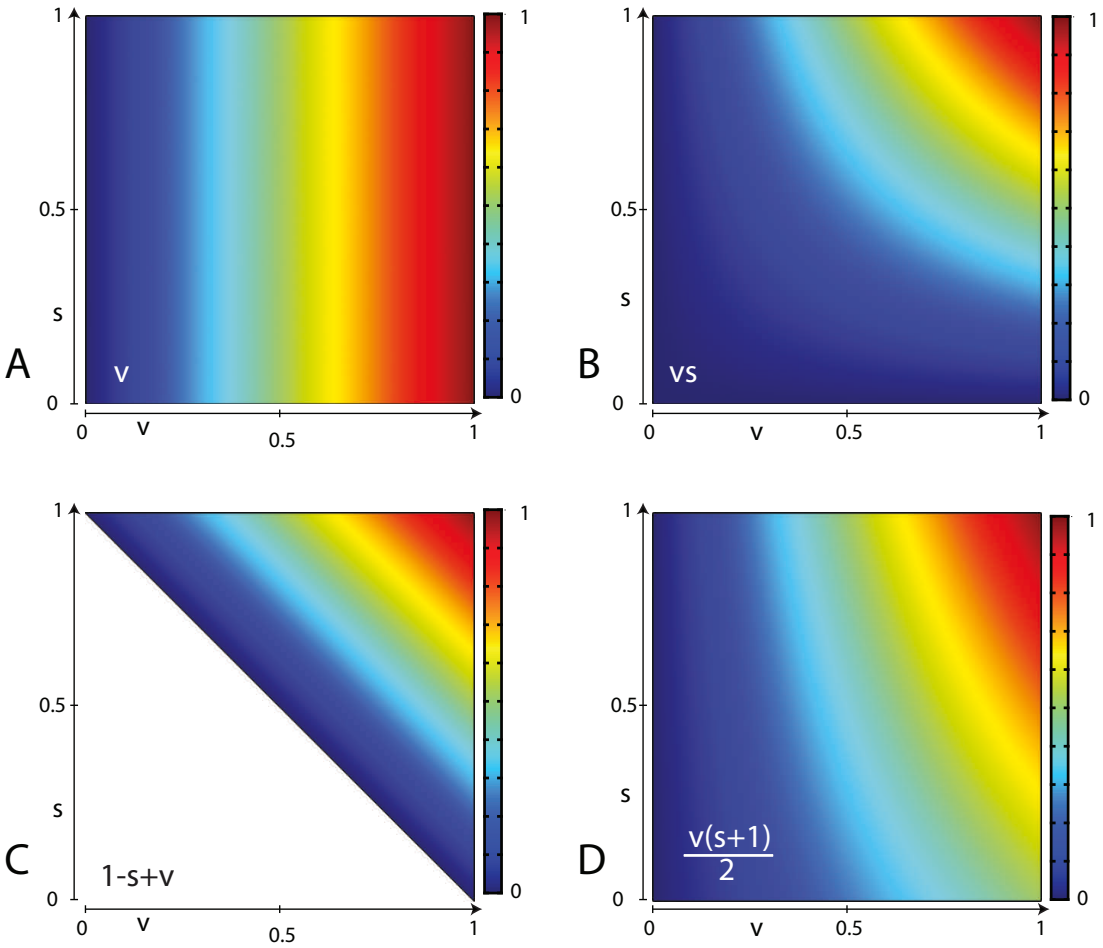

Figure 5.2: *Plot A shows the function* $g_i(s,v) = v$. *Plot B shows the function* $g_{i+1}(s,v) = vs$. *Plot C shows the function* $g_{i+2}(s,v) = -(1-s-v)$ *when considered with the condition of* $g_{i+3}(s,v) = s+v \geq 1$ *and Plot D shows the function* $v\frac{s+1}{2}$.

extension to the volume filling principles, though we note that s and v should not be considered to be "in competition" with one another. The current form of the model must also introduce further conditions that prevent the considering of the feature of $s > 1$ promoting invasion through a "follow the leader"/"Indian chain" dynamic (Schlüter, 2013; Friedl and Wolf, 2003*b*). As such we impose the conditions that $s + v \geq 1$ and $s \leq 1$, otherwise, instead of limiting movement ($g_1(s, v)$), movement would be encouraged in the opposite direction and instead of limiting tissue degradation ($g_2(s, v)$ and $g_3(s, v)$), the tissue degradation term would cause the density of ECM to increase. Furthermore, we note that the degradation of ECM term stops v from being degraded below $s - 1 + v = 0$ and that the remodelling of ECM is only negative where $c + v \geq 1$, therefore the minimum v value that can be achieved is $v = 1 - s$ and we have the condition for the model of $v + s \geq 1$.

We consider the impact this has on the haptotactic sensitivity function where we now have $(s - 1 + v)(1 - c - v)$ by plotting in Figure 5.3 this function at four values of $c = 0, 0.25, 0.5, 0.75$. Care must be taken when reading this figure to ensure that the correct scale of the axis and value is read as we have imposed the conditions of $c + v \leq 1$ and $v + s \geq 1$.

5.3 Results

We consider the same dummy variables (Δvm_s and Δvm_t) and functions ($\varnothing = 1 - c - v$ and Δv_{total}) as in the previous chapter in addition to the function of $\gamma = s + v - 1$ which is used to show where there is potential tissue to be degraded by MMP-2, as well as verifying that $s + v \geq 1$ to ensure that ECM degradation has a negative impact on total ECM density. The function γ also

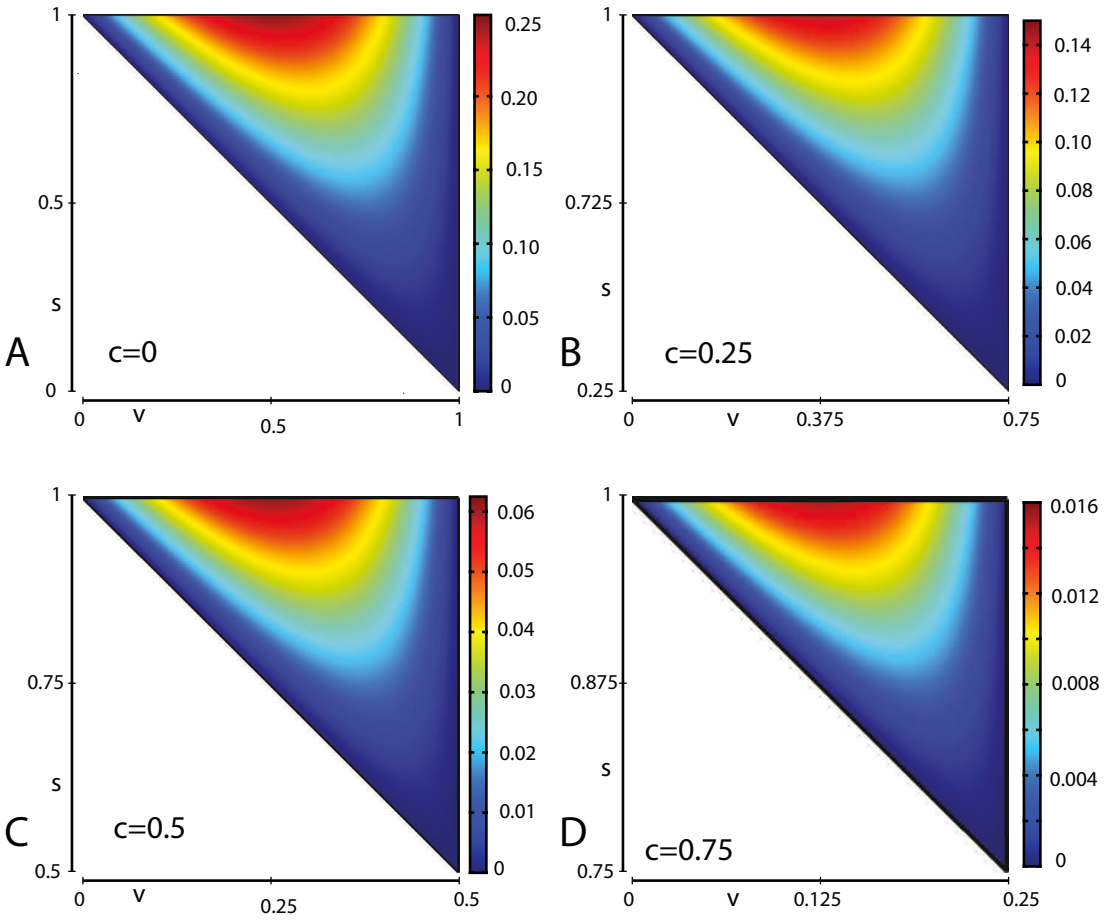

Figure 5.3: *Plots A-D are of the function* $(s-1+v)(1-c-v)$*, which is the value of haptotactic sensitivity function where* $g_1 = s-1+v$*. Each plot (A-D) is the representation of the function where* $c = 0, 0.25, 0.5$ *and* 1*, respectively. We draw particular attention to the ranges of* s *and* v *in each plot and the value of the maximum as these decrease from plot* $A \rightarrow$ *plot* $B \rightarrow$ *plot* $C \rightarrow$ *plot* D*.*

serves to illustrate how the suitability modifier affects the degradation of ECM or movement of cancer cells. We also consider the function $\lambda_1 = m_t(1-s)$ to show where there is an overlap of MT1-MMP and suitability modifier of value < 1 which indicates the amount of suitability modifier that is in the process of being remodelled back to the neutral state and indicates the regions that retard cancer cell movement. The third and final function that we introduce is $\lambda_2 = m_s(1-s)$ which allows us to identify the regions in which MMP-2 degradation of ECM is being impacted upon.

We now present the computational simulation results of our invasion model in a 2-dimensional spatial domain (all parameter values are from the baseline set found in Table 4.4). We consider 6 Invasion Scenarios formed from varying either the initial conditions of the model or the parameter δ_s to identify characteristics of results obtained by the model that may offer insight into either *in vivo* or *in vitro* experiments.

We plot the time evolution of the various variables as well as noting some results that are not immediately obvious from these plots, namely, the amount of tissue degradaded by MMP-2 and MT1-MMP individually and offer a comparison of these values.

The first grouping of scenarios (Invasion Scenarios 1A, 1B, 2) considers an initial mass of cancer cells represented by a Gaussian distribution in the centre of a two dimensional square domain along with two specific forms the surrounding media can take (two initial condition data for s) along with $v(0) = 1 - c(0)$, $m_s(0) = m_t(0) = T(0) = f(0) = 5c(0)$. These can be seen as comparable with Invasion Scenario 0A. The second grouping of scenarios (Invasion Scenarios 3A-) consider an initial strip of cancer cells on the left hand side of the domain and how they proceed to invade through some varyingly heterogeneous surrounding

media along with $v(0) = 1 - c(0)$, $m_s(0) = m_t(0) = T(0) = f(0) = c(0)$. These can be seen as comparable with Invasion Scenario 0B.

Invasion Scenario 1A is the first scenario we consider in which the tissue is considered to have a neutral effect on invasion in the top half of the domain by having a matrix suitability modifier $s = 1$, with the lower half of the domain having moderate characteristics limiting invasion by having the matrix suitability modifier of $s = \frac{1}{2}$, as shown in Figure 5.4 C. This splits the domain into two regions where the upper region, which has $s(t = 0) = 1$ and therefore has dynamics present in this region that are identical to that of simulating the model presented in Chapter 4, where the suitability modifier is not considered at all. The only minor difference in comparing it with the previous model is that there is no zero flux boundary across the line defined by $y = 0$ and therefore some movement of cancer cells from the unrestricted upper region into the lower region is possible.

The lower region, on the other hand, is the first simulated result where the effects of the suitability modifier are considered. This creates an asymmetric invasion of the cancer cells as can be seen from the plots in Figure 5.4 with a reduced invasion in the lower half of the domain (cf. Figure 5.4 D) and also an increased overall ECM profile in the lower half of the domain (cf. Figure 5.4 E).

Figures 5.5 & 5.6 show the corresponding evolution of the various enzyme concentrations. The plots in Figures 5.5 F & 5.6 F show that any free TIMP2 that is produced or released from a complex is quickly bound to either free MT1-MMP or MMP-2. The plots in Figures 5.5 D & 5.6 D show that while MMP-2 can freely diffuse throughout the environment, its profile is affected by the source term coming from the asymmetric cancer cell invasion dynamics. The plots in Figures 5.5 E & 5.6 E show how the degradative effect of MT1-MMP is limited by its dependence on transport by the cancer cells. This is demonstrated by a

reduced invasive profile in the bottom half of each plot.

In Figure 5.7 we note that there is a higher amount of degradation of tissue in the upper half of the region where we have considered $s(t = 0) = 1$. This shows the degree to which the suitability modifier has limited ECM degradation.

In Figure 5.8 we perform domain integrations of the variables v, c, $\varnothing$, λ_s, λ_t, Δv_{total}, $\Delta v m_s$, $\Delta v m_t$, m_s and m_t to better examine the contributions of these variables to the dynamics of the model across the considered timeframe of $t = 0 - 40$, corresponding to 4.6 days. We specifically note that while the domain integration of Δv_{total} reaches ~ 16 by $t = 40$, this should not be taken to mean that the entirety of the ECM has been degraded as the ECM is remodelled (gained density/recovered) over time. Indeed we note that the domain integration of v at $t = 40$ is approximately $\frac{7}{8}$th the value of what it was initially. By plotting the domain integrations of m_s and m_t we have shown that the difference between $\Delta v m_s$ and $\Delta v m_t$ is not down to the relative concentrations of MMP-2 and MT1-MMP (which are the same) but instead due to their relative locations (cf. Figure 5.4 and 5.5) where MMP-2 can diffuse past the boundary of the cancer cells, which defines the full extent of MT1-MMP location, and gain access to ECM that MT1-MMP cannot reach.

Finally, in Figure 5.9 we plot the location for the free space $\varnothing = 1 - c - v$ and the function $s - 1 + v$ to gain insight into how the suitability modifier is influencing cellular locomotion ($g_1 = s - 1 + v$) and ECM degradation ($g_2 = g_3 = s - 1 + v$). We note that degradation of ECM can only happen where $s - 1 + v > 0$ and that haptotaxis of cancer cells to ECM gradients can only occur where both $1 - c - v > 0$ and $s - 1 + v > 0$. While we refer the reader back to Figure 5.3 to see the plotting of $(s - 1 + v)(1 - c - v)$ for s against v for various chosen c to get an idea of what some of these values may be, we can use Figure 5.9 to

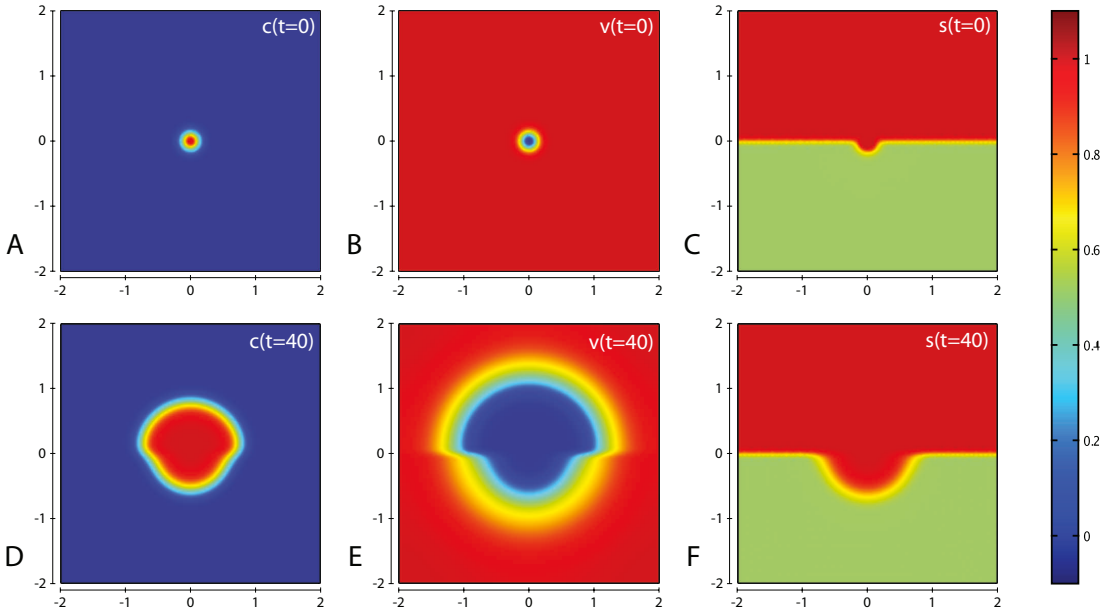

Figure 5.4: *Invasion Scenario 1A. Plots A-C show the initial values of the cancer cell and ECM densities as well as the initial stucture of the matrix suitability modifier with D-F showing their resultant profiles at* $t = 40$ *(corresponding to ∼4.6 days). Simulations are performed using the baseline parameter set of Table 4.4 along with* $\delta_s = 0.025$.

see the locations where both $1 - c - v > 0$ and $s - 1 + v > 0$ and can draw the conclusion that the suitability modifier has blocked haptotaxis in the bottom half of the domain where $s - 1 + v = 0$ at all points where $c > 0$ despite the volume filling term not blocking haptotaxis at this location.

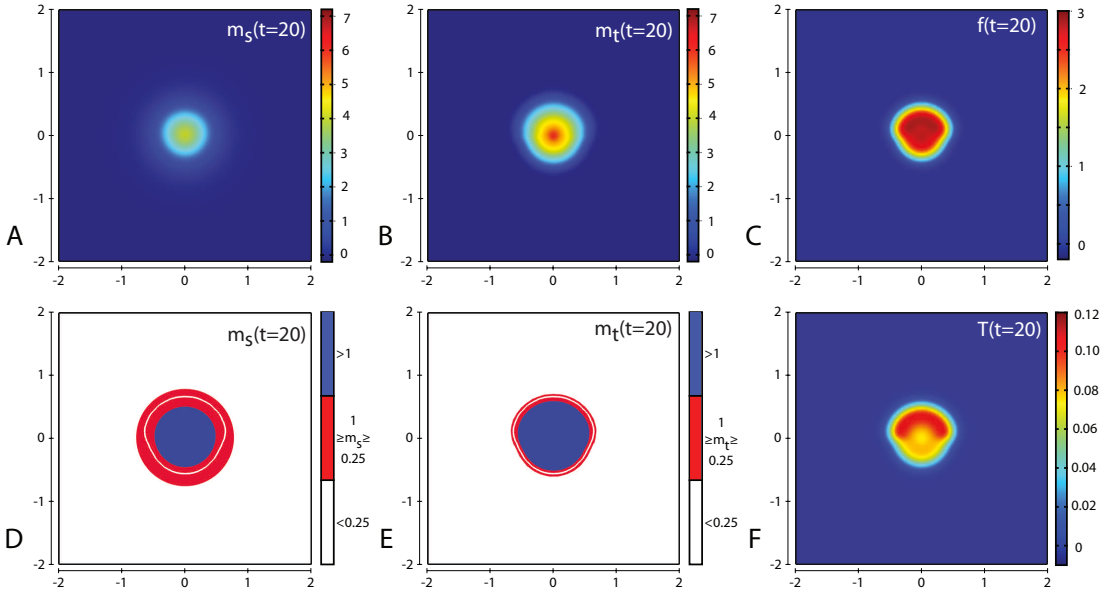

Figure 5.5: *Invasion Scenario 1A. The concentrations of MMP-2, MT1-MMP, the intermediary complex f and TIMP2 are shown in plots A,B,C and F respectively at $t = 20$ (corresponding to ∼2.3 days). Plots D, E show the MMP-2 and MT1-MMP concentrations at $t = 20$ with appropriate thresholds near the invasive front of the cancer cell invasion. The white contour line shows the cancer cell density at level 0.01 chosen to represent the maximum extent of invasion. Simulations are performed using the baseline parameter set of Table 4.4 along with $\delta_s = 0.025$.*

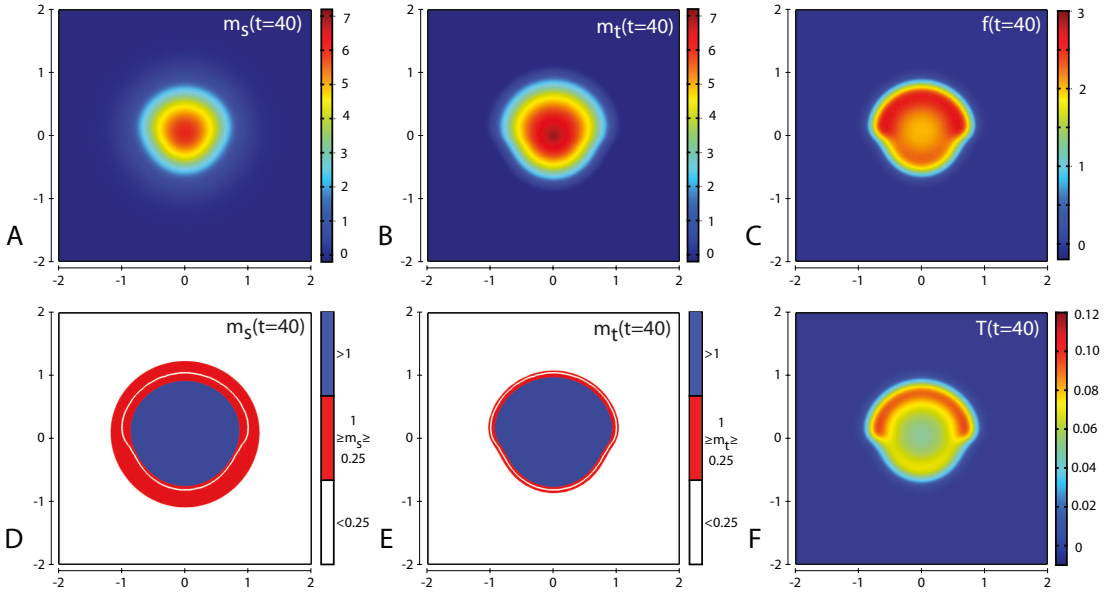

Figure 5.6: *Invasion Scenario 1A. The concentrations of MMP-2, MT1-MMP, the intermediary complex f and TIMP2 are shown in plots A,B,C and F respectively at $t = 40$ (corresponding to ∼4.6 days). Plots D, E show the MMP-2 and MT1-MMP concentrations at $t = 40$ with appropriate thresholds near the invasive front of the cancer cell invasion. The white contour line shows the cancer cell density at level 0.01 chosen to represent the maximum extent of invasion. Simulations are performed using the baseline parameter set of Table 4.4 along with $\delta_s = 0.025$.*

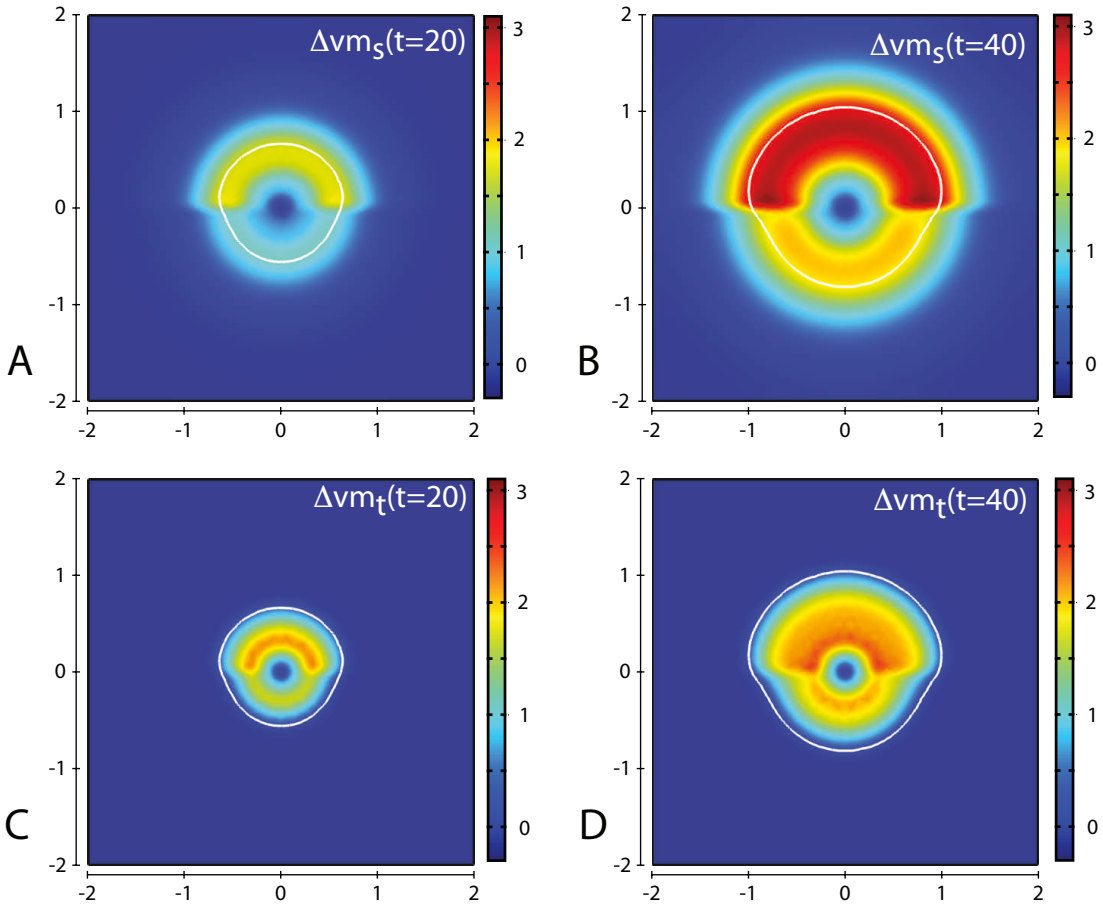

Figure 5.7: *Invasion Scenario 1A. Plots A & B show the profiles of the density of ECM degraded solely by m_s, while plots C & D show the profiles of the density of ECM degraded solely by m_t at $t = 20$ and 40 (corresponding to ∼2.3 and 4.6 days, respectively). The white contour line in plots A-D shows the cancer cell density at level 0.01 chosen to represent the maximum extent of invasion. Simulations are performed using the baseline parameter set of Table 4.4 along with $\delta_s = 0.025$.*

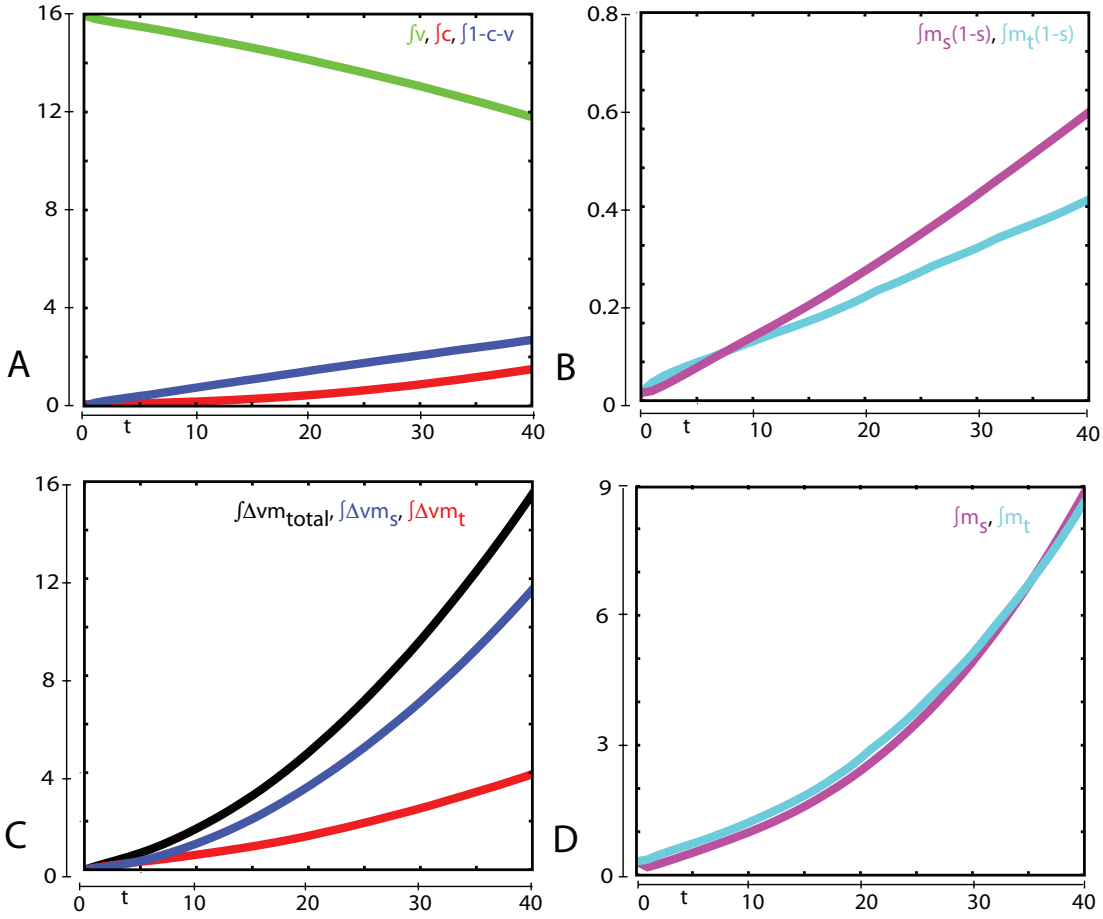

Figure 5.8: *Invasion Scenario 1A. Domain integrations of various variables and functions where plot A features* $\int c, \int v$ *and* $\int \varnothing = \int 1-c-v$ *representing the total amount of cancer cell density (red), ECM density (green) and amount of free space (blue), respectively. Plot B features* $\int \lambda_2 = \int m_s(1-s)$ *and* $\int \lambda_1 = \int m_t(1-s)$ *to represent the amount of overlap between the suitability modifier with MMP-2 (magenta) and with MT1-MMP (cyan), respectively. Plot C features* $\int \Delta v_{total}$, $\int \Delta v m_s$, *and* $\int \Delta v m_t$, *to represent the total amount of ECM degraded (black), total ECM degraded by MMP-2 (blue) and total ECM degraded by MT1-MMP (red). Plot D features* $\int m_s$ *and* $\int m_t$ *to represent the total amount of MMP-2 (magenta) and MT1-MMP (cyan), respectively. Simulations are performed using the baseline parameter set of Table 4.4 along with* $\delta_s = 0.025$.

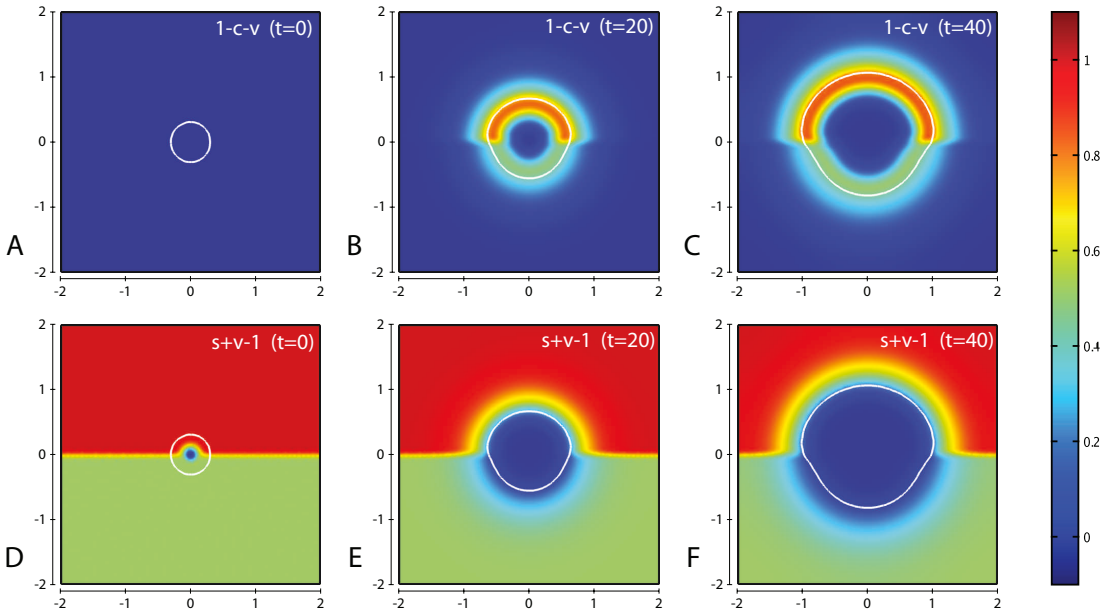

Figure 5.9: *Invasion Scenario 1A. The function of* $\varnothing = 1 - c - v$ *is plotted in plots A-C for the times of* $t = 0, 20$ *and* 40 *while the function of* $s - 1 + v$ *is plotted in plots D-F for the times of* $t = 0, 20$ *and* 40*, relating to* $0, \sim 2.3$ *days and* ~ 4.6 *days respectively. The white contour line in all plots shows the cancer cell density at level 0.01 chosen to represent the maximum extent of invasion. Simulations are performed using the baseline parameter set of Table 4.4 along with* $\delta_s = 0.025$.

Invasion Scenario 1B follows on from Invasion Scenario 1A, which we note offers a clear comparison between the dynamic of results obtained from the model presented in Chapter 4 (cf. upper region of plots D, E and F in Figure 5.4) and results obtained when the suitability modifier is actively impacting the spread of cancer cells and the degradation of ECM (cf. lower region of plots D, E and F in Figure 5.4). We now proceed to consider what impact having a considerably high value of δ_s in a scenario that is otherwise the same as Invasion Scenario 1A. By having such a high value for δ_s, we are representing the unfit matrix being very quickly remodelled into a neutral state. By doing so, we will again be able to compare the upper and lower regions (separated by the line $y = 0$) to determine what effect a rapidly neutralised suitability modifier will have on the growth and spread of cancer cells.

We offer only a minimal interpretation and presentation of the results of this Invasion Scenario as we note that this is only minimally varied from that of Invasion Scenario 1A. As such, we have condensed the results presented into a singular figure of Figure 5.10 where we show the resultant profiles at $t = 40$ (corresponding to ~ 4.6 days) of cancer cell density, ECM, suitability modifier and concentrations of MMP-2, MT1-MMP, the intermediate complex of TIMP2:MT1-MMP:proMMP-2 and TIMP2 in the plots of A-F and I, respectively. We also consider the presence of MMP-2 and MT1-MMP when within defined concentration ranges.

It can be seen from the plot in Figure 5.10 A that the cancer cells invade in an almost symmetric manner (unlike the scenario in Figure 5.4 D). However, we can also see from the plot in Figure 5.10 B that there is a reduced ECM profile in the upper half of the domain compared with the lower half. This is due to a limiting of ECM degradation beyond the cancer cell boundary in the lower half of the domain which can only be due to a reduction in ECM degradation by MMP-2. While the cancer cell profile is near symmetric and the ECM profile is

asymmetric, we note that the remaining variable of m_s, m_t, T and f all appear to be as symmetric as the cancer cell profile. This is due to the reliance of these variables on cancer cells for production or activation depending on enzymes found to cancer cells.

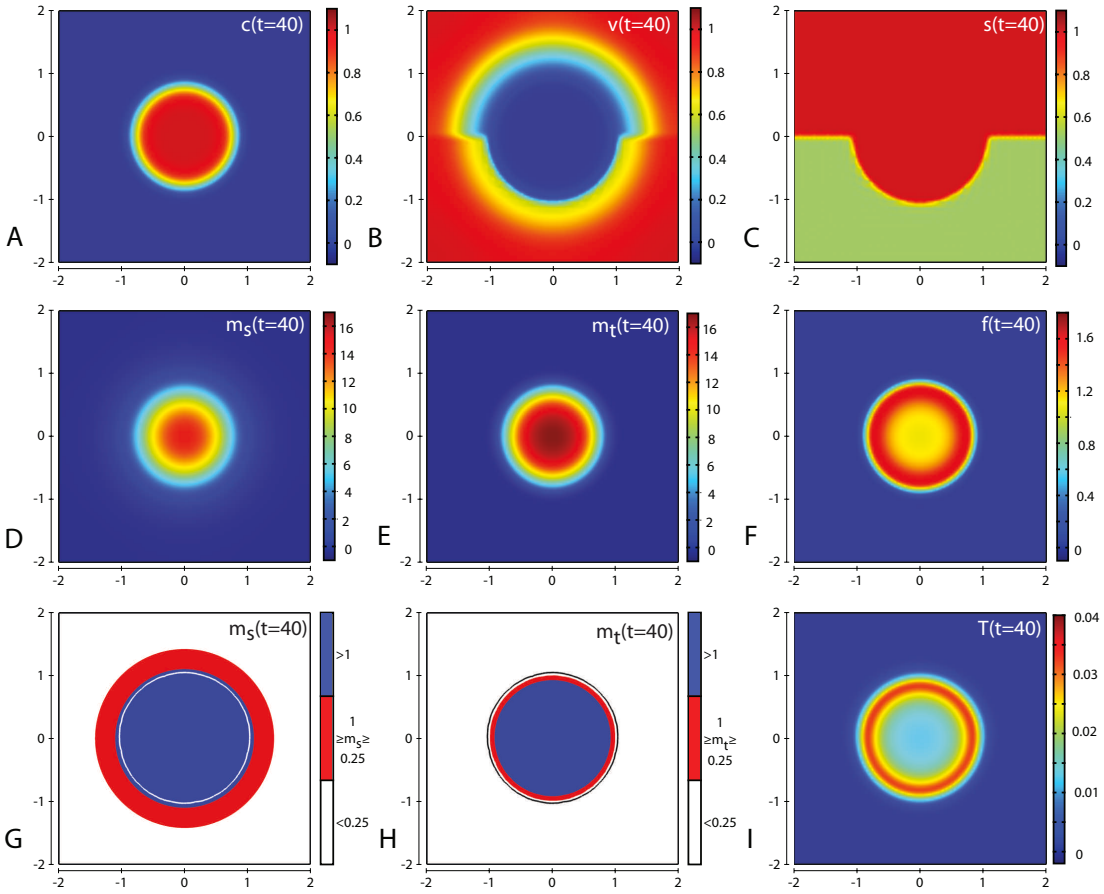

Figure 5.10: *Invasion Scenario 1B. Simulations are performed using the baseline parameter set of Table 4.4 along with the key constant of* $\delta_s = 10$. *Plots A-C show the values of the cancer cell and ECM densities as well as the initial layout of the matrix suitability modifier at* $t = 40$ *(corresponding to ∼4.6 days). Plots D-G show the concentrations of MMP-2, MT1-MMP, the intermediary complex* f *and TIMP2 at* $t = 40$ *(corresponding to ∼4.6 days). Plots H, I show the MMP-2 and MT1-MMP concentrations at* $t = 40$ *with appropriate thresholds near the invasive front of the cancer cell invasion. The black contour line shows the cancer cell density at level 0.01 chosen to represent the maximum extent of invasion.*

Invasion Scenario 2 considers the tissue to have neutral effects on invasion in a diagonal strip across the region by having a matrix suitability modifier $s = 1$, while the remaining domain is considered to have characteristics that strongly limit invasion by having the matrix suitability modifier of $s = \frac{1}{4}$, as shown in Figure 5.11 C. All parameters are kept at the baseline values and we use the same initial conditions as Invasion Scenario 1A, with the exception of $s(t = 0)$ defined above. As can be seen from the plots in Figure 5.11 we observe an asymmetric invasion by the cancer cells, with a reduced invasion in the region where s was originally $s = \frac{1}{4}$ (cf. Figure 5.11 D) and also a reduced degradation of ECM in this region (cf. Figure 5.11 E).

Figures 5.12 & 5.13 show the corresponding evolution of the various enzyme concentrations using the baseline parameter set. The plots in Figures 5.12 F & 5.12 F show that we retain the characteristic of any free TIMP2 that is produced or released from a complex is quickly bound to either free MT1-MMP or MMP-2. In comparing these two plots, it can be seen that there is a higher TIMP2 concentration in the invading front when there is a more suitable matrix to be invaded, i.e. where $s = 1$. Evaluation of the other enzyme concentrations shown in Figures 5.12 A–E & 5.12 A–E shows similar insight as was obtained from Invasion Scenario 1A.

Plots showing the simulation results obtained in a two-dimensional domain where asymmetric invasion of the ECM is achieved by the cancer cells. We use the matrix suitability modifier s to represent a medium with neutral abilities in the upper half of the region ($s = 1$; red) and with a reduced, moderate, suitability for invasion in the lower half ($s = 0.5$; green).

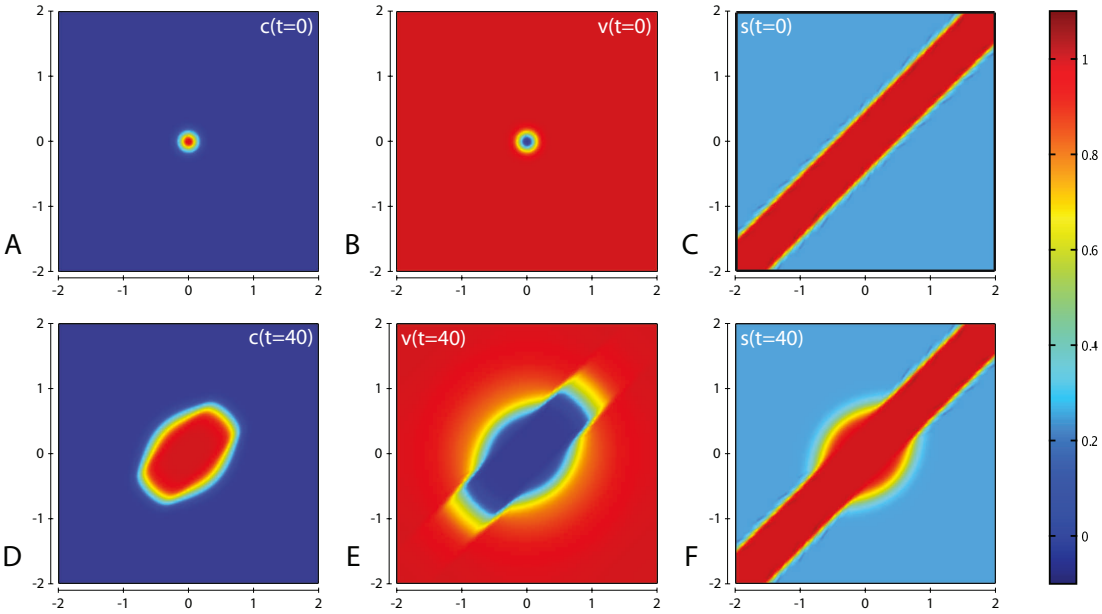

Figure 5.11: *Invasion Scenario 2. Plots A-C show the initial values of the cancer cell and ECM densities as well as the initial layout of the matrix suitability modifier with D-F showing their resultant profiles at* $t = 80$ *(corresponding to* $\sim$*9.2 days). Simulations are performed using the baseline parameter set of Table 4.4 along with the key constant of* $\delta_s = 0.025$.

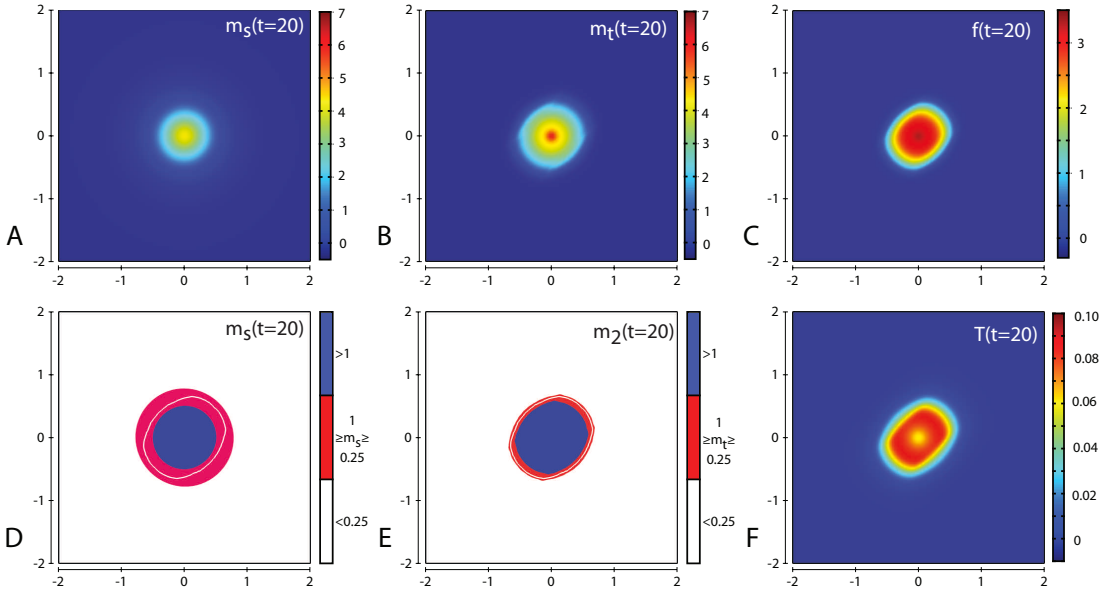

Figure 5.12: *Invasion Scenario 2. Plots A-C show the initial values of the cancer cell and ECM densities as well as the initial layout of the matrix suitability modifier with D-F showing their resultant profiles at* $t = 40$ *(corresponding to ∼4.6 days). Simulations are performed using the baseline parameter set of Table 4.4 along with the key constant of* $\delta_s = 0.025$.

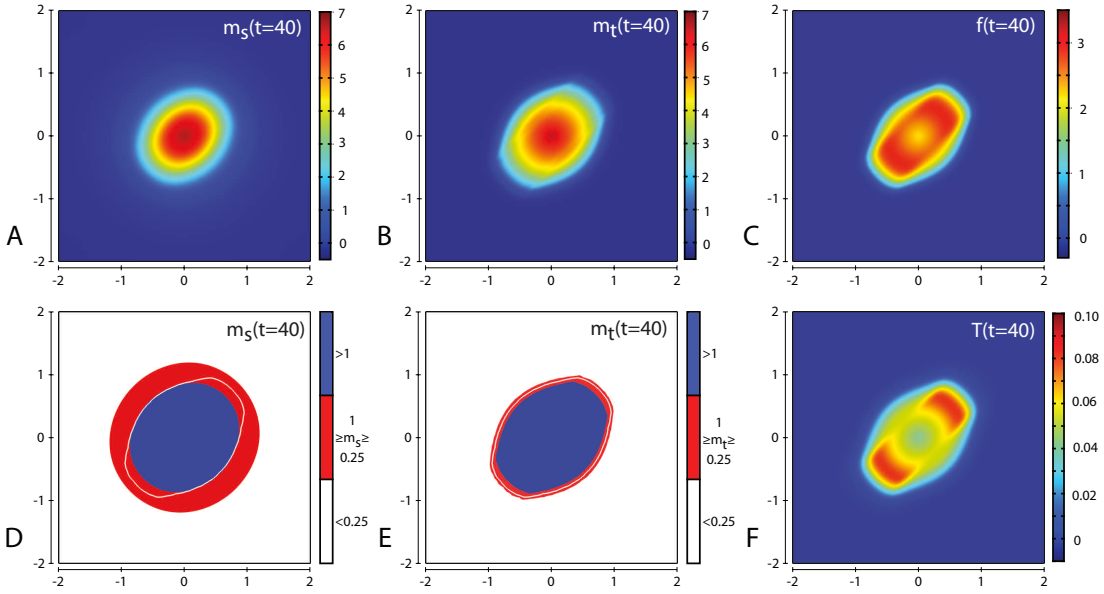

Figure 5.13: *Invasion Scenario 2. Plots A-C show the initial values of the cancer cell and ECM densities as well as the initial layout of the matrix suitability modifier with D-F showing their resultant profiles at* $t = 40$ *(corresponding to ∼4.6 days). Simulations are performed using the baseline parameter set of Table 4.4 along with the key constant of* $\delta_s = 0.025$.

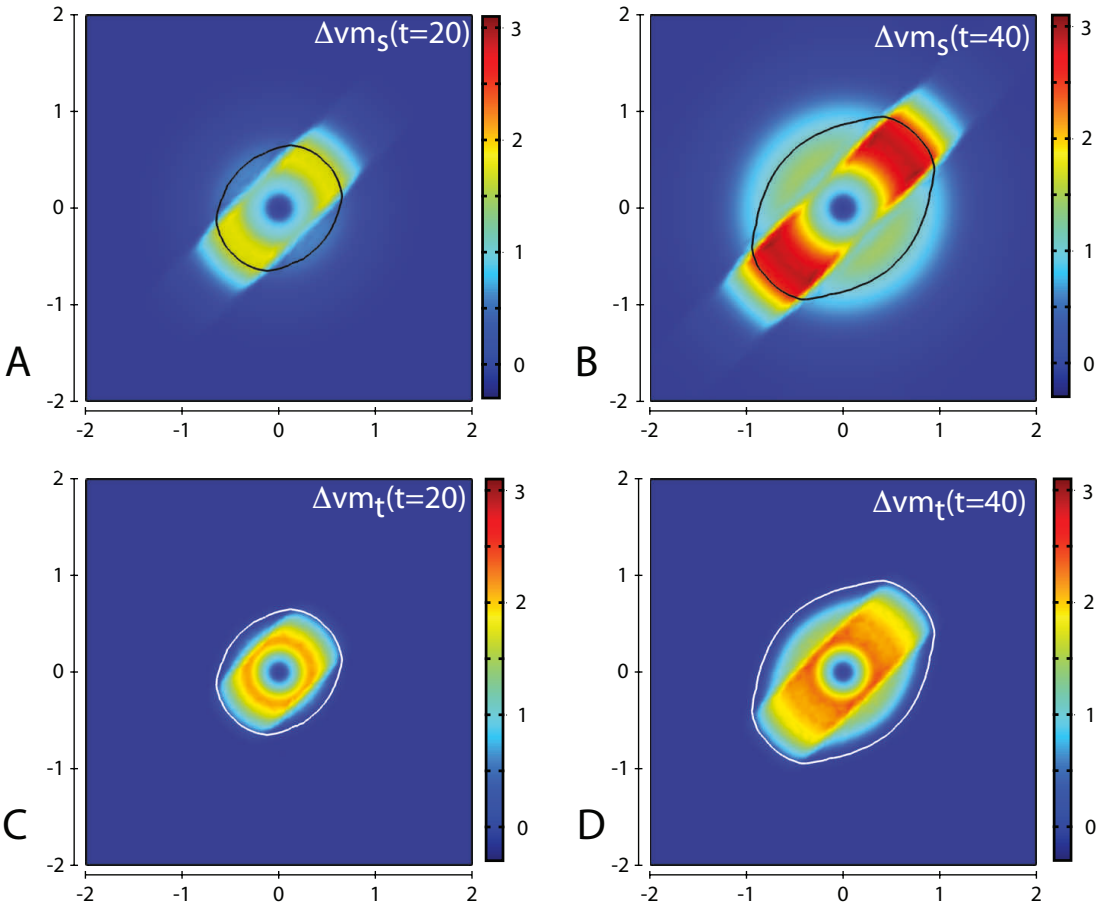

Figure 5.14: *Invasion Scenario 2. Plots A & B show the profiles of the density of ECM degraded solely by m_s, while plots C & D show the profiles of the density of ECM degraded solely by m_t at $t = 20$ and 40 (corresponding to ∼2.3 and 4.6 days, respectively). The white contour line in plots C & D and black contour line in plots A & B shows the cancer cell density at level 0.01 chosen to represent the maximum extent of invasion. Simulations are performed using the baseline parameter set of Table 4.4 along with the key constant of $\delta_s = 0.025$.*

Comparison of Invasion Scenarios 0A, 1A, 1B, 2 is offered up here where in recognising that the six Invasion Scenarios proposed in this chapter can be separated into two groups that bear similarities to the Invasion Scenarios of the previous chapter, we compare the results obtained from each to see what conclusions we can draw from the results. Here, we consider the first three Invasion Scenarios proposed in this chapter of 1A, 1B and 2 with the first Invasion Scenario proposed in the previous chapter of 0A.

We can compare Invasion Scenarios 1A and 1B in order to examine the effect of the parameter δ_s on cancer cell invasion. Invasion Scenarios 0A and 1B can be compared to establish the connection between no consideration of a suitability modifier ($s(t = 0) = 1$) and the case where the suitability modifier is quickly remodelled by MT1-MMP ($\delta_s >> 0$). In comparing the initial overlap of $c(0)(1 - s(0))$ for IS1A & 1B with IS2, we find that they begin at different values. This means that we cannot directly compare IS2 with either IS1A or IS1B to obtain precise results for the effect of the parameter δ_s, however some general trends may be commented on, such as the effect of $s(0)$ on later time cancer cell invasion. Further, IS2 can be compared with IS0A to understand the effects that the suitability modifier has had on cancer cell invasion when presented with the scenario of $s(t = 0)$ and δ_s in IS2.

We present three tables; Tables (5.1, 5.2) and (5.3), to show domain integration data and some functions thereof obtained from the model presented in this chapter of equations (5.1)-(5.7) when solved with the parameters defined in the previous chapter in Table 4.4. This has been done so that there is able to be a meaningful comparison with the results obtained in the previous chapter for Invasion Scenarios 0A&B. One such method for comparing total amount of MMPs present at various time steps is to scale the subdomain integration over a suitable domain or other term. We have decided to scale it against the subdomain

integration of c here. We also consider the proportion of ECM that has been degraded by the two functionally different MMPs and how much the suitability matrix has changed.

We label the functions identified in Table 5.3 as the following: $\alpha = \frac{m_s}{c}, \beta = \frac{m_t}{c}, \gamma = \frac{m_s}{m_t+m_s}, \delta = \frac{m_t}{m_t+m_s}, \epsilon = \frac{\Delta v_{ms}}{\Delta v_{mtotal}}, \zeta = \frac{\Delta v_{m_t}}{\Delta v_{m_{total}}}, \eta = \frac{s}{s(t=0)}, \theta = s - s(t = 0), \iota = \frac{T}{c}$

While a parameter sensitivity is offered in the previous chapter, the inclusion of the suitability matrix incorporates a new parameter (δ_s) and more importantly, further consequences that can be discussed. As we note that Invasion Scenarios 1A&B are identical with the exception of the parameter δ_s, we choose to consider the impact of the parameter δ_s on cancer cell invasion by varying it and in doing so we can view Invasion Scenarios 1A&B.

We explore the following functions in Table (5.4): $A = [\int s(25)\,\mathrm{d}\mathbf{x}]^{\delta_s=\psi} - \int s(0)\,\mathrm{d}\mathbf{x}$, $B = [\int c\,\mathrm{d}\mathbf{x}]^{\delta_s=\psi} - [\int c\,\mathrm{d}\mathbf{x}]^{\delta_s=0.025}$, $C = [\int \Delta v_{total}]^{\delta_s=\psi} - [\int \Delta v_{total}]^{\delta_s=0.025}$, $D = [\frac{\int \Delta v_{m_t}}{\int \Delta v_{total}}]^{\delta_s=\psi} - [\frac{\int \Delta v_{m_t}}{\int \Delta v_{total}}]^{\delta_s=0.025}$, $E = t_c$.

We consider 8 possible parameter values for δ_s of 0, 0.005, 0.015, 0.025, 0.05, 0.1, 1, 10 and record various data from each simulation. We first show in Table 5.4 (A) the amount that the suitability modifier has changed by where it logically proceeds that we consider the minimum to be 0 where $\delta_s = 0$ and record the changes from this choice of δ_s instead of from $\delta_s = 0.025$, (B) the amount specific results change from the values obtained for the choice of $\delta_s = 0.025$ for the results of the total cancer cell density, (C) the total ECM degradation and (D) the proportion of the ECM degradation that has been achieved by MT1-MMP. We note that the values of $[\int c\,\mathrm{d}\mathbf{x}]^{\delta_s=0.025} = 0.64, [\int \Delta v_{total}]^{\delta_s=0.025} = 6.98$ and $[\frac{\int \Delta v_{m_t}}{\int \Delta v_{total}}]^{\delta_s=0.025} = 0.28$ were recorded to provide the values that the other choices for δ_s are recorded to deviate from. As a final result (E), we consider the time,

IS	t	c	v	$\varnothing$	m_s	m_t	T	f	s
0A	0	0.06	15.94	0	0.31	0.31	0.31	0.31	
1A	0	0.06	15.94	0	0.31	0.31	0.31	0.31	
1B	0	0.06	15.94	0	0.31	0.31	0.31	0.31	
2	0	0.06	15.94	0	0.31	0.31	0.31	0.31	
0A	20	0.57	13.14	2.29	5.29	6.02	0.04	1.19	NA
1A	20	0.44	14.14	1.42	2.41	2.69	0.08	1.69	12.10
1B	20	0.57	13.51	1.92	5.22	5.88	0.04	1.24	12.38
2	20	0.53	14.48	0.99	2.62	2.95	0.08	1.91	6.87
0A	40	2.01	9.11	4.88	24.75	25.69	0.07	3.14	NA
1A	40	1.51	11.79	2.70	8.84	8.62	0.16	4.81	12.30
1B	40	1.97	10.01	4.02	24.32	25.24	0.07	3.08	12.90
2	40	1.39	12.99	1.62	9.08	8.36	0.13	4.26	7.18

Table 5.1: *Invasion Scenarios 0A, 1A&B, 2. The domain integration of the model variables at* $t = 0, 20$ *and* $t = 40$ *(corresponding to 0 days,* $\sim$*2.3 days and* $\sim$*4.6 days). We note that all the Invasion Scenarios detailed here have the same initial conditions with the exception of* s *and therefore identical domain integration values at* $t = 0$ *for the remaining variables.*

IS	t	Δv_{total}	Δv_{ms}	Δv_{mt}
0A	0	0	0	0
1A	0	0	0	0
1B	0	0	0	0
2	0	0	0	0
0A	20	7.29	6.21	1.08
1A	20	4.83	3.43	1.40
1B	20	6.25	5.18	1.07
2	20	4.06	2.56	1.50
0A	40	25.72	23.04	2.68
1A	40	15.45	11.55	3.94
1B	40	21.66	19.01	2.65
2	40	10.80	7.46	3.34

Table 5.2: *Invasion Scenarios 0A, 1A&B, 2. The domain integration of how much degradation has occurred due to each and both of the MMPs considered at* $t = 0, 20$ *and* $t = 40$ *(corresponding to 0 days,* $\sim$*2.3 days and* $\sim$*4.6 days). We note that all the Invasion Scenarios detailed here have the same initial conditions with the exception of* s *and therefore identical domain integration values at* $t = 0$ *for the remaining variables.*

	α	β	γ	δ	ϵ	ζ	η	θ	ι
Scenario0A	12.31	12.78	0.49	0.51	0.90	0.10	NA	NA	0.03
Scenario1A	5.85	5.71	0.51	0.49	0.75	0.25	1.02	0.27	0.11
Scenario1B	12.35	12.81	0.49	0.51	0.88	0.12	1.07	0.87	0.04
Scenario2	6.53	6.01	0.52	0.48	0.69	0.31	1.05	0.37	0.09

Table 5.3: *Comparison of Invasion Scenarios 0A–2. The subdomain integration of functions of the model variables where we define these functions (α–$\$\iota$) in the text. Results are found at $t = 40$ unless otherwise specified. The values of the subdomain integration for specific variables for Invasion Scenario 0A, 1A, 1B, 2 can be found in Tables 5.1 and 5.2.*

t_c, when the switch from more degradation being due to MT1-MMP to more degradation from MMP-2.

From columns A–C we can determine that an increase in parameter δ_s causes an increase in the amount of suitability modifier that has been remodelled, an increase in the amount of total cancer cells and an increase in the total degradation of ECM.

Additionally, we find from these data is that the proportion of ECM that is degraded by MT1-MMP is reduced for the cases where δ_s is reduced and increased for when we have an increased δ_s. This result appears paradoxical at first as we would expect that by decreasing δ_s we would increase the amount of time that certain ECM is considered unavailable to be degraded by MMP-2. Indeed, when we compare the results obtained from Table 5.3 for proportion of degradation by

MT1-MMP between Invasion Scenario 1A and 1B at $t = 50$, we find that there is a marked reduction in the amount of degradation of ECM by MT1-MMP in IS1B from 1A (25% to 12%) where the parameter δ_s has increased from $\delta_s = 0.025$ to $\delta_s = 10$. This results in a contradiction that requires further examination and so we consider the plots of $\int \Delta v m_s$ and $\int \Delta v m_t$ to find some clarity. We find that for early times we have more than half of the degradation being done by MT1-MMP with a switch occurring at $t = t_c$ where more than half of the degradation is being done by MMP-2. We note that as degradation by MMP-2 increases at a quadratic rate of a higher power, the proportion of degradation as a result of MT1-MMP decreases as the time progresses. In comparing the amount of degradation by MMP-2 for each δ_s, we do find that there is an increase as δ_s increases however this is balanced at lower timeframes by the increase in t_c for increasing δ_s. As such we have identified that for lower timeframes, there is an increase in the proportion of degradation of ECM by MT1-MMP for increasing δ_s whereas for longer timeframes, there is the reverse where an a decrease in the proportion of degradation of ECM by MT1-MMP for increasing δ_s

We compare the data obtained for Invasion Scenario 0A and 1B in Tables 5.1 and 5.2 and find that having a high δ_s is almost analogous to having no suitability modifier considered with the exception of a reduced degradation of ECM in advance of the cancer invasion boundary where $s < 1$ (cf. Figure 4.8 E and Figure 5.4 E). We show in Figure 5.15 that the amount of overlap between cancer cells and the suitability matrix, that is to say the value of $c(1 - s)$, increases for a decreasing δ_s where there is virtually no overlap across the considered timeframe for the case where $\delta_s = 10$.

We note that for the case where there is a high δ_s, which is understood as a case where the suitability modifier is rapidly remodelled upon contact with the MT1-MMP attached to cancer cells, we recover many of the details, though not

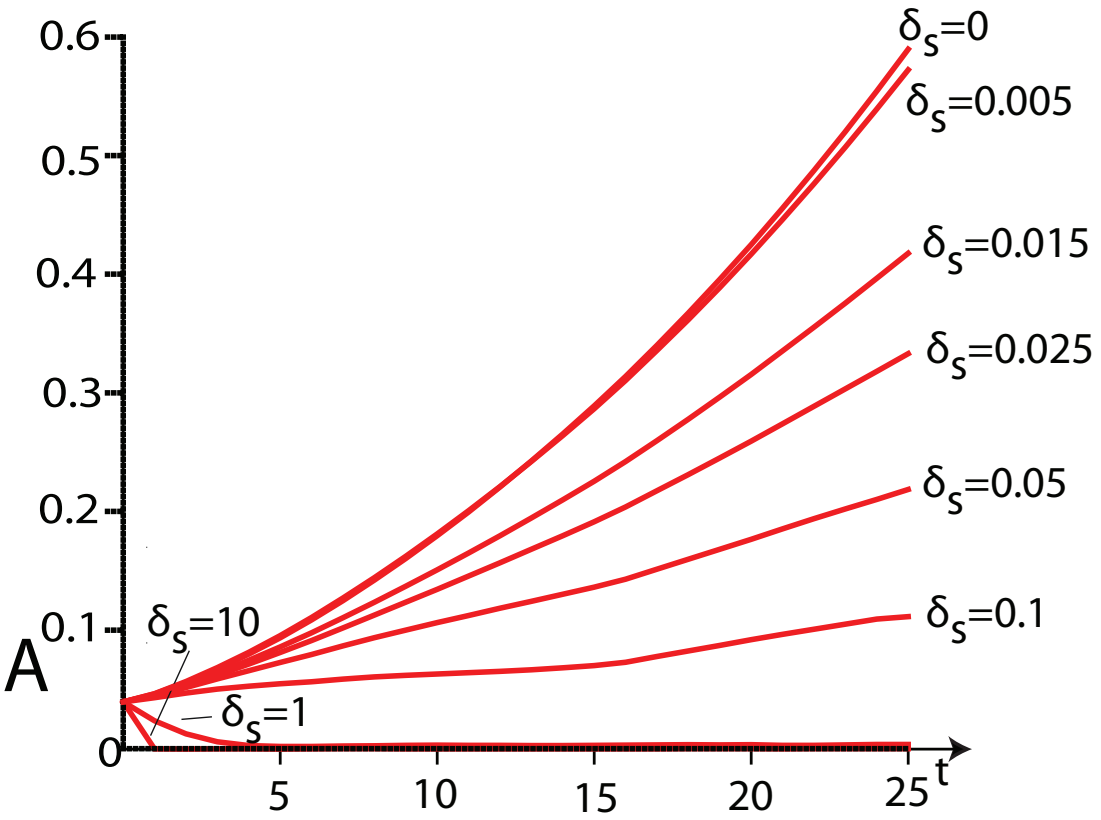

Figure 5.15: *Invasion Scenario 1A. We show the values of* $c(1-s)$ *across a timescale of* $t = 0 - 25$ *for varying values of the parameter that represents the remodelling of the suitability of the matrix,* $\delta_s = 0, 0.005, 0.015, 0.025, 0.05, 0.1, 1$ *and* 10*. Simulations are performed using the baseline parameter set of Table 4.4 along with the indicated values of* δ_s*.*

ψ	A	B	C	D	E
0	0	-0.08	-0.24	-0.01	-0.06
0.005	0.03	-0.06	-0.18	-0.01	-0.04
0.015	0.08	-0.03	-0.07	-0.01	-0.02
0.025	0.11	0	0	0	0
0.05	0.17	0.04	0.11	0	0.05
0.1	0.22	0.08	0.24	0.01	0.14
1	0.44	0.16	0.65	0.03	0.89
10	0.57	0.19	1.05	0.04	0.90

Table 5.4: *The amount that functions A–E, defined in the text, have increased or decreased at t=25 for when the parameter δ_s has a range of values 0-10 where we measure the variation from $\delta_s = 0$ in A and $\delta_s = 0.025$ for B-E.*

all, that are representative of the model from the previous chapter. The reason for the similarity, though not replication, is that as MT1-MMP rapidly remodels the suitability modifier, $g_1 = g_2 = g_3 = v$ where $c > 0$. As g_1 and g_3 would only matter where there already exists either cancer cells or MT1-MMP attached to cancer cells, it is only g_2 that offers meaningful difference from the model of the previous chapter where $g_2 = v$. We have therefore determined that for cases where δ_s is high, we have a model that is an extension from the previous model only where MMP-2 is limited in its ability to degrade the ECM in advance of the cancer cell boundary. By setting the diffusion rate of MMP-2 to 0, we would in fact have the two models converging as $\delta_s \to \infty$.

Invasion Scenario 2 can be seen as an alternative exploration from that of Invasion Scenario 1A of the effects of the suitability modifier where the two scenarios have the same parameters and initial conditions with the exception of

We note that there appears to be two classifications of results where Scenario 0A and 1B exist as one such classification while Scenario 1A and 2 represent the other. More specifically, we note that for Invasion Scenarios 0A and 1B we have that invasion has not been significantly hampered by the suitability matrix (where Invasion Scenario 0A is equivalent to a neutral $s(t = 0) = 1$ and as such is the scenario the others are compared to to measure the effect of the suitability modifier).

When examining Table 5.3, we make the following remarks:

(i) the ratio of total MT1-MMP to MMP-2 across the entire domain is approximately equal for all scenarios (ii) in the scenarios where MT1-MMP is less significant than MMP-2 (Invasion Scenarios 0A and 1B: where there is comparatively less a proportion of ECM degraded by MT1-MMP when compared to MMP-2 and there is either no suitability modifier to remodel or a high value of δ_s) we have that there is a higher proportion of MT1-MMP than MMP-2 despite the previously shown results of the MMP-2 being freely diffusive and as such being able to extend past the cancer cell invasive boundary while MT1-MMP is restricted by the movement of the cancer cells and cannot extend beyond the cancer cell invasive boundary.

The subdomain integration of TIMP2 concentration divided by the cancer cell density is either $\sim 0.03 - 0.04$ (Scenarios 0A, 1B) or $\sim 0.09 - 0.11$ (Scenarios 1A, 2) at $t = 40$ where we note that the stable steady state would provide a TIMP2 concentration of 0.01nM and a cancer cell density of 1 across the 4 by 4 domain providing a TIMP2 concentration scaled by the cancer density of 0.01, a value below either result obtained from the dynamically evolving results. The approximately threefold results for TIMP2 concentration scaled by cancer cell density in the second grouping of scenarios correlates with the the scenarios

where the cancer cells have been the least successful in growing and spreading. We further note that as the function of the domain integrals $\frac{T}{c}$ reduces (Invasion Scenario 1A and 2 $\rightarrow$ 1B and 0A) we see am increase in total cancer cell density (1.51 and 1.39 $\rightarrow$1.97 and 2.01). From this we may suspect that an increase in TIMP2 concentration may lead to a decrease in invasion from the ability of TIMP2 to inhibit the matrix degrading capabilities of MMP-2 however upon inspection of the spatial layout of TIMP2 in Invasion Scenario 1A in Figures 5.5 F & 5.6 F we see the increase in TIMP2 concentration is in the top half of the domain where we have an increased and active invasion. This paradoxical definition of an increased invasion where there is an increased concentration of TIMP2 while a lower overall TIMP-2 concentration benefits invasion means that TIMP2 cannot be an effective indicator of tumour invasiveness on its own.

t	c	v	m_s	m_t	T	f	s	Δv_{total}	$\Delta v m_s$	$\Delta v m_t$
0	2.00	14.00	2.00	2.00	2.00	2.00	9.00	0	0	0
100	7.26	6.74	147.60	147.90	0.09	6.71	11.30	43.24	36.02	7.22

Table 5.5: *Invasion Scenario 3A. Table showing the subdomain integration at* $t = 0$ *and* $t = 100$ *(corresponding to 0 days and ∼11.5 days) of the model variables in addition to the inclusion of how much degradation has occurred due to each and both of the MMPs considered.*

Invasion Scenario 3A examines computational simulation results of cancer cell invasion in a more heterogeneous environment such as would be expected in certain *in vitro* experiments (and also *in vivo*). For this scenario, we used the baseline parameter set, except for the parameter δ_s which is reduced by a factor of ten to a value of 0.0025. The plots in Figures 5.16 D–F show that the cancer cells take a longer time to invade the less suitable regions of ECM resulting in a heterogeneous invasion pattern. In Figure 5.16 F, we can see that there are regions of higher cancer cell density (small red zones) in advance of regions of lower cancer cell density (small green zones) but without having broken off from the main mass entirely. The corresponding plots of the concentrations of MMP-2 and MT1-MMP at $t = 10, 50, 100$.

Figure 5.17 shows the plots of the corresponding MMP-2 and MT1-MMP concentrations. Plots A-C show the MMP-2 concentration at $t = 10, 50$ and 100 (corresponding to ∼1.15, 5.75 and 11.5 days, respectively), while plots D–F show the MT1-MMP concentration at $t = 10, 50$ and 100 respectively.

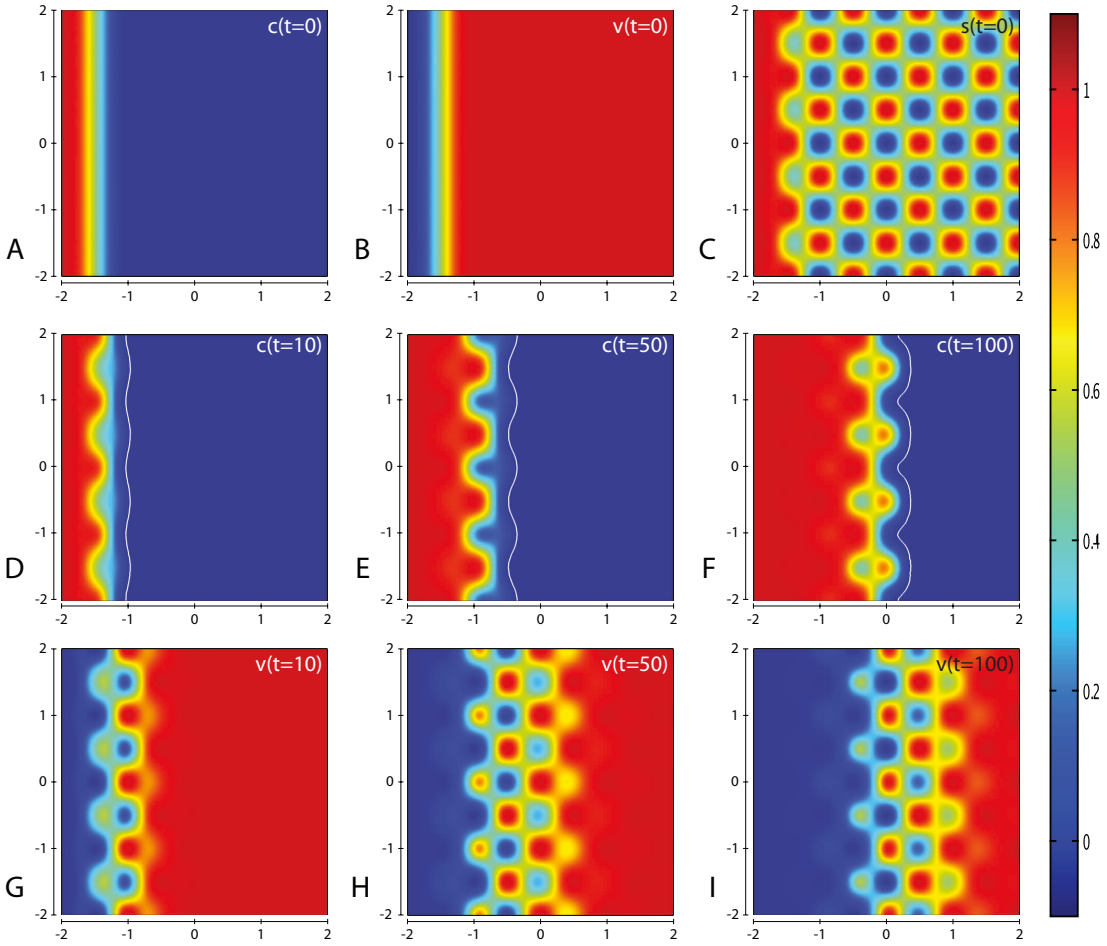

Figure 5.16: *Invasion Scenario 3A. Plots showing the simulation results obtained in a two-dimensional domain with a spatially complex matrix suitability modifier s to more accurately depict the observations of certain in vivo experiments. Plots A-C show the initial values of the cancer cell and ECM densities as well as the initial structure of the matrix suitability modifier. Plots D-F show the resultant profiles of cancer cell density at $t = 10, 50$ and 100 (corresponding to $\sim$1.15, 5.75 and 11.5 days, respectively). The white contour line shows the cancer cell density at level 0.01 chosen to represent the maximum extent of invasion. Plots G-I show the resultant profiles of ECM density at $t = 10, 50$ and 100. The simulations were performed using the baseline parameter set with the exception of the parameter $\delta_s = 0.0025$.*

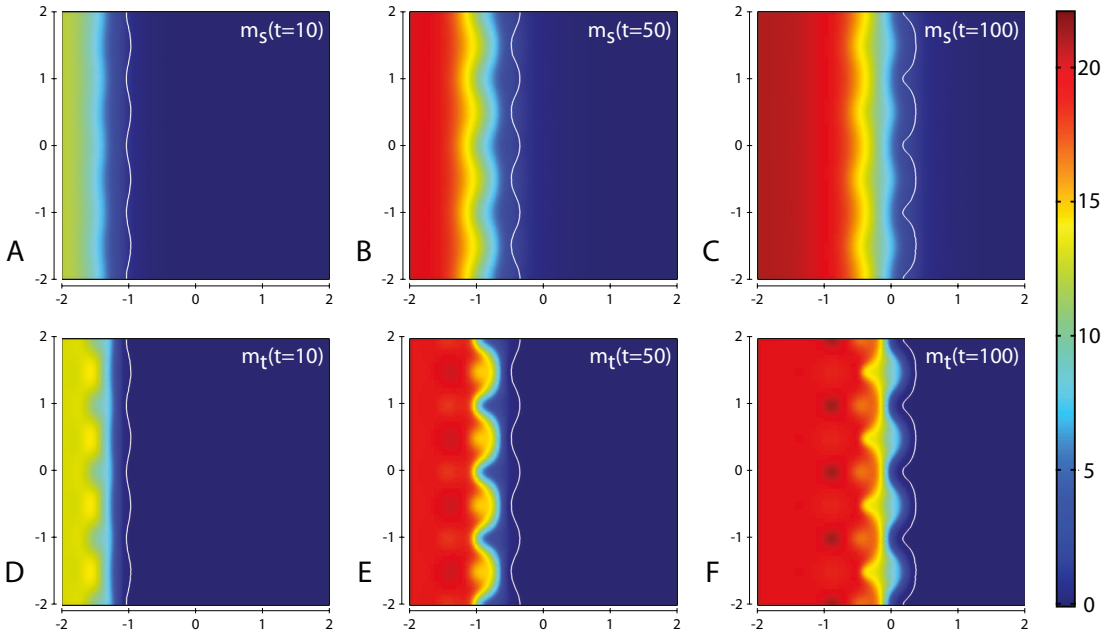

Figure 5.17: *Invasion Scenario 3A. Plots showing the simulation results obtained in a two-dimensional domain with a spatially complex matrix suitability modifier s to more accurately depict the observations of in vivo experiments. Plots A-C show the evolution of MMP-2 concentration at $t = 10, 50$ and 100 (corresponding to ∼1.15, 5.75 and 11.5 days, respectively). Plots D-F show the evolution of MT1-MMP concentration at $t = 10, 50$ and 100 respectively. The white contour line shows the cancer cell density at level 0.01 chosen to represent the maximum extent of invasion. Simulations are performed using the baseline parameter set with the exception of $\delta_s = 0.0025$.*

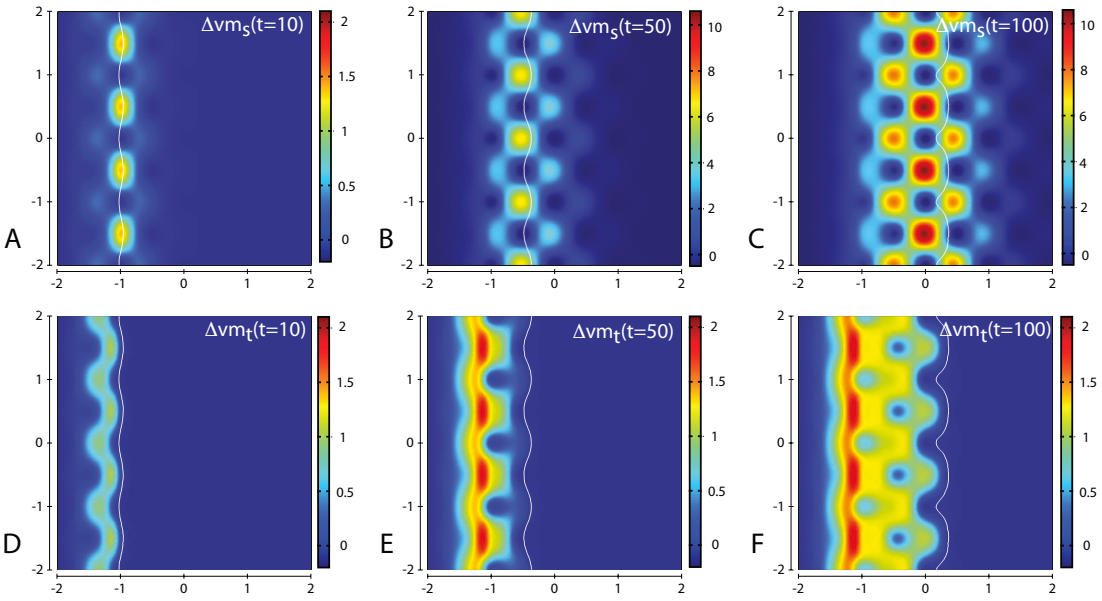

Figure 5.18: *Invasion Scenario 3A. Plots showing the simulation results obtained in a two-dimensional domain with a spatially complex matrix suitability modifier s to more accurately depict the observations of in vivo experiments. Plots A-C show the profiles of the density of ECM degraded solely by m_s, while plots D-F show the profiles of the density of ECM degraded solely by m_t at $t = 10, 50$ and 100 (corresponding to $\sim$1.15, 5.75 and 11.5 days, respectively). The white contour line shows the cancer cell density at level 0.01 chosen to represent the maximum extent of invasion. Simulations are performed using the baseline parameter set with the inclusion of $\delta_{s_u} = 0.025$.*

Invasion Scenarios 3B-E are variations of Invasion Scenario 3A where by considering different initial distributions of the suitability modifier ($s(t = 0)$) while imposing $\int s\mathrm{d}\Omega_{total}$ remaining the same (Ω represents the entire domain) with the additional constraints of $\int s\mathrm{d}\Omega_i$ remaining the same for defined smaller regions Ω_i. We note that the initial condition for Invasion Scenario 3A was determined in part by the term $0.5cos(\frac{4\pi x}{2})cos(k\pi y2$ where $k = 4$, for information in the final $\frac{3}{4}$ of the domain. As such, the natural division is for 26 Ω_i where,

$$\int s\mathrm{d}\Omega_1 = P, \int s\mathrm{d}\Omega_2 = Q, \int s\mathrm{d}\Omega_3 = R, \tag{5.8}$$

$$\int s\mathrm{d}\Omega_4 = S, \int s\mathrm{d}\Omega_j = T \tag{5.9}$$

For positive k and some constants P, Q, R, S and T where $j = 5, ..., 16$

Therefore, we choose to consider the cases where $k = 0, 2, 6, 8$ as Invasion Scenarios 3B-E, respectively. In considering the case where $k = 0$, we note that we no longer have the condition of $\int s\mathrm{d}\Omega_j = T$ for $j = 5, ..., 16$ but instead have $\int s\mathrm{d}\Omega_k = U(k)$ for $k = 1, ..., 8$ and $U(k) = (P + Q, R + S, 2T, 2T, 2T, 2T, 2T)^T$.

As the results of each of these Invasion Scenarios of 3C-F will be qualitatively the same as those obtained in Invasion Scenario 3A and Invasion Scenario 3B will be qualitatively similar to Invasion Scenario 0B, we present only the initial condition for $s(t = 0)$ for each scenario while the results of the domain integration of c will be presented in the next subsection in Figure 5.20.

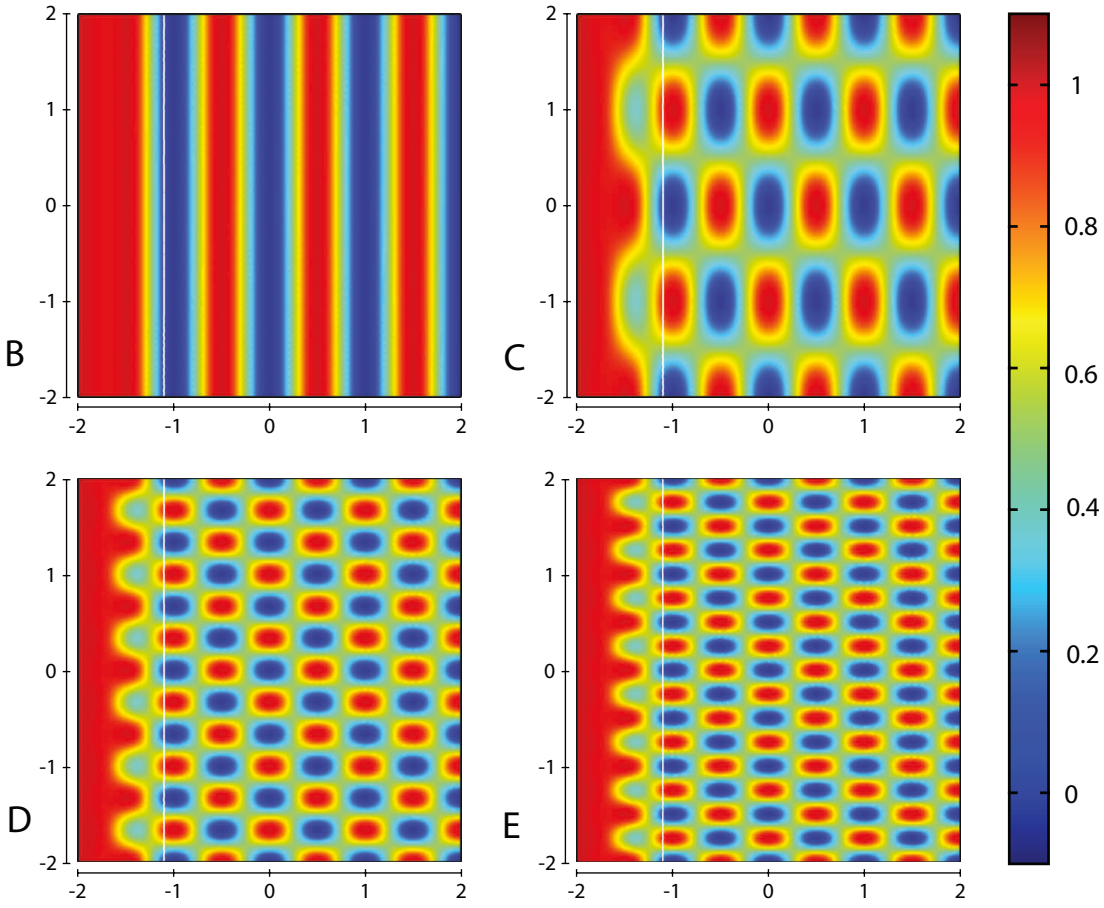

Figure 5.19: *Plots of the initial condition $s(t = 0)$ for Invasion Scenarios 3B-E*

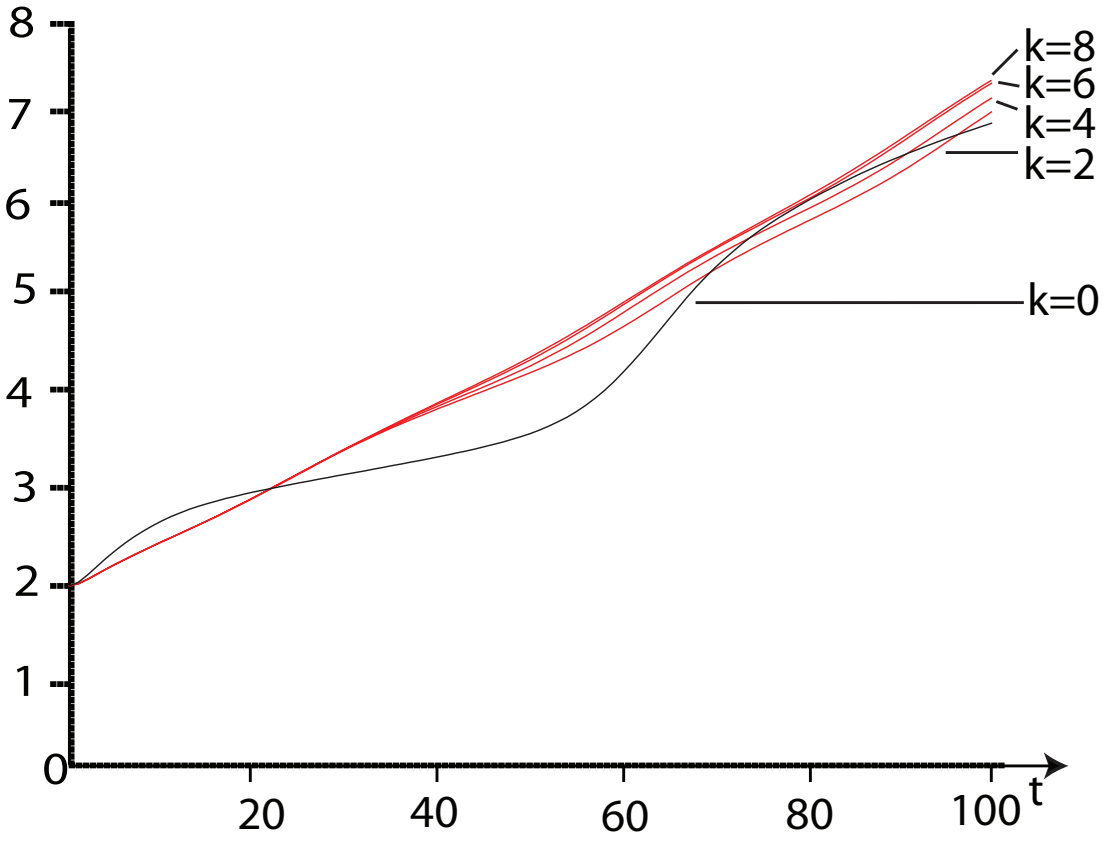

Figure 5.20: *Plot of the domain integration of cancer cells, $\int c \mathrm{d}\Omega_{total}$, for Invasion Scenarios 3A-E*

Comparison of Invasion Scenarios 3A-E enables considering the effect of changing the distribution of the initial condition for $s(t = 0)$ while maintaining the properties of $\int s \mathrm{d}\Omega_{total}$ and $\int s \mathrm{d}\Omega_i$ for $i = 1, ..., 16$ remaining the same for all of the Invasion Scenarios 3A-E.

In comparing the domain integrations of cancer cells in Figure 5.20, we find that the results are the same for $t < 35$ for Invasion Scenarios where $k > 0$. After this time, however, there is a breaking of the fellowship where the domain integration of the cancer cells becomes stratified where the Invasion Scenarios with higher k values show increased total cancer cell density. This suggests that a location with a suitability modifier value that is twice as restrictive as another location

will have less than twice the impact on cancer invasion over time. This can be understood as the remodelling term of the suitability modifier of $\delta_s m_t(1-s)$ will not provide a linear rate of remodelling over the time period it will take to obtain a value of $s = 1$ as there will be an increase in the amount of MT1-MMP present as more cancer cells reach the location of overlap. This affect will be even more pronounced for a lower δ_s, higher cancer diffusion or higher haptotaxis rate. This highlights the importance of effectively modelling the spatial aspect of the suitability modifier as even though we have subdomain integrations over each subdomain, Ω_i being the same between the Invasion Scenarios, there is still a difference in the total amount of cancer cells present at later times.

5.4 Discussion

By including a suitability modifier in the model considered in the previous chapter, we have found that this modification can provide a wide range of new results as well as providing an additional function for MT1-MMP which has now become much more significant to cancer cell invasion for specific types of tissue that may be considered to be closer to 3D in vitro models as well in vivo models.

Additionally we introduced the concept of "matrix suitability", governed by the variable s in our model. By considering the suitability of the matrix as a factor affecting ECM degradation and the movement of enzymes and cancer cells, we were able to generate heterogeneity in the ECM caused solely by matrix degradation. This meant we were able to focus on the effects of these gradients explicitly caused by matrix degradation rather than ECM density gradients due to some intrinsic tissue heterogeneity. This also allows for the consideration of stable spatially heterogeneous conditions in the initial ECM layout (while $v(t = 0) = 1$) where the ECM remodelling term of $\mu_v(1 - c - v)$ will not affect this initial heterogeneous condition over time. More specifically, if we were to not include the suitability modifier at all and wanted to have an initially heterogeneous ECM, we would have to have a spatially heterogeneous $v(t = 0)$. ECM that is not in the cancer-ECM interface would then be remodelled by the term $\mu_v(1-c-v)$ to the non-spatially heterogeneous value of 1 before cancer cells have come into contact with the region. The only 3 ways of preventing this would be to (i) consider a small enough domain that the remodelling of ECM has not fully taken place by the time cancer cells have reached the specified region, (ii) have a low enough parameter value μ_v (down to the point of being zero) for the same reason as in the first case and (iii) have the ECM remodelling term by dependent upon the spatially significant initial condition of v.

We found the parameter δ_s to be significant in determining the morphology of the cancer mass as evidenced by the comparison between Invasion Scenario 1A and 1B where the only difference was the increase in the parameter δ_s. We found that for a high enough δ_s, the results of the model are similar to, but do not tend to, those obtained for when there is no suitability modifier considered (Invasion Scenario 0A), unless there is a lack of diffusion for the MMP-2 proteins.

An increase in parameter δ_s causes an increase in the amount of suitability modifier that has been remodelled, an increase in the amount of total cancer cells and an increase in the total degradation of ECM.

We observed the time dependence on the effect of the parameter δ_s where when we compared the proportion of degradation of ECM by MT1-MMP for varying values of δ_s, we found that at $t = 25$ the relation was an increase for increasing δ_s whereas at $t = 50$ the relation was reversed with a decrease for increasing δ_s. This was due to the effect on the point measured as t_c which measured the time where the switch from more degradation occurring due to MMP-2 instead of MT1-MMP occurs where as t increases further, we will maintain this relation of an increase in δ_s will further reduce the proportion of ECM degradation caused by MT1-MMP.

Further, we have found that the ratio of MT1-MMP to MMP-2 is unaffected by either the suitability modifier or the rate at which it is remodelled, however, when there is a need for the suitability to be remodelled ($s(t = 0) < 1$), there is a higher proportion of total ECM degraded by MT1-MMP. We find that the total amount of TIMP2 when scaled by total cancer cell population is markedly increased to threefold in Invasion Scenarios 1A and 2 when compared to Invasion Scenarios 0A and 1B. This overall increase in relative TIMP2 concentration can be seen to be a result of an increase in TIMP2 at areas where there is active

degradation of ECM and a stabilised, reduced TIMP2 concentration at the area where cancer cell invasion has been completely successful ($c = 1$).

We formulated Invasion Scenarios 3A-E in such a way as to investigate the effect of a changing initial condition for the suitability modifier while maintaining 16 regions of constant total suitability modifier. We find that the initial spatial layout of the suitability modifier is important as while a location with a suitability value of $1 - 2\beta$ will have twice the impact as a suitability value of $1 - \beta$ for some constant β, when it comes to remodelling these locations to the value of 1, it will take t_1 for the first case and t_2 for the second case where $t_2 \leq t_1 \leq 2t_2$ due to the increase in MT1-MMP that is moved to the location that is being remodelled. This effect will therefore become more significant for an increase in the parameters of D_c, χ and a decrease in the parameter δ_s.

In summation, the computational simulation results showed that the matrix suitability modifier and its regulation played an important role in determining the precise pattern of invasion. As has been observed in the experimental data of Sabeh, Shimizu-Hirota and Weiss (2009) and Li et al. (2008), we have shown that the architecture of the tissue can negatively impact invasion under circumstances of pore-size being below on optimal level or in environments of cross-linked collagen type I and IV, with both of these conditions requiring tissue remodelling specifically by MT1-MMP. In addition to this, invasion is reduced where TIMP2 is over or under produced. To investigate the matrix suitability modifier from a biological perspective, experiments would need to be carried out to obtain the initial layout of the suitability modifier as well as the parameter δ_s. The first step in doing this would be to find out the effects of different tissue pore size on cancer cell migration to establish what range of pore sizes would be considered a neutral modifier, what range of pore sizes allow migration at reduced levels and what range of pore sizes completely block migration. This could be done by

using the approaches of Nyström et al. (2005) and Martins et al. (2009) where they performed *in vitro* experiments using a collagen:matrigel assay to investigate the invasiveness of cancer cells to establish a quantitative "invasive index" in organotypic cultures. Once there is quantitative data for these effects, obtaining data on the structure of the tissue through effective imaging techniques such as those described in Wolf et al. (2009) would allow one to generate realistic initial conditions of the matrix suitability modifier. An estimate of the parameter δ_s could then be obtained by validating the model against experiments similar to those found in Sabeh, Shimizu-Hirota and Weiss (2009) or Li et al. (2008), who performed *in vitro* experiments using a cross-linked native type I collagen assay to investigate the importance of MT1-MMP in cancer invasion.

Chapter 6

Stochastic Modelling of the MMP-2 Activation System at Invadopodia

6.1 Introduction

In this chapter we move from the much larger spatial scale considered in the previous two chapters to discuss MMP-2 activation by MT1-MMP proteins at the smaller subcellular scale of invadopodia (of volume 2×10^{-15} L Murphy and Courtneidge, 2011). While MMP-2, with its relatively high diffusion rate, is not responsible for localised ECM degradation at invadopodia, it is capable of degrading many components of the ECM, including type IV collagen. Type IV collagen is the main component of the basement membrane, a cellular barrier which cannot be degraded by MT1-MMP. Initially, we present a model of an invadopodium in isolation before analysing this model with simulations to show the affect an invadopodium has in the context of its surroundings, as well as the

Cube of length (cm)	**Volume (L)**	**Maximum number of cancer cells in domain**
1	1×10^{-3}	67, 000, 000
0.1	1×10^{-6}	67, 000
0.01	1×10^{-9}	67
0.0025	1.59×10^{-11}	1
0.000126	2×10^{-15}	a fraction equal to the volume of an invadopodia Murphy and Courtneidge (2011)

Table 6.1: *A clarification on the scales involved at various spatial scales in regards to the amount of cancer cells that can fill the volume. The values are based off of the cancer cell volume filling value in the previous two chapters of* $6.7 \times 10^7 cells\ cm^{-3}$.

affect that the surroundings have on the invadopodia.

Invadopodia are actin-rich membrane protrusions from a cell that form adhesion sites with the ECM and propagate ECM degradation by the releases of matrix degrading enzymes (Chen, 1989; Kelly et al., 1994). As such, they are of particular significance when it comes to cancer cell invasion (Basbaum and Werb, 1996; Weaver, 2006; Yamaguchi and Condeelis, 2007). This ECM degradation fuels migration of the cell through the ECM (Chen and Wand, 1999). Invadopodia are distinct from other cell protrusions (e.g. filopodia, lamellipodia, podosomes) in size and function (Chen and Wand, 1999; Murphy and Courtneidge, 2011). The maximum number of cancer cells that is capable of filling various volumes is listed in Table 6.1 to illustrate the spatial scale involved.

MT1-MMP is found to be the most critical of the matrix degrading enzymes

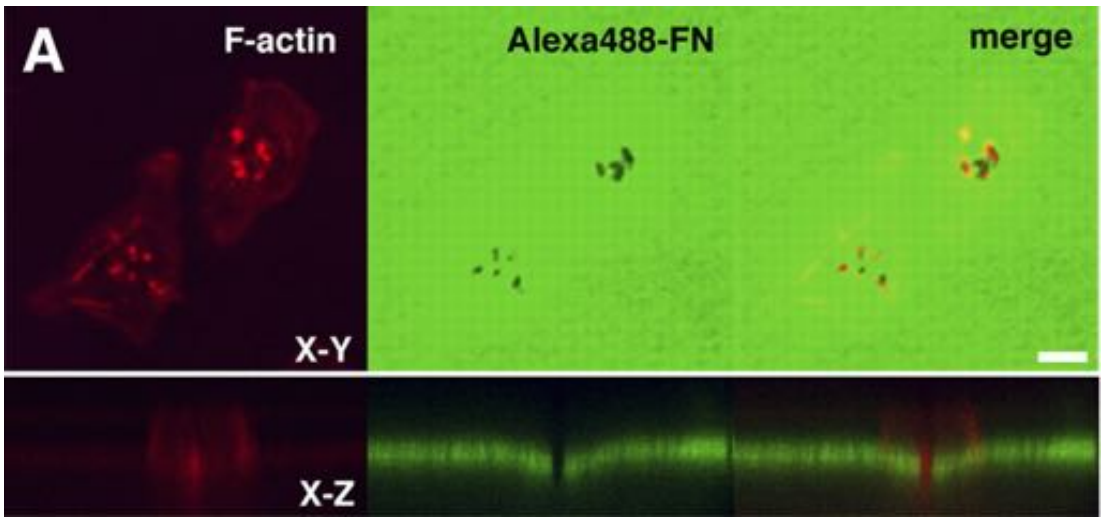

Figure 6.1: *Image showing focalised ECM degradation as a result of invadopodia. Reproduced from Yamaguchi et al. (2005), published under a creative commons licence.*

at invadopodia where they are not required for invadopodia formation but are essential for invadopodia function (Artym et al., 2006). A single carcinoma cell may feature 1–10 invadopodia at one time and these are generally formed in a cluster (Linder, 2007). This clustering causes focalised degradation of ECM as can be seen in Figure 6.1. MT1-MMP shuttling to invadopodia is essential for cancer cell invasion (Nakahara et al., 1997) and causes increased MMP-2 activation. Kwiatkowska et al. (2011) found that blocking this shuttling to lamellipodia can downregulate MMP-2 expression.

The precise number of MMP-2 proteins that can be activated at invadopodia must be estimated from the total amount produced by an entire cell. Here, we provide three methods of estimating this value using the property that a cell may produce MMP-2 at a rate of 100,000–1,000,000 h^{-1}. In all three methods, we will assume that the volume of a cell is 1.59×10^{-11}L and the volume of an invadopodium is 2×10^{-15}L, as in Table 6.1. Further, we will consider a cancer cell without invadopodia to be a sphere of radius 15.6μm and a single invadopodium to be a

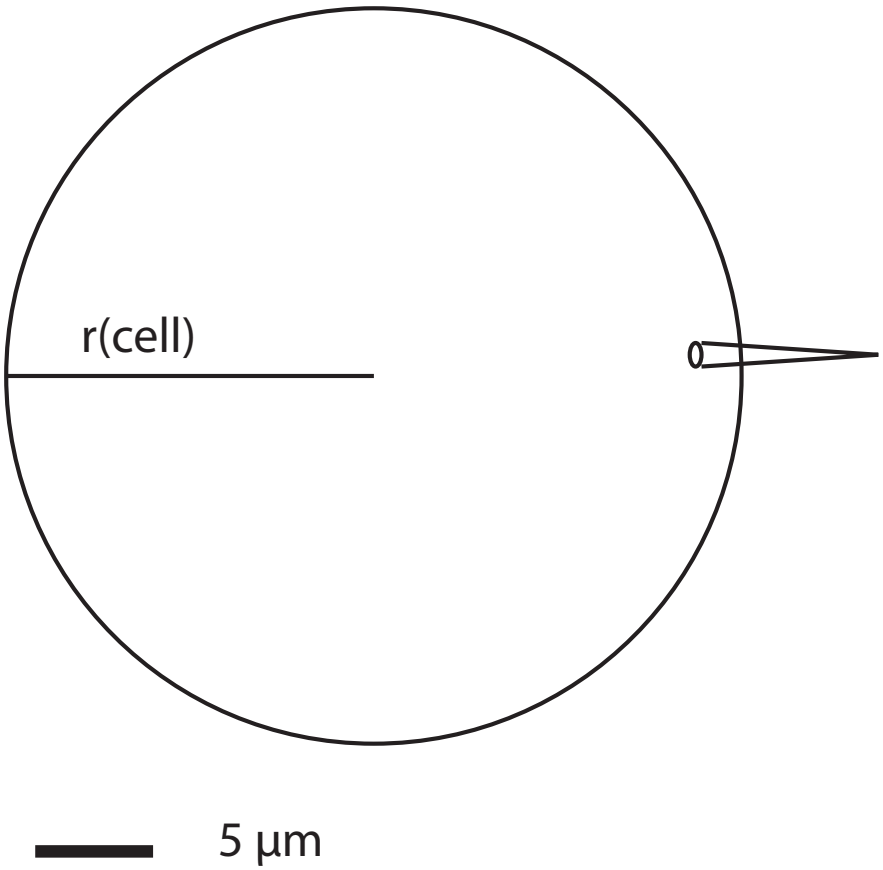

Figure 6.2: *Schematic diagram illustrating a cell with an invadopodium used to approximate the amount of MMP-2 proteins that can be activated at an invadopodium. Scale bar = 5μm.*

cone of radius 0.5μm and height 7.5μm where we note that these values maintain the volumes defined previously.

A method based off dividing the volume of the cell by that of the invadopodium provides an estimate of 12–126 proteins per hour. A method based off comparing the relative surface areas of the cell and invadopodium provides an estimate of 380–3800 proteins per hour. A third method, where additional details are provided below, provides an estimate of 2–30 proteins per hour.

The region defined as that in which enzyme reactions between membrane bound

and freely diffusive proteins can take place is termed the *active region*. The active regions of invadopodia is referred to as the *invadopodial regions*.

If we consider this active region to be up to a cm from the cell membrane then the volume of the active region for a cell without invadopodia would be $V_{ac} = \frac{4}{3}\pi((r+a)^3 - r^3) = \frac{4}{3}\pi(3r^2a + 3ra^2 + a^3)\text{cm}^3$. For simplicity, we neglect the minor difference as would be caused by the overlap of the active region of the cell and the invadopodia. The volume of the active region of the invadopodia is $V_{ai} = \pi(r+a)^2\frac{h+a}{3} - \pi r^2\frac{h}{3} = \frac{4\pi}{3}(\frac{r^2}{4} + \frac{ar(h+a)}{2} + \frac{a^2(h+a)}{4})$. Therefore, the amount of MMP-2 proteins that can be produced at invadopodia is estimated to be $(\frac{V_{ai}}{V_{ac}} \times 100)\%$ of 100,000–1,000,000h^{-1}. We plot $\frac{V_{ai}}{V_{ac}} \times 100$ in Figure 6.3. Therefore, the number of MMP-2 proteins that can be produced at invadopodia is estimated to be $0.0025 - 0.003\%$ of the range 100,000–1,000,000h^{-1}, or, 2-30 proteins per hour.

Taking the three methods into account, we choose to consider a default range for the amount of MMP-2 proteins to be activated of 0–216 proteins (0–180nM) per hour. This can be achieved by simulating the invadopodial region with zero flux boundary conditions with a corresponding initial proMMP-2 concentration of 0–180nM and no production.

Stochastic simulations are widely used for intracellular dynamics in computational cell biology (Cai and Wang, 2007; Bressloff and Newby, 2013; Sturrock, 2013). Traditionally, intracellular chemical reactions have been modelled with deterministic reaction rate equations (RREs), namely ordinary differential equations (ODEs). The justification for modelling these reactions stochastically lies in the low population number of mRNAs as well as the fact that small fluctuations in their levels have a knock-on effect where each mRNA may produce 1000s of active proteins.

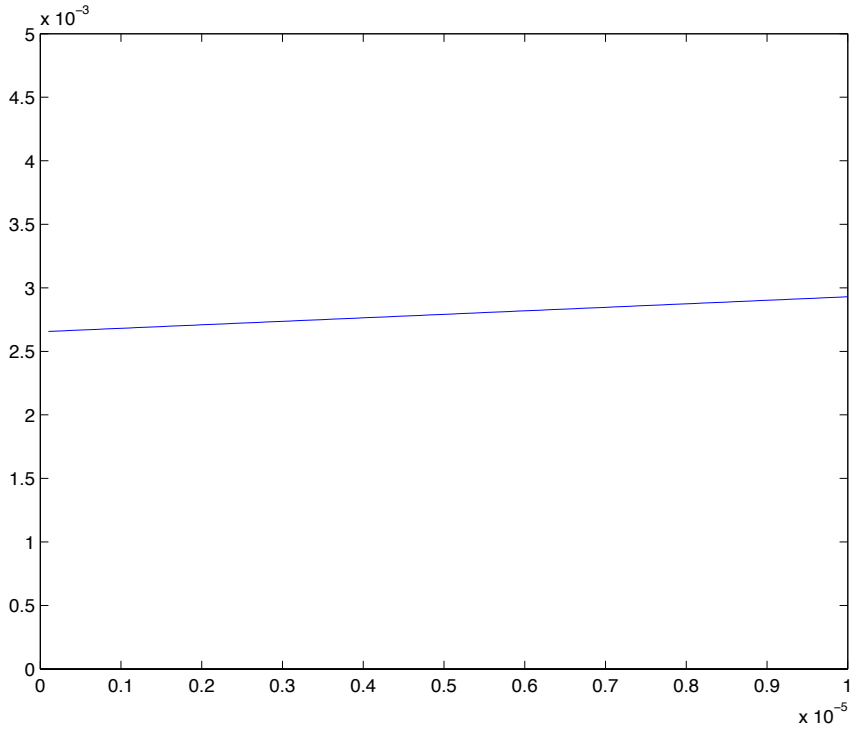

Figure 6.3: *Identifying the proportion of MMP-2 proteins that are produced by an invadopodium is achieved by plotting the function* $\frac{V_{ai}}{V_{ac}} \times 100$ *for various values of the radius defining the invadopodial region,* a*, where* h=7.5μm *and* r=0.5μm*. The minimum value of* a *is considered to be* 0.001μm *with a maximum* a *of* 0.1μm*, which we note is one fifth the radius of the invadopodium.*

At invadopodia, only a small number of proteins (0-432) comes into play in a relatively short time (1-2 hours). The knock-on effect from a localised increase in the activation of MMP-2 increases the degradation of ECM across the considered domain. However the most significant knock-on effect is that the increased ECM degradation occurring at invadopodia as a result of MT1-MMP activity can fuel locomotion of the entire cell through a medium (Chen and Wand, 1999). We therefore apply stochastic methods when considering the activation system of MMP-2 by MT1-MMP and TIMP2 at invadopodia.

We formulate our model based on the Gillespie Algorithm (SSA: stochastic simulation algorithm Gillespie, 1977), which is explained in detail in Higham (2008). We will use this approach to model the system of activation of MMP-2 by MT1-MMP as outlined in Figure 6.4.

We will therefore be simulating a similar scenario to that which is considered in a deterministic way with a system of ODEs in Karagiannis and Popel (2004), which was later developed to consider the tip endothelial cell in sprouting angiogenesis in Karagiannis and Popel (2006). We note that continuum modelling is an appropriate method of modelling the protein interactions considered in this chapter when applied to a domain considering one or more cancer cells as the larger spatial and temporal scales results in a large amount of proteins and less consequences in fluctuations of their populations.

The other notable attempt at modelling MT1-MMP mediated MMP-2 activation along with related interactions in regards to cancer cell invasion is that of Hoshino et al. (2012). The focus of their work is an invadopodium of size $\sim 1.39\mu m^3$ with a total domain of size $\sim 73.61\mu m^3$. They modelled the invadopodium and surrounding environment as a 3D discretised space of 2601 compartments of dimensions $0.0973\mu m \times 0.0973\mu m \times 3\mu m$ where the invadopodium consisted of

49 clustered compartments. The freely diffusive proteins and protein complexes were modelled with reaction diffusion equations while the interactions of proteins within the invadopodium were modelled by a systems of 39 ODEs in ACell (Ichikawa, 2001). The main finding of their work is that the rapid turnover of MT1-MMP is responsible for the increased degradation of ECM at invadopodia. This was determined from both of their *in silico* and *in vitro* modelling approaches where the blocking of vesicle transport blocked ECM degradation.

6.2 Model Development

A schematic diagram of the MMP-2 activation system from its pro-enzyme form is shown in Figure 6.4. The N-terminal inhibitory domain of a freely diffusive TIMP2 protein binds to the active site (catalytic region) of the membrane bound MT1-MMP. This blocks catalytic activity on the part of MT1-MMP. The C-terminal domain that remains free on TIMP2 binds with the C-terminal hemopexin domain of proMMP-2. This stochiometric trimer of form 1:1:1 is then split by a free MT1-MMP protein concluding the activation of MMP-2 from its proenzyme form. Additionally, we consider an alternative route by which the trimer of MT1-MMP:TIMP2:proMMP-2 can be formed by the initial formation of the complex TIMP2:proMMP-2 that can then bind to a free MT1-MMP protein. As both proMMP-2 and MMP-2 bind to TIMP2 with a high rate in comparison to the dissociation rate (Olson et al., 1997), we consider this reaction to be irreversible. Before we present the reaction equations, we must define the notation involved.

Notation for the stochastic model largely follows the mathematical literature (Higham, 2008):

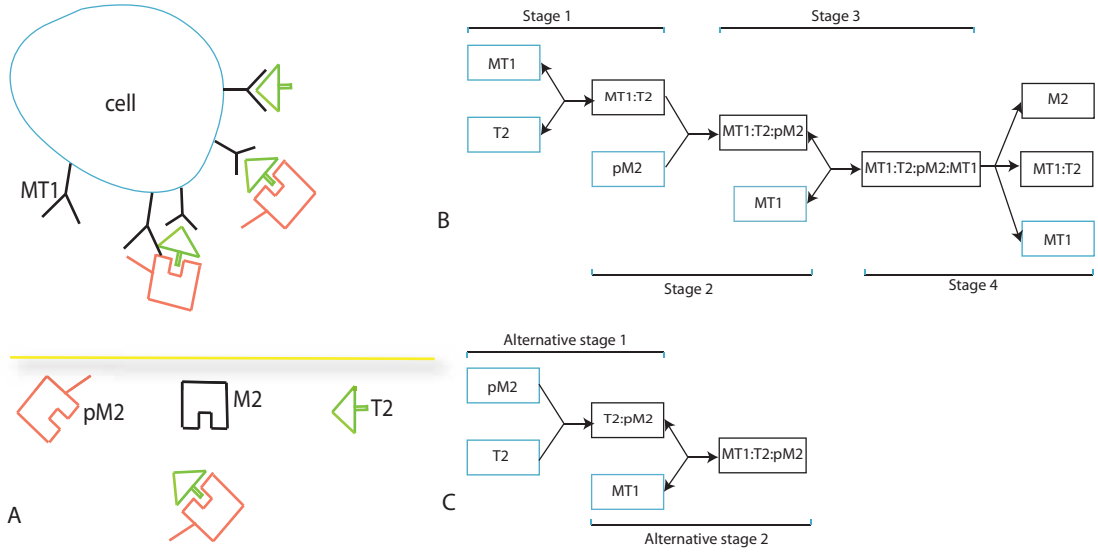

Figure 6.4: *The schematic diagram of MMP-2 activation. Plot A indicates whether a protein or complex is bound to the membrane of the cell or capable freely diffusing throughout the domain. Plot B illustrates the first pathway by which proMMP-2 can become activated while plot C illustrates the alternative route by which proMMP-2 can become activated. In all plots, 'MT1' represents MT1-MMP, 'T2' represents TIMP2, pM2 represents proMMP-2 and M2 represents MMP-2, while in plots B and C, a protein/complex is in a blue box if it is directly produced by a cancer cell and black if it is formed from later reactions.*

N : the number of chemical species.

M : the number of chemical reactions or reaction channels that the chemical species partake in.

$\mathbf{X}(t)$: the *state vector*, elements of which are defined below.

$X_i(t)$: elements of the state vector represent the number of elements of chemical species i, where $i = 1, ..., N$.

$\nu_{\mathbf{j}}$: the *stochiometric vector*, also known as the *state-change vector*, details how the state vector is modified by chemical reaction j where $j = 1, ..., M$.

A: the *stochiometric matrix* is a matrix whose columns are made up of the stochiometric vectors, i.e., $A = [\nu_1, ..., \nu_M]$.

We define the state vector of our model as follows:

$$\mathbf{X}(t) = \begin{pmatrix} X_1(t) \\ X_2(t) \\ X_3(t) \\ X_4(t) \\ X_5(t) \\ X_6(t) \\ X_7(t) \\ X_8(t) \\ X_9(t) \end{pmatrix} = \begin{pmatrix} \text{proMMP-2} \\ \text{MMP-2} \\ \text{MT1-MMP} \\ \text{TIMP2} \\ \text{MT1-MMP:TIMP2} \\ \text{MT1-MMP:TIMP2:proMMP-2} \\ \text{MT1-MMP:TIMP2:proMMP-2:MT1-MMP} \\ \text{MMP-2:TIMP2} \\ \text{proMMP-2:TIMP2} \end{pmatrix}, \quad (6.1)$$

and we can proceed to write out the chemical reactions outlined above in a manner that will be easier for our modelling efforts.

Stage 1: $X_3 + X_4 \xrightarrow{c_1} X_5$ (6.2)

$X_5 \xrightarrow{c_2} X_3 + X_4$ (6.3)

Stage 2: $X_5 + X_1 \xrightarrow{c_3} X_6$ (6.4)

Stage 3: $X_6 + X_3 \xrightarrow{c_5} X_7$ (6.5)

$X_7 \xrightarrow{c_6} X_6 + X_3$ (6.6)

Stage 4: $X_7 \xrightarrow{c_7} X_5 + X_2 + X_3$ (6.7)

Alternative stage 1: $X_1 + X_4 \xrightarrow{c_8} X_9$ (6.8)

Alternative stage 2: $X_3 + X_9 \xrightarrow{c_1} X_6$ (6.9)

$X_6 \xrightarrow{c_2} X_3 + X_9$ (6.10)

$X_2 + X_4 \xrightarrow{c_8} X_8$ (6.11)

Now that we have formulated the system in this way, it is easier to see what each of the reactions defined by equations (6.2)–(6.11) does to the state vector $\mathbf{X}(t)$. For example, for one reaction taking us from $t = t_1$ to $t = t_2$ of equation (6.7) to occur we require an $X_7(t_1) \geq 1$ with the result being $X_7(t_2) = X_7(t_1) - 1$, $X_9(t_2) = X_9(t_1) + 1$, $X_2(t_2) = X_2(t_1) + 1$, $X_3(t_2) = X_3(t_1) + 1$ with the remaining $X_j(t_2) = X_j(t_1)$ for $j = 1, 4, 5, 6, 8$. In formalising this, $\mathbf{X}(t_1 + \tau) = \mathbf{X}(t_1) + \nu_{\mathbf{j}}$ where τ is the adaptively determined timestep for the chemical reaction j to occur

and $\nu_{\mathbf{j}}$ are defined as the columns of the stochiometric matrix A where:

$$A = \begin{pmatrix} 0 & 0 & -1 & 1 & 0 & 0 & 0 & -1 & 0 & 0 & 0 \\ 0 & 0 & 0 & 0 & 0 & 0 & 1 & 0 & 0 & 0 & -1 \\ -1 & 1 & 0 & 0 & -1 & 1 & 1 & 0 & -1 & 1 & 0 \\ -1 & 1 & 0 & 0 & 0 & 0 & 0 & -1 & 0 & 0 & -1 \\ 1 & -1 & -1 & 1 & 0 & 0 & 1 & 0 & 0 & 0 & 0 \\ 0 & 0 & 1 & -1 & -1 & 1 & 0 & 0 & 1 & -1 & 0 \\ 0 & 0 & 0 & 0 & 1 & -1 & -1 & 0 & 0 & 0 & 0 \\ 0 & 0 & 0 & 0 & 0 & 0 & 0 & 0 & 0 & 0 & 1 \\ 0 & 0 & 0 & 0 & 0 & 0 & 0 & 1 & -1 & 1 & 0 \end{pmatrix}. \tag{6.12}$$

We are left with two issues that need to be dealt with. Firstly, how we will choose which of the chemical reactions takes place and secondly, in what manner will we define their respective timesteps represented by τ. It is in both of these steps that we will find our stochasticity. By using the Gillespie Algorithm, we obtain the following iterative method of identifying which reaction will next take place and what the time length, τ, for this reaction to take place will be where we use the function *rand* in Matlab to generate a random number, r, from a uniform distribution in the interval (0,1). The reaction rates determined in units involving concentrations $(c_1, ..., c_8)$ are transformed into appropriate form $(a_1, ..., a_{11})$ where the probability of a reaction, j, to take place is determined by $\frac{a_j}{\sum_{i=1}^{11} a_i}$.

A minimal form of one iteration of our model is presented below in equations (6.13)–(6.29) where the probability of which reaction takes place is initially defined before the reaction that is chosen to take place and the time that this takes is determined. The molecule population and the probability of which reaction would take place would therefore be updated in the next iteration.

$$a_1 = \frac{c_1}{N_A v} \times X_3 \times X_4 \tag{6.13}$$

$$a_2 = c_2 \times X_5 \tag{6.14}$$

$$a_3 = \frac{c_3}{N_A v} \times X_1 \times X_5 \tag{6.15}$$

$$a_4 = c_4 \times X_6 \tag{6.16}$$

$$a_5 = \frac{c_5}{N_A v} \times X_6 \times X_3 \tag{6.17}$$

$$a_6 = c_6 \times X_7 \tag{6.18}$$

$$a_7 = c_7 \times X_7 \tag{6.19}$$

$$a_8 = \frac{c_8}{N_A v} \times X_1 \times X_7 \tag{6.20}$$

$$a_9 = \frac{c_1}{N_A v} \times X_3 \times X_9 \tag{6.21}$$

$$a_{10} = c_2 \times X_6 \tag{6.22}$$

$$a_{11} = \frac{c_8}{N_A v} \times X_2 \times X_4 \tag{6.23}$$

$$\alpha = \sum_{i=1}^{11} a_i \tag{6.24}$$

$$\beta_k = \frac{\sum_{i=1}^{k} a_i}{\alpha} \tag{6.25}$$

$$j = \min(k) \text{ s.t. } r < \beta_k \tag{6.26}$$

$$\tau = \frac{1}{\alpha} ln(\frac{1}{r}) \tag{6.27}$$

$$X = X + \nu_j \tag{6.28}$$

$$t = t + \tau \tag{6.29}$$

Rate constants for the model are established by collecting those that were used in previous chapters as well as the biological literature and are presented in Table 6.2. We note that there is a high level of uncertainty when it comes to parameter c_5 which can be fitted to the experimental results of English et al. (2001) and Butler et al. (1998), similarly done in the ODE model considered in Karagiannis

and Popel (2004) to obtain a value of $\sim 4.3 \times 10^3 M^{-1}$. Indeed, we show how the proposed stochastic model can obtain a similar approximation to this value in Figure 6.5. This is, however, significantly lower than the parameter value of $2 \times 10^6 M^{-1}$ used in Hoshino et al. (2012) and $4.3 \times 10^4 M^{-1}$ used in the previous chapters of this work and that of Deakin and Chaplain (2013). As such, while we continue to use the value of $4.3 \times 10^4 M^{-1}$, we acknowledge that a more accurate, biologically obtained, estimate for this parameter is required.

We examine the activation system of MMP-2 mediated by MT1-MMP and TIMP2 and as such consider a spatial region around the external boundary of invadopodia. We define this spatial region of interest to be approximately the same size as the invadopodia itself of 2×10^{-15}L. This is equivalent to choosing a value of $a =\sim 0.3\mu$m. As we lack significant data for the production rates of proMMP-2, TIMP2 and MT1-MMP, we consider the system to be closed by setting $\alpha_{\text{pM2}} = \alpha_{\text{MT1}} = \alpha_{\text{T2}} = 0$.

We initially consider two cases with differing initial conditions, where we show the results of the proposed schematic when run over 1 hour with zero-flux boundary conditions. We present the cases concurrently, divided into two figures detailing the population dynamics across the initial 60s (Figure 6.6) and then the entire lifespan of the invadopodium, defined as 1 hour (Figure 6.7).

For the first case, we consider proMMP-2($t = 0$) = 60nM, MT1-MMP($t = 0$) = 70nM and TIMP2($t = 0$) = 50nM, while all other enzymes and enzyme complexes are assumed to be zero. In the second case, we consider proMMP-2($t = 0$) = 60nM, MT1-MMP($t = 0$) = 47.5nM and TIMP2($t = 0$) = 50nM where, again, all other enzymes and enzyme complexes are assumed to be zero. We note that when we define the I.C.s to be of form pM2=z_1, T2=z_2 and T2:pM2=z_3, we can vary the initial conditions of these three proteins and complexes and maintain

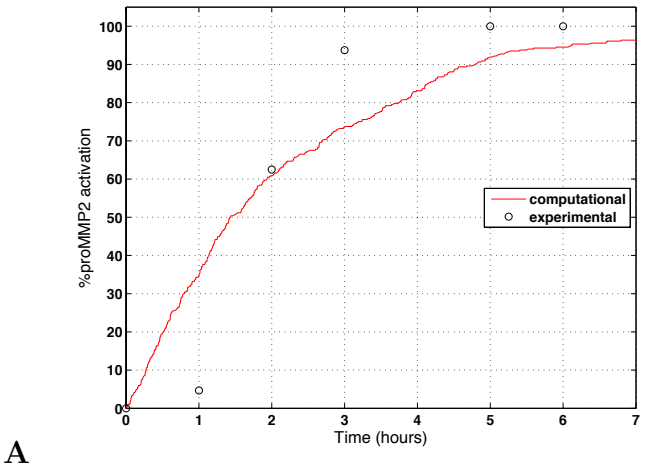

A

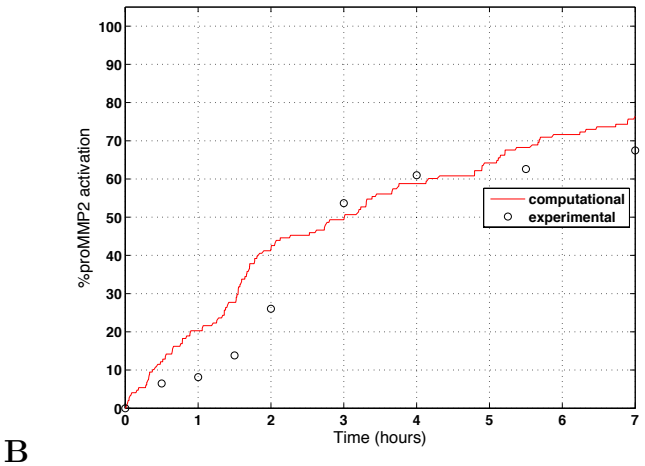

B

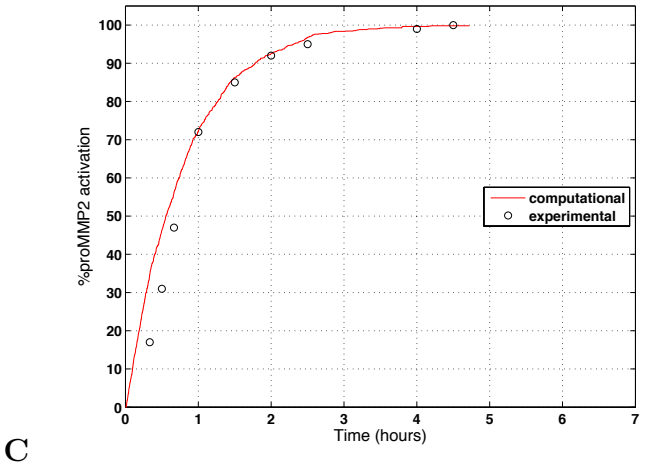

C

Figure 6.5: *Plots showing comparisons of the stochastic model with the parameters of Table 6.2 with the exception of* $c_5 = 4.3 \times 10^3 M^{-1} s^{-1}$. *The experimental data of Butler et al. (1998) is represented in plots A & B and English et al. (2001) in plot C.*

Parameter	**Dimensionalised value**	**Source**
c_1	$2.74 \times 10^6\ M^{-1}s^{-1}$	Toth et al. (2000)
c_2	$2 \times 10^{-4}\ s^{-1}$	Toth et al. (2000)
c_3	$1.406 \times 10^5\ M^{-1}s^{-1}$	Olson et al. (1997)
c_4	$4.7 \times 10^{-3}\ s^{-1}$	Olson et al. (1997)
c_5	$4.3 \times 10^4\ M^{-1}s^{-1}$	estimated
c_6	$9 \times 10^{-7}\ s^{-1}$	Karagiannis and Popel (2004)
c_7	$2 \times 10^{-2}\ s^{-1}$	Karagiannis and Popel (2004)
c_8	$3.26 \times 10^4\ M^{-1}s^{-1}$	Olson et al. (1997)
$c_{shuttle}$	$\frac{1}{t_{\text{shuttle}}} s^{-1}$	definition
α_{pM2}	0	
α_{MT1}	0	
α_{T2}	0	
N_A	6.022×10^{23}	Perrin (1909)
volume (v)	2×10^{-15}L	estimated

Table 6.2: *List of parameter values used in this chapter (unless otherwise stated).*

qualitatively similar results provided the conditions of $z_1 + z_2 + 2 \times z_3 = C_1$ and $\frac{z_1 + z_3}{z_2 + z_3} = C_2$ are met, for some constants C_1 and C_2.

We note that the plots of Figure 6.6 are qualitatively similar. However, there are some noticeable differences where the first difference we remark upon is one we have not found to be significant. In the first case, the complex MT1-MMP:TIMP2:proMMP-2 (brown) is first formed at $t =\sim$ 7s in comparison to $t =\sim$ 3s in the second case. Further, the number of TIMP2 proteins in the first case has almost reached zero in half the timeframe while this number has not dropped below 8 in the entire timeframe in the second case. This difference is caused by the amount of TIMP2 binding to MT1-MMP where we remark that MT1-MMP(t=60)=25 in the first case compared to the very low value of MT1-MMP proteins in the second case by this time.

It is in the plots of Figure 6.7 that we notice a much more significant difference between the two cases. Critically, there is minimal MMP-2 present by the end of the simulation for the second case. This is the result of TIMP2 proteins binding to every available MT1-MMP protein meaning that there is a lack of free MT1-MMP proteins that are able to take place in the severing of the pro domain as indicated in stages 3 and 4 of Figure 6.4. In fact, the only enzymes and enzyme complexes larger than 10 in case ii are MT1-MMP:TIMP2:proMMP-2 (brown), proMMP-2 (red) and MT1-MMP:TIMP2 (green).

We note that from 10 simulations (not shown) where there were the same initial conditions as presented in case ii, the percentage of MMP-2 activated by t=3600s varied between 0 and 15 with mean value $\sim$4.4% and standard deviation of $\sim$3.2. This compares to the percentage of MMP-2 activated by t=3600s where we consider the volume of the well-mixed system to be 2×10^{-11}L, where Higham (2008) showed that the Gillespie Method converges to the ODE model of the interactions

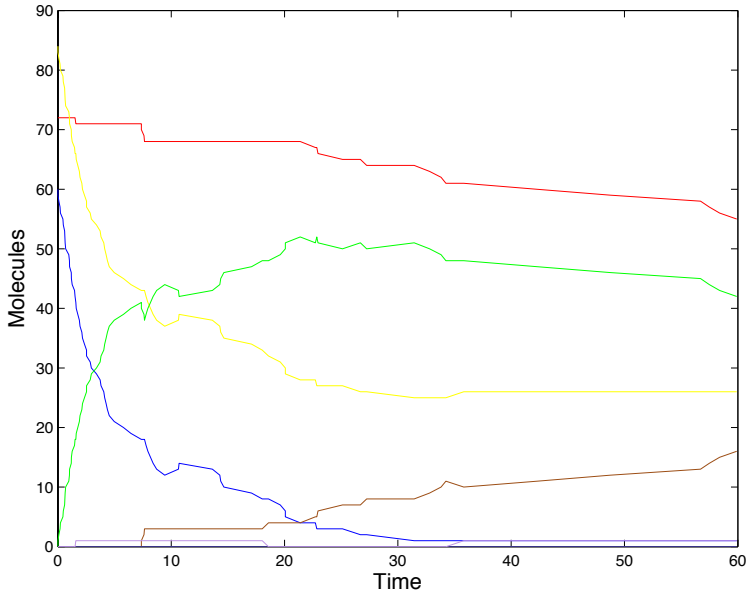

A

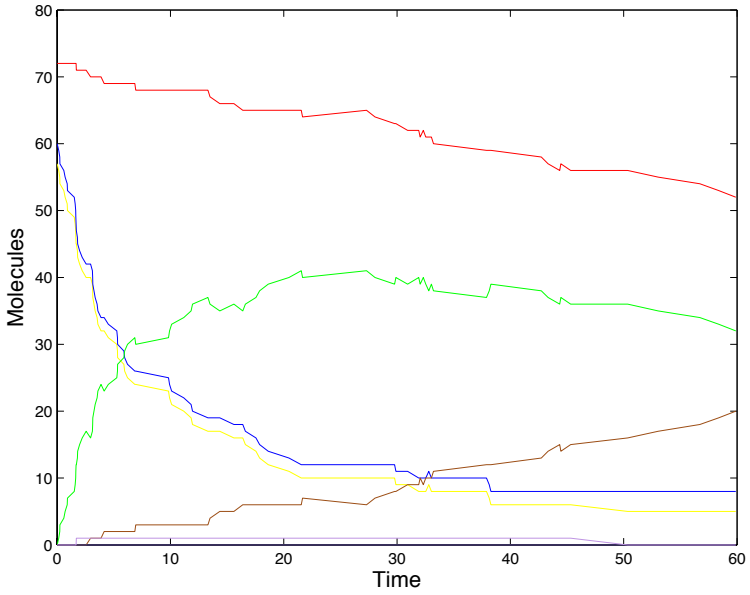

B

Figure 6.6: *Plots showing the short time dynamics (t=0-60s) of the MMP-2 activation system. Plot A represents the first case while plot B represents the second case. proMMP-2 is presented in red, MT1-MMP in yellow, TIMP2 in blue, MT1-MMP:TIMP2 in green, MT1-MMP:TIMP2:proMMP-2 in brown, MT1-MMP:TIMP2:proMMP-2:MT1-MMP in dark blue, MMP-2 in black and TIMP2:proMMP-2 in lavender.*

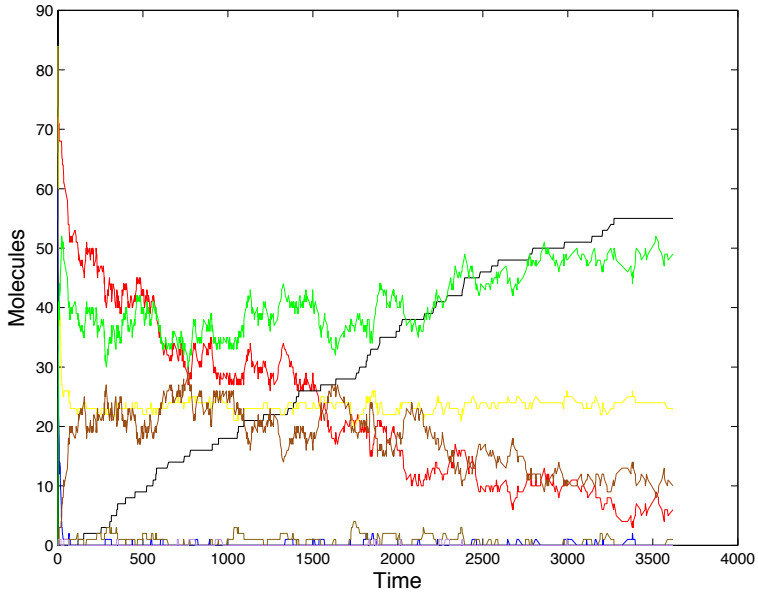

A

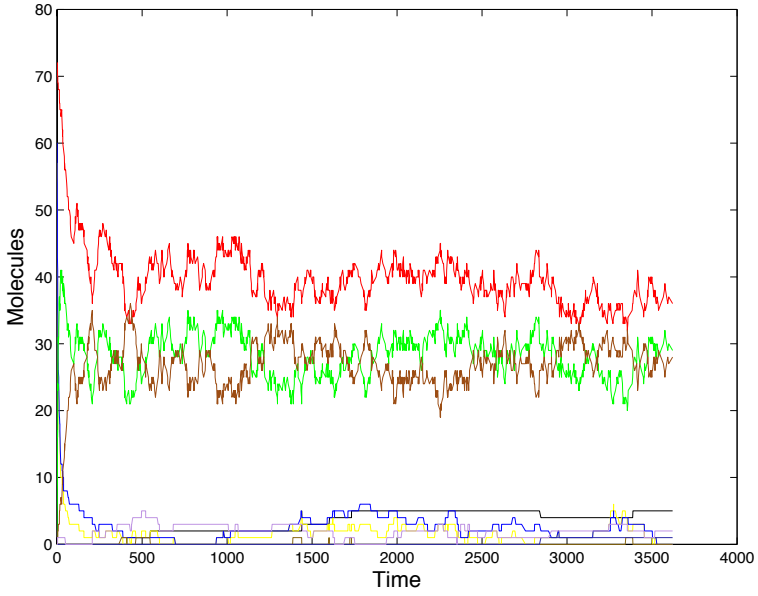

B

Figure 6.7: *Full term dynamics (t=0-3600s) of the MMP-2 activation system where no MT1-MMP shuttling takes place. Plot A represents the first case while plot B represents the second case. proMMP-2 is presented in red, MT1-MMP in yellow, TIMP2 in blue, MT1-MMP:TIMP2 in green, MT1-MMP:TIMP2:proMMP-2 in brown, MT1-MMP:TIMP2:proMMP-2:MT1-MMP in dark blue, MMP-2 in black and TIMP2:proMMP-2 in lavender.*

at high volumes, of 6.0%.

The conclusions that we can draw from these observations are that when the initial number of TIMP2 proteins is larger than the initial amount of MT1-MMP proteins, rapid binding of MT1-MMP to TIMP2 can prevent there from being any free MT1-MMP proteins to take place in the activation of MMP-2. However, we can also conclude that stochastic effects allow for the production of some MMP-2 proteins despite this with the maximum of 11% of the proMMP-2 being activated in the simulations run.

We have proposed a method of examining invadopodia in isolation from the cell and the majority of the surrounding ECM by imposing zero-flux boundary conditions on a domain defined as the invadopodial region (the difference between the volume of one cone of radius, r, and height, h, and a larger cone of radius, $r + a$, and height, $h + a$). While there may be experiments that can be set up to study just such a scenario, we consider the additional dynamics of freely diffusive proteins capable of diffusing into the invadopodial region to be more reflective of the majority of potential *in vivo* and *in vitro* experiments. We note that due to the relatively high diffusion rate of the freely-diffusive proteins ($O(10^8 cm^2 s^{-1})$ Collier et al., 2011), this would not be an inconsequential amount. We must therefore expand the model to capture the dynamics involved with the activation process of MMP-2 in a more expansive set of biological considerations.

We define a scenario similar to the experimental results shown in Figure 6.1 by using the schematic illustrated in Figure 6.8, where we consider a layer of ECM constituent parts of dimensions $5 \times 50 \times 50 \mu$m with a single cancer cell, placed on top of this region with a cell-ECM interface of $5 \times 10^{-6} cm^{-2}$ and consider the ECM degradation that would take place through both MT1-MMP and MMP-2.

MT1-MMP shuttling to invadopodia is, by necessity, dependent on the consideration of a region larger than an isolated invadopodium. As such, we can now appropriately model MT1-MMP shuttling to invadopodia. MT1-MMP shuttling to invadopodia is independent of all other reactions so we treat this separately and we consider an additional MT1-MMP shuttled to the invadopodia after a time t_{shuttle}. To couple this with the SSA time steps, we consider a production of a single MT1-MMP protein every $t_{shuttle}$ and apply the additional number of MT1-MMP proteins after every cycle of the SSA. Note that this can be interpreted as adding ν_s to the state vector, $\mathbf{X}(\text{t})$, where this adds one protein of MT1-MMP, $\nu_s = (0, 0, 1, 0, 0, 0, 0, 0, 0)^T$.

Reactions involving one or more membrane-bound proteins/complexes can take place only within the active region defined by the sensing radius a and reactions between two freely diffusive proteins can take place both outside and inside this defined region. Once again we define the invadopodia to be a cone of radius 0.5μm and height 7.5μm.

Since the number of enzymes used to form complexes at invadopodia is much lower than the total number of these enzymes in the domain, combined with the high diffusion rate of these enzymes, we consider the concentration of proMMP-2, TIMP2 and TIMP2:proMMP-2 to be constant within the invadopodial region by considering a replacement protein to be instantly transported within the invadopodial region when a complex is formed that would otherwise use them up. Further, we define the separation of complexes to no longer release these proteins

and we model these modified reactions within the invadopodial region as:

$$\text{Stage 1:} \qquad X_3 + X_4 \xrightarrow{c_1} X_4 + X_5, \tag{6.30}$$

$$X_5 \xrightarrow{c_2} X_3, \tag{6.31}$$

$$\text{Stage 2:} \qquad X_5 + X_1 \xrightarrow{c_3} X_1 + X_6, \tag{6.32}$$

$$X_6 \xrightarrow{c_4} X_5, \tag{6.33}$$

$$\text{Stage 3:} \qquad X_6 + X_3 \xrightarrow{c_5} X_7, \tag{6.34}$$

$$X_7 \xrightarrow{c_6} X_6 + X_3, \tag{6.35}$$

$$\text{Stage 4:} \qquad X_7 \xrightarrow{c_7} X_5 + X_3 + X_2, \tag{6.36}$$

$$X_3 + X_9 \xrightarrow{c_1} X_6 + X_9, \tag{6.37}$$

$$X_6 \xrightarrow{c_2} X_3, \tag{6.38}$$

with a corresponding stochiometric matrix B of form:

$$B = \begin{pmatrix} 0 & 0 & 0 & 0 & 0 & 0 & 0 & 0 & 0 \\ 0 & 0 & 0 & 0 & 0 & 0 & 1 & 0 & 0 \\ -1 & 1 & 0 & 0 & -1 & 1 & 1 & -1 & 1 \\ 0 & 0 & 0 & 0 & 0 & 0 & 0 & 0 & 0 \\ 1 & -1 & -1 & 1 & 0 & 0 & 1 & 0 & 0 \\ 0 & 0 & 1 & -1 & -1 & 1 & 0 & 1 & -1 \\ 0 & 0 & 0 & 0 & 1 & -1 & -1 & 0 & 0 \\ 0 & 0 & 0 & 0 & 0 & 0 & 0 & 0 & 0 \\ 0 & 0 & 0 & 0 & 0 & 0 & 0 & -1 & 1 \end{pmatrix}. \tag{6.39}$$

We consider the amount of ECM to be degraded as a result of the invadopodium to be the sum of degradation by MT1-MMP at the invadopodium and the degradation of MMP-2 activated at the invadopodium. For simplicity, we consider the amount of ECM degraded by either MT1-MMP or MMP-2 to be a linear relation to the sum of their respective lifespans. As such, the total amount of ECM degradation is assumed to be of the form:

$$\delta_1 \int \mathrm{X}(3)dt + \delta_2 \int \mathrm{X}(2)dt. \tag{6.40}$$

In order to consider a simple method by which the dissolution of the invadopodia is the result of MT1-MMP dissociating cortactin, we set

$$\delta_3 \int \mathrm{X}(3)dt, \tag{6.41}$$

to be dissociation of cortactin and that the invadopodia lifespan ends when this value passes some critical value χ.

While the total amount of degraded ECM will generally be unaffected by differently defined sizes of regions of ECM in our formulation, the distribution of the ECM degradation by MMP-2 will differ as we impose zero-flux boundary conditions on this region of ECM.

Since we have insufficient data for the linked parameters of $\delta_3, t_{\text{shuttle}}$ and χ, we simply leave δ_3 undefined and determine $\delta_3\chi$ from running the default parameter set indicated in Table 6.2 along with the chosen default value of MT1-MMP shuttling of $\frac{1}{t_{\text{shuttle}}} = 0.18\text{s}^{-1}$ to obtain the amount of cortactin degraded over a 1 hour lifespan of $\delta_3 \int_0^{3600} \mathrm{X}(3)\,\mathrm{dt} = \chi$. We then set the lifespan of an invadopodia to be the lowest time, t, s.t. $\delta_3 \int \mathrm{X}(3)\,\mathrm{dt} \geq \chi$. In doing so, we have uncoupled the lifespan of invadopodia from being one hour and linked it to the amount of cortactin that has been degraded. Finally, an estimate for the range of permissible rates of MT1-MMP shuttling $\frac{1}{t_{\text{shuttle}}}$ is identified.

In making these approximations, we make no quantitative predictions for the levels of cortactin dissociated. However we are able to provide qualitative results for the lifespan of invadopodia, how this is affected by MT1-MMP shuttling as well as the resultant MMP-2 activation and ECM degradation across the lifespan of an invadopodium.

While we have to consider the two regions of the invadopodial region and the domain minus the invadopodial region, we formulate our model by considering the domain minus the invadopodial region to be in stasis in terms of the population concentrations of all enzymes with the exception of MMP-2 and the invadopodial region is assumed to be in stasis for the populations of the freely diffusive proteins. We assume that any MMP-2 proteins that are produced in the invadopodial region are instantly transported to the region made up of the domain minus invadopodial region. This allows us to calculate the lifespan of each active MMP-2 protein, defined as the time until it is inhibited by TIMP-2, by using the Gillespie Algorithm to be $\tau_i = \dfrac{log(1/\text{rand})}{2.5 \times 10^{-2}}$ where rand is a function that generates a random number uniformly distributed in the interval (0,1). We note that this is not dependent on the volume of the region considered so will be unchanged by the size of the region of ECM that we consider. Since τ_i is in the range 0–100s and $D_{ms} = 1.29 \times 10^8 cm^2 s^{-1}$ (with a correspondingly high root mean squared displacement), MMP-2 activated at invadopodia are active over a much larger spatial scale than the invadopodia themselves. We have therefore shown that it is appropriate to consider MMP-2 activated at invadopodia to be considered as instantly acting over the larger well-mixed region. We note that the size of the larger domain does not affect the production of MMP-2 or the lifespan of the proteins and so does not need to be explicitly defined.

In order to identify suitable forms of initial conditions for a scenario where the majority of ECM degradation happens at invadopodia and for the amount of

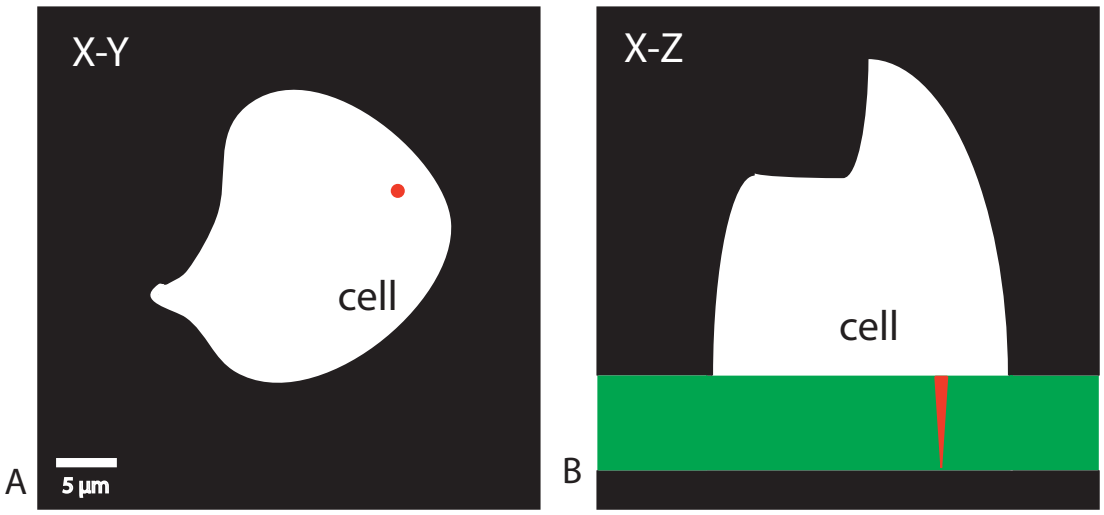

Figure 6.8: *Schematic diagram showing the location of the invadopodium and its relative size when compared to a cell.*

MT1-MMP shuttled to the invadopodium as determined by biologically realistic approximations, we note that, as illustrated in Figure 6.7, we have found that there are minor amounts of active MT1-MMP or MMP-2 proteins when TIMP2($t = 0$) >MT1-MMP($t = 0$), and therefore a correspondingly minor amount of ECM degradation. We therefore choose initial conditions for MT1-MMP($t = 0$) = 47nM and TIMP2($t = 0$) = 50nM. Additionally, we choose to use an initial concentration of proMMP-2 of 60nM.

In order to obtain an estimate for the default shuttling rate of MT1-MMP to invadopodia, t_{shuttle}, we define it to be the rate that allows for the production of 60nM of MMP-2 after an hour from the initial conditions prescribed above. We have done so as we note that this is also the fastest shuttling rate allowed as the amount of activated MMP-2 after one hour is 10% the initial amount of proMMP-2 proteins from simulations performed with the increased TIMP-2 concentration of 143nM. This follows as a limit from Artym et al. (2006) where they note that complete inhibition of matrix degradation at invadopodia occurs

when the TIMP2 concentration is 143nM (3 μg/ml). As such, we have identified a default MT1-MMP shuttling rate of $t_{\text{shuttle}} = 5.56s$.

In performing ten computational simulations with these defined initial conditions and default shuttling rate, we obtain a mean value of $\int_0^{3600} \text{X}(3)\,\text{dt}$ of 7028.6 with standard deviation of 339.8. This means that we take χ to be equal to $\delta_3 \times 7028.6$ and assume that instead of invadopodia terminating at one hour, they now terminate once $\int \text{X}(3) \geq 7028.6$.

6.3 Results

In order to identify the permissible range of values for the MT1-MMP shuttling rate, we note that the default rate is the fastest possible shuttling rate and proceed to identify the slowest MT1-MMP shuttling rate. We performed groups of ten computational simulations for increasing $t_{shuttle}$ until we identified a limit of $t_{shuttle} = 17.8$s. This limit was determined as we have not observed invadopodia having a lifespan of over 2 hours in the biological literature. We present these findings in Table 6.3.

From the available data, presented in Table 6.3, we are now able to establish a range of permissible rates of MT1-MMP shuttling to invadopodia of $t_{\text{shuttle}} = 5.56 - 17.8$s. We note that decreasing the shuttling rate of MT1-MMP, $\frac{1}{t_{\text{shuttle}}}$, causes an increase in the lifespan of the invadopodium. Despite the increase in invadopodium lifespan, the total amount of MT1-MMP proteins shuttled to the invadopodium over the course of its lifespan is decreased with decreasing shuttling rate of MT1-MMP.

The amount of ECM degraded by MT1-MMP at, and MMP-2 activated at, the

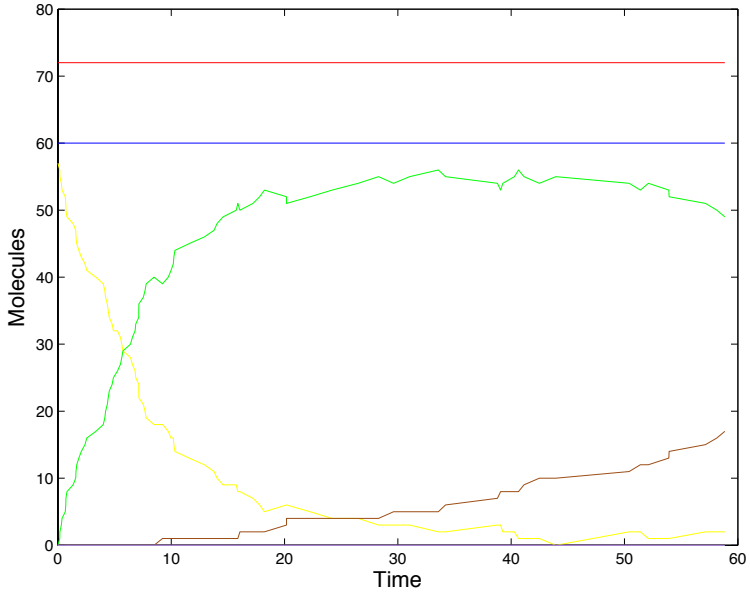

A

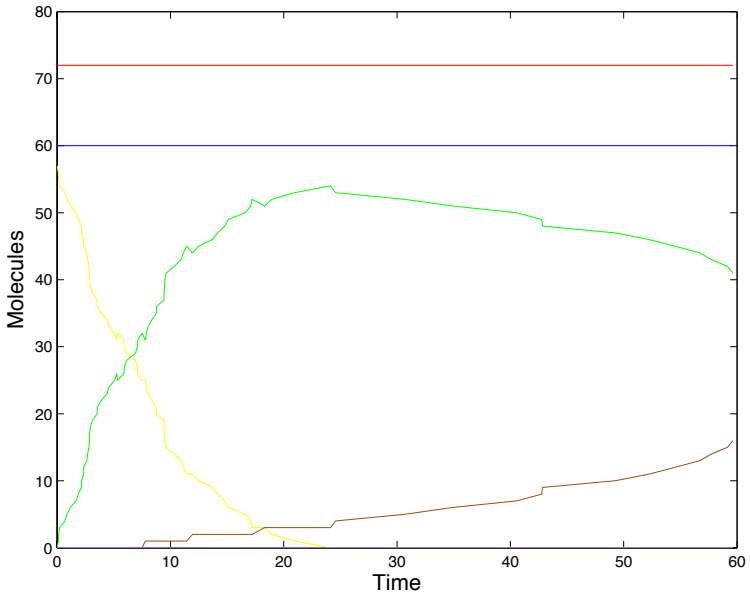

B

Figure 6.9: *Short time dynamics (t=0-60s) of the MMP-2 activation system. Plot A has a shuttling rate of 5.56s while plot B has no MT1-MMP shuttling. proMMP-2 is presented in red, MT1-MMP in yellow, TIMP2 in blue, MT1-MMP:TIMP2 in green, MT1-MMP:TIMP2:proMMP-2 in brown, MT1-MMP:TIMP2:proMMP-2:MT1-MMP in dark blue, MMP-2 in black and TIMP2:proMMP-2 in lavender.*

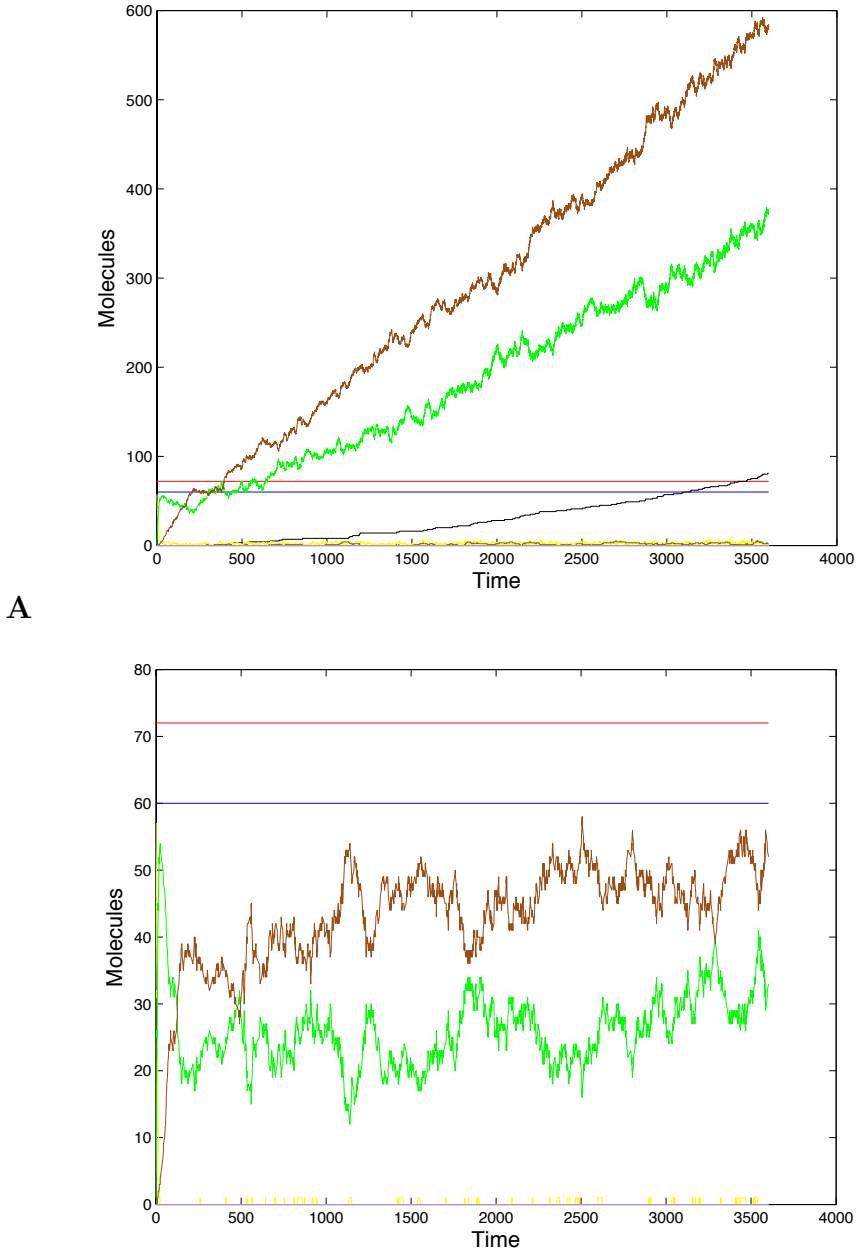

Figure 6.10: *Full term dynamics (t=0-3600s) of the MMP-2 activation system. Plot A has a shuttling rate of 5.56s while plot B has no MT1-MMP shuttling. proMMP-2 is presented in red, MT1-MMP in yellow, TIMP2 in blue, MT1-MMP:TIMP2 in green, MT1-MMP:TIMP2:proMMP-2 in brown, MT1-MMP:TIMP2:proMMP-2:MT1-MMP in dark blue, MMP-2 in black and TIMP2:proMMP-2 in lavender.*

t_{shuttle}	**Invadopodium Lifespan (s)**	**MT1-MMP Shuttled**	**Activated MMP-2**	**Sum of MMP-2 Lifespans**
5.56	3527.2 ± 105.6	817 ± 30	68 ± 10	2640.0 ± 400.1
9	4915.4 ± 144.8	792 ± 26	68 ± 10	2722.1 ± 501.5
13	6110.0 ± 125.5	754 ± 19	68 ± 10	2887.9 ± 514.4
17.8	7276.1 ± 279.3	742 ± 34	62 ± 4	2444.1 ± 357.6

Table 6.3: *Mean with standard deviation values for when the time between MT1-MMP molecules shuttling to MT1-MMP is varied from 5.56s to 17.8s. Further, we note here that the total amount of ECM degraded by MT1-MMP will remain near constant across the computational simulations regardless of the lifespan of the invadopodia by definition.*

invadopodium, as defined by $\delta_3 \int \mathrm{X}(3)$ and $\delta_3 \int \mathrm{X}(3)$, respectively, remains approximately the same (~ 7028.6 and ~ 2500) as the shuttling rate of MT1-MMP to invadopodium changes. As the lifespan of invadopodium is strictly increasing with decreasing shuttling rate of MT1-MMP, the rate of degradation by MT1-MMP proteins at invadopodia decreases as well as the rate of ECM degradation by MMP-2 proteins activated at the invadopodia. As such, we have found that while the amount of ECM degraded by invadopodia is not linked to the MT1-MMP shuttling rate, the rate of ECM degradation is directly linked to the MT1-MMP shuttling rate. Further, from computational simulations where we assume MT1-MMP shuttling to invadopodia has been blocked, $\frac{1}{t_{\text{shuttle}}} = 0$, we find that there is only minimal levels of ECM degraded by either MT1-MMP or MMP-2 proteins.

.

6.4 Discussion

We have studied MMP-2 activation at the smaller spatial and temporal scales that are relevant when considering invadopodia by formulating a SSA model. We have identified that stochastic effects on the scale of invadopodia can allow for a significant activation of MMP-2 (up to 25% over 1 hour) in comparison to the approximation of the ODE model presented of 3.06% when there is a constraint on the initial conditions of TIMP2($t = 0$) = 0.95MT1-MMP($t = 0$). Further, we found that when TIMP2($t = 0$) > 0.95MT1-MMP($t = 0$), little to no ECM degradation of ECM takes place ($\delta_1 \int$MT1-MMP+$\delta_2 \int$MMP-2 is very small as can be seen from plot B of Figure 6.7).

In contrast to the *in silico* approach in Hoshino et al. (2012), we consider MT1-MMP shuttling to invadopodia to be responsible for the increased ECM degradation at invadopodia. However, our result would match their *in vitro* observation that the blocking of vesicle transport of MT1-MMP would eliminate this increased ECM degradation.

6.5 Future Work

The results of our model can be formulated into a manner similar to the biological imaging shown in Figure 6.1 by using the schematic illustrated in Figure 6.11, where where we consider a layer of ECM constituent parts of dimensions $5 \times 50 \times 50 \mu$m with a single cancer cell, placed on top of this region with a cell-ECM interface of $5 \times 10^{-6} cm^{-2}$ and consider the ECM degradation that would take place through both MT1-MMP and MMP-2. The size of the region of ECM degraded by each invadopodium would be determined by the size and shape of

	Radius by Height (μm)	**Volume of Invadopodial Region (L)**	**MT1-MMP shuttling rate**
A	0.5 7.5	1.99×10^{-15}	$\frac{1}{t_{\text{shuttleA}}}$
B	0.4 5	1.12×10^{-15}	$\frac{1}{t_{\text{shuttleB}}}$
C	0.6 8	2.48×10^{-15}	$\frac{1}{t_{\text{shuttleC}}}$
D	0.3 6	1.05×10^{-15}	$\frac{1}{t_{\text{shuttleD}}}$
E	0.8 9	3.60×10^{-15}	$\frac{1}{t_{\text{shuttleE}}}$

Table 6.4: *Characteristics of the invadopodia labelled A-E*

each invadopodial region, along with the amount of ECM within that region that is predicted to be degraded. Further, the amount of ECM degraded across the entire domain will be dependent upon the amount of free MT1-MMP at regions other than the invadopodia as well as MMP-2 across the entire domain.

We consider 5 invadopodium labelled A-E in Figure 6.11. We consider each invadopodia to have a related domain of volume 1.05×10^{-15}–3.60×10^{-15}L and MT1-MMP shuttling rate as described in Table 6.4. We define this related domain to be the region in which enzyme reactions can take place between membrane bound and freely diffusible proteins, prescribed from a radius of $a = 0.2\mu$m from the invadopodia.

We present the form that a typical result of such a model would take in Figure 6.12 where for simplicity, we have defined the amount and distribution of ECM degraded by each invadopodium to be identical.

Further fruitful extensions of the model would seem to fall in into three categories.

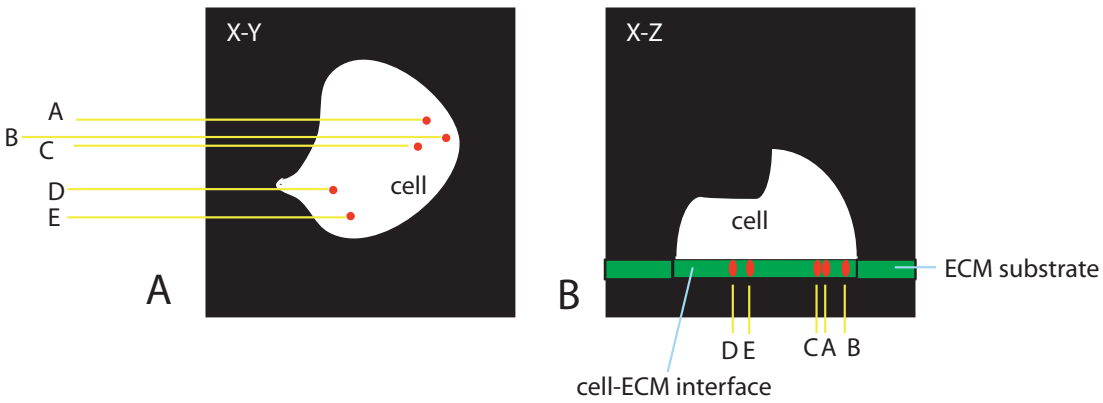

Figure 6.11: *The location of the 5 considered invadopodia (A-E).*

The first is to include further dynamics relating to MT1-MMP such as dimerisation, catalytic shuttling etc. as was incorporated in the ODE model of Karagiannis and Popel (2004). The impact of these additional processes on invadopodial function is not yet clear and so such an extension may offer insights into complimentary biological works. The second is having an adaptive invadopodium shape which adapts according to the lifespan of the invadopodium. This could be coupled with a computational model that maps the lifecycle of invadopodia including retraction and formation such as that proposed in Enderling et al. (2008) or the implementation of a moving boundary framework such as that proposed in Trucu et al. (2013). The third is to incorporate the proposed model into one which considers the entire cell. To do so would provide the benefits of being able to include intracellular processes and be useful for the identification of significant pathways for MT1-MMP shuttling and resultant ECM degradation.

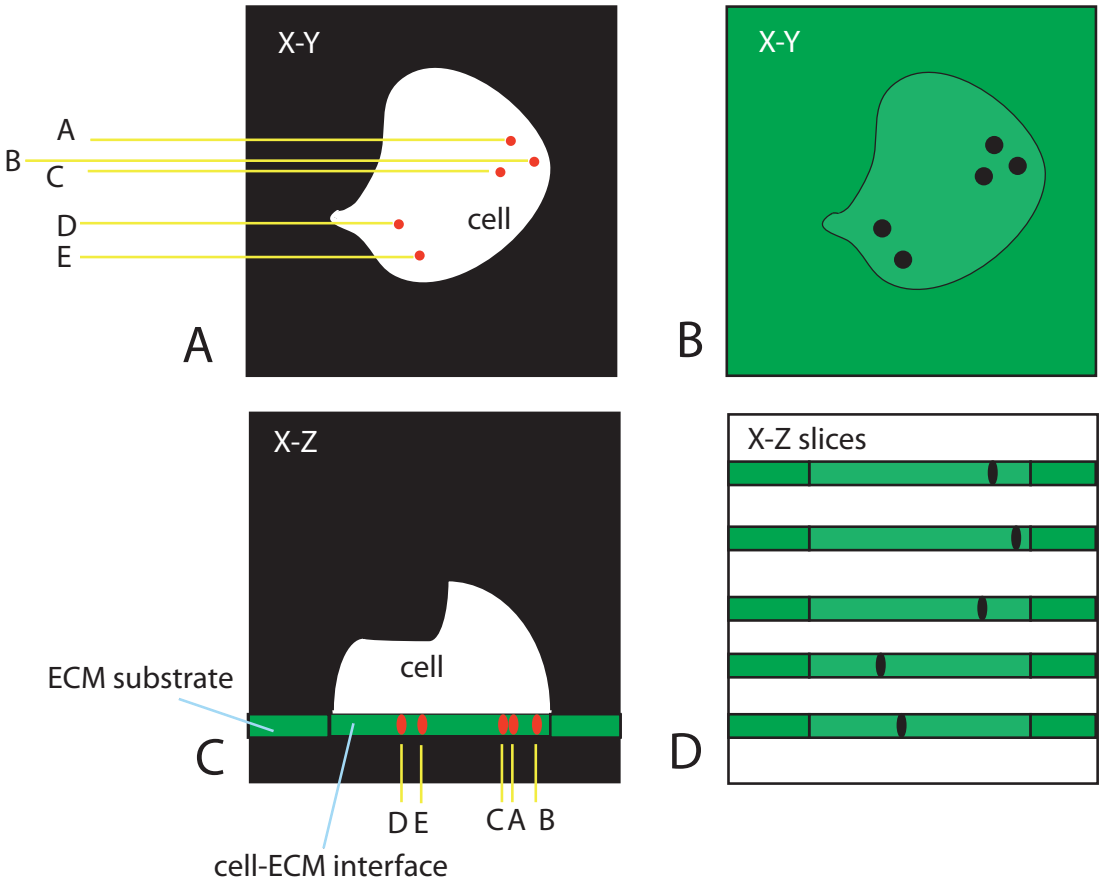

Figure 6.12: *Results of the proposed model in the future work would be of this form. In this case, we have defined the related distribution and amount of ECM degraded by each invadopodium to be identical as the figure is currently an artificial construct rather than the direct interpretation of results of the model.*

Chapter 7

Conclusions and Future Work

Throughout this presented work, we have concurrently studied two aspects of cancer cell invasion. Firstly, degradation of tissue mediated by the soluble MMP-2 and the membrane bound MT1-MMP, secondly the activation system of MMP-2 mediated by MT1-MMP and TIMP2. We applied the study of these elements of cancer cell invasion in three circumstances. In Chapter 4, we established a novel model of cancer invasion at the tissue scale through a system of PDEs, advancing upon previous mathematical models of cancer cell invasion that consider generic matrix degrading enzymes and could be considered to be parallel to works that focus on the uPA system in cancer cell invasion. The potential of the presented model to consider rich ECM environments is explored in Chapter 5 where we consider only a minor modification to the system of PDEs, where we note that the original model can be recovered. In the third and final research chapter, Chapter 6, we considered a motivating problem that happens on the smaller scale, that of subcellular invadopodia.

To establish the bare bones of the cancer cell invasion model in Chapter 4, we drew on existing models in an examination of the most appropriate way in which

to model the competition for space between the cancer cells and ECM constituent parts through the haptoatactic sensitivity function and production terms of both the cancer cell population and ECM density. We then developed this framework to consider degradation of ECM mediated by MT1-MMP and MMP-2 where the latter protein is activated solely through the cleavage by MT1-MMP of the pro domain region of proMMP-2 when the proMMP-2 protein is in a complex formation of MT1-MMP, TIMP2 and proMMP-2. Rather than considering all of the intermediary complexes that would be involved in this process, a simplified schematic for this activation process was proposed to minimise computational expense.

Parameterisation of the presented model came under two parts. Initially, a number of parameters could be drawn from the literature where similar mathematical models of cancer cell invasion with ECM degradation mediated by generic matrix degrading enzymes. The second part of the parameterisation came with the consideration of the specific matrix degrading enzymes of MMP-2 and MT1-MMP and the activation process of MMP-2 mediated by MT1-MMP and TIMP2. To completer the parameterisation, we were required to briefly study two submodels of MMP-2 activation in order to validate the simplified schematic of MMP-2 activation by the use of biologically estimated parameters.

Despite the steps taken, there remained one parameter that was very poorly parameterised. While this parameter is featured in every research chapter, we feel that it is sufficient to remark upon it in the context of the initial research chapter, only. The rate in which a free MT1-MMP protein binds to the complex of MT1-MMP, TIMP2 and proMMP-2 was considered to be $3 \times 10^3 M^{-1}s^{-1}$ in Karagiannis and Popel (2004) and $2 \times 10^6 M^{-1}s^{-1}$ where we chose to consider this reaction rate to be $4.3 \times 10^4 M^{-1}s^{-1}$. As we consider this to be a significant potential source of errors in our model, a better biological estimation of the rate

at which this reaction takes place must be found before further validation of the presented models against biological data and meaningful predictions can take place.

By considering the definition of volume filling/competition for space, we noted that only results of $c + v \leq 1 + \alpha$ may be biologically relevant, where $0 \leq \alpha << 1$, and only when the case of $c + v > 1$ is short lasting and righted to be $c + v \leq 1$. We noted that by considering volume filling terms in the haptotactic sensitivity function, the likelihood of finite tie blow-up solutions was reduced and the production terms of the cancer cells and ECM ensured that the populations of c and v were reduced, but not below zero, such that $c + v \leq 1$. Future work, which would compliment the effects of considering volume filling terms in the haptotactic sensitivity function of reducing the likelihood of finite time blow-up solutions, would be in the consideration of cell-cell and cell-ECM adhesion through the use of integer-PDEs, as outlined in the earlier chapter focusing on providing a literature review. There would also be exciting possibilities that could be considered in such models that have not, to the best of the author's knowledge, been investigated. MT1-MMP that is unbound from TIMP2 has the ability to not only degrade extracellular components but can cause the dissociation of integrals responsible for cellular adhesion. As a decrease in cellular adhesion has been linked to an increased invasiveness of cancer cells, such a consideration in an integro-PDE model of cancer cell invasion may provide a means of modelling a cancer cell population that becomes progressively more invasive over time at a rate determined by the amount of free MT1-MMP.

We identified an appropriate form of considering the significance of the degradation by the two types of matrix degrading proteins to be in measuring the running total of how much degradation of ECM has taken taken place from each of the specific MMPs. We found that the majority of bulk collagenolytic activity was

due to degradation of ECM by MMP-2 after a short time interval. Where we considered the cancer-ECM interface to be defined as the region between c=0.01 and v=0.01, we were able to provide approximations for the concentrations of MMP-2 (0A: 1-4nM, 0B:1-5.5nM) and MT1-MMP (0A&OB: 0.1-5nM) within this region. These values are broadly defined by the parameters $\alpha_{mt}, \alpha_T, \beta_{mt}and\beta_{ms}$, which can be modified to form a closer match with biological observations that may be obtained. We specifically note that where the parameter defining the production rate of TIMP2, α_T, was modified in isolation of all other parameters, there was found to be a value that allowed for a peak amount of the activated MMP-2 steady state. We performed our simulations at the approximate value of this peak of $\alpha_T = 4$ where we note that the ratio of the steady state concentrations of the active MMP-2 to MT1-MMP can be modified to match desired results through the varying of parameter for the production rate of TIMP2 (Figure 4.19) with the knock on effect to the steady state concentrations of the intermediate complex, f, and TIMP2 as indicated in Figure 4.20.

In Chapter 5, we introduced the concept of the "suitability of the matrix" through only a small modification to the equations defining the model. This allowed for a much larger range of richly composed ECM constructs that can be considered with the model. We found the parameter δ_s to be significant in determining the morphology of the cancer mass as evidenced by the comparison between Invasion Scenario 1A and 1B where the only difference was the increase in the parameter δ_s. We found that for a high enough δ_s, the results of the model are similar to, but do not tend to, those obtained for when there is no suitability modifier considered (Invasion Scenario 0A), unless there is a lack of diffusion for the MMP-2 proteins. Specifically, an increase in parameter δ_s causes an increase in the amount of suitability modifier that has been remodelled, an increase in the amount of total cancer cells and an increase in the total degradation of ECM.

A new role for MT1-MMP was now considered in which it was able modify the suitability of the ECM to a neutral state. This granted a much more significant role for MT1-MMP in determining the invasiveness of the cancer in some structured ECM in which there was considered to be a low initial suitability of the matrix. However, we note that the ratio of active MT1-MMP to active MMP-2 is unaffected by the suitability of the matrix, as considered in this model.

A qualitative result that occurred across all simulations of the model proposed in Chapters 4 & 5 was that near the leading front of the cell invasion boundary (though not directly upon the boundary) there is an increase in both the concentrations of the intermediate complex f and TIMP2 from the concentration where the cancer population has stabilised at the maximum non-dimensionalised value of 1. This increase in the intermediate complex, f, was shown to not be due to the initial condition being higher than this increased amount where in Invasion Scenario 0B f began near its steady state and reached a maximum of almost twice this value. An increase in TIMP2 and the intermediate complex, f, is therefore considered to take place at areas where there is active degradation of ECM.

Computational simulation results showed that the matrix suitability modifier and its regulation played an important role in determining the precise pattern of invasion. As has been observed in the experimental data of Sabeh, Shimizu-Hirota and Weiss (2009) and Li et al. (2008), we have shown that the architecture of the tissue can negatively impact invasion under circumstances of pore-size being below an optimal level or in environments of cross-linked collagen type I and IV, with both of these conditions requiring tissue remodelling specifically by MT1-MMP. Pampaloni et al. (2007) propose that 3D *in vitro* models can be used to closer approximate whole-animal systems than 2D cell cultures where we note that the model proposed in Chapter 4 may be sufficient for 2D *in vivo* cell cultures

whereas the marginally more complex model of Chapter 5 is more appropriately compared with 3D *in vitro* or *in vivo* observations.

To further investigate the matrix suitability modifier from a biological perspective, a number of biologically motivated works would need to take place. Firstly, through imaging of defined 3D tissue constructs *in vitro*, quantification of ECM constructs can take place. If this is coupled with the effect on cancer cell invasion through these mediums, we can obtain quantification of the suitability of the matrix and estimates of the parameter for the remodelling of suitability, δ_s. These biological experiments could follow the approaches of the *in vitro* experiments performed in Nyström et al. (2005) and Martins et al. (2009) where instead of using a collagen:matrigel assay, a 3D construct such as is considered in Sabeh, Shimizu-Hirota and Weiss (2009) or Li et al. (2008) could be used to investigate the invasiveness of cancer cells to establish a quantitative "invasive index" in organotypic cultures. Once such thorough quantification of the parameter δ_s has been undertaken with a working knowledge of how to quantify the suitability of the matrix, comparison with accurate *in vivo* imaging data will allow for the consideration of patient-specific predictions for how the cancer cell invasion will progress.

If we were to investigate the impact of new inhibitors on cancer cell invasion, the reduced schematic of MMP-2 activation would be too focused and would need to be expanded back to the original format before the impact of selective inhibitors to specific parts of the MMP-2 activation system could be considered.

To expand on these models mathematically, a multi scale approach, such as that considered in Trucu et al. (2013), would more accurately allow for the consideration of dynamics at the leading edge of the cancer cell mass. As we have considered remodelling of the suitability of the matrix to be the sole domain of

MT1-MMP, which are bound to cancer cells, the leading edge of the cancer cell mass will face movement through ECM that is considered to be the least suitable to move through. As such, the leading edge of cancer cell invasion would benefit from a more focussed approach to better approximate the overall morphology of the cancer cell mass.

Further, in order for a tumour to grow past 2–3mm in diameter, there needs to be sufficient nutrients attracted towards the tumour through angiogenesis (Folkman and Hochberg, 1973). As the models proposed in Chapters 4 & 5 can provide estimates for how the cancer cell mass will progress for spatial considerations beyond the 2-3mm limit, the inclusion of oxygen distribution and related dynamics offers exciting capabilities for the inclusion of additional heterogeneity in the ECM and cancer environment. This could be done through the inclusion of some of the dynamics from the many mathematical models for angiogenesis, which are covered in the review papers of Mantzaris et al. (2004), Chaplain and Lolas (2006) and Scianna et al. (2013).

In Chapter 6, we studied MMP-2 activation at the smaller spatial and temporal scales that are relevant when considering invadopodia by considering a stochastic approach with and without MT1-MMP shuttling to invadopodia. We identified that stochastic effects could cause significant fluctuations in the activation of MMP-2 which is in contrast to the ordinarily tightly regulated MMP system. The possibility of an increased activation of MMP-2 at invadopodia in conjunction with the shuttling of MT1-MMP to invadopodia allows for a potentially significant increase in overall ECM degradation.

We identified a default value of MT1-MMP shuttling to invadopodia in accordance to the biologically observed scenario (Yamaguchi et al., 2005) of the majority of ECM degradation on the cell level being the result of MT1-MMP focalised at

invadopodia. We constructed this scenario in accordance to the biological observation of ECM degradation at invadopodia being wiped out at set TIMP2 concentrations (Artym et al., 2006). In order to predict a range of MT1-MMP shuttling rates, we made the assumption that invadopodia have a lifetime dependent upon the amount of cortactin dissociated by MT1-MMP and then found the limits of MT1-MMP shuttling that allowed for the lifetime of invadopodia to be within biologically observed timeframes.

If we were to instead couple the dynamics proposed in this model to a model of invadopodia formation and lifespan, more accurate approximations of generic invadopodia could be approximated. Further, with the consideration of a growing and moving invadopodia, we would be able to model a moving domain where interactions with the membrane bound MT1-MMP and associated complexes can take place.

We could again make use of a multi scale mathematical approach of the form considered in Trucu et al. (2013) when applied to an individual cell as in Peng (2015), coupled with a model for invadopodia formation and regulation, to approximate the amount of MMP-2 activated following a cell boundary and how this compares to the increase of MMP-2 activated at invadopodia as a result of MT1-MMP shuttling. Adapting such a model would allow for the examination of how MT1-MMP is shuttled to invadopodia intracellularly and open up possible avenues of research related to what causes and affects this shuttling with the result it would have on MMP-2 activation and ECM degradation.

Bibliography

Adler, J. (1973), 'A method for measuring chemotaxis and use of the method to determine optimum conditions for chemotaxis by Escherichia coli', *J. Gen. Microbiol.* **74**(1), 77–91.

Adler, J. and Tso, W. (1974), '"Decision"-making in bacteria: Chemotactic response of Escherichia coli to conflicting stimuli', *Science* **184**(4143), 1292–1294.

Alberts, B., Johnson, A., Lewis, J., Raff, M., Roberts, K. and Walter, P. (2008), *Molecular biology of the cell: Fifth Edition*, Vol. 4.

Andasari, V. (2011), Mathematical modelling of cancer cell invasion of tissue: discrete and continuum approaches to studying the central role of adhesion, PhD thesis, University of Dundee.

Andasari, V., Gerisch, A., Lolas, G., South, A. and Chaplain, M. (2011), 'Mathematical modeling of cancer cell invasion of tissue: biological insight from mathematical analysis and computational simulation', *J. Math. Biol.* **63**(1), 141–171.

Andasari, V., Roper, R., Swat, M. and Chaplain, M. (2012), 'Integrating intracellular dynamics using CompuCell3D and Bionetsolver: applications to multiscale modelling of cancer cell growth and invasion', *PLoS One* **7**(3), e33726.

Anderson, A. (2005), 'A hybrid mathematical model of solid tumour invasion: the importance of cell adhesion', *Math. Med. Biol.* **22**(2), 163–186.

Anderson, A., Chaplain, M., Newman, E., Steele, R. and Thompson, A. (2000), 'Mathematical modelling of tumour invasion and metastasis', *Comput. Math. Meth. Med.* **2**(2), 129–154.

Anderson, A., Weaver, A., Cummings, P. and Quaranta, V. (2006), 'Tumor morphology and phenotypic evolution driven by selective pressure from the microenvironment', *Cell* **127**(5), 905–915.

Araujo, R. and McElwain, D. (2004), 'A history of the study of solid tumour growth: the contribution of mathematical modelling', *Bull. Math. Biol.* **66**(5), 1039–1091.

Armstrong, N., Painter, K. and Sherratt, J. (2006), 'A continuum approach to modelling cell–cell adhesion', *J. Theor. Biol.* **243**(1), 98–113.

Artym, V., Zhang, Y., Seillier-Moiseiwitsch, F., Yamada, K. and Mueller, S. (2006), 'Dynamic interactions of cortactin and membrane type 1 matrix metalloproteinase at invadopodia: defining the stages of invadopodia formation and function', *Cancer Res.* **66**(6), 3034–3043.

Aubert, M., Badoual, M., Fereol, S., Christov, C. and Grammaticos, B. (2006), 'A cellular automaton model for the migration of glioma cells', *Phys. Biol.* **3**(2), 93.

Baker, T., Tickle, S., Wasan, H., Docherty, A., Isenberg, D. and Waxman, J. (1994), 'Serum metalloproteinases and their inhibitors: markers for malignant potential.', *Br. J. Cancer* **70**(3), 506.

Barrett, A., Woessner, J. F. and Rawlings, N. (2012), *Handbook of proteolytic enzymes*, Vol. 1, Elsevier.

Basbaum, C. and Werb, Z. (1996), 'Focalized proteolysis: spatial and temporal

regulation of extracellular matrix degradation at the cell surface', *Curr. Opin. Cell Biol.* **8**(5), 731–738.

Bellomo, N. and Delitala, M. (2008), 'From the mathematical kinetic, and stochastic game theory to modelling mutations, onset, progression and immune competition of cancer cells', *Phys. Life Rev.* **5**(4), 183–206.

Bellomo, N., Li, N. and Maini, P. (2008), 'On the foundations of cancer modelling: selected topics, speculations, and perspectives', *Math. Model. Meth. Appl. Sci.* **18**(04), 593–646.

Bianconi, E., Piovesan, A., Facchin, F., Beraudi, A., Casadei, R., Frabetti, F., Vitale, L., Pelleri, M., Tassani, S., Piva, F., Perez-Amodiof, S., Strippoli, P. and Canaidera, S. (2013), 'An estimation of the number of cells in the human body', *Ann. Human Biol.* **40**(6), 463–471.

Bissell, M., Radisky, D., Rizki, A., Weaver, V. and Petersen, O. (2002), 'The organizing principle: microenvironmental influences in the normal and malignant breast', *Differentiation* **70**(9-10), 537–546.

Böttger, K., Hatzikirou, H., Chauviere, A. and Deutsch, A. (2012), 'Investigation of the migration/proliferation dichotomy and its impact on avascular glioma invasion', *Math. Model. Nat. Phen.* **7**(01), 105–135.

Bray, D. (1992), *Cell Movements*, New York: Garland Publishing.

Bressloff, P. and Newby, J. (2013), 'Stochastic models of intracellular transport', *Reviews Mod. Phys.* **85**(1), 135.

Britton, N. (2012), *Essential mathematical biology*, Springer Science & Business Media.

Burton, A. (1966), 'Rate of growth of solid tumours as a problem of diffusion', *Growth* **30**(2), 157–176.

Butler, G., Butler, M., Atkinson, S., Will, H., Tamura, T., Schade van Westrum, S., Crabbe, T., Clements, J., d'Ortho, M. and Murphy, G. (1998), 'The TIMP2 membrane type 1 metalloproteinase "receptor" regulates the concentration and efficient activation of progelatinase A: a kinetic study', *J. Biol. Chem.* **273**(2), 871–880.

Byrne, H. (2010), 'Dissecting cancer through mathematics: from the cell to the animal model', *Nat. Rev. Cancer* **10**(3), 221–230.

Byrne, H. and Chaplain, M. (1995), 'Growth of nonnecrotic tumors in the presence and absence of inhibitors', *Math. Biosci.* **130**(2), 151–181.

Byrne, H. and Chaplain, M. (1996), 'Growth of necrotic tumors in the presence and absence of inhibitors', *Math. Biosci.* **135**(2), 187–216.

Cai, X. and Wang, X. (2007), 'Stochastic modeling and simulation of gene networks–a review of the state-of-the-art research on stochastic simulations', *EEE Signal Process. Mag.* .

Carter, S. (1967), 'Haptotaxis and the mechanism of cell motility', *Nature* **213**, 256–260.

Chang, S., Shefelbine, S. and Buehler, M. (2012), 'Structural and mechanical differences between collagen homo-and heterotrimers: relevance for the molecular origin of brittle bone disease', *Biophys. J.* **102**(3), 640–648.

Chaplain, M. and Lolas, G. (2005), 'Mathematical modelling of cancer cell invasion of tissue: The role of the urokinase plasminogen activation system', *Math. Models and Meth. Appl. Sci.* **15**(11), 1685–1734.

Chaplain, M. and Lolas, G. (2006), 'Mathematical modelling of cancer invasion of tissue: dynamic heterogeneity.', *NHM* **1**(3), 399–439.

Chaplain, M., McDougall, S. and Anderson, A. (2006), 'Mathematical modeling of tumor-induced angiogenesis', *Annu. Rev. Biomed. Eng.* **8**, 233–257.

Chen, W. (1989), 'Proteolytic activity of specialized surface protrusions formed at rosette contact sites of transformed cells', *J. Exp. Zool.* **251**(2), 167–185.

Chen, W. and Wand, J. (1999), 'Specialized surface protrusions of invasive cells, invadopodia and lamellipodia, have differential MT1-MMP, MMP-2, and TIMP-2 localization', *Ann. NY Acad. Sci.* **878**(1), 361–371.

Chiquet, M., Koch, M., Matthisson, M., Tannheimer, M. and Chiquet-Ehrismann, R. (1996), 'Regulation of extracellular matrix synthesis by mechanical stress', *Biochem. Cell Biol.* **74**(6), 737–744.

Clark, I., Swingler, T., Sampieri, C. and Edwards, D. (2008), 'The regulation of matrix metalloproteinases and their inhibitors', *Int. J. Biochem. Cell Biol.* **40**(6-7), 1362–1378.

Collier, I., Legant, W., Marmer, B., Lubman, O., Saffarian, S., Wakatsuki, T., Elson, E. and Goldberg, G. (2011), 'Diffusion of MMPs on the surface of collagen fibrils: the mobile cell surface-collagen substratum interface', *PLoS ONE* **6**(9), e24029.

Daley, W., Peters, S. and Larsen, M. (2008), 'Extracellular matrix dynamics in development and regenerative medicine', *J. Cell. Sci.* **121**(Pt 3), 255–264.

Deakin, A. (1975), 'Model for the growth of a solid in vitro tumor.', *Growth* **39**(1), 159–165.

Deakin, N. and Chaplain, M. (2013), 'Mathematical modeling of cancer invasion: the role of membrane-bound matrix metalloproteinases', *Front. Oncol.* **3**(70).

Deisboeck, T., Wang, Z., Macklin, P. and Cristini, V. (2011), 'Multiscale cancer modeling', *Ann. Rev. Biomed. Eng.* **13**.

Deryugina, E., Ratnikov, B., Monosov, E., Postnova, T., DiScipio, R., Smith, J. and Strongin, A. (2001), 'MT1-MMP initiates activation of pro-MMP-2 and integrin αvβ3 promotes maturation of MMP-2 in breast carcinoma cells', *Exp. Cell Res.* **263**(2), 209–223.

Dillon, R., Owen, M. and Painter, K. (2008), 'A single-cell-based model of multicellular growth using the immersed boundary method', *AMS Contemp. Math* **466**, 1–15.

Dölz, R., Engel, J. and Kühn, K. (1988), 'Folding of collagen IV', *Eur. J. Biochem.* **178**(2), 357–366.

Domschke, P., Trucu, D., Gerisch, A. and Chaplain, M. (2014), 'Mathematical modelling of cancer invasion: Implications of cell adhesion variability for tumour infiltrative growth patterns', *J. Theor. Biol.* **361**, 41–60.

Donzé, A., Fanchon, E., Gattepaille, L., Maler, O. and Tracqui, P. (2011), 'Robustness analysis and behavior discrimination in enzymatic reaction networks', *PLoS ONE* **6**(9), e24246.

d'Ortho, M., Will, H., Atkinson, S., Butler, G., Messent, A., Gavrilovic, J., Smith, B., Timpl, R., Zardi, L. and Murphy, G. (1997), 'Membrane-type matrix metalloproteinases 1 and 2 exhibit broad-spectrum proteolytic capacities comparable to many matrix metalloproteinases.', *Eur. J. Biochem.* **250**(3), 751–757.

Drasdo, D., Bode, J., Dahmen, U., Dirsch, O., Dooley, S., Gebhardt, R., Ghallab, A., Godoy, P., Häussinger, D., Hammad, S., Hoehme, S., Holzhütter, H.,

Klingmüller, U., Kuepfer, L., Timmer, J., Zerial, M. and Hengstler, J. (2014), 'The virtual liver: state of the art and future perspectives', *Arch. Toxicol.* **88**(12), 2071–2075.

Drasdo, D. and Hoehme, S. (2005), 'A single-cell-based model of tumor growth in vitro: monolayers and spheroids', *Phys. Biol.* **2**(3), 133–147.

Drasdo, D. and Höhme, S. (2003), 'Individual-based approaches to birth and death in avascular tumors', *Math. Comp. Model.* **37**(11), 1163–1175.

Egeblad, M. and Werb, Z. (2002), 'New functions for the matrix metalloproteinases in cancer progression', *Nat. Rev. Cancer* **2**(3), 161–174.

Ehrlich, H. and Krummel, T. (1996), 'Regulation of wound healing from a connective tissue perspective', *Wound Repair Regen.* **4**(2), 203–210.

Enderling, H., Alexander, N., Clark, E., Branch, K., Estrada, L., Crooke, C., Jourquin, J., Lobdell, N., Zaman, M., Guelcher, S., Anderson, A. and Weaver, A. (2008), 'Dependence of invadopodia function on collagen fiber spacing and cross-linking: computational modeling and experimental evidence', *Biophys. J.* **95**(5), 2203–2218.

English, W., Holtz, B., Vogt, G., Knauper, V. and Murphy, G. (2001), 'Characterization of the role of the "MT-loop": an eight-amino acid insertion specific to progelatinase A (MMP2) activating membrane-type matrix metalloproteinases', *J. Biol. Chem.* **276**(45), 42018–42026.

Eroschenko, V. and Di Fiore, M. (2013), *DiFiore's atlas of histology with functional correlations*, Lippincott Williams & Wilkins.

Folkman, J. and Hochberg, M. (1973), 'Self-regulation of growth in three dimensions', *J. Exp. Med.* **138**(4), 745–753.

Friedl, P. and Wolf, K. (2003*a*), 'Proteolytic and non-proteolytic migration of tumour cells and leucocytes', *Biochem. Soc. Symp.* **70**, 277–285.

Friedl, P. and Wolf, K. (2003*b*), 'Tumour-cell invasion and migration: diversity and escape mechanisms', *Nat. Rev. Cancer* **3**(5), 362–374.

Friedl, P. and Wolf, K. (2008), 'Tube travel: the role of proteases in individual and collective cancer cell invasion', *Cancer Res.* **68**(18), 7247–7249.

Gatenby, R. and Gawlinski, E. (1996), 'A reaction-diffusion model of cancer invasion', *Cancer Res.* **56**(24), 5745–5753.

Gatenby, R. and Gawlinski, E. (2003), 'The glycolytic phenotype in carcinogenesis and tumor invasion insights through mathematical models', *Cancer Res.* **63**(14), 3847–3854.

Gatenby, R., Gawlinski, E., Gmitro, A., Kaylor, B. and Gillies, R. (2006), 'Acid-mediated tumor invasion: a multidisciplinary study', *Cancer Res.* **66**(10), 5216–5223.

Gerisch, A. and Chaplain, M. (2008), 'Mathematical modelling of cancer cell invasion of tissue: local and non-local models and the effect of adhesion', *J. Theor. Biol.* **250**(4), 684–704.

Gerlee, P. and Anderson, A. (2007), 'An evolutionary hybrid cellular automaton model of solid tumour growth', *J. Theor. Biol.* **246**(4), 583–603.

Gerlee, P. and Anderson, A. (2008), 'A hybrid cellular automaton model of clonal evolution in cancer: the emergence of the glycolytic phenotype', *J. Theor. Biol.* **250**(4), 705–722.

Gerlee, P. and Anderson, A. (2009*a*), 'Evolution of cell motility in an individual-based model of tumour growth', *J. Theor. Biol.* **259**(1), 67–83.

Gerlee, P. and Anderson, A. (2009*b*), 'Evolution of cell motility in an individual-based model of tumour growth', *J. Theor. Biol.* **259**(1), 67–83.

Gerlee, P. and Anderson, A. (2010), 'Diffusion-limited tumour growth: simulations and analysis', *Math. Biosci. Eng.* **7**(2), 385.

Ghaemi, M. and Shahrokhi, A. (2006), 'Combination of the cellular Potts model and lattice gas cellular automata for simulating the avascular cancer growth', pp. 297–303.

Gilles, C., Polette, M., Seiki, M., Birembaut, P. and Thompson, E. (1997), 'Implication of collagen type I-induced membrane-type 1-matrix metalloproteinase expression and matrix metalloproteinase-2 activation in the metastatic progression of breast carcinoma.', *Lab. Invest.* **76**(5), 651–660.

Gillespie, D. (1977), 'Exact stochastic simulation of coupled chemical reactions', *J. Phys. Chem.* **81**(25), 2340–2361.

Gioia, M., Monaco, S., Fasciglione, G., Coletti, A., Modesti, A., Marini, S. and Coletta, M. (2007), 'Characterization of the mechanisms by which gelatinase a, neutrophil collagenase, and membrane-type metalloproteinase MMP-14 recognize collagen i and enzymatically process the two α-chains', *J. Molecular Biol.* **368**(4), 1101–1113.

Gohji, K., Fujimoto, N., Hara, I., Fujii, A., Gotoh, A., Okada, H., Arakawa, S., Kitazawa, S., Miyake, H., Kamidono, S. and M., N. (1998), 'Serum matrix metalloproteinase-2 and its density in men with prostate cancer as a new predictor of disease extension', *Int. J. Cancer* **79**(1), 96–101.

Greenspan, H. (1972), 'Models for the growth of a solid tumor by diffusion', *Stud. Appl. Math* **51**(4), 317–340.

Greenspan, H. (1974), 'On the self-inhibited growth of cell cultures.', *Growth* **38**(1), 81–95.

Greenspan, H. (1976), 'On the growth and stability of cell cultures and solid tumors', *J. Theor. Biol.* **56**(1), 229–242.

Gross, J. and Lapiere, C. (1962), 'Collagenolytic activity in amphibian tissues: a tissue culture assay', *Proc. Nat. Acad. Sci. USA* **48**(6), 1014–1022.

Guo, P., Imanishi, Y., Cackowski, F., Jarzynka, M., Tao, H., Nishikawa, R., Hirose, T., Hu, B. and Cheng, S. (2005), 'Up-regulation of angiopoietin-2, matrix metalloprotease-2, membrane type 1 metalloprotease, and laminin 5 gamma 2 correlates with the invasiveness of human glioma', *Am. J. Pathol.* **166**(3), 877–890.

Haas, T., Davis, S. and Madri, J. (1998), 'Three-dimensional type i collagen lattices induce coordinate expression of matrix metalloproteinases MT1-MMP and MMP-2 in microvascular endothelial cells', *J. Biol. Chem.* **273**(6), 3604–3610.

Hanahan, D. and Weinberg, R. (2000), 'The hallmarks of cancer', *Cell* **100**(1), 57–70.

Hanahan, D. and Weinberg, R. (2011), 'Hallmarks of cancer: the next generation', *Cell* **144**(5), 646–674.

Hatzikirou, H., Basanta, D., Simon, M., Schaller, K. and Deutsch, A. (2010), 'go or grow: the key to the emergence of invasion in tumour progression?', *Math. Med. Biol* p. dqq011.

Hatzikirou, H., Breier, G., Deutsch, A. and Meyers, R. (2008), 'Cellular automaton models of tumor invasion', *Encyclop. Complexity Sys. Sci.* pp. 1–18.

Hatzikirou, H. and Deutsch, A. (2008), 'Cellular automata as microscopic models of cell migration in heterogeneous environments', *Curr. Top. Develop. Biol.* **81**, 401–434.

Hayflick, L. and Moorhead, P. (1961), 'The serial cultivation of human diploid cell strains', *Exp. Cell Res.* **25**(3), 585–621.

Higham, D. (2008), 'Modeling and simulating chemical reactions', *SIAM Rev.* **50**(2), 347–368.

Hillen, T. and Painter, K. (2001), 'Global existence for a parabolic chemotaxis model with prevention of overcrowding', *Adv. Appl. Math.* **26**(4), 280–301.

Hillen, T. and Painter, K. (2009), 'A users guide to PDE models for chemotaxis', *J. Math. Biol.* **58**(1-2), 183–217.

Holmbeck, K., Bianco, P., Caterina, J., Yamada, S., Kromer, M., Kuznetsov, S., Mankani, M., Robey, P., Poole, A., Pidoux, I., J.M., W. and H., B.-H. (1999), 'MT1-MMP-deficient mice develop dwarfism, osteopenia, arthritis, and connective tissue disease due to inadequate collagen turnover', *Cell* **99**(1), 81–92.

Holzhütter, H., Drasdo, D., Preusser, T., Lippert, J. and Henney, A. (2012), 'The virtual liver: a multidisciplinary, multilevel challenge for systems biology', *Wiley Interdiscip. Rev.: Syst. Biol. Med.* **4**(3), 221–235.

Hooke, R. (1665), *Micrographia: or Some Physiological Descriptions of Miniature Bodies Made by Magnifying Glasses.*, London: J. Martyn and J. Allestry.

Horstmann, D. (2003), 'From 1970 until present: the Keller-Segel model in chemotaxis and its consequences', *Jahresberichte der DMV* **105**(3), 103–165.

Hoshino, D., Koshikawa, N., Suzuki, T., Quaranta, V., Weaver, A., Seiki, M. and Ichikawa, K. (2012), 'Establishment and validation of computational model for MT1-MMP dependent ECM degradation and intervention strategies', *PLoS Comput. Biol.* **8**(4), e1002479.

Hotary, K., Allen, E., Brooks, P., Datta, N., Long, M. and Weiss, S. (2003), 'Membrane type I matrix metalloproteinase usurps tumor growth control imposed by the three-dimensional extracellular matrix', *Cell* **114**(1), 33–45.

Hotary, K., Allen, E., Punturieri, A., Yana, I. and Weiss, S. (2000), 'Regulation of cell invasion and morphogenesis in a three-dimensional type I collagen matrix by membrane-type matrix metalloproteinases 1, 2, and 3', *J. Cell Biol.* **149**(6), 1309–1323.

Hu, M. and Polyak, K. (2008), 'Microenvironmental regulation of cancer development', *Curr. Opin. Genet. Dev.* **18**(1), 27–34.

Hynes, R. (2009), 'The extracellular matrix: not just pretty fibrils', *Science* **326**(5957), 1216–1219.

Ichikawa, K. (2001), 'A-Cell: graphical user interface for the construction of biochemical reaction models', *Bioinformatics* **17**(5), 483–484.

Inada, M., Wang, Y., Byrne, M., Rahman, M., Miyaura, C., López-Otín, C. and Krane, S. (2004), 'Critical roles for collagenase-3 (MMP13) in development of growth plate cartilage and in endochondral ossification', *Proc. Natl. Acad. Sci. USA* **101**(49), 17192–17197.

Jiang, Y., Pjesivac-Grbovic, J., Cantrell, C. and Freyer, J. (2005), 'A multiscale model for avascular tumor growth', *Biophys. J.* **89**(6), 3884–3894.

Kadler, K., Baldock, C., Bella, J. and Boot-Handford, R. (2007), 'Collagens at a glance', *J. Cell Sci.* **120**(12), 1955–1958.

Karagiannis, E. and Popel, A. (2004), 'A theoretical model of type I collagen proteolysis by matrix metalloproteinase (MMP) 2 and membrane type 1 MMP in the presence of tissue inhibitor of metalloproteinase 2', *J. Biol. Chem.* **279**(37), 39105–39114.

Karagiannis, E. and Popel, A. (2006), 'Distinct modes of collagen type I proteolysis by matrix metalloproteinase (MMP) 2 and membrane type I MMP during the migration of a tip endothelial cell: insights from a computational model', *J. Theor. Biol.* **238**(1), 124–145.

Keener, J. and Sneyd, J. (1998), *Mathematical physiology*, Vol. 1, Springer.

Keller, E. and Segel, L. (1970), 'Initiation of slime mold aggregation viewed as an instability', *J. Theor. Biol.* **26**(3), 399–415.

Keller, E. and Segel, L. (1971*a*), 'Model for chemotaxis', *J. Theor. Biol.* **30**(2), 225–234.

Keller, E. and Segel, L. (1971*b*), 'Traveling bands of chemotactic bacteria: a theoretical analysis', *J. Theor. Biol.* **30**(2), 235–248.

Kelly, T., Mueller, S., Yeh, Y. and Chen, W. (1994), 'Invadopodia promote proteolysis of a wide variety of extracellular matrix proteins', *J. Cellular Physiol.* **158**(2), 299–308.

Kerr, J., Wyllie, A. and Currie, A. (1972), 'Apoptosis: a basic biological phenomenon with wide-ranging implications in tissue kinetics', *Br. J. Cancer* **26**(4), 239–257.

Kerrigan, J., Mansell, J. and Sandy, J. (2000), 'Matrix turnover', *J. Orthod.* **27**(3), 227–233.

Kessenbrock, K., Plaks, V. and Werb, Z. (2010), 'Matrix metalloproteinases: regulators of the tumor microenvironment', *Cell* **141**(1), 52–67.

Khalil, A. and Friedl, P. (2010), 'Determinants of leader cells in collective cell migration', *Integr. Biol.* **2**(11-12), 568–574.

Kim, Y., Stolarska, M. and Othmer, H. (2007), 'A hybrid model for tumor spheroid growth in vitro i: theoretical development and early results', *Math. Mod. Meth. in Appl. Sci.* **17**(supp01), 1773–1798.

Kinoh, H., Sato, H., Tsunezuka, Y., Takino, T., Kawashima, A., Okada, Y. and Seiki, M. (1996), 'MT-MMP, the cell surface activator of proMMP-2 (pro-gelatinase A), is expressed with its substrate in mouse tissue during embryo-genesis', *J. Cell. Sci.* **109**, 953–959.

Klein, R., Zheng, M., Ambesi, A., Van De Water, L. and McKeown-Longo, P. (2003), 'Stimulation of extracellular matrix remodeling by the first type III repeat in fibronectin', *J. Cell Sci.* **116**(22), 4663–4674.

Kleiner, D. and Stetler-Stevenson, W. (1999), 'Matrix metalloproteinases and metastasis', *Cancer Chemother. Pharmacol.* **43 Suppl**, 42–51.

Kolomecki, K., Stepien, H., Bartos, M. and Kuzdak, K. (2001), 'Usefulness of VEGF, MMP-2, MMP-3 and TIMP-2 serum level evaluation in patients with adrenal tumours', *Endocr. Regul.* **35**(1), 9–16.

Kühn, K. (1995), 'Basement membrane (type IV) collagen', *Matrix Biology* **14**(6), 439–445.

Kumar, S. and Weaver, V. (2009), 'Mechanics, malignancy, and metastasis: the force journey of a tumor cell', *Cancer Metastasis Rev.* **28**(1-2), 113–127.

Kuznetsova, N., McBride, D. and Leikin, S. (2003), 'Changes in thermal stability and microunfolding pattern of collagen helix resulting from the loss of $\alpha 2$ (I) chain in osteogenesis imperfecta murine', *J. Molecular Biol.* **331**(1), 191–200.

Kwiatkowska, A., Kijewska, M., Lipko, M., Hibner, U. and Kaminska, B. (2011), 'Downregulation of Akt and FAK phosphorylation reduces invasion of glioblastoma cells by impairment of MT1-MMP shuttling to lamellipodia and downregulates MMPs expression', *Biochim. Biophys. Acta* **1813**(5), 655–667.

Li, J. and Lowengrub, J. (2014), 'The effects of cell compressibility, motility and contact inhibition on the growth of tumor cell clusters using the Cellular Potts Model', *J. Theor Biol.* **343**, 79–91.

Li, X., Ota, I., Yana, I., Sabeh, F. and Weiss, S. (2008), 'Molecular dissection of the structural machinery underlying the tissue-invasive activity of membrane type-1 matrix metalloproteinase', *Mol. Biol. Cell* **19**(8), 3221–3233.

Linder, S. (2007), 'The matrix corroded: podosomes and invadopodia in extracellular matrix degradation', *Trends Cell Biol.* **17**(3), 107–117.

López-Otín, C. and Overall, C. (2002), 'Protease degradomics: a new challenge for proteomics', *Nat. Rev. Mol. Cell Biol.* **3**(7), 509–519.

Lowengrub, J., Frieboes, H., Jin, F., Chuang, Y., Li, X., Macklin, P., Wise, S. and Cristini, V. (2010), 'Nonlinear modelling of cancer: bridging the gap between cells and tumours', *Nonlinearity* **23**(1), R1–R9.

Lu, P., Takai, K., Weaver, V. and Werb, Z. (2011), 'Extracellular matrix degradation and remodeling in development and disease', *Cold Spring Harb. Perspect. Biol.* **3**(12), a005058.

Lu, P., Weaver, V. and Werb, Z. (2012), 'The extracellular matrix: a dynamic niche in cancer progression', *J. Cell Biol.* **196**(4), 395–406.

Lund, D., Mouly, V. and Cornelison, D. (2014), 'MMP-14 is necessary but not sufficient for invasion of three-dimensional collagen by human muscle satellite cells', *Am. J. Physiol. Cell Physiol.* **307**(2), C140–C149.

Macklin, P. and Lowengrub, J. (2006), 'An improved geometry-aware curvature discretization for level set methods: application to tumor growth', *J. Comp. Phys.* **215**(2), 392–401.

Macklin, P. and Lowengrub, J. (2007), 'Nonlinear simulation of the effect of microenvironment on tumor growth', *J. Theor. Biol.* **245**(4), 677–704.

Macklin, P. and Lowengrub, J. (2008), 'A new ghost cell/level set method for moving boundary problems: application to tumor growth', *J. Sci. Comp.* **35**(2-3), 266–299.

Macklin, P., McDougall, S., Anderson, A., Chaplain, M., Cristini, V. and Lowengrub, J. (2009), 'Multiscale modelling and nonlinear simulation of vascular tumour growth', *J. Math. Biol.* **58**(4-5), 765–798.

Malemud, C. (2005), 'Matrix metalloproteinases (MMPs) in health and disease: an overview.', *Front. Biosci.* **11**, 1696–1701.

Mallet, D. and Pettet, G. (2006), 'A mathematical model of integrin-mediated haptotactic cell migration', *Bull. Math. Biol.* **68**(2), 231–253.

Mantzaris, N., Webb, S. and Othmer, H. (2004), 'Mathematical modeling of tumor-induced angiogenesis', *J. Math. Biol.* **49**(2), 111–187.

Marchant, B., Norbury, J. and Sherratt, J. (2001), 'Travelling wave solutions to a haptotaxis-dominated model of malignant invasion', *Nonlinearity* **14**(6), 1653–1671.

Martins, V., Vyas, J., Chen, M., Purdie, K., Mein, C., South, A., Storey, A., McGrath, J. and O'Toole, E. (2009), 'Increased invasive behaviour in cutaneous squamous cell carcinoma with loss of basement-membrane type VII collagen', *J. Cell. Sci.* **122**(Pt 11), 1788–1799.

McBride, D., Choe, V., Shapiro, J. and Brodsky, B. (1997), 'Altered collagen structure in mouse tail tendon lacking the $\alpha 2$ (I) chain', *J. Molecular Biol.* **270**(2), 275–284.

Meyskens, F., Thomson, S. and Moon, T. (1984), 'Quantitation of the number of cells within tumor colonies in semisolid medium and their growth as oblate spheroids', *Cancer Res.* **44**(1), 271–277.

Monaco, S., Sparano, V., Gioia, M., Sbardella, D., Di Pierro, D., Marini, S. and Coletta, M. (2006), 'Enzymatic processing of collagen IV by MMP-2 (gelatinase A) affects neutrophil migration and it is modulated by extracatalytic domains', *Protein Sci.* **15**(12), 2805–2815.

Moreira, J. and Deutsch, A. (2002), 'Cellular automaton models of tumor development: a critical review', *Adv. Complex Sys.* **5**(02n03), 247–267.

Mouw, J., Ou, G. and Weaver, V. (2014), 'Extracellular matrix assembly: a multiscale deconstruction', *Nature Rev. Molecular Cell Biol.* **15**(12), 771–785.

Murphy, D. and Courtneidge, S. (2011), 'The "ins" and "outs" of podosomes and invadopodia: characteristics, formation and function', *Nat. Rev. Molecular Cell Biol.* **12**(7), 413–426.

Murray, J. (2002), *Mathematical Biology. I: An Introduction. II: Spatial models and Biomedical Applications*, Vol. 17.

Nagase, H. and Woessner, J. (1999), 'Matrix metalloproteinases', *J. Biol. Chem.* **274**(31), 21491–21494.

Nakada, M., Nakada, S., Demuth, T., Tran, N., Hoelzinger, D. and Berens, M. (2007), 'Molecular targets of glioma invasion', *Cell. Mol. Life Sci.* **64**(4), 458–478.

Nakahara, H., Howard, L., Thompson, E., Sato, H., Seiki, M., Yeh, Y. and Chen, W.-T. (1997), 'Transmembrane/cytoplasmic domain-mediated membrane type 1-matrix metalloprotease docking to invadopodia is required for cell invasion', *Proc. Nat. Acad. Sci.* **94**(15), 7959–7964.

Nguyen, M., Arkell, J. and Jackson, C. (2000), 'Three-dimensional collagen matrices induce delayed but sustained activation of gelatinase A in human endothelial cells via MT1-MMP', *Int. J. Biochem. Cell Biol.* **32**(6), 621–631.

Nöel, A., Gutiérrez-Fernández, A., Sounni, N., Behrendt, N., Maquoi, E., Lund, I., Cal, S., Hoyer-Hansen, G. and López-Otín, C. (2012), 'New and paradoxical roles of matrix metalloproteinases in the tumor microenvironment', *Front. Pharmacol.* **3**, 140.

Nyström, M., Thomas, G., Stone, M., Mackenzie, I., Hart, I. and Marshall, J. (2005), 'Development of a quantitative method to analyse tumour cell invasion in organotypic culture', *J. Pathol.* **205**(4), 468–475.

Oberg, A., Höyhtyä, M., Tavelin, B., Stenling, R. and Lindmark, G. (1999), 'Limited value of preoperative serum analyses of matrix metalloproteinases (MMP-2, MMP-9) and tissue inhibitors of matrix metalloproteinases (TIMP-1, TIMP-2) in colorectal cancer.', *Anticancer Res.* **20**(2B), 1085–1091.

Olson, M., Gervasi, D., Mobashery, S. and Fridman, R. (1997), 'Kinetic analysis of the binding of human matrix metalloproteinase-2 and-9 to tissue inhibitor of metalloproteinase (TIMP)-1 and TIMP-2', *J. Biol. Chem.* **272**(47), 29975–29983.

Orme, M. and Chaplain, M. (1996), 'A mathematical model of vascular tumour growth and invasion', *Math. Comput. Model.* **23**(10), 43–60.

Overall, C. and López-Otín, C. (2002), 'Strategies for MMP inhibition in cancer: innovations for the post-trial era', *Nat. Rev. Cancer* **2**(9), 657–672.

Painter, K., Armstrong, N. and Sherratt, J. (2010), 'The impact of adhesion on cellular invasion processes in cancer and development', *J. Theor. Biol.* **264**(3), 1057–1067.

Painter, K. and Hillen, T. (2002), 'Volume-filling and quorum-sensing in models for chemosensitive movement', *Can. Appl. Math. Quart* **10**(4), 501–543.

Pampaloni, F., Reynaud, E. and Stelzer, E. (2007), 'The third dimension bridges the gap between cell culture and live tissue', *Nat. Rev. Molecular Cell Biol.* **8**(10), 839–845.

Patlak, C. (1953), 'Random walk with persistence and external bias', *Bull. Math. Biophys.* **15**(3), 311–338.

Peng, L. (2015), Multiscale mathematical modelling of cancer invasion, PhD thesis, University of Dundee.

Perrin, J. (1909), 'Mouvement brownien et réalité moléculaire', **18**, 5–104.

Perumpanani, A., Sherratt, J., Norbury, J. and Byrne, H. (1996), 'Biological lnferences from a mathematical model for malignant invasion', *Invasion Metastasis* **16**, 209–22l.

Perumpanani, A., Sherratt, J., Norbury, J. and Byrne, H. (1999), 'A two parameter family of travelling waves with a singular barrier arising from the modelling of extracellular matrix mediated cellular invasion', *Physica D* **126**(3), 145–159.

Perumpanani, A., Simmons, D., Gearing, A., Miller, K., Ward, G., Norbury, J., Schneemann, M. and Sherratt, J. (1998), 'Extracellular matrix-mediated chemotaxis can impede cell migration', *Proc. Roy. Soc. London, Ser. B* **265**(1413), 2347–2352.

Petrella, B. and Brinckerhoff, C. (2006), 'Tumor cell invasion of von Hippel Lindau renal cell carcinoma cells is mediated by membrane type-1 matrix metalloproteinase', *Molecular Cancer* **5**(1), 66.

Powathil, G., Gordon, K., Hill, L. and Chaplain, M. (2012), 'Modelling the effects of cell-cycle heterogeneity on the response of a solid tumour to chemotherapy: biological insights from a hybrid multiscale cellular automaton model', *J. Theor. Biol.* **308**, 1–19.

Preziosi, L. and Tosin, A. (2009), 'Multiphase and multiscale trends in cancer modelling', *Math. Model. Nat. Phen.* **4**(03), 1–11.

Provenzano, P., Inman, D., Eliceiri, K., Knittel, J., Yan, L., Rueden, C., White, J. and Keely, P. (2008), 'Collagen density promotes mammary tumor initiation and progression', *BMC Med.* **6**, 11.

Quaranta, V., Rejniak, K., Gerlee, P. and Anderson, A. (2008), 'Invasion emerges from cancer cell adaptation to competitive microenvironments: quantitative predictions from multiscale mathematical models', **18**(5), 338–348.

Quesada, V., Ordonez, G., Sanchez, L., Puente, X. and Lopez-Otin, C. (2009), 'The Degradome database: mammalian proteases and diseases of proteolysis', *Nucleic Acids Res.* **37**(Database issue), D239–243.

Ramis-Conde, I., Chaplain, M., Anderson, A. and Drasdo, D. (2009), 'Multi-scale modelling of cancer cell intravasation: the role of cadherins in metastasis', *Phys. Biol.* **6**(1), 016008.

Ramis-Conde, I., Drasdo, D., Anderson, A. and Chaplain, M. (2008), 'Modeling the influence of the E-cadherin-β-catenin pathway in cancer cell invasion: a multiscale approach', *Biophy. J.* **95**(1), 155–165.

Rejniak, K. (2005), 'A single-cell approach in modeling the dynamics of tumor microregions', *Math. Biosci. Eng.* **2**(3), 643–655.

Rejniak, K. (2007), 'An immersed boundary framework for modelling the growth of individual cells: an application to the early tumour development', *J. Theor. Biol.* **247**(1), 186–204.

Rejniak, K. (2012), 'Homeostatic imbalance in epithelial ducts and its role in carcinogenesis', *Scientifica* **2012**.

Rejniak, K. and Anderson, A. (2011), 'Hybrid models of tumor growth', *WIRES Syst. Biol. Med.* **3**(1), 115–125.

Rejniak, K. and Dillon, R. (2007), 'A single cell-based model of the ductal tumour microarchitecture', *Comp. Math. Meth. Med.* **8**(1), 51–69.

Rejniak, K. and McCawley, L. (2010), 'Current trends in mathematical modeling of tumor-microenvironment interactions: a survey of tools and applications', *Exp. Biol. Med. (Maywood)* **235**(4), 411–423.

Rejniak, K., Wang, S., Bryce, N., Chang, H., Parvin, B., Jourquin, J., Estrada, L., Gray, J., Arteaga, C., Weaver, A., Quaranta, V. and Anderson, A. (2010), 'Linking changes in epithelial morphogenesis to cancer mutations using computational modeling', *PLoS Comp. Biol.* **6**(8), e1000900.

Roose, T., Chapman, S. and Maini, P. (2007), 'Mathematical models of avascular tumor growth', *SIAM Rev.* **49**(2), 179–208.

Rowe, R. and Weiss, S. (2009), 'Navigating ECM barriers at the invasive front: the cancer cell-stroma interface', *Ann. Rev. Cell Develop.* **25**, 567–595.

Rubenstein, B. and Kaufman, L. (2008), 'The role of extracellular matrix in glioma invasion: a cellular potts model approach', *Biophys. J.* **95**(12), 5661–5680.

Sabeh, F., Li, X., Saunders, T., Rowe, R. and Weiss, S. (2009), 'Secreted versus membrane-anchored collagenases: relative roles in fibroblast-dependent collagenolysis and invasion.', *J. Biol. Chem.* **284**(34), 23001–23011.

Sabeh, F., Shimizu-Hirota, R. and Weiss, S. (2009), 'Protease-dependent versus -independent cancer cell invasion programs: three-dimensional amoeboid movement revisited', *J. Cell Biol.* **185**(1), 11–19.

Sahai, E. (2005), 'Mechanisms of cancer cell invasion', *Curr. Opin. Genet. Dev.* **15**(1), 87–96.

Sakai, K., Nakamura, T., Suzuki, Y., Imizu, T. and Matsumoto, K. (2011), '3-D collagen-dependent cell surface expression of MT1-MMP and MMP-2 activation regardless of integrin $\beta 1$ function and matrix stiffness', *Biochem. Biophys. Res. Comm.* **412**(1), 98–103.

Sato, H., Takino, T., Okada, Y., Cao, J., Shinagawa, A., Yamamoto, E. and Seiki, M. (1994), 'A matrix metalloproteinase expressed on the surface of invasive tumour cells', *Nature* **370**(6484), 61–65.

Schlüter, D. (2013), A multiscale systems biology study of in vitro cell migration and cancer cell invasion, PhD thesis, University of Dundee.

Scianna, M., Bell, C. and Preziosi, L. (2013), 'A review of mathematical models for the formation of vascular networks', *J. Theor. Biol.* **333**, 174–209.

Scianna, M. and Preziosi, L. (2012), 'Multiscale developments of the cellular potts model', *Multiscale Model. Sim.* **10**(2), 342–382.

Scott, J. (1968), 'Hilltopping as a mating mechanism to aid the survival of low density species', *J. Res. Lepid* **7**(4), 191–204.

Shapiro, S. and Senior, R. (1999), 'Matrix metalloproteinases: matrix degradation and more', *Am. J. Resp. Cell Molecular Biol.* **20**(6), 1100–1102.

Sherratt, J. (1993), 'Cellular growth control and travelling waves of cancer', *SIAM J. Appl. Math.* **53**(6), 1713–1730.

Smallbone, K., Gavaghan, D., Gatenby, R. and Maini, P. (2005), 'The role of acidity in solid tumour growth and invasion', *J. Theor. Biol.* **235**(4), 476–484.

Song, N., Sung, H., Choi, J., Han, S., Jeon, S., Song, M., Lee, Y., Park, C., Park, S., Lee, K., Yoo, K., Noh, D., Ahn, S., Lee, S. and Kang, D. (2012), 'Preoperative serum levels of matrix metalloproteinase-2 (MMP-2) and survival of breast cancer among Korean women', *Cancer Epidemiol. Biomark. Prev.* **21**(8), 1371–1380.

Sonnenschein, C. and Soto, A. (2013), 'The aging of the 2000 and 2011 hallmarks of cancer reviews: a critique', *J. Biosci.* **38**(3), 651–663.

Steeg, P. (2006), 'Tumor metastasis: mechanistic insights and clinical challenges', *Nat. Med.* **12**(8), 895–904.

Stevens, A. and Othmer, H. (1997), 'Aggregation, blowup, and collapse: the ABC's of taxis in reinforced random walks', *SIAM J. Appl. Math.* **57**(4), 1044–1081.

Stott, E., Britton, N., Glazier, J. and Zajac, M. (1999), 'Stochastic simulation of

benign avascular tumour growth using the Potts model', *Math. Comp. Model.* **30**(5), 183–198.

Sturrock, M. (2013), Spatio-temporal modelling of gene regulatory networks containing negative feedback loops, PhD thesis, University of Dundee.

Szabó, A. and Merks, R. (2013), 'Cellular potts modeling of tumor growth, tumor invasion, and tumor evolution', *Front. Oncol.* **3**.

Tam, E., Moore, T., Butler, G. and Overall, C. (2004), 'Characterization of the distinct collagen binding, helicase and cleavage mechanisms of matrix metalloproteinase 2 and 14 (gelatinase A and MT1-MMP): the differential roles of the MMP hemopexin c domains and the MMP-2 fibronectin type II modules in collagen triple helicase activities', *J. Biol. Chem.* **279**(41), 43336–43344.

Tektonidis, M., Hatzikirou, H., Chauvière, A., Simon, M., Schaller, K. and Deutsch, A. (2011), 'Identification of intrinsic in vitro cellular mechanisms for glioma invasion', *J. Theor. Biol* **287**, 131–147.

Terranova, V., DiFlorio, R., Lyall, R., Hic, S., Friesel, R. and Maciag, T. (1985), 'Human endothelial cells are chemotactic to endothelial cell growth factor and heparin.', *J. Cell Biol.* **101**(6), 2330–2334.

Thomlinson, R. and Gray, L. (1955), 'The histological structure of some human lung cancers and the possible implications for radiotherapy', *Br. J. Cancer* **9**(4), 539–549.

Toth, M., Bernardo, M., Gervasi, D., Soloway, P., Wang, Z., Bigg, H., Overall, C., DeClerck, Y., Tschesche, H., Cher, M., Brown, S., Mobashery, S. and Fridman, R. (2000), 'Tissue inhibitor of metalloproteinase (TIMP)-2 acts synergistically

with synthetic matrix metalloproteinase (MMP) inhibitors but not with TIMP-4 to enhance the (Membrane type 1)-MMP-dependent activation of pro-MMP-2', *J. Biol. Chem.* **275**(52), 41415–41423.

Tracqui, P. (2009), 'Biophysical models of tumour growth', *Rep. Prog. Phys.* **72**(5).

Trucu, D., Lin, P., Chaplain, M. and Wang, Y. (2013), 'A multiscale moving boundary model arising in cancer invasion', *Multiscale Model. Simul.* **11**(1), 309–335.

Tso, W. and Adler, J. (1974), 'Negative chemotaxis in Escherichia coli', *J. Bacteriol.* **118**(2), 560–576.

Turner, S. and Sherratt, J. (2002), 'Intercellular adhesion and cancer invasion: a discrete simulation using the extended Potts model', *J. Theor. Biol.* **216**(1), 85–100.

Tutton, M., George, M., Eccles, S., Burton, S., Swift, R. and Abulafi, A. (2003), 'Use of plasma MMP-2 and MMP-9 levels as a surrogate for tumour expression in colorectal cancer patients', *Int. J. Cancer* **107**(4), 541–550.

Vakonakis, I. and Campbell, I. (2007), 'Extracellular matrix: from atomic resolution to ultrastructure', *Curr. Opin. Cell Biol.* **19**(5), 578–583.

Vargas, D. and Zaman, M. (2011), 'Computational model for migration of a cell cluster in three-dimensional matrices', *Ann. Biomed. Eng.* **39**(7), 2068–2079.

Vu, T. and Werb, Z. (2000), 'Matrix metalloproteinases: effectors of development and normal physiology', *Genes Dev.* **14**(17), 2123–2133.

Wang, W., Wyckoff, J., Frohlich, V., Oleynikov, Y., Hüttelmaier, S., Zavadil, J., Cermak, L., Bottinger, E., Singer, R., White, J., Segall, J. and Condeelis, J.

(2002), 'Single cell behavior in metastatic primary mammary tumors correlated with gene expression patterns revealed by molecular profiling', *Cancer Res.* **62**(21), 6278–6288.

Weaver, A. (2006), 'Invadopodia: specialized cell structures for cancer invasion', *Clin. Exp. Metastasis* **23**(2), 97–105.

Webb, S., Sherratt, J. and Fish, R. (1999), 'Alterations in proteolytic activity at low pH and its association with invasion: a theoretical model', *Clin. Exp. Metastasis* **17**(5), 397–407.

Werb, Z. (1997), 'ECM and cell surface proteolysis: regulating cellular ecology', *Cell* **91**(4), 439–442.

Wojciak-Stothard, B., Denyer, M., Mishra, M. and Brown, R. (1997), 'Adhesion, orientation, and movement of cells cultured on ultrathin fibronectin fibers', *In Vitro Cell. Dev. Biol. Animal* **33**(2), 110–117.

Wolf, K., Alexander, S., Schacht, V., Coussens, L., von Andrian, U., van Rheenen, J., Deryugina, E. and Friedl, P. (2009), 'Collagen-based cell migration models in vitro and in vivo', *Semin. Cell Dev. Biol.* **20**(8), 931–941.

Wurzel, M., Schaller, C., Simon, M. and Deutsch, A. (2005), 'Cancer cell invasion of brain tissue: guided by a prepattern?', *J. Theor. Med.* **6**(1), 21–31.

Yamaguchi, H. and Condeelis, J. (2007), 'Regulation of the actin cytoskeleton in cancer cell migration and invasion', *BBA: Molecular Cell Res.* **1773**(5), 642–652.

Yamaguchi, H., Lorenz, M., Kempiak, S., Sarmiento, C., Coniglio, S., Symons, M., Segall, J., Eddy, R., Miki, H., Takenawa, T. and Condeelis, J. (2005), 'Molecular mechanisms of invadopodium formation the role of the N-WASP–Arp2/3 complex pathway and cofilin', *J. Cell Biol.* **168**(3), 441–452.

Zhang, Y., Mao, X., Schwend, T., Littlechild, S. and Conrad, G. (2013), 'Resistance of Corneal RFUVA-Cross-Linked Collagens and Small Leucine-Rich Proteoglycans to Degradation by Matrix Metalloproteinases', *Invest. Ophthalmol. Vis. Sci.* **54**(2), 1014–1025.

Zheng, X., Wise, S. and Cristini, V. (2005), 'Nonlinear simulation of tumor necrosis, neo-vascularization and tissue invasion via an adaptive finite-element/level-set method', *Bull. Math. Biol.* **67**(2), 211–259.

Zhou, Z., Apte, S., Soininen, R., Cao, R., Baaklini, G., Rauser, R., Wang, J., Cao, Y. and Tryggvason, K. (2000), 'Impaired endochondral ossification and angiogenesis in mice deficient in membrane-type matrix metalloproteinase I', *Proc. Natl. Acad. Sci. U.S.A.* **97**(8), 4052–4057.

Zigrino, P., Drescher, C. and Mauch, C. (2001), 'Collagen-induced proMMP-2 activation by MT1-MMP in human dermal fibroblasts and the possible role of $\alpha 2\beta 1$ integrins', *Eur. J. Cell Biol.* **80**(1), 68–77.

Zucker, S. and Cao, J. (2009), 'Selective matrix metalloproteinase (MMP) inhibitors in cancer therapy: ready for prime time?', *Cancer Biol. Therapy* **8**(24), 2371–2373.